Universität
Hamburg

Department
Physik

Spinor Tonks-Girardeau gases and ultracold molecules

Dissertation
zur Erlangung des Doktorgrades
des Departments Physik
der Universität Hamburg

vorgelegt von
Frank Deuretzbacher

aus Halle (Saale)

Hamburg
2008

Gutachterin/Gutachter der Dissertation:	Prof. Dr. Daniela Pfannkuche Prof. Dr. Stephanie M. Reimann Prof. Dr. Maciej Lewenstein
Gutachterin/Gutachter der Disputation:	Prof. Dr. Daniela Pfannkuche Prof. Dr. Klaus Sengstock
Datum der Disputation:	15. Dezember 2008
Vorsitzender des Prüfungsausschusses:	PD Dr. Alexander Chudnovskiy
Vorsitzender des Promotionsausschusses:	Prof. Dr. Robert Klanner
Dekan des Fachbereiches für Mathematik, Informatik und Naturwissenschaften:	Prof. Dr. Arno Frühwald

Abstract

The research field of ultracold atomic quantum gases has been developing rapidly during the last years. That is due to the extremely flexible toolbox of the experimenters, which allows them to simulate for example a plenty of very different solid-state phenomena and to perform ultraslow chemical reactions in a controlled reversible manner.

One of the newest research objects are one-dimensional atomic systems in optical lattices. In cigar-shaped optical traps the free motion of the particles can be restricted to one dimension. The tight transverse confinement, moreover, extremely strengthens the effective forces leading to strong correlations between the particles.

In the first chapters of this thesis I study properties of quasi-one-dimensional Bose gases with contact interactions. For this reason I have developed an exact diagonalization approach, which allows for an accurate construction of the many-body wave function of few particles. During the development of the exact-diagonalization programming code I oriented myself on experiments, which have been performed in the group of K. Sengstock on spinor Bose-Einstein condensates.

At first I study the influence of the interaction strength on the properties of a spin polarized Bose gas. As long as the repulsive forces are weak, the particles behave like typical bosons, i. e., due to the permutation symmetry of the many-particle wave function they favor to occupy the same single-particle state. In that regime, the main impact of the weak repulsion is a broadening and flattening of the single-particle wave function in order to reduce the mean distance between the bosons. In the opposite limit, an extremely strong (or even infinite) repulsive contact force prevents the bosons from staying at the same position, thereby mimicing Pauli's exclusion principle. Indeed it is observed that hard-core bosons behave in many respects like noninteracting fermions.

Here I study the interaction-driven fermionization of quasi-one-dimensional bosons and its effect on the most important measurable quantities. It is shown that the momentum distribution reflects the permutation symmetry and the correlations of the many-particle wave function. Moreover, it clearly distinguishes between the above mentioned interaction regimes. In this work the boundaries of these regimes are determined for small finite-size systems.

Next, I study a one-dimensional Bose gas of hard-core particles (i. e. the repulsive contact forces between the point-like particles shall be infinite) with spin degrees of freedom. For that reason an easy-to-use analytical formula of the exact many-body wave function of the highly correlated bosons is derived. The construction scheme is based on M. Girardeau's original idea of a Fermi-Bose map for spinless particles. As a striking consequence of our mapping we find that one-dimensional hard-core particles (bosons or fermions) with spin degrees of freedom behave in many respects like noninteracting spinless fermions and noninteracting distinguishable spins. Therefore, the energy spectrum of this highly correlated many-particle system can be constructed easily. Moreover, the analytical formula of the many-body wave function is the basis of an illustrative construction scheme for the spin densities, which resemble a chain of localized spins.

Again, the momentum distribution is particularly interesting. Now its form strongly depends on the spin configuration of the one-dimensional system. The momentum distribution of spinless hard-core bosons shows striking differences from that of spinless noninteracting fermions. Here, by contrast, in some spin configurations the momentum distribution of the system shows clear fermionic signatures. Moreover, the construction scheme for the wave functions is also applicable to isospin-$1/2$ bosons, which e. g. represent Bose-Bose mixtures and two-level atoms.

The second part of this thesis deals with the ultracold chemical reaction of ^{40}K and ^{87}Rb atoms. C. Ospelkaus *et al.* produced molecules from atom pairs in a controlled reversible manner by means of a Feshbach resonance. This groundbreaking experiment was an important step towards the production of ultracold polar molecules (in their internal vibrational ground state). This might enable the realization of quantum gases with long-range interactions in the near future. Here, I develop a theoretical approach for the description of the molecule formation in a three-dimensional optical lattice. This approach might also be useful for other atomic mixtures with large mass ratios.

Zusammenfassung

Das Gebiet der ultrakalten Quantengase hat sich in den letzten Jahren rasant entwickelt. Das liegt auch an dem schier unerschöpflichen Werkzeugkasten der Experimentatoren, der z. B. die quantenmechanische Simulation unterschiedlichster Festkörperphänomene und die kontrollierte Durchführung chemischer Reaktionen ermöglicht, die bei ultratiefen Temperaturen sozusagen in Zeitlupe ablaufen.

Die neuesten Untersuchungsobjekte sind eindimensionale Systeme in optischen Gittern. Ein zigarrenförmiges Einschlusspotential beschränkt dabei die freie Bewegung der Teilchen auf eine Dimension, was darüber hinaus zur Folge hat, dass die effektiven Kräfte zwischen den Teilchen extrem verstärkt werden. Das führt zu starken Korrelationen zwischen den Teilchen.

In den ersten Kapiteln dieser Dissertation werden die quantenmechanischen Eigenschaften von quasi-eindimensionalen Bose-Gasen mit einer extrem kurzreichweitigen Kontaktwechselwirkung untersucht. Zu diesem Zweck wurde eine Exakte Diagonalisierung entwickelt, die eine genaue Konstruktion der Vielteilchenwellenfunktion von wenigen Teilchen ermöglicht. Als Vorbild dienten Experimente der Gruppe von K. Sengstock zu Spinor Bose-Einstein Kondensaten.

Es wurde zunächst der Einfluss der Wechselwirkungsstärke auf die Eigenschaften eines spinpolarisierten Bose-Gases untersucht. Solange die abstoßenden Kontaktkräfte zwischen den Teilchen klein sind, verhalten sie sich wie typische Bosonen, die sich auf Grund der Symmetrie der Vielteilchenwellenfunktion unter beliebigen Teilchenvertauschungen bevorzugt im selben stationären Bewegungszustand aufhalten. Die Einteilchenwellenfunktion, die diesen stationären Bewegungszustand beschreibt, wird durch die repulsiven Kontaktkräfte lediglich verbreitert, um den mittleren Abstand zwischen den Teilchen zu reduzieren. Eine sehr starke (unendlich große) abstoßende Kontaktkraft hindert die Bosonen hingegen in ihrem Bestreben, den selben quantenmechanischen Zustand einzunehmen. Die unendlich starke Abstoßung simuliert vielmehr das Pauli-Prinzip, wodurch sich die Bosonen, ähnlich wie Fermionen, nicht mehr am selben Ort aufhalten können. Es wird tatsächlich beobachtet, dass Bosonen unter diesen Bedingungen viele Eigenschaften von nichtwechselwirkenden Fermionen annehmen.

Diese sogenannte Fermionisierung quasi-eindimensionaler Bosonen mit zunehmender Kontaktabstoßung wird hier im Detail anhand wichtiger Messgrößen untersucht. Dabei zeigt insbesondere die Impulsverteilung des Systems ein interessantes Verhalten, da sich in ihrer Form sowohl die Permutationssymmetrie als auch die Korrelationen der Gesamtwellenfunktion widerspiegeln. Es wird in dieser Arbeit erstmals gezeigt, dass sich bestimmte Merkmale der Impulsverteilung auch zur Bestimmung der Grenzen der oben beschriebenen typischen Wechselwirkungsbereiche eignen.

Im nächsten Schritt wird ein eindimensionales Bose-Gas mit Spinfreiheitsgraden und (unendlich) starker Kontaktabstoßung untersucht. Zu diesem Zweck wird, aufbauend auf den Ideen von M. D. Girardeau, eine vergleichsweise einfache analytische Formel für die exakten Vielteilchen-Eigenfunktionen des Hamiltonoperators entwickelt. Die verblüffende Konsequenz dieser Formel ist die Aussage, dass sich eindimensionale Teilchen (sowohl Bosonen als auch Fermionen) mit Spinfreiheitsgraden im Bereich unendlich starker Kontaktabstoßung gleichzeitig wie nichtwechselwirkende spinlose Fermionen und nichtwechselwirkende unterscheidbare Spins verhalten. Dadurch setzt sich das Energiespekrum solcher Systeme in einfacher Weise aus dem Spektrum dieser beiden Teilchensorten zusammen. Außerdem lässt sich aus der Formel der exakten Vielteilchen-Wellenfunktionen ein anschauliches Konstruktionsverfahren für die Spindichten

ableiten. Es zeigt sich, dass diese einer Kette von lokalisierten Spins gleichen, deren Orientierung sich in einfacher Weise von der angegebenen Wellenfunktion ablesen lässt.

Besonders interessant ist abermals das Verhalten der Impulsverteilung, deren Form stark von der Spinkonfiguration des eindimensionalen Systems abhängt. Es zeigt sich nun auch im Impulsraum eine große Ähnlichkeit zwischen Bosonen und Fermionen. Darüber hinaus ist das Konstruktionsverfahren auch auf Isospin-$1/2$ Bosonensysteme anwendbar, welche sich z. B. durch Mischungen oder mit Hilfe von Zwei-Niveau Atome realisieren lassen.

Der zweite Teil dieser Arbeit widmet sich dem Gebiet der ultrakalten Chemie. In dem von C. Ospelkaus *et al.* durchgeführten Experiment wurden Kalium- und Rubidiumatome mit Hilfe einer Feshbachresonanz kontrolliert zur Reaktion gebracht. Dieses Schlüsselexperiment ermöglichte erst kürzlich die Herstellung von ultrakalten polaren Molekülen (im internen Vibrationsgrundzustand), wodurch in naher Zukunft möglicherweise Quantengase mit langreichweitigen Wechselwirkungen realisiert werden können. Es wird hier ein einfaches Verfahren entwickelt, welches eine genaue Beschreibung der Kalium-Rubidium Verbindung in einem dreidimensionalen optischen Gitter ermöglicht. Die dabei entwickelte Methode könnte auch für andere Mischsysteme mit großen Massenunterschieden der einzelnen Bestandteile von Bedeutung sein.

Publikationen

Teile dieser Dissertation sind in meiner Diplomarbeit [1] und in den folgenden Arbeiten veröffentlicht worden:

Publications

Parts of this thesis have been published in my diploma thesis [1] and in the following papers:

[2] F. Deuretzbacher, K. Bongs, K. Sengstock and D. Pfannkuche, *Evolution from a Bose-Einstein condensate to a Tonks-Girardeau gas: An exact diagonalization study*, Physical Review A **75**, 013614 (2007).

[3] F. Deuretzbacher, K. Plassmeier, D. Pfannkuche, F. Werner, C. Ospelkaus, S. Ospelkaus, K. Sengstock and K. Bongs, *Heteronuclear molecules in an optical lattice: Theory and experiment*, Physical Review A **77**, 032726 (2008).

[4] F. Deuretzbacher, K. Fredenhagen, D. Becker, K. Bongs, K. Sengstock and D. Pfannkuche, *Exact Solution of Strongly Interacting Quasi-One-Dimensional Spinor Bose Gases*, Phys. Rev. Lett. **100**, 160405 (2008).

Contents

Chapter 1

Introduction

The subject of this thesis are Tonks-Girardeau gases with spin degrees of freedom and ultracold heteronuclear Feshbach molecules. A Tonks-Girardeau gas is a one-dimensional Bose gas of point-like hard spheres. It is named after Lewi Tonks und Marvin D. Girardeau. In 1936 L. Tonks first derived the equation of state of a one-dimensional gas of hard spheres [5], motivated by the research done at the laboratories of General Electric on monoatomic films of caesium on tungsten. Later in 1960 M. D. Girardeau found an elegant way to construct the exact many-particle wave function of one-dimensional hard-core bosons from that of spinless noninteracting fermions [6].

More precisely, he found out that the wave function of one-dimensional hard-core bosons $\psi^{(\infty)}_{\text{bosons}}$ can be constructed exactly from the corresponding wave function of spinless noninteracting fermions $\psi^{(0)}_{\text{fermions}}$ simply by a multiplication of the latter with the so-called unit antisymmetric function A: $\psi^{(\infty)}_{\text{bosons}} = A\,\psi^{(0)}_{\text{fermions}}$ [see Eq. (3.7) for the definition of A]. This equation constitutes a bijective map between noninteracting fermions and bosons with infinite δ repulsion. As a direct consequence the energy spectra of the two systems and all the properties which are calculated from the square of the wave function are identical. However, the momentum distributions are still quite different due to the different permutation symmetries of the bosonic and fermionic wave functions.

Girardeau's idea turned out to be extremely useful for the understanding of one-dimensional systems and it inspired other theorists to search for further exact solutions. Shortly later in 1963 E. H. Lieb and W. Liniger solved exactly a gas of one-dimensional spinless bosons which interact via contact potentials of *finite* strength *in the thermodynamic limit* [7, 8]. That solution was generalized to particles with arbitrary permutation symmetry by C. N. Yang [9] and to bosons at finite temperatures by C. N. Yang and C. P. Yang [10]. These papers form the basis of an effective harmonic-fluid approach to the low-energy properties of one-dimensional systems by means of the Luttinger liquid model [11, 12, 13] (see Ref. [14] for an introduction to the method).

However, although these systems seemed to be rather interesting for many theorists it was impossible during a couple of decades to realize the quasi-one-dimensional regime in experiments. That situation changed with the rapid progress in the field of ultracold atoms. Since the realization of Bose-Einstein condensation (BEC) in atomic gases in 1995 the first groundbreaking experiments have mainly been performed in the weakly interacting regime in two or three dimensions (see Refs. [15, 16] for a review). In first experiments with cigar-shaped optical dipole traps [17] dark solitons [18] and quantum phase fluctuations [19] have been studied in the weakly interacting regime. However, extremely elongated trap geometries, which are needed to reach the strongly interacting regime, became only recently available in optical lattices [20]. Finally, in the year 2004 two experimental groups even reached the Tonks-Girardeau regime [21, 22]. Moreover, Luttinger-

liquid behavior, which has been theoretically predicted in Ref. [23] for ultracold atomic gases, has been observed in several experiments with cold atoms in optical lattices [24, 25] and electrons in quantum wires [26] and carbon nanotubes [27, 28, 29].

When one-dimensional systems with stronger interactions came into reach experimentally it was realized that these systems have an inhomogeneous trapping potential with a finite size so that the methods, which are based on the approach of E. H. Lieb and W. Liniger, were not directly applicable. Moreover, it is rather difficult to extract correlation properties from the Lieb-Liniger solution. The solution of Girardeau [6] on the other hand is valid for arbitrary trap geometries but unfortunately only for an infinitely strong δ repulsion. It was thus necessary to develop new approaches which account for the finite size, the inhomogeneity and the finite interaction strength of the atomic gases. These new approaches are based on the Lieb-Liniger method [30, 31, 32, 33, 34, 35], quantum Monte Carlo techniques [36, 37], the numerical density-matrix renormalization group (DMRG) approach [38, 39, 40], the Multi-Configuration Time-Dependent Hartree (MCTDH) method [41, 42] and the numerical exact-diagonalization technique [1, 2, 3, 4, 43, 44], which is used throughout this thesis.

In the experiments of Kinoshita *et al.* [21, 45] the strength of the effective one-dimensional δ repulsion has been tuned by means of the transverse confinement. This is possible since in the quasi-one-dimensional regime the effective one-dimensional interaction becomes proportional to the transverse level spacing of the cigar-shaped trap. Accordingly, I study in chapter 3 the interaction-driven evolution of a one-dimensional spin-polarized few boson system from a Bose-Einstein condensate to a Tonks-Girardeau gas. I use the exact-diagonalization method for the analysis of the system, which I explain in detail in chapter 2 for the specific system of bosons with spin-dependent contact forces. It is shown in chapter 3 that the momentum distribution of the spin-polarized system shows a particularly interesting evolution when the interaction strength is increased.

In chapter 4 I analyze the ground-state properties of a Tonks-Girardeau gas with additional spin degrees of freedom. So far most experiments, which studied the ground-state properties and the spin dynamics of weakly interacting isospin-$1/2$ [46], spin-1 [47, 48, 49] or spin-2 [50, 51, 52, 53] Bose-Einstein condensates, have been successfully explained within the mean-field picture and the single-mode approximation [54, 55, 56, 57, 58, 59, 60]. Moreover, coherent spin dynamics of only two atoms at each site of a deep three-dimensional optical lattice has been studied in a series of recent experiments [61, 62, 63]. However, in cigar-shaped traps with stronger interactions the single-mode approximation is not applicable [64, 65, 66]. In that regime interesting spin textures have been observed [67, 53], which are so far not completely understood. The results of chapter 4 contribute to an understanding of these quasi-one-dimensional systems with spin degrees of freedom from the viewpoint of an infinitely strong repulsion between the particles.

Girardeau's concept of a bijective map between bosons and fermions has been extended to other systems such as fermionic Tonks-Girardeau gases [68] and very recently also to mixtures [69] and two-level atoms [70, 71]. Surprisingly, thus far no Fermi-Bose map existed for the important system of particles with spin degrees of freedom. A solution of that problem is given in chapter 4 based on Girardeau's original idea for spinless bosons [6]. There, an easy-to-use analytical formula for the many-body wave functions of hard-core particles with spin is given. That formula constitutes a bijective map between noninteracting spinless fermions and noninteracting distinguishable spins on the one hand and hard-core particles with spin on the other hand. As a result the energy spectrum of the strongly interacting spinful particles is simply the sum of the spectra of noninteracting spinless fermions and noninteracting distinguishable spins. Further, an illustrative construction scheme for the spin densities is derived and it is shown for the example of three spin-1 bosons that the analytical limiting solutions can be used to approximate realistic systems

with large but finite interactions. Again, the momentum distribution shows a particularly interesting behavior, which is now strongly dependent on the spin configuration of the one-dimensional system and which exhibits fermionic features in some spin configurations.

Finally, chapter 5 deals with the production of ultracold heteronuclear molecules from ^{40}K and ^{87}Rb atoms by means of radio-frequency (rf) association in the vicinity of a magnetic-field Feshbach resonance [72, 73, 74]. In the first sections of that chapter I introduce important concepts concerning the interactions in ultracold atomic gases. In particular I solve the problem of two atoms in a three-dimensional rotationally symmetric harmonic trap, which interact via a box-like potential. In the zero-range limit I obtain the result of Busch *et al.* [75], which shows that the extremely short-range interaction potentials of ultracold atoms can be modeled by a regularized δ potential. That solution (which already includes the interaction between the particles) is the basis of a detailed theoretical analysis of the experiment of C. Ospelkaus *et al.* [72] in the following sections of chapter 5. In particular it was necessary for a precise determination of the two-atom wave function to account for the coupling between center-of-mass and relative motion due to the anharmonic corrections of the single lattice sites and the different masses of the atoms. We derive a simple exact-diagonalization approach to that problem, which allows us not only to precisely determine the location of the Feshbach resonance but also the efficiency of the rf association and the lifetime of the molecules.

Chapter 2

Modeling of ultracold spin-1 atoms

The main results of Secs. 2.5 to 2.9 have been published in my diploma thesis [1] and the main parts of the exact diagonalization have been implemented during that time.

In this chapter I describe the methods which are the basis of the following chapters 3 and 4. In Sec. 2.1 I present the Hamiltonian of the system and I discuss its properties and symmetries. In the corresponding subsections 2.1.1 and 2.1.2 I derive the effective Zeeman Hamiltonian and interaction potential respectively. In Secs. 2.3 to 2.8 I describe the implementation of a numerical diagonalization of the many-particle Hamiltonian (2.5) and finally, in Sec. 2.9, I compare my numerical results to known exact solutions in some limiting cases: the Tonks-Girardeau solution [6] for a quasi-one-dimensional spin-polarized system, the solution of C. K. Law, H. Pu and N. P. Bigelow [56] for a zero-dimensional system of bosonic spins and the two-particle solution [75, 76].

2.1 Hamiltonian for spin-1 atoms

Spin-independent harmonic trap: We consider a neutral ^{87}Rb atom with spin $f = 1$. The atom is confined by means of an optical dipole trap which provides a spin-independent harmonic potential

$$V_{\text{trap}} = \frac{1}{2} m \Big(\omega_x^2 x^2 + \omega_y^2 y^2 + \omega_z^2 z^2 \Big) \otimes \mathbb{1} \, .$$

Here, m is the mass of the ^{87}Rb atom (see appendix D), ω_x, ω_y and ω_z are the trap frequencies of the x-, y- and z-direction, and $\mathbb{1}$ is the 3×3 dimensional identity matrix. V_{trap} is a 3×3 dimensional matrix since a spin-1 particle with motional and spin degrees of freedom is described by a 3-component wave function

$$\psi(\vec{r}) = \sum_{m_f = -1,0,1} \psi_{m_f}(\vec{r}) |m_f\rangle \, ,$$

with $|1\rangle = (1,0,0)^T$, $|0\rangle = (0,1,0)^T$ and $|{-1}\rangle = (0,0,1)^T$. In each spin state the atom feels the same trapping potential since V_{trap} is diagonal in spin space. Furthermore, V_{trap} commutes with the parity operators of the x-, y- and z-direction $\Pi_x : x \to -x$, $\Pi_y : y \to -y$ and $\Pi_z : z \to -z$ since $V_{\text{trap}}(x,y,z) = V_{\text{trap}}(\pm x, \pm y, \pm z)$. In most experiments of Refs. [52, 53] the transverse trap frequencies ω_y and ω_z are much larger than the axial trap frequency ω_x so that the system becomes quasi-one-dimensional.

Zeeman Hamiltonian: A homogeneous magnetic field along the z-axis couples to the atomic spin leading to the Zeeman Hamiltonian

$$V_Z = -\frac{\mu_B B}{2} f_z - \frac{\mu_B^2 B^2}{2C_{\text{hfs}}} \left(\mathbb{1} - \frac{1}{4} f_z^2 \right). \tag{2.1}$$

Here, μ_B is Bohr's magneton, B is the strength of the applied magnetic field, f_z is the dimensionless spin-1 matrix of the z-direction and C_{hfs} is the hyperfine constant (see appendix D). The dimensionless spin-1 matrices are given by

$$f_x = \frac{1}{\sqrt{2}} \begin{pmatrix} 0 & 1 & 0 \\ 1 & 0 & 1 \\ 0 & 1 & 0 \end{pmatrix}, \quad f_y = \frac{1}{\sqrt{2}} \begin{pmatrix} 0 & -\mathbb{i} & 0 \\ \mathbb{i} & 0 & -\mathbb{i} \\ 0 & \mathbb{i} & 0 \end{pmatrix} \quad \text{and} \quad f_z = \begin{pmatrix} 1 & 0 & 0 \\ 0 & 0 & 0 \\ 0 & 0 & -1 \end{pmatrix}.$$

The first term of V_Z is the usual linear and the second term is the quadratic Zeeman energy. Its origin is explained in subsection 2.1.1.

Interaction Hamiltonian: Two spin-1 atoms interact with each other via a short-ranged spin-dependent potential which is given by [54, 55]

$$V_{\text{int.}} = \delta(\vec{r}_1 - \vec{r}_2) \left(g_0 \mathbb{1}^{\otimes 2} + g_2 \vec{f}_1 \cdot \vec{f}_2 \right) \tag{2.2}$$

with the interaction strengths g_0 and g_2 (note that g_0 and g_2 have dimension energy $\times$ volume since the δ potential has dimension $1/\text{volume}$). $V_{\text{int.}}$ is a 9×9 dimensional matrix since two spin-1 particles with motional and spin degrees of freedom are described by a 9-component wave function

$$\psi(\vec{r}_1, \vec{r}_2) = \sum_{m_f, m_f' = -1,0,1} \psi_{m_f, m_f'}(\vec{r}_1, \vec{r}_2) |m_f, m_f'\rangle \,,$$

with $|m_f, m_f'\rangle = |m_f\rangle \otimes |m_f'\rangle$. $\mathbb{1}^{\otimes 2} = \mathbb{1} \otimes \mathbb{1}$, $\vec{f}_1 = (f_{x,1}, f_{y,1}, f_{z,1}) = (f_x \otimes \mathbb{1}, f_y \otimes \mathbb{1}, f_z \otimes \mathbb{1})$ are the spin-1 matrices of the first atom and $\vec{f}_2 = (f_{x,2}, f_{y,2}, f_{z,2}) = (\mathbb{1} \otimes f_x, \mathbb{1} \otimes f_y, \mathbb{1} \otimes f_z)$ are the spin-1 matrices of the second atom. The scalar product $\vec{f}_1 \cdot \vec{f}_2$ has to be evaluated according to

$$\vec{f}_1 \cdot \vec{f}_2 = f_{x,1} f_{x,2} + f_{y,1} f_{y,2} + f_{z,1} f_{z,2} = (f_x \otimes \mathbb{1})(\mathbb{1} \otimes f_x) + \ldots = f_x \otimes f_x + \ldots \,.$$

The first term of the interaction potential (2.2) is spin-independent (i. e. diagonal in spin space) and the second term is spin-dependent (i. e. non-diagonal in spin space). The scalar product $\vec{f}_1 \cdot \vec{f}_2$ can be expressed by means of the $\vec{F}^2$ operator and the identity matrix. We use

$$\vec{F}^2 = \left(\vec{f}_1 + \vec{f}_2 \right)^2 = \vec{f}_1^{\,2} + \vec{f}_2^{\,2} + 2\vec{f}_1 \cdot \vec{f}_2 = 4\mathbb{1}^{\otimes 2} + 2\vec{f}_1 \cdot \vec{f}_2 \qquad \left(\vec{f}_1^{\,2} = \vec{f}_2^{\,2} = 2\mathbb{1}^{\otimes 2} \right).$$

Thus,

$$\vec{f}_1 \cdot \vec{f}_2 = \vec{F}^2/2 - 2\mathbb{1}^{\otimes 2}$$

and we can rewrite the interaction Hamiltonian (2.2) according to

$$V_{\text{int.}} = \delta(\vec{r}_1 - \vec{r}_2) \left[(g_0 - 2g_2)\mathbb{1}^{\otimes 2} + (g_2/2)\vec{F}^2 \right]. \tag{2.3}$$

Therefore, $V_{\text{int.}}$ commutes with $F_z = f_{z,1} + f_{z,2}$ and $\vec{F}^2$. The interaction strengths g_0 and g_2 are given by [54, 55]

$$g_0 = \frac{4\pi\hbar^2}{m} \times \frac{a_0 + 2a_2}{3} \quad \text{and} \quad g_2 = \frac{4\pi\hbar^2}{m} \times \frac{a_2 - a_0}{3}$$

with the scattering lengths a_0 and a_2 ($\hbar$ is Planck's constant). The interaction potential which the atoms feel depends on the 2-atom spin $\vec{F}$ leading to the scattering lengths a_0 (if $F = 0$) and a_2 (if $F = 2$). For ^{87}Rb, $a_0 = 101.8\,a_B$ and $a_2 = 100.4\,a_B$ [77] (a_B is the Bohr radius). Therefore, the spin-dependent part of the interaction is approximately 200 times smaller than the spin-independent part of the interaction, $g_0/|g_2| \approx 200$. I will derive the interaction Hamiltonian in subsection 2.1.2.

Total Hamiltonian of 2 atoms: By summing up the kinetic energy and all the contributions to the potential energy we obtain the total Hamiltonian

$$\begin{aligned} H = &\sum_{i=1}^{2}\left[-\frac{\hbar^2}{2m}\Delta_i + \frac{1}{2}m\Big(\omega_x^2 x_i^2 + \omega_y^2 y_i^2 + \omega_z^2 z_i^2\Big)\right]\otimes\mathbb{1}^{\otimes 2} \\ &-\sum_{i=1}^{2}\left[\frac{\mu_B B}{2}f_{z,i} + \frac{\mu_B^2 B^2}{2C_{\text{hfs}}}\left(\mathbb{1}^{\otimes 2} - \frac{1}{4}f_{z,i}^2\right)\right] + \delta(\vec{r}_1 - \vec{r}_2)\Big(g_0\mathbb{1}^{\otimes 2} + g_2\vec{f}_1\cdot\vec{f}_2\Big). \end{aligned} \tag{2.4}$$

Conserved quantities: The above Hamiltonian (2.4) conserves the parities of the x-, y- and z-directions Π_x, Π_y and Π_z, and the z-component of the total spin F_z. For zero magnetic fields $B = 0$ the square of the total spin $\vec{F}^2$ is also conserved. For nonzero magnetic fields $B \neq 0$ the square of the total spin $\vec{F}^2$ is not conserved due to the quadratic Zeeman Hamiltonian. $\vec{F}^2$ commutes with F_z and $\vec{f}_1\cdot\vec{f}_2$ but not with $\big(f_{z,1}^2 + f_{z,2}^2\big)$.

The linear Zeeman energy is often negligible: The linear Zeeman energy is often by far the largest energy contribution to the total energy; see Sec. 2.2. However, since the above Hamiltonian (2.4) commutes with F_z one can diagonalize H within subspaces with same M_F. Within these subspaces the linear Zeeman energy is only a constant offset.

Further, the linear Zeeman energy has no influence on the population dynamics of the system. In current experiments the probability is measured to find a particle in spin state $|m_f\rangle$ $(m_f = -1, 0, 1)$. The corresponding two-particle projection operator is given by $P_{m_f} = |m_f\rangle\langle m_f| \otimes \mathbb{1} + \mathbb{1} \otimes |m_f\rangle\langle m_f|$. These projection operators P_{m_f} commute with F_z. Supposed that the initial two-particle state is given by $|\psi\rangle$ then the time evolution of this state is given by $e^{-\mathbb{i}Ht/\hbar}|\psi\rangle$. The time evolution of the population of the hyperfine state m_f is thus

$$\langle\psi|e^{\mathbb{i}Ht/\hbar}P_{m_f}e^{-\mathbb{i}Ht/\hbar}|\psi\rangle = \langle\psi|e^{\mathbb{i}H't/\hbar}\underbrace{e^{\mathbb{i}H_{Z,\text{lin.}}t/\hbar}e^{-\mathbb{i}H_{Z,\text{lin.}}t/\hbar}}_{=\mathbb{1}}P_{m_f}e^{-\mathbb{i}H't/\hbar}|\psi\rangle$$

and therefore independent of $H_{Z,\text{lin.}}$. Here we have decomposed the Hamiltonian H into the linear Zeeman energy $H_{Z,\text{lin.}}$ and the remainder H' and we have used that $H_{Z,\text{lin.}}$ commutes with H' so that the relation $e^{-\mathbb{i}(H_{Z,\text{lin.}}+H')t/\hbar} = e^{-\mathbb{i}H_{Z,\text{lin.}}t/\hbar}e^{-\mathbb{i}H't/\hbar}$ holds.

Weak coupling between spin and motional degrees of freedom: The spin and the motional degrees of freedom are only weakly coupled by the Hamiltonian (2.4). To see this, we decompose H into three parts. The first part,

$$H_{\text{mot.}} = \sum_{i=1}^{2}\left[-\frac{\hbar^2}{2m}\Delta_i + \frac{1}{2}m\Big(\omega_x^2 x_i^2 + \omega_y^2 y_i^2 + \omega_z^2 z_i^2\Big) + g_0\delta(\vec{r}_1 - \vec{r}_2)\right]\otimes\mathbb{1}^{\otimes 2},$$

acts only in position space, the second part,

$$H_{\text{spin}} = -\sum_{i=1}^{2}\left[\frac{\mu_B B}{2}f_{z,i} + \frac{\mu_B^2 B^2}{2C_{\text{hfs}}}\left(\mathbb{1}^{\otimes 2} - \frac{1}{4}f_{z,i}^2\right)\right],$$

acts only in spin space and the third part,

$$H_{\text{mot.–spin}} = g_2 \delta(\vec{r}_1 - \vec{r}_2) \vec{f}_1 \cdot \vec{f}_2 \,,$$

weakly couples the motional to the spin degrees of freedom. The shape of the motional wave function is mainly determined by $H_{\text{mot.}}$ since it already contains the (large) spin-independent interaction. Due to the weak coupling of the motional and the spin degrees of freedom via $H_{\text{mot.–spin}}$ it is often a good strategy to diagonalize H in the eigenbasis of $(H_{\text{mot.}} + H_{\text{spin}})$. [1]

Generalization to N atoms: Generalization of the above two-particle Hamiltonian (2.4) to N particles is straightforward

$$\begin{aligned} H = &\sum_{i=1}^{N} \left[-\frac{\hbar^2}{2m}\Delta_i + \frac{1}{2}m\Big(\omega_x^2 x_i^2 + \omega_y^2 y_i^2 + \omega_z^2 z_i^2\Big)\right] \otimes \mathbb{1}^{\otimes N} \\ &- \sum_{i=1}^{N} \left[\frac{\mu_B B}{2} f_{z,i} + \frac{\mu_B^2 B^2}{2C_{\text{hfs}}} \left(\mathbb{1}^{\otimes N} - \frac{1}{4} f_{z,i}^2 \right) \right] + \sum_{i<j} \delta(\vec{r}_i - \vec{r}_j) \left(g_0 \mathbb{1}^{\otimes N} + g_2 \vec{f}_i \cdot \vec{f}_j \right). \end{aligned} \tag{2.5}$$

Here, $f_{z,i} = \mathbb{1}^{\otimes(i-1)} \otimes f_z \otimes \mathbb{1}^{\otimes(N-i)}$ $\big(f_{x,i}$, $f_{y,i}$ accordingly$\big)$ and the scalar product $\vec{f}_i \cdot \vec{f}_j$ has to be evaluated according to $\vec{f}_i \cdot \vec{f}_j = f_{x,i} f_{x,j} + f_{y,i} f_{y,j} + f_{z,i} f_{z,j}$.

2.1.1 Derivation of the Zeeman Hamiltonian

For the derivation of the Zeeman Hamiltonian (2.1) we have to regard that the atomic spin $\vec{f}$ is composed of a nuclear spin $\vec{i}$ and an electron spin $\vec{s}$. ^{87}Rb atoms have a nuclear spin of $i = 3/2$ and an electron spin of $s = 1/2$ resulting in a total spin of $f = 1$ or 2. Both spins interact with each other and an external magnetic field

$$H_Z = g_e \mu_B B s_z - \cancel{g_n \mu_n B i_z} + C_{\text{hfs}} \vec{s} \cdot \vec{i}. \tag{2.6}$$

Here, $g_e \approx 2$ is the electron g-factor, g_n is the nuclear g-factor, μ_n is the nuclear magneton, $\vec{s} = (s_x, s_y, s_z)$ and $\vec{i} = (i_x, i_y, i_z)$ are the dimensionless spin-$1/2$ and spin-$3/2$ matrices respectively. We can savely neglect the second term of Eq. (2.6) since $g_n \mu_n / g_e \mu_B \approx 10^{-11}$. H_Z can be diagonalized exactly analytically. Its energy spectrum is plotted in Fig. 2.1.

At zero magnetic field H_Z consists only of the spin-spin coupling which is diagonal in the basis of total spin. Using

$$\vec{f}^{\,2} = (\vec{s} + \vec{i})^2 = \vec{s}^{\,2} + \vec{i}^{\,2} + 2\vec{s} \cdot \vec{i} \quad \Rightarrow \quad \vec{s} \cdot \vec{i} = \vec{f}^{\,2}/2 - 9/4\, \mathbb{1} \tag{2.7}$$

we obtain the hyperfine shifts

$$\begin{aligned} C_{\text{hfs}}\, \vec{s} \cdot \vec{i} \,|f = 1, m_f\rangle &= -5/4\, C_{\text{hfs}}\, |f = 1, m_f\rangle \quad \text{and} \\ C_{\text{hfs}}\, \vec{s} \cdot \vec{i} \,|f = 2, m_f\rangle &= +3/4\, C_{\text{hfs}}\, |f = 2, m_f\rangle. \end{aligned}$$

[1] So far I did not discuss the additional symmetry restrictions of the two-particle wave function. In the weakly interacting regime $\big[$when $g_0/(l_x l_y l_z)$ is small compared to the level spacings $\hbar\omega_x$, $\hbar\omega_y$ and $\hbar\omega_z\big]$ the two bosons occupy the same motional (mean-field) ground state and one can describe the system within the symmetric spin space by using a renormalized spin-dependent interaction strength g_2 (see the discussion in Sec. 2.2; this is the so-called single-mode approximation which is e. g. used in Ref. [56]). In the strongly interacting regime, however, the motional wave functions are highly correlated and nonsymmetric within different spin components (see Secs. 4.1 and 4.2).

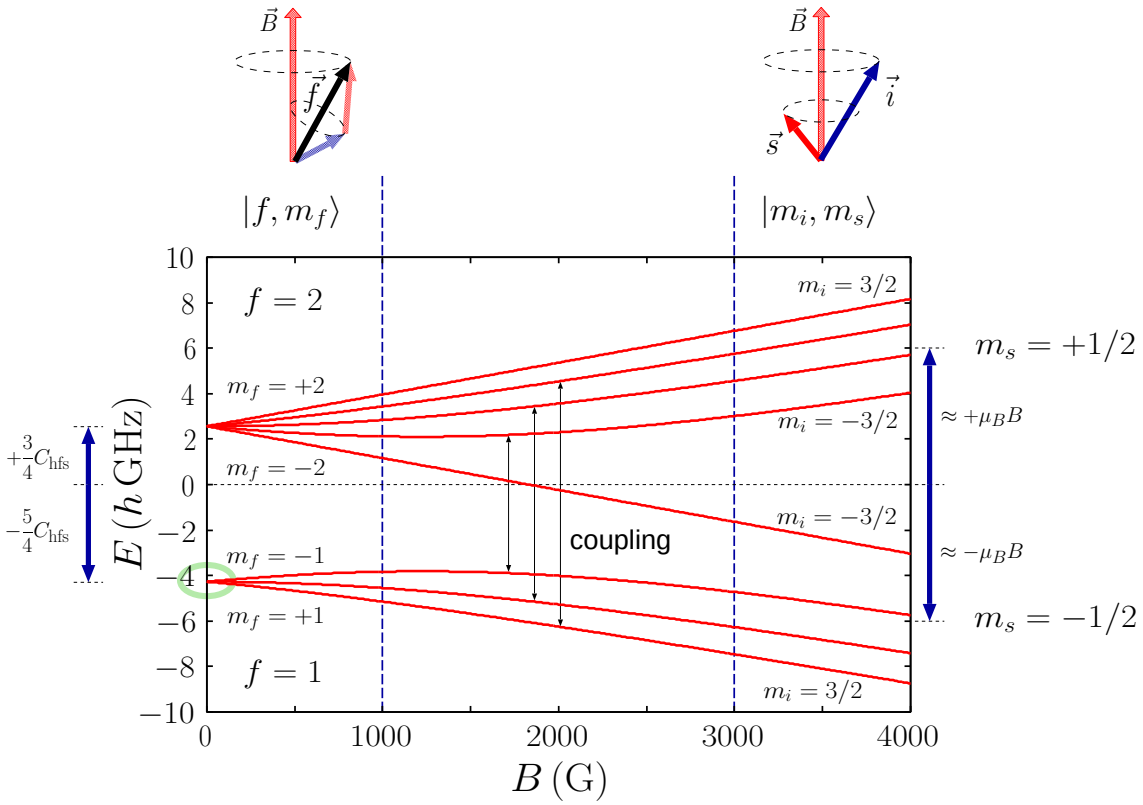

Figure 2.1: Zeeman energy of ^{87}Rb atoms in dependence of the magnetic field $|\vec{B}|$. For small $|\vec{B}|$ the nuclear spin $\vec{i}$ and the electron spin $\vec{s}$ couple to the total spin $\vec{f}$ which precesses around the magnetic field axis. For large $|\vec{B}|$ both spins $\vec{i}$ and $\vec{s}$ precess independently around $\vec{B}$. Although the experiments are performed at very low magnetic fields (green circle) the nonlinear behavior of the energy due to the coupling between $f = 1$ and $f = 2$ states is not negligible.

The energy shifts are drawn as blue arrows leftmost in Fig. 2.1. Thus all $f = 2$ states are shifted upwards by $E_Z = +3/4C_{\text{hfs}}$ and all $f = 1$ states are shifted downwards by $E_Z = -5/4C_{\text{hfs}}$.
For small magnetic fields it is often sufficiently accurate to approximate the real eigenstates by $\vec{f}^2$ eigenstates (f and m_f are 'good' quantum numbers). By using Eq. (2.7) and the Wigner-Eckart theorem [78]

$$P_f s_z P_f = \frac{\langle \vec{s} \cdot \vec{f} \rangle_f}{\langle \vec{f}^2 \rangle_f} P_f f_z P_f$$

(P_f is the projection operator onto the Hilbert space with spin f and the expectation values have to be calculated with states from this subspace) we obtain the first-order approximation of the Zeeman energy

$$E_Z \approx \langle f, m_f | H_Z | f, m_f \rangle = \underbrace{\left[g_e \frac{f(f+1) - 3}{2f(f+1)} \right]}_{=:g_f \text{ (Landé factor)}} \mu_B B m_f + C_{\text{hfs}} \big[f(f+1)/2 - 9/4 \big].$$

The Landé factor of the $f = 1$ states is $g_1 = -1/2$ and for the $f = 2$ states we obtain $g_2 = 1/2$ (for an illustrative calculation of the Landé factor see Ref. [1]). The first-order low-$|\vec{B}|$ result is

thus given by

$$E_Z(f=1) \approx -5/4 C_{\text{hfs}} - \mu_B B m_f/2 \quad \text{and} \quad E_Z(f=2) \approx +3/4 C_{\text{hfs}} + \mu_B B m_f/2\,. \quad (2.8)$$

This behavior can be seen in Fig. 2.1 in the region $B < 1000\,\text{G}$. Note that for $f = 2$ the state with $m_f = 2$ has highest energy whereas for $f = 1$ the state with $m_f = -1$ has highest energy due to the negative sign of the Landé factor.

Let us now consider the other extreme case of large magnetic fields $2\mu_B B \gg C_{\text{hfs}}$. Here it is sufficiently accurate to approximate the real eigenstates by (i_z, s_z) eigenstates (m_i and m_s are 'good' quantum numbers). By using the relations

$$\vec{s}\cdot\vec{i} = i_z \otimes s_z + \frac{1}{2}(i_+ \otimes s_- + i_- \otimes s_+) \quad (2.9)$$

with $i_\pm \equiv i_x \pm \mathbb{i} i_y$ (and analog for $s_\pm$) and

$$i_\pm |i, m_i\rangle = \sqrt{i(i+1) - m_i(m_i \pm 1)}\,|i, m_i \pm 1\rangle \quad \text{(and analog for } s_\pm) \quad (2.10)$$

we obtain the first-order approximation of the Zeeman energy in the region of large magnetic fields

$$E_Z \approx \langle m_i, m_s | H_Z | m_i, m_s\rangle = 2\mu_B B m_s + C_{\text{hfs}} m_i m_s. \quad (2.11)$$

Thus in the region $B > 3000\,\text{G}$ we observe two multiplets which are shifted by an average energy of $\Delta E \approx \pm\mu_B B$ (see the blue arrows rightmost of Fig. 2.1). The average spacing between the four states of each multiplet is $\Delta E \approx C_{\text{hfs}}/2$. Note again that the ordering within the lower multiplet is inverted since $m_s = -1/2$.

In the intermediate region $1000\,\text{G} < B < 3000\,\text{G}$ the energy depends nonlinearly on B (except for the fully stretched states) and the coupling between states with same m_f $\big(|1, m_f\rangle \leftrightarrow |2, m_f\rangle, m_f = -1, 0, 1\big)$ continuously rotates $\vec{f}^{\,2}$ into (i_z, s_z) eigenstates. Note, that the energy of the fully stretched states $\big(|2, 2\rangle = |3/2, 1/2\rangle$ and $|2,-2\rangle = |-3/2,-1/2\rangle\big)$ depends linearly on B for all magnetic fields since they are not coupled to other states. They are thus eigenstates of H_Z for all magnetic fields and their energy is exactly given by Eqs. (2.8) or (2.11). To determine the energy of the other states for all magnetic fields we have to calculate and diagonalize the 8×8 matrix of H_Z. Since only pairs of states with same m_f are mutually coupled this task reduces to a diagonalization of three 2×2 matrices. Here we do this calculation only for the pair of states $|2, -1\rangle$ and $|1, -1\rangle$. We switch into the (i_z, s_z) representation since the calculation of the off-diagonal matrix element is easier to perform with the given Eqs. (2.9) and (2.10). The state $|2, -1\rangle$ transforms into the state $|-3/2, 1/2\rangle$ and the state $|1, -1\rangle$ transforms into the state $|-1/2, -1/2\rangle$ (see Fig. 2.1). The matrix element of H_Z between these states is $\langle -3/2, 1/2|H_Z|-1/2, -1/2\rangle = \sqrt{3}/2\, C_{\text{hfs}}$. The resulting 2×2 matrix is given by $\big[$see Eq. (2.11) for the diagonal elements$\big]$

$$H_Z^{(\text{subspace})} = \begin{pmatrix} -3/4\, C_{\text{hfs}} + \mu_B B & \sqrt{3}/2\, C_{\text{hfs}} \\ \sqrt{3}/2\, C_{\text{hfs}} & +1/4\, C_{\text{hfs}} - \mu_B B \end{pmatrix}. \quad (2.12)$$

The eigenvalues of this matrix are

$$E_\pm = -C_{\text{hfs}}/4 \pm \sqrt{C_{\text{hfs}}^2 - C_{\text{hfs}}\mu_B B + \mu_B^2 B^2}. \quad (2.13)$$

For small magnetic fields one can perform a Taylor expansion in B. For the lower energy $\big($which belongs to the state $|\psi_-\rangle \approx |1, -1\rangle\big)$ we obtain

$$E_Z(|1, -1\rangle) = -\frac{C_{\text{hfs}}}{4} - C_{\text{hfs}}\sqrt{1 - \frac{\mu_B B}{C_{\text{hfs}}} + \frac{\mu_B^2 B^2}{C_{\text{hfs}}}} \approx -\frac{5C_{\text{hfs}}}{4} + \frac{\mu_B B}{2} - \frac{3\mu_B^2 B^2}{8C_{\text{hfs}}}. \quad (2.14)$$

The result now contains the hyperfine shift, the linear and the quadratic Zeeman energy. Similar calculations can be performed for the other states. The general result for the Zeeman shift, which is valid for all quantum numbers (f, m_f), is given by

$$E_Z = -\frac{C_{\text{hfs}}}{4} + (-1)^f \left[C_{\text{hfs}} + \frac{\mu_B B}{2} m_f + \frac{\mu_B^2 B^2}{2C_{\text{hfs}}} \left(1 - \frac{m_f^2}{4} \right) \right]. \tag{2.15}$$

In current experiments all the atoms are initially prepared in spin state $f = 1$ and the magnetic field strength is of the order of a few Gauss, which is indicated by the green circle in Fig. 2.1. During observation time the total spin of the atomic system $\vec{F} = \sum_i \vec{f}_i$ is conserved. Thus the hyperfine shift and the linear Zeeman energy are only a constant offset which has no influence on the system. The quadratic Zeeman shift, however, is of the order of the interaction energy and thus not negligible.

The off-diagonal elements of H_Z also lead to a mixing of $f = 1$ and $f = 2$ states. The above state $|\psi_-\rangle$, e.g., is a superposition $|\psi_-\rangle = \alpha|1, -1\rangle + \beta|2, -1\rangle$. Assuming a magnetic field strength of one Gauss, which is a typical experimental value, we obtain $\alpha = 0.99999998$ and $\beta = 0.0002$. Such a small admixture of $f = 2$ states has no influence on the properties of the system and we can safely assume $\alpha = 1$ and $\beta = 0$. In the effective Zeeman Hamiltonian for the spin $f = 1$ atoms (2.1) we have neglected the constant hyperfine shift and the small admixture of the $|f = 2, m_f\rangle$ states.

2.1.2 Derivation of the Interaction Hamiltonian

The interaction potential depends on the total spin of the valence electrons: We consider the interaction between two ^{87}Rb atoms at zero magnetic field $B = 0$. Again, we have to regard that the atomic spins are composed of a nuclear spin $\vec{i}$ and an electron spin $\vec{s}$. At close distances the electron spins of the two atoms couple to the total electron spin $\vec{S} = \vec{s}_1 + \vec{s}_2$. The interaction between the two atoms depends on the absolute value of S: In the singlet state, $S = 0$, it is more attractive than in the triplet state, $S = 1$, since in the first case the electron density between the Rb cores is higher; see Fig. 2.2. The interaction Hamiltonian is therefore given by

$$V_{\text{int.}}(r) = V_s(r) P_{S=0} + V_t(r) P_{S=1} \tag{2.16}$$

where $P_{S=0}$ ($P_{S=1}$) is the projection operator into the $S = 0$ (1) subspace and where V_s (V_t) is the singlet (triplet) interaction potential.

Delta approximation: We consider situations where the range of the singlet and triplet potential R_s and R_t is much smaller than the typical wave length of the wave functions of the interacting particles. This length scale is of the order of the oscillator length $l_{\text{osc.}}$, i. e., we consider situations where $\max(R_s, R_t) \ll l_{\text{osc.}}$.[2] Under these conditions the whole impact of the interaction potential reduces to a boundary condition on the logarithmic derivative of the wave function of the relative

[2] To be more precisely: Of course the interaction potentials V_s and V_t may have many bound states which lead to the formation of tightly bound molecules; see Fig. 5.1(a) and the discussion in Secs. 5.1 and 5.2. The extent of these molecules is much smaller than the range of the interaction. But here we are not interested in these tightly bound molecules but in the deformation of the low-energy wave functions of the trap by the short-ranged interaction; see the wave functions in Fig. 5.6 (apart from the red wave function in (a)). These low-energy trap states are in fact highly excited states and thus they are metastable (the ground-state molecule has lowest energy). However, the formation of tightly bound molecules is suppressed due to several conservation laws and since the overlap with the trap states is negligibly small so that there is enough observation time to study the metastable low-energy trap states.

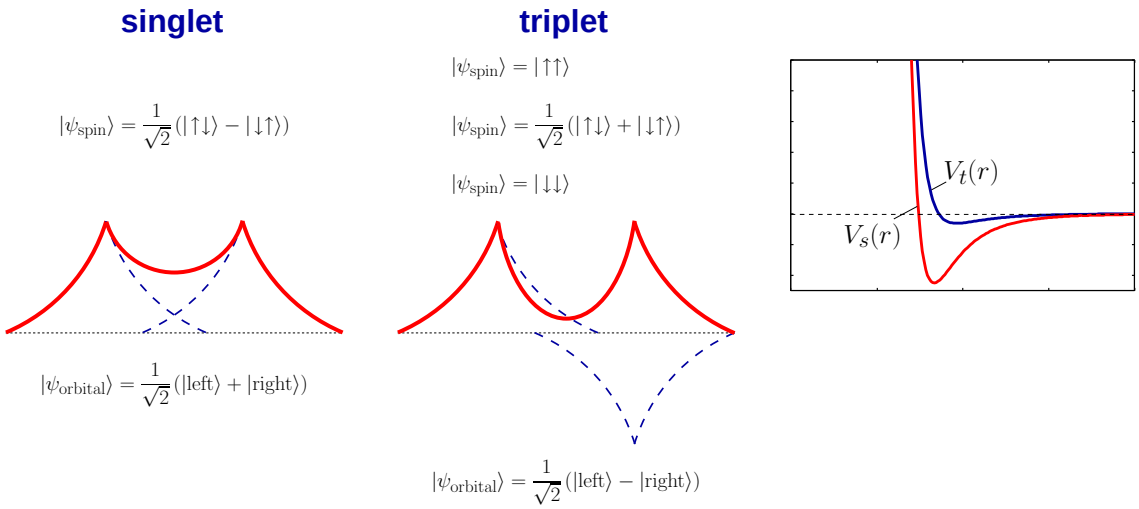

Figure 2.2: *The interaction potential depends on the total spin of the valence electrons*— At short distances the electron spins couple to a totel spin $\vec{S} = \vec{s}_1 + \vec{s}_2$. In the singlet state, the spin function is antisymmetric and the orbital function of the two electrons is symmetric, leading to a higher electron density (red) between the positive Rb cores. By contrast, in the triplet state, the spin function is symmetric and the orbital function is antisymmetric, leading to a lower electron density between the cores. Thus, in the singlet state, the Rb cores can come closer to each other so that the singlet interaction potential $V_s(r)$ is more attractive than the triplet potential $V_t(r)$.

motion at zero distance between the particles

$$\left.\frac{(r\psi_{s/t})'}{r\psi_{s/t}}\right|_{r=0} = -\frac{1}{a_{s/t}}$$

where ψ_s (ψ_t) is the wave function in the singlet (triplet) state and where a_s (a_t) is the scattering length of the singlet (triplet) interaction potential. [3] I will show in Sec. 5.3 that the above boundary condition is equivalent to the pseudopotential

$$V_{\text{pseudop.},s/t}(r) = \frac{2\pi\hbar^2 a_{s/t}}{\mu}\delta(\vec{r})\frac{\partial}{\partial r}\,r\,.$$

Thus, for our purposes, it is sufficiently accurate (and much easier to handle) to approximate the real interaction potentials V_s and V_t by a regularized δ potential:

$$V_{\text{int.}}(r) = \frac{2\pi\hbar^2}{\mu}\delta(\vec{r})\frac{\partial}{\partial r}\,r\,\left(a_s P_{S=0} + a_t P_{S=1}\right). \tag{2.17}$$

Accurate values for the singlet and triplet scattering lengths have been calculated in Ref. [77]: $a_s = 90.0\,a_B$ and $a_t = 98.99\,a_B$. The regularized δ potential acts only on wave functions with zero relative angular momentum $l_{\rm rel} = 0$. We want to use the pseudopotential in an exact diagonalization where the basis wave functions are harmonic oscillator eigenstates. Thus, the wave functions of the relative motion with $l_{\rm rel} = 0$ are given by

$$\psi_{\text{basis, rel.}}(r) \propto \mathfrak{L}_n^{1/2}(r^2)e^{-r^2/2} \qquad \text{(compare with Eq. 5.49)}$$

[3] For the definition of the scattering length see Fig. 5.3 and Eq. 5.17. The above boundary condition follows from Eq. 5.17 in the limit $R_{s/t} \to 0$. A discussion of the boundary condition is given in Secs. 5.2 and 5.3.

where $\mathfrak{L}_a^b(z)$ are the generalized Laguerre polynomials. The derivative of these wave functions at the origin is zero

$$\frac{\partial}{\partial r}\mathfrak{L}_n^{1/2}(r^2)e^{-r^2/2}\bigg|_{r=0} = 0\,.$$

We hence obtain

$$\frac{\partial}{\partial r}\Big[r\psi_{\text{basis, rel.}}(r)\Big]\bigg|_{r=0} = \psi_{\text{basis, rel.}}(0) + \cancel{0\cdot\psi'_{\text{basis, rel.}}(0)}\,. \tag{2.18}$$

Thus, we can neglect the operator $\frac{\partial}{\partial r}r$ in Eq. 2.17 and obtain the interaction potential [4]

$$V_{\text{int.}}(r) = \frac{2\pi\hbar^2}{\mu}\delta(\vec{r})\big(a_s P_{S=0} + a_t P_{S=1}\big). \tag{2.19}$$

Effective interaction Hamiltonian for spin-1 atoms: Since the interaction between two atoms depends on the absolute value of the total electron spin S (singlet or triplet), the atomic spin f can in principle be changed after the scattering. However, typical trap frequencies are orders of magnitude smaller than the hyperfine splitting $2C_{\text{hfs}}$. Thus, when the system is very cold, two atoms in $f = 1$ will remain in the same multiplet after the scattering since there is not enough energy to promote either atom to $f = 2$. Therefore, the effective low-energy interaction preserves the spin f of the individual atoms [54]. I will show in the following that, in the $f_1 = f_2 = 1$ subspace (i. e. the subspace where both atoms have spin 1), the interaction potential is given by

$$V_{\text{int.}}(r) = \frac{2\pi\hbar^2}{\mu}\delta(\vec{r})\big(a_{F=0}P_{F=0} + a_{F=2}P_{F=2}\big) \tag{2.20}$$

where $P_{F=0}$ ($P_{F=2}$) is the projection operator into the $F = 0\,(2)$ subspace $\big(\vec{F} = \vec{f}_1 + \vec{f}_2$ is the total spin of the two atoms$\big)$ and where $a_{F=0}$ and $a_{F=2}$ are the corresponding scattering lengths.

Derivation of Eq. (2.20) from Eq. (2.19)— At zero magnetic field two interacting atoms with nuclear and electron spins $\big(\vec{i}_1, \vec{s}_1\big)$ and $\big(\vec{i}_2, \vec{s}_2\big)$ are described by the Hamiltonian

$$H = C_{\text{hfs}}\left(\vec{i}_1\cdot\vec{s}_1 + \vec{i}_2\cdot\vec{s}_2\right) + \big(H_{\text{kin.}} + V_{\text{trap}}\big)\otimes\mathbb{1} + \frac{2\pi\hbar^2}{\mu}\delta(\vec{r})\big(a_s P_{S=0} + a_t P_{S=1}\big).$$

The first term H_{hfs} is the hyperfine coupling between the nuclear and electron spins and the remainder H' consists of the kinetic, potential and interaction energy of the two atoms. The differences of the energy eigenvalues of H_{hfs} are of the order of a few hGHz: $\Delta E_{\text{hfs}} = 2C_{\text{hfs}} \approx 7\,h$GHz. By contrast, the differences of the energy eigenvalues of H' are typically of the order of a few hHz up to several hkHz $\big($the largest trap frequencies which have been achieved in deep optical lattices are of the order of $\approx 0.1\,h$MHz; see Table 2.1$\big)$. Thus, to first order, H is well approximated by H_{hfs}. Using Eq. 2.7 we obtain

$$H_{\text{hfs}} = \frac{C_{\text{hfs}}}{2}\left(\vec{f}_1^{\,2} + \vec{f}_2^{\,2} - 9\mathbb{1}\right).$$

Therefore, the eigenvectors of H_{hfs} are given by the eigenvectors of $\left(\vec{f}_1^{\,2} + \vec{f}_2^{\,2}\right)$ and the eigenvalues are given by

$$E_{\text{hfs}} = \frac{C_{\text{hfs}}}{2}\Big[f_1(f_1+1) + f_2(f_2+1) - 9\Big]\,,$$

[4] The second summand of Eq. 2.18 is negligible as long as $\psi'_{\text{basis, rel.}}(0) < \infty$ (or, more precisely, as long as $\psi'_{\text{basis, rel.}}(r)$ does not have a $1/r$ singularity at the origin). The wave functions of noninteracting particles are always smooth at $r = 0$.

i. e.,

$$E_{\text{hfs}} = \begin{cases} -5C_{\text{hfs}}/2 & \text{if } f_1 = f_2 = 1 \\ -C_{\text{hfs}}/2 & \text{if } f_1 = 1 \text{ and } f_2 = 2 \text{ or } f_1 = 2 \text{ and } f_2 = 1 \\ 3C_{\text{hfs}}/2 & \text{if } f_1 = f_2 = 2\,. \end{cases}$$

The ground-state multiplet is ninefold degenerate since two spins with $f = 1$ can couple to one state with spin $F = 0$, three states with $F = 1$ and five states with $F = 2$.

Let us now switch on H'. Then, the degeneracy of the ground-state multiplet is lifted and we observe the following energy structure: There is one state with an energy of $-5C_{\text{hfs}}/2+E_1(a_s, a_t)$, there are three states with an energy of $-5C_{\text{hfs}}/2 + E_2(a_s, a_t)$ and there are five states with an energy of $-5C_{\text{hfs}}/2 + E_3(a_s, a_t)$. That is not surprising since H commutes with F_z and $\vec{F}^2$. [5] Hence, the degenerate eigenstates have spin $F = 0, 1$ and 2, respectively. Since $\left(\vec{f}_1^{\,2} + \vec{f}_2^{\,2}\right)$ does not commute with $P_{S=0}$ and $P_{S=1}$, each state contains admixtures from the higher multiplets of H_{hfs} due to the coupling to these states via the interaction (2.19). However, according to the above discussion, these admixtures are negligible since $\Delta E_{\text{hfs}} \gg \Delta E'$. Therefore, we may approximate H within the lowest multiplet by the Hamiltonian

$$H = E_1(a_s, a_t)P_{f_1=f_2=1,\,F=0} + E_2(a_s, a_t)P_{f_1=f_2=1,\,F=1} + E_3(a_s, a_t)P_{f_1=f_2=1,\,F=2}$$

where $P_{f_1=f_2=1,\,F}$ projects into the subspace where both atoms have spin 1 and total spin F. In the following we abbreviate these projectors by P_F.

Each energy is related to a scattering length $\big(E_1 \leftrightarrow a_{F=0},\ E_2 \leftrightarrow a_{F=1}$ and $E_3 \leftrightarrow a_{F=2}\big)$ via Eq. (5.50) and thus we may write the low-energy interaction Hamiltonian according to

$$V_{\text{int.}}(r) = \frac{2\pi\hbar^2}{\mu}\delta(\vec{r})\big(a_{F=0}P_{F=0} + a_{F=1}P_{F=1} + a_{F=2}P_{F=2}\big).$$

Finally we regard that the $F = 1$ spin functions are antisymmetric and thus the corresponding relative wave functions must be antisymmetric too (we are considering bosons). These wave functions are zero at $r = 0$ and thus the matrix elements of the operator $\delta(\vec{r})P_{F=1}$ are always zero for bosonic wave functions. After neglecting this part of the above Hamiltonian, we finally arrive at Eq. (2.20).

An alternative notation: We may express the operator $P_{F=0}$ as a linear combination of the operators $\mathbb{1}$, $\vec{f}_1 \cdot \vec{f}_2$ and $P_{F=1}$:

$$P_{F=0} = \alpha\mathbb{1} + \beta\vec{f}_1 \cdot \vec{f}_2 + \gamma P_{F=1}\,.$$

First, we convert the operator $\vec{f}_1 \cdot \vec{f}_2$:

$$\begin{aligned} &\vec{F}^2 = \left(\vec{f}_1 + \vec{f}_2\right)^2 = \vec{f}_1^{\,2} + \vec{f}_2^{\,2} + 2\vec{f}_1 \cdot \vec{f}_2 \\ &\Leftrightarrow\ 2\vec{f}_1 \cdot \vec{f}_2 = \vec{F}^2 - 4\mathbb{1} \quad \Leftrightarrow \quad \vec{f}_1 \cdot \vec{f}_2 = \vec{F}^2/2 - 2\mathbb{1} \end{aligned}$$

and obtain the equation

$$P_{F=0} = (\alpha - 2\beta)\mathbb{1} + \frac{\beta}{2}\vec{F}^2 + \gamma P_{F=1}\,. \tag{2.21}$$

In order to determine the coefficients, we calculate the expectation value of (2.21) with the $\big(\vec{F}^2, F_z\big)$ eigenvectors $|F = 0, m_F = 0\rangle$, $|F = 1, m_F\rangle$ and $|F = 2, m_F\rangle$. We obtain a set of

[5] I checked these commutation relations by means of MATHEMATICA

three coupled equations

$$\begin{aligned} 1 &= \alpha - 2\beta && \text{(expectation value with } |F=0, m_F=0\rangle\text{)} \\ 0 &= \alpha - 2\beta + \beta + \gamma && \text{(expectation value with } |F=1, m_F\rangle\text{)} \\ 0 &= \alpha - 2\beta + 3\beta && \text{(expectation value with } |F=2, m_F\rangle\text{)} \end{aligned}$$

from which we easily extract the coefficients $\alpha = 1/3$, $\beta = -1/3$ and $\gamma = -2/3$. Thus, the operator $P_{F=0}$ may be rewritten as

$$P_{F=0} = \frac{1}{3}\mathbb{1} - \frac{1}{3}\vec{f}_1 \cdot \vec{f}_2 - \frac{2}{3}P_{F=1}\,. \tag{2.22}$$

In an analogous calculation we obtain for $P_{F=2}$:

$$P_{F=2} = \frac{2}{3}\mathbb{1} + \frac{1}{3}\vec{f}_1 \cdot \vec{f}_2 - \frac{1}{3}P_{F=1}\,. \tag{2.23}$$

Using Eqs. (2.22) and (2.23) we obtain from Eq. (2.20)

$$V_{\text{int.}}(r) = \frac{2\pi\hbar^2}{\mu}\delta(\vec{r})\left(\frac{a_{F=0}+2a_{F=2}}{3}\mathbb{1} + \frac{a_{F=2}-a_{F=0}}{3}\vec{f}_1\cdot\vec{f}_2 - \cancel{\frac{2a_{F=0}+a_{F=2}}{3}P_{F=1}}\right).$$

Again, we can neglect the third summand since the expectation value of the operator $\delta(\vec{r})P_{F=1}$ is always zero for bosonic wave functions. Using $\mu = m/2$ we finally obtain Eq. (2.2).

2.2 Energy scales and parameter regimes

Energy scales: *Trap frequencies*— Before I proceed I will calculate the typical energy scales of our system. Table 2.1 shows typical trap frequencies of several experiments. The trap frequencies of each direction ω_x, ω_y and ω_z can be varied independently. The trap frequencies of the optical dipole traps used in Hamburg vary from a few to several hundred Hz. In the experiments of Kinoshita *et al.* at Penn State University an extremely elongated, quasi-one-dimensional trap was used. Here, the axial trap frequency was only $\omega_x = 2\pi \times 27.5\,\text{Hz}$ whereas the transverse trap frequencies were three orders of magnitude larger $\omega_y = \omega_z \lesssim 2\pi \times 70.7\,\text{kHz}$. Large trap frequencies in all three dimensions can be achieved in a deep optical lattice (Mainz).

Table 2.1: Trap frequencies of several experiments.

	ω_x	ω_y	ω_z
Hamburg 1D [53]	$2\pi \times 16.7\,\text{Hz}$	$2\pi \times 118\,\text{Hz}$	$2\pi \times 690\,\text{Hz}$
Hamburg 3D [53]	$2\pi \times 92\,\text{Hz}$	$2\pi \times 103\,\text{Hz}$	$2\pi \times 138\,\text{Hz}$
Penn State [21]	$2\pi \times 27.5\,\text{Hz}$	up to $2\pi \times 70.7\,\text{kHz}$	up to $2\pi \times 70.7\,\text{kHz}$
Mainz [63]	$2\pi \times 43.6\,\text{kHz}$	$2\pi \times 43.6\,\text{kHz}$	$2\pi \times 43.6\,\text{kHz}$

Interaction energy— According to the discussion in section 2.1, the level spacing of the trap has to be compared to the spin-independent interaction energy since the interplay of these two energy contributions determines the shape of the motional wave function. To get a rough estimate, we

calculate the spin-independent interaction energy of two atoms which reside in the ground state of the harmonic trap (see Sec. 2.4 for the eigenfunctions of the harmonic oscillator)

$$\psi(\vec{r}_1,\vec{r}_2)=\prod_{i=1,2}\phi_0(x_i)\phi_0(y_i)\phi_0(z_i)\qquad\text{with}\qquad\phi_0(u)=\frac{1}{\sqrt{l_u\sqrt{\pi}}}e^{-\frac{1}{2}(u/l_u)^2}\,.$$

Here, $l_u=\sqrt{\hbar/(m\omega_u)}$ is the oscillator length of the $u=x,y,z$-direction. According to Eq. (2.2), the spin-independent interaction energy of the above state is given by

$$E_{\text{int.},0}=g_0\int d\vec{r}\psi(\vec{r},\vec{r})^2=g_0\int dx\phi_0^4(x)\int dy\phi_0^4(y)\int dz\phi_0^4(z).$$

The one-dimensional integrals $I_u=\int du\phi_0^4$ have dimension $1/l_u$. To see this, we decompose each quantity into a dimensionless quantity (which we mark by a tilde symbol) and its unit

$$u=\widetilde{u}l_u,\quad\phi_0(u)=\widetilde{\phi}_0(u)\frac{1}{\sqrt{l_u}}\quad(u=x,y,z).$$

By inserting these relations into the corresponding interaction integrals we obtain $I_u=\widetilde{I}_u/l_u$ with $\widetilde{I}_x=\widetilde{I}_y=\widetilde{I}_z=1/\sqrt{2\pi}$. The interation energy becomes $\left(\omega_u=2\pi\times f_u\right)$

$$E_{\text{int.},0}=\frac{g_0}{l_xl_yl_z\sqrt{2\pi}^3}=\frac{4\pi\hbar^2}{m}\times\frac{a_0+2a_2}{3}\times\sqrt{\frac{m^3\cancel{(2\pi)^3}}{\hbar^3}}\times\sqrt{f_xf_yf_z}\times\frac{1}{\cancel{\sqrt{2\pi}^3}}\,.$$

As can be seen, the interaction energy increases when the trap frequencies are made larger since then the particles are enclosed within a smaller volume, $E_{\text{int.},0}\propto 1/(l_xl_yl_z)\propto\sqrt{f_xf_yf_z}$.
Again, we decompose each quantity into a product of a dimensionless number and its unit in order to calculate the interaction energy in units of hHz

$$\begin{gathered}\hbar=\widetilde{\hbar}\,\text{Js},\quad m=\widetilde{m}\,\text{kg},\quad a_i=\widetilde{a}_i\,a_B\;(i=0,2)\quad a_B=\widetilde{a}_B\,\text{m},\\ f_u=\widetilde{f}_u\,\text{Hz}\;\;(u=x,y,z),\quad h=\widetilde{h}\,\text{Js}\quad\Leftrightarrow\quad\text{J}=1/\widetilde{h}\,h\text{Hz}\,,\end{gathered}$$

with $\widetilde{\hbar}=1.05457163\times10^{-34}$, $\widetilde{m}=1.443160648\times10^{-25}$, $\widetilde{a}_0=101.8,\ldots$, (see appendix D for the constants). Finally we obtain the interaction energy in hHz

$$E_{\text{int.},0}=\underbrace{\left[\frac{4\pi\widetilde{\hbar}^2}{\widetilde{m}}\times\frac{\widetilde{a}_0+2\widetilde{a}_2}{3}\times\widetilde{a}_B\times\sqrt{\frac{\widetilde{m}^3}{\widetilde{\hbar}^3}}\times\frac{1}{\widetilde{h}}\right]}_{=:C_{\text{int.}}}\sqrt{\widetilde{f}_x\widetilde{f}_y\widetilde{f}_z}\,h\text{Hz}\tag{2.24}$$

with $C_{\text{int.}}\approx4\times10^{-4}$ in typical experiments. The spin-dependent interaction energy $E_{\text{int.},2}$ is approximately 200 times smaller since $|g_2|/g_0\approx1/200$.

Linear Zeeman energy— In the experiments performed in Hamburg and Mainz [63, 49] the magnetic field strength was of the order of 1 G. According to Eq. (2.1), the splitting of the linear Zeeman energy is given by $\Delta E_{Z,\text{lin.}}=\mu_BB/2$. Similar to the above calculation we determine the constant $C_{Z,\text{lin.}}$ which gives the linear Zeeman energy $\Delta E_{Z,\text{lin.}}$ in hHz if B is given in G

$$\Delta E_{Z,\text{lin.}}=\underbrace{\left[\frac{\widetilde{\mu}_B}{2\widetilde{h}10^4}\right]}_{C_{Z,\text{lin.}}}\widetilde{B}\,h\text{Hz}$$

with $\mu_B = \widetilde{\mu}_B\,\mathrm{J/T}$, $B = \widetilde{B}\,\mathrm{G}$, $1\,\mathrm{T} = 10^4\,\mathrm{G}$ and $C_{Z,\mathrm{lin.}} \approx 700 \times 10^3$. Thus, for a magnetic field strength of 1 G we obtain 700 hkHz which is by far the largest energy scale in our system. However, as discussed in section 2.1, the linear Zeeman energy has no influence on the population dynamics of our system and within subspaces with same M_F it is only a constant, negligible offset. Hence, this large energy contribution can often be neglected.

Quadratic Zeeman energy— The energy shift due to the quadratic Zeeman Hamiltonian is given by $\Delta E_{Z,\mathrm{quad.}} = \mu_B^2 B^2/(8C_{\mathrm{hfs}})$; see Eq. (2.1). Similar to the above calculation we obtain

$$\Delta E_{Z,\mathrm{quad.}} = \underbrace{\left[\frac{\widetilde{\mu}_B^2}{8\times 10^{17}\,\widetilde{h}^2\,\widetilde{C}_{\mathrm{hfs}}}\right]}_{C_{Z,\mathrm{quad.}}} \widetilde{B}^2\,h\mathrm{Hz}$$

with $\widetilde{C}_{\mathrm{hfs}} \approx 3.4 \times 10^9$ and $C_{Z,\mathrm{quad.}} \approx 72$. Hence, for a magnetic field strength of 1 G we obtain a quadratic Zeeman energy of 72 hHz.

Parameter regimes: Let me now calculate the different energy contributions for some typical experiments with ultracold ^{87}Rb atoms.

Two atoms in a deep optical lattice well— In the spin-dynamics experiments of Widera *et al.* [63] a deep optical lattice was used to confine two atoms at each lattice site. Around the minima, the sites are well approximated by harmonic oscillator potentials. From Eq. (2.24) and the frequencies of Table 2.1, we calculate a spin-independent interaction energy of $E_{\mathrm{int.},0} \approx 3.6\,h$kHz. That is only 0.08 times the level spacing. Thus, we expect that both atoms reside in the Gaussian ground state of the trap which is only slightly deformed by the repulsion between the atoms.

The linear Zeeman energy can be neglected since the z-component of the total spin F_z is conserved. Further, the spatial two-atom ground-state wave function is permutationally symmetric so that the dynamics takes place within the symmetric spin space which is spanned by the two states $|m_{f,1}, m_{f,2}\rangle = |0,0\rangle$ and $(|1,-1\rangle + |-1,1\rangle)/\sqrt{2}$. Moreover, the dynamics of the system depends on the initial state and the ratio of the quadratic Zeeman energy compared to the spin-dependent interaction energy. This ratio can be tuned by the magnetic field and the confinement.

The spin-dependent interaction energy is of the order of $E_{\mathrm{int.},2} \approx -16.6\,h$Hz. This energy has to be compared to the shift of the quadratic Zeeman energy when two spins are flipped: $2\Delta E_{Z,\mathrm{quad.}}$. Both energies are of the same order for a magnetic field strength of approximately 0.34 G since $2\Delta E_{Z,\mathrm{quad.}}(0.34\,\mathrm{G}) \approx 16.6\,h$Hz. Thus, we expect that the interplay of both energy contributions strongly influences the population dynamics of the two atoms around 0.34 G.

Large particle numbers and weak interactions— For both Hamburg experiments [53] we obtain a two-particle interaction energy of $E^{(2)}_{\mathrm{int.},0} \approx 0.5\,h$Hz. That is quite weak compared to the smallest level spacing of the trap, $E^{(2)}_{\mathrm{int.},0}/(\hbar\omega_x) \approx 0.03$ (1D) or ≈ 0.005 (3D). We are therefore in the weakly interacting regime. Of course the N-particle interaction energy grows rapidly with the number of particles $E^{(N)}_{\mathrm{int.},0} \propto N(N-1)/2$ and since the number of particles is typically given by $N = 3\times 10^5$ [51] we obtain for a condensate: $E^{(N)}_{\mathrm{int.},0} \approx 41\,h$GHz. That is quite much compared to the kinetic and potential energy $E_{\mathrm{kin.}} + E_{\mathrm{trap}} = 1/2(16.7+118+690)\,h\mathrm{Hz}\times 3\times 10^5 \approx 0.12\,h$GHz (1D) and thus we expect that the ground-state wave function is substantially deformed to reduce the interaction energy. However, due to the weak two-particle interaction, we can still assume that all the particles reside in the same mean-field orbital.

Few atoms in a quasi-one-dimensional trap— For the quasi-one-dimensional trap of Kinoshita *et al.* [21] we obtain a two-particle interaction of $E_{\mathrm{int.},0} \approx 146\,h$Hz. That is approximately 5.3 times larger than the level spacing of the x-direction but ≈ 500 times smaller than the level spacing of

the transverse y- and z-directions. Thus we expect, on the one hand, that the atoms reside in the ground state of the transverse directions so that we can describe the system by a one-dimensional Schrödinger equation. On the other hand, we expect a substantial deformation of the ground-state wave function with strong correlations between the particles along the axial direction.

2.3 Exact diagonalization and second quantization

Exact diagonalization: The exact diagonalization method is usually used to calculate the low-energy eigenspectrum and eigenfunctions of a time-independent Hamiltonian. The evolution of a wave function $|\psi(t)\rangle$ is determined by the time-dependent Schrödinger equation

$$\mathrm{i}\hbar\frac{d}{dt}|\psi(t)\rangle = H(t)|\psi(t)\rangle.$$

In the case of a time-independent Hamiltonian $H(t) = H$, the energy eigenfunctions change as a function of time only by a complex phase factor $|\psi(t)\rangle = e^{-\mathrm{i}Et/\hbar}|\psi\rangle$. The eigenfunctions $|\psi\rangle$ and eigenenergies E are determined by the stationary Schrödinger equation

$$H|\psi\rangle = E|\psi\rangle. \tag{2.25}$$

In order to solve this eigenvalue problem we choose an arbitrary basis of the Hilbert space $\{|n\rangle, n = 1, 2, \ldots\}$ and project Eq. (2.25) on the individual states $|n\rangle$

$$\langle n|H\sum_{n'}|n'\rangle\langle n'|\psi\rangle = E\langle n|\psi\rangle \quad \text{(for all } n\text{)}.$$

This set of equations can be written in matrix form

$$\begin{pmatrix} H_{11} & H_{12} & H_{13} & \cdots \\ H_{21} & H_{22} & H_{23} & \cdots \\ H_{31} & H_{32} & H_{33} & \cdots \\ \vdots & \vdots & \vdots & \ddots \end{pmatrix} \begin{pmatrix} c_1 \\ c_2 \\ c_3 \\ \vdots \end{pmatrix} = E \begin{pmatrix} c_1 \\ c_2 \\ c_3 \\ \vdots \end{pmatrix} \tag{2.26}$$

with $H_{nn'} \equiv \langle n|H|n'\rangle$ and $c_n \equiv \langle n|\psi\rangle$. The eigenenergies of the stationary Schrödinger equation (2.25) are given by the eigenvalues of the Hamiltonian matrix $(H_{nn'})$ and correspondingly the eigenfunctions $|\psi\rangle$ are determined from the eigenvectors $(c_1, c_2, \ldots)$ of Eq. (2.26) by $|\psi\rangle = \sum_n c_n|n\rangle$. In the case of a complete basis $\{|n\rangle\}$ the result is exact.

We diagonalize the Hamiltonian matrix $(H_{nn'})$ numerically by using efficient algorithms (ARPACK, NAG). The dimension of the Hilbert space of our problem is infinite but we must restrict the basis $\{|n\rangle\}$ to a finite number due to CPU and memory limitations resulting in deviations between the real and the numerically obtained eigenenergies and eigenfunctions. The accuracy of our calculations depends on a 'good choice' of basis functions $|n\rangle$ and their number. Our main task is to generate the basis and to calculate the Hamiltonian matrix $(H_{nn'})$ and, afterwards, to calculate the desired observables from the given coefficients of the eigenvectors.

Second quantization: When dealing with many particles it is a rather cumbersome task to construct permutationally symmetric or antisymmetric wave functions and to calculate matrix elements of some operators by using these wave functions. Second quantization is an efficient tool to calculate these matrix elements. Here, I will give a brief description of the method for bosons.

In second quantization bosonic many-particle wave functions are represented by number states $|n_1, n_2, \ldots\rangle$, where n_i is the number of bosons which occupy the ith single-particle basis state.

All many-particle operators can be expressed by means of creation and annihilation operators $a_i^\dagger$ and a_i. These operators act as follows on the occupation number states

$$a_i^\dagger|\ldots,n_i,\ldots\rangle=\sqrt{n_i+1}|\ldots,n_i+1,\ldots\rangle,\quad a_i|\ldots,n_i,\ldots\rangle=\sqrt{n_i}|\ldots,n_i-1,\ldots\rangle, \tag{2.27}$$

and they obey the commutation relations

$$\left[a_i,a_j^\dagger\right]=\delta_{ij},\qquad \left[a_i,a_j\right]=0,\qquad \text{and}\qquad \left[a_i^\dagger,a_j^\dagger\right]=0\,.$$

One important class of many-particle operators, such as the density operator, can be written as a sum of single-particle operators $\sum_\nu f^\nu$. Such an operator is translated into second quantization by the prescription

$$\sum_\nu f^\nu=\sum_{ij}\langle i|f|j\rangle a_i^\dagger a_j\,. \tag{2.28}$$

A second class of operators, such as the interaction operator, is a double sum of two-particle operators $\sum_{\mu<\nu} g^{\mu\nu}$. These operators are constructed by the prescription:

$$\sum_{\mu<\nu} g^{\mu\nu}=\frac{1}{2}\sum_{ijkl}\langle ij|g|kl\rangle a_i^\dagger a_j^\dagger a_k a_l\,. \tag{2.29}$$

An introduction into second quantization is given in the book of Gordon Baym [79] and a derivation of formula (2.28) is presented in the book of Eugen Fick [80]. [6]

2.4 Single-particle basis

The first step of an exact diagonalization is to choose a proper basis. I have decided for the energy eigenfunctions of the noninteracting bosons. Thus, the number states $|n_1,n_2,\ldots\rangle$ represent permutationally symmetric energy eigenstates of noninteracting bosons with n_i bosons occupying the ith energy eigenstate of the single-particle problem. Here, I determine the energy eigenvalues and eigenfunctions of one particle since they occur in the matrix elements $\langle i|f|j\rangle$ and $\langle ij|g|kl\rangle$ of Eqs. (2.28) and (2.29). In the case of one particle Eq. (2.5) becomes

$$H=\left[-\frac{\hbar^2}{2m}\Delta+\frac{1}{2}m\Big(\omega_x^2x^2+\omega_y^2y^2+\omega_z^2z^2\Big)\right]\otimes\mathbb{1}-\frac{\mu_B B}{2}f_z-\frac{\mu_B^2B^2}{2C_{\text{hfs}}}\left(\mathbb{1}-\frac{1}{4}f_z^2\right).$$

The energy spectrum of H is given by

$$E=\left(n_x+\frac{1}{2}\right)\hbar\omega_x+\left(n_y+\frac{1}{2}\right)\hbar\omega_y+\left(n_z+\frac{1}{2}\right)\hbar\omega_z-\frac{\mu_B B}{2}\alpha-\frac{\mu_B^2B^2}{2C_{\text{hfs}}}\left(1-\frac{1}{4}\alpha^2\right) \tag{2.30}$$

with $n_x,n_y,n_z=0,1,2,\ldots$ and $\alpha=0,\pm1$. The corresponding eigenfunctions are given by

$$\psi_{n\alpha}(\vec{r})=\psi_{n_x}(x)\psi_{n_y}(y)\psi_{n_z}(z)|\alpha\rangle$$

[6] The general formula of a two-particle operator, which is valid for bosons and fermions, is given by $\sum_{\mu<\nu} g^{\mu\nu}=1/2\sum_{ijkl}\langle ij|g|kl\rangle a_i^\dagger a_j^\dagger a_l a_k$, i. e., the annihilation operators a_k and a_l occur in reversed order. This is equal to Eq. (2.29) for bosons since a_k and a_l commute. But for fermions both equations are not equal since the fermionic annihilation operators anticommute.

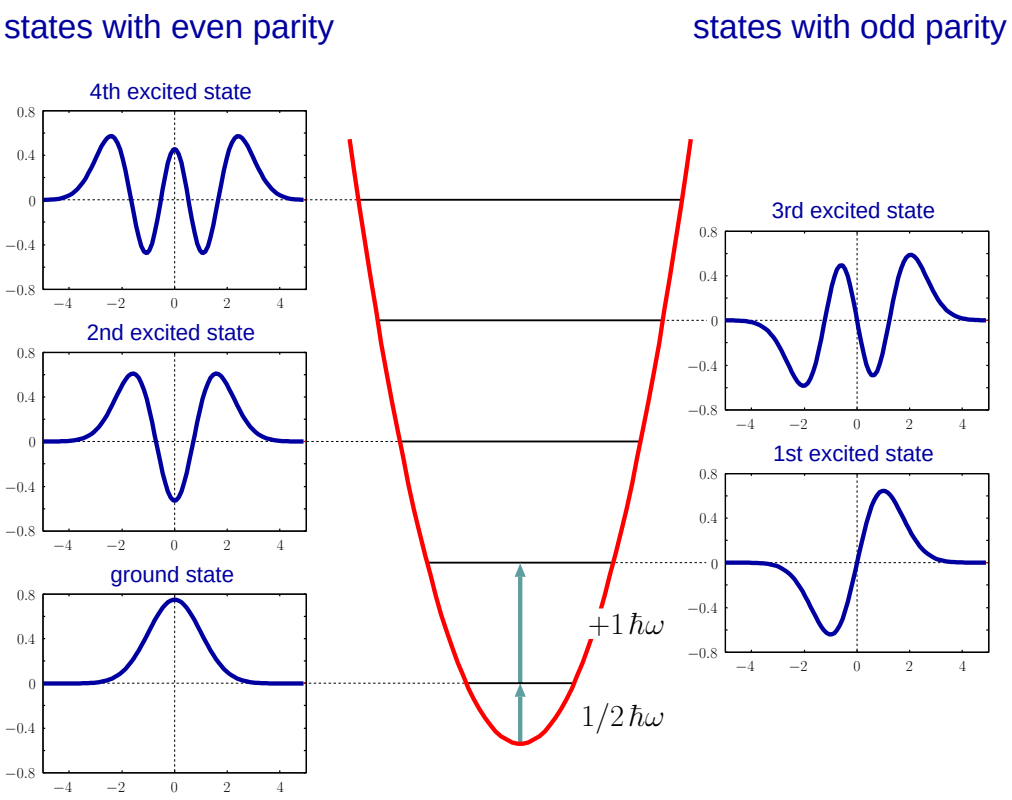

Figure 2.3: Energy spectrum and eigenfunctions of the one-dimensional harmonic oscillator.

where $n = (n_x, n_y, n_z)$ is a multi-index, $\psi_{n_u}(u)$ $(u = x, y, z)$ are the eigenfunctions of the one-dimensional harmonic oscillator and $|\alpha\rangle = |f = 1, m_f = \alpha\rangle$ $(\alpha = 0, \pm 1)$ are the eigenfunctions of $\vec{f}^{\,2} = 2\mathbb{1}$ and f_z. The wave functions $\psi_{n_u}(u)$ are given by

$$\psi_{n_u}(u) = \frac{1}{\sqrt{l_u \, 2^{n_u} \, n_u! \, \sqrt{\pi}}} H_{n_u}(u/l_u) e^{-\frac{1}{2}(u/l_u)^2}$$

where $l_u = \sqrt{\hbar/(m\omega_u)}$ is the oscillator length of the u-direction and

$$H_{n_u}(u/l_u) = \sum_{s=0}^{\lfloor n_u/2 \rfloor} (-1)^s \frac{n_u!}{(n_u - 2s)! \, s!} (2\,u/l_u)^{n_u - 2s}$$

are the Hermite polynomials. $\lfloor x \rfloor$ is the largest integer smaller than x. The eigenfunctions of the one-dimensional harmonic oscillator have a well-defined parity

$$\Pi_u \psi_{n_u}(u) = \psi_{n_u}(-u) = (-1)^{n_u} \psi_{n_u}(u) \, .$$

The energy spectrum and the lowest harmonic oscillator eigenfunctions are visualized in Fig. 2.3.

2.5 Generation of the many-particle basis

In the following chapters we want to study the low-energy properties of the system. We assume here that the low-energy eigenfunctions of the interacting system can be accurately represented by

a superposition of low-energy basis functions of the noninteracting system. [7] Therefore, we construct all the basis functions of the noninteracting system below a certain energy cutoff. Moreover, we make use of the conserved quantities, namely the parities Π_x, Π_y and Π_z, and the z-component of the total spin F_z. The parities Π_x, Π_y and Π_z of a many-particle state are given by

$$\Pi_u|N\rangle = \prod_{(i\alpha)}\Big[(-1)^{n_{ui}}\Big]^{N_{i\alpha}}|N\rangle \qquad (u = x, y, z) \tag{2.31}$$

with $|N\rangle = |\ldots;(N_{i\alpha} : n_{xi}, n_{yi}, n_{zi}, \alpha);\ldots\rangle$. In this notation $N_{i\alpha}$ particles occupy the single-particle state $|n_{xi}, n_{yi}, n_{zi}, \alpha\rangle$. I have developed the following recursive construction scheme for the many-particle basis states:

Given a magnetization $F_z = M$, we construct the noninteracting ground state $|(N-M:0,0,0,0);(M:0,0,0,1)\rangle$ with $N-M$ particles in state $|n_x, n_y, n_z, \alpha\rangle = |0,0,0,0\rangle$ and M particles in state $|0,0,0,1\rangle$, i. e., all the particles reside in the motional ground state $|n_x, n_y, n_z\rangle = |0,0,0\rangle$, $N-M$ particles have spin $|\alpha\rangle = |0\rangle$ and M particles have spin $|\alpha\rangle = |1\rangle$ to achieve a magnetization of M. [8] We have put as many as possible particles into the $|\alpha\rangle = |0\rangle$ spin state since it has the lowest quadratic Zeeman energy. We have 4 possibilities to construct excited states, based on this ground state, by adding the energy differences $\Delta E_x = \hbar\omega_x$, $\Delta E_y = \hbar\omega_y$, $\Delta E_z = \hbar\omega_z$ and $2\Delta E_{Z,\text{quad.}}$:

$$\begin{aligned}
&|(N-M-1:0,0,0,0);(M:0,0,0,1);(1:1,0,0,0)\rangle && (+\Delta E_x)\\
&|(N-M-1:0,0,0,0);(M:0,0,0,1);(1:0,1,0,0)\rangle && (+\Delta E_y)\\
&|(N-M-1:0,0,0,0);(M:0,0,0,1);(1:0,0,1,0)\rangle && (+\Delta E_z)\\
&|(N-M-2:0,0,0,0);(M+1:0,0,0,1);(1:0,0,0,-1)\rangle && (+2\Delta E_{Z,\text{quad.}}).
\end{aligned}$$

In the first three states we have occupied the first excited state of the x-, y- and z-direction by one particle and in the fourth state we have taken 2 particles out of the spin state $|\alpha\rangle = |0\rangle$ and put them into the spin states $|\alpha\rangle = |1\rangle$ and $|\alpha\rangle = |-1\rangle$. By comparing the energies of these 4 states we find the first excited state of the many-particle basis. We choose this state and discard the remaining three states. Similarly, we find the second excited state(s) of the many-particle basis by adding excitations to the first excited state. We repeat the procedure until we have found all the basis functions below a certain energy cutoff.

The recursion generates only states with the same magnetization M since the z-component of the total spin F_z is conserved during the process $2\times|0\rangle \rightarrow |1\rangle + |-1\rangle$. Finally, we select all the many-particle states with the same parities $(\Pi_x, \Pi_y, \Pi_z) = (1,1,1), (\text{–}1,1,1), \ldots$ (there are $2^3 = 8$ possibilities) and save them in the corresponding files.

Often we already know at the beginning that the system will be two- (if $\omega_x, \omega_y \ll \omega_z$), one- (if $\omega_x \ll \omega_y, \omega_z$) ore zero-dimensional (if the two-particle interaction is much smaller than the level spacing of the trap). Then, we allow only for the excitations $(\Delta E_x, \Delta E_y, 2\Delta E_{Z,\text{quad.}})$ if the system is two-dimensional, $(\Delta E_x, 2\Delta E_{Z,\text{quad.}})$ if the system is one-dimensional or $2\Delta E_{Z,\text{quad.}}$ if the system is zero-dimensional.

On the one hand, the described construction scheme is quite flexible, but, on the other hand, it is rather time consuming — especially in the three-dimensional case — due to the many comparisons of energies. It turned out to be better to generate in a first step the spinless many-particle wave functions $|\ldots;(N_{i\alpha} : n_{xi}, n_{yi}, n_{zi});\ldots\rangle$ and in a second step all the possible spinful many-particle wave functions from a given spinless one. Such a recursion has been implemented by Kim

[7] We test the validity of this assumption later in Sec. 2.9.

[8] For $M < 0$ we construct the ground state $|(N-M:0,0,0,0);(M:0,0,0,-1)\rangle$.

Plassmeier [81] and I used his program lately during my Ph.D. thesis. Furthermore, I applied my program almost exclusively to one-dimensional trapping geometries and in this case we do not need to compare energies since all the newly generated (spinless) states have the same energy:

$$|N:n_x=0\rangle \overset{+\Delta E_x}{\longrightarrow} |(N-1:0);(1:1)\rangle \overset{+\Delta E_x}{\longrightarrow}$$
$$|(N-1:0);(1:2)\rangle \text{ and } |(N-2:0);(2:1)\rangle \overset{+\Delta E_x}{\longrightarrow}$$
$$|(N-1:0);(1:3)\rangle,\ |(N-2:0);(1:1);(1:2)\rangle \text{ and } |(N-3:0);(3:1)\rangle \overset{+\Delta E_x}{\longrightarrow} \dots .$$

However, I hopefully demonstrated that it is possible to construct recursively all the many-particle basis states below a certain energy cutoff with well-defined magnetization and parities.

2.6 Calculation of the Hamiltonian matrix

In this section I will calculate the matrix elements of the many-particle Hamiltonian (2.5). I have chosen the permutationally symmetric eigenfunctions of the noninteracting Hamiltonian as basis states. First, I introduce an alternative notation for the occupation number states

$$|\dots;(N_{i\alpha}:n_{xi},n_{yi},n_{zi},\alpha);\dots\rangle \quad \overset{\text{new notation}}{\longrightarrow} \quad |\dots,N_{i\alpha},\dots\rangle \tag{2.32}$$

where $i=(n_{xi},n_{yi},n_{zi})$ is a multi-index. Here, each position within the occupation number state corresponds to a single-particle state $|n_{xi},n_{yi},n_{zi},\alpha\rangle$. These states shall represent the bosonic eigenfunctions of the noninteracting Hamiltonian.

The Hamiltonian (2.5) consists of two parts: $H=H_0+V_{\text{int.}}$. The first part H_0 is the Hamiltonian of the noninteracting system and the second part $V_{\text{int.}}$ is the interaction Hamiltonian. H_0 is already diagonal in the chosen representation but $V_{\text{int.}}$ is non-diagonal.

First I will calculate the **Hamiltonian of the noninteracting system** which is given by

$$\begin{aligned} H_0 = &\sum_{i=1}^{N}\left[-\frac{\hbar^2}{2m}\Delta_i+\frac{1}{2}m\Big(\omega_x^2x_i^2+\omega_y^2y_i^2+\omega_z^2z_i^2\Big)\right]\otimes\mathbb{1}^{\otimes N}\\ &-\sum_{i=1}^{N}\left[\frac{\mu_B B}{2}f_{z,i}+\frac{\mu_B^2B^2}{2C_{\text{hfs}}}\left(\mathbb{1}^{\otimes N}-\frac{1}{4}f_{z,i}^2\right)\right]. \end{aligned} \tag{2.33}$$

H_0 is a single-particle operator. According to Eq. (2.28) we obtain its second-quantized form [9]

$$\begin{aligned} H_0 = \sum_{(i\alpha)(j\beta)}\langle i\alpha|\Bigg[&-\frac{\hbar^2}{2m}\Delta\otimes\mathbb{1}+\frac{1}{2}m\Big(\omega_x^2x^2+\omega_y^2y^2+\omega_z^2z^2\Big)\otimes\mathbb{1}\\ &-\frac{\mu_B B}{2}f_z-\frac{\mu_B^2B^2}{2C_{\text{hfs}}}\left(\mathbb{1}-\frac{1}{4}f_z^2\right)\Bigg]|j\beta\rangle a_{i\alpha}^\dagger a_{j\beta}\,. \end{aligned} \tag{2.34}$$

[9] My notation is a little bit inconsistent: The indices $i,j=1,2,\dots,N$ in the first-quantized operators (2.33) and (2.36) are simple numbers. By contrast, in the second-quantized operators (2.34), (2.37) and in the occupation number states (2.32) $i=(n_{xi},n_{yi},n_{zi})$, $j=(n_{xj},n_{yj},n_{zj})$, $k=(n_{xk},n_{yk},n_{zk})$ and $l=(n_{xl},n_{yl},n_{zl})$ symbolize multi-indices.

Using Eq. (2.30) and the orthonormality of the single-particle basis $\langle i\alpha|j\beta\rangle = \delta_{ij}\delta_{\alpha\beta}$ we obtain

$$H_0 = \sum_{(i\alpha)} \Bigg[\left(n_{xi} + \frac{1}{2}\right)\hbar\omega_x + \left(n_{yi} + \frac{1}{2}\right)\hbar\omega_y + \left(n_{zi} + \frac{1}{2}\right)\hbar\omega_z - \frac{\mu_B B}{2}\alpha - \frac{\mu_B^2 B^2}{2C_{\text{hfs}}}\left(1 - \frac{1}{4}\alpha^2\right)\Bigg] a_{i\alpha}^\dagger a_{i\alpha}\,.$$

Now we multiply from left with the conjugate transpose of $|N\rangle = |\ldots, N_{i\alpha}, \ldots\rangle$ and from right with $|N'\rangle = |\ldots, N'_{i\alpha}, \ldots\rangle$, use Eqs. (2.27), the orthonormality of the occupation number states $\langle N|N'\rangle = \delta_{NN'}$ and obtain the matrix elements

$$\langle N|H_0|N'\rangle = \delta_{NN'} \sum_{(i\alpha)} N_{i\alpha} \Bigg[\left(n_{xi} + \frac{1}{2}\right)\hbar\omega_x + \left(n_{yi} + \frac{1}{2}\right)\hbar\omega_y + \left(n_{zi} + \frac{1}{2}\right)\hbar\omega_z - \frac{\mu_B B}{2}\alpha - \frac{\mu_B^2 B^2}{2C_{\text{hfs}}}\left(1 - \frac{1}{4}\alpha^2\right)\Bigg]. \tag{2.35}$$

Next, we calculate the matrix elements of the **Interaction Hamiltonian** which is given by

$$V_{\text{int.}} = \sum_{i<j} \delta(\vec{r}_i - \vec{r}_j)\left(g_0 \mathbb{1}^{\otimes N} + g_2 \vec{f}_i \cdot \vec{f}_j\right). \tag{2.36}$$

$V_{\text{int.}}$ is a two-particle operator. According to Eq. (2.29) we obtain the second-quantized form

$$V_{\text{int.}} = \frac{1}{2} \sum_{\substack{(i\alpha)(j\beta)\\(k\gamma)(l\delta)}} \langle ij|\delta(\vec{r}_1 - \vec{r}_2)|kl\rangle \,\langle \alpha\beta|\left(g_0 \mathbb{1}^{\otimes 2} + g_2 \vec{f}_1 \cdot \vec{f}_2\right)|\gamma\delta\rangle \; a_{i\alpha}^\dagger a_{j\beta}^\dagger a_{k\gamma} a_{l\delta}\,. \tag{2.37}$$

We introduce the abbreviations

$$I_{ijkl} = \langle ij|\delta(\vec{r}_1 - \vec{r}_2)|kl\rangle = \int d\vec{r}_1 d\vec{r}_2\, \delta(\vec{r}_1 - \vec{r}_2)\langle ij|\vec{r}_1\vec{r}_2\rangle\langle \vec{r}_1\vec{r}_2|kl\rangle = \int d\vec{r}\,\psi_i(\vec{r})\psi_j(\vec{r})\psi_k(\vec{r})\psi_l(\vec{r})$$

for the interaction integrals and

$$g_{\alpha\beta\gamma\delta} = \langle \alpha\beta|\left(g_0 \mathbb{1}^{\otimes 2} + g_2 \vec{f}_1 \cdot \vec{f}_2\right)|\gamma\delta\rangle$$

for the interaction-strength matrix. Next, we multiply from left with the conjugate transpose of $|N\rangle = |\ldots, N_{i\alpha}, \ldots\rangle$, from right with $|N'\rangle = |\ldots, N'_{i\alpha}, \ldots\rangle$ and obtain the matrix elements

$$\langle N|V_{\text{int.}}|N'\rangle = \frac{1}{2} \sum_{\substack{(i\alpha)(j\beta)\\(k\gamma)(l\delta)}} g_{\alpha\beta\gamma\delta}\, I_{ijkl}\, \langle N|a_{i\alpha}^\dagger a_{j\beta}^\dagger a_{k\gamma} a_{l\delta}|N'\rangle\,.$$

These matrix elements have been calculated in my diploma thesis [1] using Eqs. (2.27) and the orthonormality of the occupation number states $\langle N|N'\rangle = \delta_{NN'}$. Here, I give only the results for completeness:

Six different bra-ket combinations can be distinguished which lead to nonzero matrix elements $\langle N|V_{\text{int.}}|N'\rangle$. In the **first case**, bra and ket are equal $|N\rangle = |N'\rangle$ and we obtain for the diagonal elements of the interaction matrix

$$\langle N|V_{\text{int.}}|N\rangle = \sum_{(i\alpha)} \frac{1}{2} g_{\alpha\alpha\alpha\alpha} I_{iiii} N_{i\alpha}(N_{i\alpha}-1) + \sum_{(i\alpha)<(j\beta)} 2 g_{\alpha\beta\alpha\beta} I_{ijij} N_{i\alpha} N_{j\beta}\,.$$

In the first term, we sum over all occupied positions within the number state $|\ldots, N_{i\alpha}, \ldots\rangle$. The second term is a double sum. The outer sum runs over all occupied positions within the number state $|\ldots, N_{i\alpha}, \ldots\rangle$ and the inner sum runs over all occupied positions to the right of position $(i\alpha)$, i. e., over all states $|\ldots, N_{i\alpha}, \ldots, N_{j\beta}, \ldots\rangle$.

In the **second case**, bra and ket differ at two positions by two particles. We obtain

$$\langle ..., N_{p\epsilon}, ..., N_{q\epsilon}, ...|V_{\text{int.}}|..., N_{p\epsilon}+2, ..., N_{q\epsilon}-2, ...\rangle = \frac{1}{2} g_{\epsilon\epsilon\epsilon\epsilon} I_{qqpp} \sqrt{(N_{p\epsilon}+2)(N_{p\epsilon}+1)N_{q\epsilon}(N_{q\epsilon}-1)}\,.$$

In the **third case**, bra and ket differ at two positions by one particle

$$\begin{aligned}&\langle ..., N_{p\epsilon}, ..., N_{q\epsilon}, ...|V_{\text{int.}}|..., N_{p\epsilon}+1, ..., N_{q\epsilon}-1, ...\rangle = \\ &\sum_{(i\alpha)\neq(p\epsilon),(q\epsilon)} 2 g_{\epsilon\alpha\epsilon\alpha} I_{qipi} \sqrt{N_{q\epsilon}(N_{p\epsilon}+1)} N_{i\alpha} \\ &+ g_{\epsilon\epsilon\epsilon\epsilon} I_{qqpq} \sqrt{N_{q\epsilon}(N_{p\epsilon}+1)}(N_{q\epsilon}-1) + g_{\epsilon\epsilon\epsilon\epsilon} I_{qppp} \sqrt{N_{q\epsilon}(N_{p\epsilon}+1)} N_{p\epsilon}\,.\end{aligned}$$

In the **fourth case**, one single-particle state of the ket is occupied with two more and two states of the ket are occupied with one less particle than in the bra

$$\begin{aligned}&\langle ..., N_{p\epsilon}, ..., N_{q\sigma}, ..., N_{s\phi}, ...|V_{\text{int.}}|..., N_{p\epsilon}+2, ..., N_{q\sigma}-1, ..., N_{s\phi}-1, ...\rangle \\ &= g_{\sigma\phi\epsilon\epsilon} I_{qspp} \sqrt{(N_{p\epsilon}+2)(N_{p\epsilon}+1)N_{q\sigma}N_{s\phi}}\,.\end{aligned}$$

In the **fifth case**, one single-particle state of the ket is occupied with two less and two states of the ket are occupied with one more particle than in the bra

$$\begin{aligned}&\langle ..., N_{p\epsilon}, ..., N_{q\sigma}, ..., N_{s\phi}, ...|V_{\text{int.}}|..., N_{p\epsilon}-2, ..., N_{q\sigma}+1, ..., N_{s\phi}+1, ...\rangle \\ &= g_{\epsilon\epsilon\sigma\phi} I_{ppqs} \sqrt{(N_{s\phi}+1)(N_{q\sigma}+1)(N_{p\epsilon}-1)N_{p\epsilon}}\,.\end{aligned}$$

Finally, in the **sixth case**, two states of the ket are occupied with one more and two states of the

ket are occupied with one less particle than in the bra

$$\langle ..., N_{p\epsilon}, ..., N_{q\sigma}, ..., N_{s\phi}, ..., N_{t\omega}, ... | V_{\text{int.}} | ..., N_{p\epsilon}+1, ..., N_{q\sigma}+1, ..., N_{s\phi}-1, ..., N_{t\omega}-1, ... \rangle$$
$$= 2 g_{\phi\omega\epsilon\sigma} I_{stpq} \sqrt{N_{s\phi} N_{t\omega} (N_{p\epsilon}+1)(N_{q\sigma}+1)}\,.$$

Recursive calculation of the interaction integrals: As has been shown in Sec. 2.2, the interaction integrals have dimension $1/(l_x l_y l_z)$ and they decompose into a product of three one-dimensional integrals for each direction

$$I_{ijkl} = \frac{1}{l_x l_y l_z} \widetilde{I}_{(n_{xi}, n_{xj}, n_{xk}, n_{xl})} \widetilde{I}_{(n_{yi}, n_{yj}, n_{yk}, n_{yl})} \widetilde{I}_{(n_{zi}, n_{zj}, n_{zk}, n_{zl})}\,.$$

Therefore, we have to determine the values of one-dimensional integrals of the form

$$\widetilde{I}_{ijkl} = \int_{-\infty}^{+\infty} dx\, \psi_i(x) \psi_j(x) \psi_k(x) \psi_l(x)$$

where the indices $i, j, k, l = 0, 1, 2, \ldots$ are simple numbers during the further discussion and where $\psi_i(x)$ are oscillator functions. In the beginning I performed a numerical integration by means of a NAG library routine (a Gaussian quadrature) which was especially suitable for these kinds of integrands consisting of polynomials which decay like e^{-ax^2} at $\pm\infty$. Later, however, Georg Deuretzbacher [82] gave me the following nice recursion formula

$$\widetilde{I}_{ijkl} = \frac{1}{2}\left[-\sqrt{\frac{i-1}{i}} \widetilde{I}_{(i-2)jkl} + \sqrt{\frac{j}{i}} \widetilde{I}_{(i-1)(j-1)kl} + \sqrt{\frac{k}{i}} \widetilde{I}_{(i-1)j(k-1)l} + \sqrt{\frac{l}{i}} \widetilde{I}_{(i-1)jk(l-1)} \right]$$

which is based on an integration by parts and two recurrence relations for the Hermite polynomials. Using this formula one can trace back each integral to the basic integral $\widetilde{I}_{0000} = 1/\sqrt{2\pi}$.

Derivation of the recursion formula— The one-dimensional interaction integrals can be written as

$$\widetilde{I}_{ijkl} = C_{ijkl} \int_{-\infty}^{+\infty} dx\, H_i(x) H_j(x) H_k(x) H_l(x) e^{-2x^2}$$

with

$$C_{ijkl} = \frac{1}{\pi \sqrt{2^{i+j+k+l} i! j! k! l!}}\,.$$

Using

$$H_i(x) = 2x H_{i-1}(x) - 2(i-1) H_{i-2}(x) \tag{2.38}$$

we obtain

$$\widetilde{I}_{ijkl} = \underbrace{C_{ijkl} \int_{-\infty}^{+\infty} dx\, 2x H_{i-1} H_j H_k H_l e^{-2x^2}}_{=\widetilde{I}^*_{ijkl}} - 2(i-1) C_{ijkl} \int_{-\infty}^{+\infty} dx\, H_{i-2} H_j H_k H_l e^{-2x^2}.$$

We use $\left(e^{-2x^2}\right)' = -4xe^{-2x^2}$ and integrate by parts:

$$\begin{aligned}\widetilde{I}^*_{ijkl} &= -\frac{1}{2}C_{ijkl}\int_{-\infty}^{+\infty} dx H_{i-1}H_jH_kH_l\frac{d}{dx}e^{-2x^2} \\ &= \cancel{-\frac{1}{2}C_{ijkl}H_iH_jH_kH_{l-1}e^{-2x^2}\Big|_{-\infty}^{+\infty}} + \frac{1}{2}C_{ijkl}\int_{-\infty}^{+\infty} dx\frac{d}{dx}\big(H_{i-1}H_jH_kH_l\big)e^{-2x^2}.\end{aligned}$$

Now we use

$$H'_n = 2nH_{n-1}$$

and obtain

$$\begin{aligned}\widetilde{I}^*_{ijkl} = (i-1)C_{ijkl}\int_{-\infty}^{+\infty} dx H_{i-2}H_jH_kH_le^{-2x^2} + j\,C_{ijkl}\int_{-\infty}^{+\infty} dx H_{i-1}H_{j-1}H_kH_le^{-2x^2} \\ +k\,C_{ijkl}\int_{-\infty}^{+\infty} dx H_{i-1}H_jH_{k-1}H_le^{-2x^2} + l\,C_{ijkl}\int_{-\infty}^{+\infty} dx H_{i-1}H_jH_kH_{l-1}e^{-2x^2}.\end{aligned}$$

It follows that

$$\begin{aligned}\widetilde{I}_{ijkl} = -(i-1)C_{ijkl}\int_{-\infty}^{+\infty} dx H_{i-2}H_jH_kH_le^{-2x^2} + j\,C_{ijkl}\int_{-\infty}^{+\infty} dx H_{i-1}H_{j-1}H_kH_le^{-2x^2} \\ +k\,C_{ijkl}\int_{-\infty}^{+\infty} dx H_{i-1}H_jH_{k-1}H_le^{-2x^2} + l\,C_{ijkl}\int_{-\infty}^{+\infty} dx H_{i-1}H_jH_kH_{l-1}e^{-2x^2}.\end{aligned}$$

Now we transform the coefficients:

$$\begin{aligned}(i-1)C_{ijkl} &= (i-1)\frac{1}{\pi\sqrt{4\cdot 2^{(i-2)+j+k+l}i(i-1)(i-2)!j!k!l!}} = \frac{1}{2}\sqrt{\frac{i-1}{i}}C_{(i-2)jkl} \\ j\,C_{ijkl} &= j\frac{1}{\pi\sqrt{4\cdot 2^{(i-1)+(j-1)+k+l}i\,j\,(i-1)!(j-1)!k!l!}} = \frac{1}{2}\sqrt{\frac{j}{i}}C_{(i-1)(j-1)kl}\end{aligned}$$

and obtain the final form of the recursion.

Building up of an integral table— Based on the recursion formula I have built up an integral table starting from the basic integral $\widetilde{I}_{0000} = 1/\sqrt{2\pi}$. All the integrals of level $L = i+j+k+l$ are obtained from the integrals of the preceding level $L-2$. Only the normal-ordered integrals with $i \geqslant j \geqslant k \geqslant l$ are saved since all the integrals, obtained by rearranging a given set of indices, are equal. The second level $L = 2$, for example, consists of the two normal-ordered integrals $\widetilde{I}_{2000}$ and $\widetilde{I}_{1100}$ which are calculated according to

$$\widetilde{I}_{2000} = -\frac{1}{2\cdot\sqrt{2}}\widetilde{I}_{0000} = -\frac{1}{4\sqrt{\pi}} \qquad \text{and} \qquad \widetilde{I}_{1100} = \frac{1}{2}\widetilde{I}_{0000} = \frac{1}{\sqrt{2}^3\sqrt{\pi}}\,.$$

All the integrals of the next level $L = 4$, namely $\widetilde{I}_{4000}$, $\widetilde{I}_{3100}$, $\widetilde{I}_{2200}$ and $\widetilde{I}_{1111}$ are superpositions of these two integrals of level $L = 2$ and so forth. Therefore, the task is to construct a chain of integrals as follows: First, the indices of level $L+2$ have to be generated from the indices of level L and then the corresponding integrals have to be calculated using the recursion. In order to accelerate the read out of the integral table, each level L is directly accessed. [10]

[10] The recursion is fairly stable: I have computed interaction integrals up to level $L = 600$ by means of the recursion and checked the accuracy by means of MATHEMATICA. For $\widetilde{I}_{150,150,150,150}$ I found a relative deviation of only 3×10^{-8}.

Calculation of the interaction-strength matrix: In order to calculate the interaction-strength matrix $g_{\alpha\beta\gamma\delta}$ we use formulas which are similar to Eqs. (2.9) and (2.10):

$$\vec{f_1}\cdot\vec{f_2} = f_z\otimes f_z + \frac{1}{2}\left(f_+\otimes f_- + f_-\otimes f_+\right)$$

and

$$f_\pm|\alpha\rangle = \sqrt{2}|\alpha\pm 1\rangle\,.$$

It follows that

$$\vec{f_1}\cdot\vec{f_2}|\gamma\delta\rangle = \gamma\delta|\gamma\delta\rangle + |\gamma+1\,\delta-1\rangle + |\gamma-1\,\delta+1\rangle\,.$$

We obtain

$$\begin{aligned} g_{\alpha\beta\gamma\delta} &= \langle\alpha\beta|\Big(g_0\mathbb{1}^{\otimes 2} + g_2\vec{f_1}\cdot\vec{f_2}\Big)|\gamma\delta\rangle \\ &= \Big(g_0+\gamma\delta g_2\Big)\delta_{\alpha\gamma}\delta_{\beta\delta} + g_2\Big(\delta_{\alpha\gamma+1}\delta_{\beta\delta-1}+\delta_{\alpha\gamma-1}\delta_{\beta\delta+1}\Big). \end{aligned} \tag{2.39}$$

Dimensionless Hamiltonian: Let me now derive the coupling constants used for the numerical computation of the Hamiltonian matrix. Within the program I have expressed all energies in units of hHz. As input parameters I have chosen the trap frequencies of each direction f_x, f_y, f_z in Hz, the magnetic field B in mG and the scattering lengths a_0 and a_2 in a_B. In calculations similar to those of Sec. 2.2 we obtain the dimensionless matrix elements of the noninteracting Hamiltonian according to

$$\begin{aligned} \langle N|\widetilde{H}_0|N'\rangle = \delta_{NN'}\sum_{(i\alpha)} N_{i\alpha}\Bigg[&\left(n_{xi}+\frac{1}{2}\right)\widetilde{f}_x + \left(n_{yi}+\frac{1}{2}\right)\widetilde{f}_y + \left(n_{zi}+\frac{1}{2}\right)\widetilde{f}_z \\ &-C^*_{Z,\text{lin.}}\widetilde{B}\alpha - C^*_{Z,\text{quad.}}\widetilde{B}^2\left(1-\frac{1}{4}\alpha^2\right)\Bigg]. \end{aligned}$$

In detail these matrix elements are derived from Eq. (2.35) as follows:

$$\hbar\omega_x = h\,f_x = \widetilde{f}_x\,h\text{Hz} \quad \text{with } f_x = \widetilde{f}_x\,\text{Hz} \qquad \text{(analog for the } y\text{- and } z\text{-direction)}$$

$$\frac{\mu_B B}{2} = \underbrace{\left[\frac{\widetilde{\mu}_B}{2\cdot 10^7\widetilde{h}}\right]}_{=C^*_{Z,\text{lin.}}}\widetilde{B}\,h\text{Hz} \quad\Rightarrow\quad C^*_{Z,\text{lin.}} = \frac{\widetilde{\mu}_B}{2\cdot 10^7\widetilde{h}} \approx 700$$

with $\mu_B = \widetilde{\mu}_B\,\text{J/T}$, $B = \widetilde{B}\,\text{mG}$, $1\,\text{T} = 10^4\,\text{G}$ and $h = \widetilde{h}\,\text{Js}$ (see appendix D for the constants).

$$\frac{\mu_B^2 B^2}{2C_{\text{hfs}}} = \underbrace{\left[\frac{\widetilde{\mu}_B^2}{2\widetilde{C}_{\text{hfs}}\,10^{23}\,\widetilde{h}^2}\right]}_{=C^*_{Z,\text{quad.}}}\widetilde{B}^2\,h\text{Hz} \quad\Rightarrow\quad C^*_{Z,\text{quad.}} = \frac{\widetilde{\mu}_B^2}{2\widetilde{C}_{\text{hfs}}\,10^{23}\,\widetilde{h}^2} \approx 2.866\times 10^{-4}$$

with $C_{\text{hfs}} = \widetilde{C}_{\text{hfs}}\,h\text{Hz}$. Using $\widetilde{H}_0 = H_0/(h\text{Hz})$ we obtain the above dimensionless Hamiltonian. Similarly we calculate the coupling constant of the interaction matrix. The result is given by

$$\langle N|\widetilde{V}_{\text{int.}}|N'\rangle = C^*_{\text{int.}}\sqrt{\widetilde{f}_x\widetilde{f}_y\widetilde{f}_z}\sum_{\substack{(i\alpha)(j\beta)\\(k\gamma)(l\delta)}}\widetilde{g}_{\alpha\beta\gamma\delta}\,\widetilde{I}_{ijkl}\,\langle N|a_i^\dagger a_j^\dagger a_k a_l|N'\rangle\,.$$

Here, we have defined $I_{ijkl} = \widetilde{I}_{ijkl}/(l_x l_y l_z)$ and $g_{\alpha\beta\gamma\delta} = \widetilde{g}_{\alpha\beta\gamma\delta}\left(4\pi\hbar^2 a_B/m\right)$. The coupling constant of the interaction is calculated as follows

$$\frac{1}{2}\frac{4\pi\hbar^2 a_B}{m}\frac{1}{l_x l_y l_z} = \underbrace{\left[\frac{1}{2}\frac{4\pi\widetilde{\hbar}^2\widetilde{a}_B}{\widetilde{m}}\sqrt{\frac{\widetilde{m}^3(2\pi)^3}{\widetilde{\hbar}^3}}\frac{1}{\widetilde{h}}\right]}_{=C^*_{\text{int.}}}\sqrt{\widetilde{f}_x\widetilde{f}_y\widetilde{f}_z}\,h\text{Hz}$$

$$\Rightarrow\; C^*_{\text{int.}} = \frac{1}{2}\frac{4\pi\widetilde{\hbar}^2\widetilde{a}_B}{\widetilde{m}}\sqrt{\frac{\widetilde{m}^3(2\pi)^3}{\widetilde{\hbar}^3}}\frac{1}{\widetilde{h}} \approx 3.083\times 10^{-5}\,.$$

Here, we used $\hbar = \widetilde{\hbar}\,\text{Js}$, $a_B = \widetilde{a}_B\,\text{m}$, $m = \widetilde{m}\,\text{kg}$ $\left(\text{mass of } {}^{87}\text{Rb}\right)$, $l_u = \sqrt{\hbar/(m\omega_u)}$, $\omega_u = 2\pi f_u$ $(u = x, y, z)$ and $h = \widetilde{h}\,\text{Js}$. Again, the interaction Hamiltonian $V_{\text{int.}}$ is related to its dimensionless counterpart according to $V_{\text{int.}} = \widetilde{V}_{\text{int.}}\,h\text{Hz}$.

2.7 Numerical diagonalization of the Hamiltonian matrix

In principle the main work is done when we built up the basis and calculated the Hamiltonian matrix. What remains is to pass the Hamiltonian matrix to an efficient sparse-matrix diagonalization routine. In the beginning I used the NAG library (mark 19). What I especially liked was the excellent documentation of the NAG making it possible (even for a beginner) to implement the diagonalization routines quickly. However, some day Kim Plassmeier realized that MATHEMATICA diagonalizes orders of magnitude faster than the NAG (mark 19) since it uses a newer algorithm of the LAPACK library. Since then I use Kim's implementation [81] of the sparse-matrix diagonalization routine of the LAPACK library. I heared that the newest NAG (mark 21) is considerably faster (since it also uses this new algorithm), however, it was not available at my university.

The results of a numerical diagonalization are the desired number of lowest eigenenergies and eigenvectors, given as an array of coefficients $(\ldots, c_N, \ldots)^T$, which are the desired coefficients of the expansion $|\psi\rangle = \sum_N c_N|N\rangle$. We will need these coefficients later together with the corresponding number states $|N\rangle$ when we want to calculate any further system properties.

2.8 Calculation of system properties

Arbitrary properties of an eigenstate $|\psi\rangle$ are given by the expectation values of the corresponding operators $\langle\psi|\mathcal{O}|\psi\rangle$. Since we know the eigenvector $(\ldots, c_N, \ldots)^T$ such an expectation value is given by

$$\langle\psi|\mathcal{O}|\psi\rangle = \sum_{NN'} c_N c_{N'}\mathcal{O}_{NN'} = \begin{pmatrix}\ldots & c_N & \ldots\end{pmatrix}\begin{pmatrix}\vdots & \\ \cdots & \mathcal{O}_{NN'} & \cdots \\ \vdots & \end{pmatrix}\begin{pmatrix}\vdots \\ c_N \\ \vdots\end{pmatrix} \tag{2.40}$$

with $\mathcal{O}_{NN'} = \langle N|\mathcal{O}|N'\rangle$. Therefore, we are done, when we know the matrix elements of the desired operator. These matrix elements will be calculated in the following for selected operators.

In the numerical implementation we mostly computed the sum of Eq. (2.40) (in the case of the densities, momentum distributions and correlation functions). In other cases, however, it is more efficient to calculate first the matrix $\mathcal{O}_{NN'}$ and to perform matrix-vector multiplications hereafter as shown in Eq. (2.40). This method was used by Kim Plassmeier for the calculation

of the expectation value $\langle \vec{F}^2 \rangle$ [81]. The main advantage of this method is that, once the matrix $\left(\mathcal{O}_{NN'}\right)$ has been calculated, one can quickly compute the expectation values of all the given eigenvectors.

Density: The density is the probability to find one particle at position $\vec{r}$. For one particle it is given by $\psi^2(\vec{r})$. The corresponding one-particle operator is the projection on position $\vec{r}$:

$$|\vec{r}\,\rangle\langle\vec{r}| \otimes \mathbb{1}_{\text{spin}}\,.$$

The matrix elements of the N-particle density are therefore given by

$$\begin{aligned}\langle N|\rho(\vec{r})|N'\rangle &= \sum_{(i\alpha)(j\beta)} \langle i\alpha|\Big[|\vec{r}\,\rangle\langle\vec{r}| \otimes \mathbb{1}_{\text{spin}}\Big]|j\beta\rangle\langle N|a^\dagger_{i\alpha}a_{j\beta}|N'\rangle \\ &= \sum_{(i\alpha)(j\beta)} \delta_{\alpha\beta}\psi_i(\vec{r})\psi_j(\vec{r})\langle N|a^\dagger_{i\alpha}a_{j\beta}|N'\rangle \end{aligned} \tag{2.41}$$

with $\psi_i(\vec{r}) = \psi_{n_{xi}}(x)\psi_{n_{yi}}(y)\psi_{n_{zi}}(z)$. We obtain for the diagonal elements

$$\langle N|\rho(\vec{r})|N\rangle = \sum_{i\alpha} \psi_i^2(\vec{r})N_{i\alpha}\,.$$

Only in one case, when bra and ket differ at two positions by one particle, we obtain nonzero non-diagonal elements which are given by

$$\langle ..., N_{p\epsilon}, ..., N_{q\sigma}, ...|\rho(\vec{r})|..., N_{p\epsilon}+1, ..., N_{q\sigma}-1, ...\rangle = \delta_{\epsilon\sigma}\psi_p(\vec{r})\psi_q(\vec{r})\sqrt{N_{q\sigma}(N_{p\epsilon}+1)}$$

The oscillator functions are computed recursively. Using (2.38) we obtain the recursion formula

$$\psi_n(x) = \sqrt{\frac{2}{n}}\,x\,\psi_{n-1}(x) - \sqrt{\frac{n-1}{n}}\,\psi_{n-2}(x)\,.$$

Spin density: The spin density is the probability to find one particle at position $\vec{r}$ in spin state $|\gamma\rangle$. The corresponding one-particle operator is the projection on state $|\vec{r}\gamma\rangle$:

$$|\vec{r}\gamma\rangle\langle\vec{r}\gamma|\,.$$

The matrix elements of the N-particle spin density are thus given by

$$\langle N|\rho_\gamma(\vec{r})|N'\rangle = \sum_{(i\alpha)(j\beta)} \delta_{\alpha\gamma}\delta_{\beta\gamma}\psi_i(\vec{r})\psi_j(\vec{r})\langle N|a^\dagger_{i\alpha}a_{j\beta}|N'\rangle\,.$$

Kinetic energy of the x-direction: The kinetic energy of one particle along the x-axis is given by

$$-\frac{\hbar^2}{2m}\frac{\partial^2}{\partial x^2} = -\frac{\hbar^2}{2ml_x^2}\frac{\partial^2}{\partial \widetilde{x}^2} = -\frac{\hbar\omega_x}{2}\frac{\partial^2}{\partial \widetilde{x}^2} = -\frac{\widetilde{f}_x}{2}\frac{\partial^2}{\partial \widetilde{x}^2}\,h\text{Hz}\,.$$

We introduce creation and annihilation operators of oscillator quantum numbers

$$b = \frac{1}{\sqrt{2}}\big(\widetilde{x} + \mathbb{i}\,\widetilde{p}_x\big) = \frac{1}{\sqrt{2}}\left(\widetilde{x} + \frac{\partial}{\partial \widetilde{x}}\right), \quad b^\dagger = \frac{1}{\sqrt{2}}\big(\widetilde{x} - \mathbb{i}\,\widetilde{p}_x\big) = \frac{1}{\sqrt{2}}\left(\widetilde{x} - \frac{\partial}{\partial \widetilde{x}}\right)$$

where the dimensionless momentum operator is given by $\widetilde{p}_x = -\mathbb{i}\,\partial/\partial\widetilde{x}$. The action of these operators on the eigenstates of the harmonic oscillator is given by

$$b^\dagger|n_x\rangle = \sqrt{n_x+1}|n_x+1\rangle, \qquad b|n_x\rangle = \sqrt{n_x}|n_x-1\rangle,$$

similar to Eqs. (2.27). We express the position operator $\widetilde{x}$ and the partial derivative $\partial/\partial\widetilde{x}$ by means of these creation and annihilation operators:

$$\widetilde{x} = \frac{1}{\sqrt{2}}\left(b + b^\dagger\right), \quad \frac{\partial}{\partial\widetilde{x}} = \frac{1}{\sqrt{2}}\left(b - b^\dagger\right).$$

We obtain for the kinetic energy

$$-\frac{\hbar^2}{2m}\frac{\partial^2}{\partial x^2} = -\frac{\widetilde{f}_x}{4}\left(b - b^\dagger\right)\left(b - b^\dagger\right) h\text{Hz} = -\frac{\widetilde{f}_x}{4}\left(b^2 - bb^\dagger - b^\dagger b + {b^\dagger}^2\right) h\text{Hz}\,.$$

The one-particle matrix elements of the kinetic energy of the x-direction are therefore given by

$$\langle i\alpha|\left[-\frac{\hbar^2}{2m}\frac{\partial^2}{\partial x^2}\right]|j\beta\rangle = -\frac{\widetilde{f}_x}{4}\, h\text{Hz}\,\delta_{\alpha\beta}\delta_{n_{yi}n_{yj}}\delta_{n_{zi}n_{zj}}$$
$$\times\left[\sqrt{n_{xj}(n_{xj}-1)}\delta_{n_{xi}n_{xj}-2} - \big(2n_{xj}+1\big)\delta_{n_{xi}n_{xj}} + \sqrt{(n_{xj}+1)(n_{xj}+2)}\delta_{n_{xi}n_{xj}+2}\right].$$

Similarly, we obtain for the **potential energy of the x-direction**

$$\langle i\alpha|\left[\frac{1}{2}m\omega_x^2 x^2\right]|j\beta\rangle = \frac{\widetilde{f}_x}{4}\, h\text{Hz}\,\delta_{\alpha\beta}\delta_{n_{yi}n_{yj}}\delta_{n_{zi}n_{zj}}$$
$$\times\left[\sqrt{n_{xj}(n_{xj}-1)}\delta_{n_{xi}n_{xj}-2} + \big(2n_{xj}+1\big)\delta_{n_{xi}n_{xj}} + \sqrt{(n_{xj}+1)(n_{xj}+2)}\delta_{n_{xi}n_{xj}+2}\right].$$

Momentum distribution: The probability to find one particle with momentum $\vec{p}$ is given by

$$|\vec{p}\,\rangle\langle\vec{p}\,| \otimes \mathbb{1}_{\text{spin}}\,.$$

The single-particle matrix element of that operator is given by

$$\langle i\alpha|\Big[|\vec{p}\,\rangle\langle\vec{p}\,| \otimes \mathbb{1}_{\text{spin}}\Big]|j\beta\rangle = \delta_{\alpha\beta}\langle i|\vec{p}\,\rangle\langle\vec{p}\,|j\rangle = \delta_{\alpha\beta}\chi_i^*(\vec{p})\chi_j(\vec{p})$$

with

$$\chi_i(\vec{p}) = \langle\vec{p}\,|i\rangle = \int d\vec{r}\langle\vec{p}\,|\vec{r}\,\rangle\langle\vec{r}\,|i\rangle = \frac{1}{\sqrt{2\pi\hbar}^3}\int d\vec{r}\,\psi_i(\vec{r})e^{-\mathrm{i}\vec{p}\cdot\vec{r}/\hbar}\,.$$

One can show that the Fourier transform of the oscillator functions is given by

$$\chi_n(p_x) = (-\mathbb{i})^n\psi_n(p_x) \tag{2.42}$$

(ψ_n is an oscillator function) and that they obey the recursive relation

$$\chi_n(p_x) = -\sqrt{\frac{2}{n}}\,\mathbb{i}\,p_x\,\chi_{n-1}(p_x) + \sqrt{\frac{n-1}{n}}\,\chi_{n-2}(p_x)\,.$$

Correlation function: The correlation function is the probability to find one particle at position $\vec{r}$ and the other at $\vec{r}\,'$. The corresponding two-particle operator is given by

$$|\vec{r}\,\vec{r}\,'\rangle\langle\vec{r}\,\vec{r}\,'| \otimes \mathbb{1}_{\text{spin}}\,.$$

The two-particle matrix elements of that operator are evaluated according to

$$\langle i\alpha\, j\beta|\Big[|\vec{r}\,\vec{r}\,'\rangle\langle\vec{r}\,\vec{r}\,'| \otimes \mathbb{1}_{\text{spin}}\Big]|k\gamma\, l\delta\rangle = \delta_{\alpha\gamma}\delta_{\beta\delta}\psi_i(\vec{r}\,)\psi_j(\vec{r}\,')\psi_k(\vec{r}\,)\psi_l(\vec{r}\,')\,.$$

The matrix elements of the N-particle correlation function are thus given by

$$\langle N|\rho(\vec{r},\vec{r}\,')|N'\rangle = \frac{1}{2}\sum_{\substack{(i\alpha)(j\beta)\\(k\gamma)(l\delta)}} \delta_{\alpha\gamma}\delta_{\beta\delta}\psi_i(\vec{r})\psi_j(\vec{r}\,')\psi_k(\vec{r})\psi_l(\vec{r}\,')\langle N|a^\dagger_{i\alpha}a^\dagger_{j\beta}a_{k\gamma}a_{l\delta}|N'\rangle\,.$$

These matrix elements are evaluated in a similar way as has been done for the interaction operator. However, take care that the product $\psi_i(\vec{r})\psi_j(\vec{r}\,')\psi_k(\vec{r})\psi_l(\vec{r}\,')$ has different symmetries than the interaction integrals $I_{ijkl} = \int d\vec{r}\,\psi_i(\vec{r})\psi_j(\vec{r})\psi_k(\vec{r})\psi_l(\vec{r})$.

Local correlation function: The local correlation function is the probability to find the two particles at the same position

$$\int d\vec{r}\,|\vec{r}\;\vec{r}\,\rangle\langle\vec{r}\;\vec{r}\,|\otimes\mathbb{1}_{\text{spin}}\,.$$

The N-particle matrix elements of that operator are given by

$$\langle N|\rho_{\text{local corr.}}|N'\rangle = \frac{1}{2}\sum_{\substack{(i\alpha)(j\beta)\\(k\gamma)(l\delta)}} \delta_{\alpha\gamma}\delta_{\beta\delta}I_{ijkl}\langle N|a^\dagger_{i\alpha}a^\dagger_{j\beta}a_{k\gamma}a_{l\delta}|N'\rangle$$

which is the interaction operator when $\delta_{\alpha\gamma}\delta_{\beta\delta}$ is replaced by the interaction-strength matrix $g_{\alpha\beta\gamma\delta}$.

Square of total spin: The operator $\vec{F}^2$ is a sum of a single- and a two-particle operator – like the Hamiltonian of our system. We calculate for two particles

$$\vec{F}^2 = \left(\vec{f}_1+\vec{f}_2\right)^2 = \vec{f}_1^{\,2}+\vec{f}_2^{\,2}+2\vec{f}_1\cdot\vec{f}_2 = 2\mathbb{1}+2\mathbb{1}+2\vec{f}_1\cdot\vec{f}_2\,.$$

Thus, the second-quantized form of that operator is given by

$$\vec{F}^2 = 2\sum_{(i\alpha)(j\beta)}\langle i\alpha|\mathbb{1}|j\beta\rangle a^\dagger_{i\alpha}a_{j\beta} + \sum_{\substack{(i\alpha)(j\beta)\\(k\gamma)(l\delta)}}\langle i\alpha\,j\beta|\vec{f}_1\cdot\vec{f}_2|k\gamma\,l\delta\rangle a^\dagger_{i\alpha}a^\dagger_{j\beta}a_{k\gamma}a_{l\delta}\,.$$

The single-particle matrix element is given by

$$\langle i\alpha|\mathbb{1}|j\beta\rangle = \delta_{ij}\delta_{\alpha\beta}$$

and the two-particle matrix element is given by [see the calculation of the interaction-strength matrix (2.39)]

$$\langle i\alpha\,j\beta|\vec{f}_1\cdot\vec{f}_2|k\gamma\,l\delta\rangle = \delta_{ik}\delta_{jl}\Big(\gamma\delta\,\delta_{\alpha\gamma}\delta_{\beta\delta}+\delta_{\alpha\gamma+1}\delta_{\beta\delta-1}+\delta_{\alpha\gamma-1}\delta_{\beta\delta+1}\Big).$$

The $\vec{F}^2$ operator has been implemented by Kim Plassmeier [81].

2.9 Testing / convergence

Since one can make mistakes in every step of an exact diagonalization, we need tests to check our results. We are here in the fortunate situation that there are many nontrivial testing cases available.

Comparison with the Tonks-Girardeau gas: One-dimensional spinless bosons with infinite δ repulsion behave in many respects like noninteracting fermions since the exact ground-state wave function is given by the absolute value of the Slater determinant [6]:

$$\psi^{(\infty)}_{\text{bosons}}(x_1,x_2,\ldots,x_N) = \big|\det\big[\psi_i(x_j)\big]\big| \qquad i,j=1,2,\ldots,N\,.$$

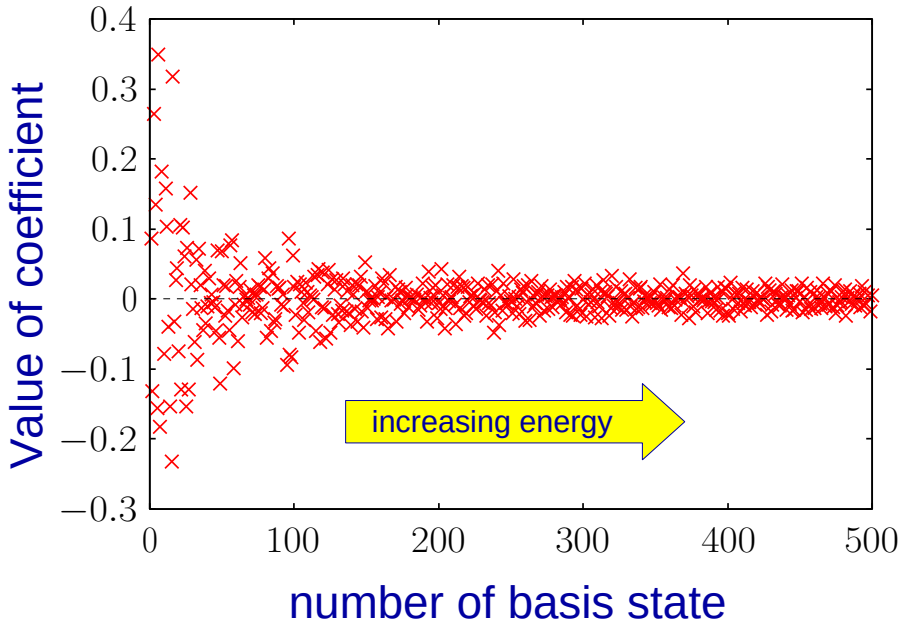

Figure 2.4: Coefficient distribution of the ground state of the spin-polarized quasi-one-dimensional strongly-interacting system. Shown are the coefficients of the expansion $|\psi\rangle = \sum_N c_N |N\rangle$.

Here, $\psi_i(x)$ is the ith eigenfunction of the single-particle Hamiltonian. It follows immediatly from this solution that all the quantities which are calculated from the square of the wave function,

$$\left[\psi^{(\infty)}_{\text{bosons}}\right]^2 = \det\left[\psi_i(x_j)\right]^2 \tag{2.43}$$

– like the N-particle density, the correlation function and all the energy contributions – are equal to those of noninteracting fermions. I will show later in Sec. 3.8 that Eq. (2.43) holds also for the excited states (but with the corresponding Slater determinant).

In our system, the particles have spin 1. But in the spin-polarized case $\langle F_z\rangle = \pm N$, when all the spins of the initial state point up- or downwards, the system can be described by a spinless wave function since the N-particle spin function $|1,1,\ldots,1\rangle$ $\big($or $|-1,-1,\ldots,-1\rangle\big)$ is the same at all times (I have shown in Sec. 2.1 that F_z is conserved and thus no spin-changing collisions can occur). Hence, the spin function can be neglected for the description of the system. Therefore, in the spin-polarized case, when the system is quasi-one-dimensional (i. e. $\omega_x \ll \omega_y, \omega_z$) and when the repulsion between the particles is strong, the bosons should behave like noninteracting fermions. In a first test, we thus checked whether the total energies of all the low-energy states were equal to those of noninteracting fermions, i. e., we checked whether the ground-state energy $E_g = N^2/2\,\hbar\omega_x$ and the level spacing $\Delta E = 1\,\hbar\omega_x$ were equal (apart from a constant offset from the Zeeman energy and the transverse directions). This is a nontrivial test of the Hamiltonian since the basis states of the noninteracting Hamiltonian are strongly mixed up in the low-energy eigenstates of the strongly interacting system, as shown in Fig. 2.4 for the ground state. Later, we also checked the density operator and the correlation function in the Tonks-Girardeau limit.

Comparison with the solution of C. K. Law, H. Pu and N. P. Bigelow [56]: In order to test the spin part of the Hamiltonian we can compare with the solution of C. K. Law *et al.* [56]. The solution is valid for zero-dimensional systems, i. e., all the particles reside in the motional ground state, and zero magnetic field. In that case the basis is finite. The occupation number states are

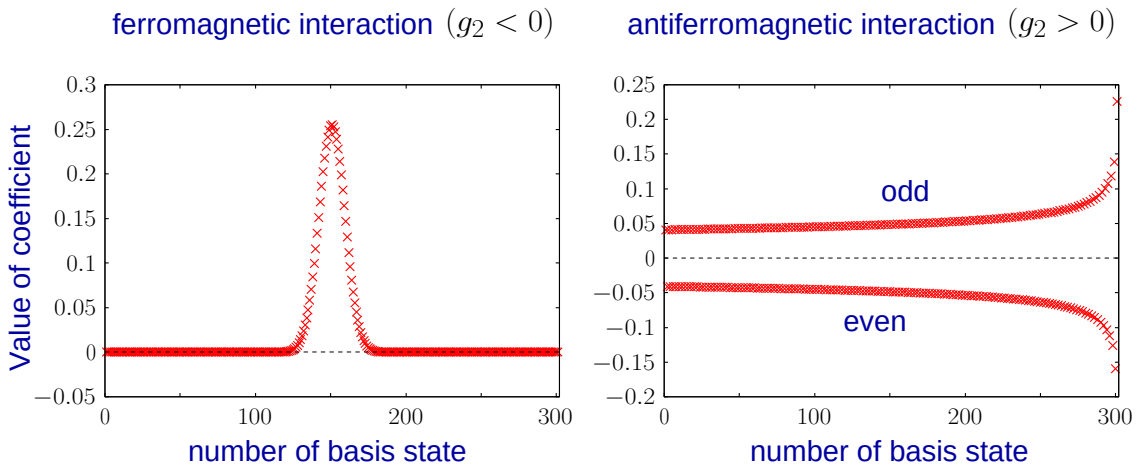

Figure 2.5: Coefficient distribution of the ground state for a zero-dimensional system at zero magnetic field. Here, the number of particles is $N = 600$ and the z-component of the total spin is $F_z = 0$. Shown are the coefficients of the expansion $|\psi\rangle = \sum_\epsilon c_\epsilon |\epsilon\rangle$ (see text).

given by $|N_0, N_1, N_{-1}\rangle$ with N_0, $N_{\pm1}$ particles in spin state $m_f = 0, \pm 1$. Let us, e. g., consider the case $F_z = 0$. Then, the basis consists of the number states $|\epsilon\rangle \equiv |N + 2 - 2\epsilon, \epsilon - 1, \epsilon - 1\rangle$ $\big(\epsilon = 1, 2, \ldots, \lfloor N/2 \rfloor + 1\big)$. The basis states are mixed up due to the spin-dependent interaction: For ferromagnetic coupling $(g_2 < 0)$ one observes a coefficient distribution in the ground state which resembles a Gaussian [see Fig. 2.5(left)] and for antiferromagnetic coupling $(g_2 > 0)$ one observes the coefficient distribution of Fig. 2.5(right). In the antiferromagnetic ground state, the coefficients c_ϵ with odd/even ϵ are greater/smaller than zero. Our numerical results agree well with the coefficient distributions of Ref. [56].

Comparison with the two-particle solution: The problem of two particles in a harmonic trap which interact via a δ potential can be solved exactly analytically. For the three-dimensional rotationally symmetric trap the solution [75] will be derived in Sec. 5.2. For the one-dimensional trap the solution [76] can be derived easily with the methods of chapter 5.

Analytical solution— We want to solve the Schrödinger equation

$$\left[-\frac{1}{2}\frac{\partial^2}{\partial x_1^2} - \frac{1}{2}\frac{\partial^2}{\partial x_2^2} + \frac{1}{2}x_1^2 + \frac{1}{2}x_2^2 + g\delta(x_1 - x_2)\right]\psi = E\psi\,.$$

Here, all energies have been expressed in units of $\hbar\omega_x$ and all lengths have been expressed in units of $l_x = \sqrt{\hbar/(m\omega_x)}$. In particular the interaction strength g has been expressed in units of $\hbar\omega_x l_x$. For the derivation of a dimensionless equation see Sec. 5.6.

The above equation separates into a center-of-mass and a relative equation. The center-of-mass equation is given by (for the transformation see Sec. 5.6)

$$\left[-\frac{1}{2}\frac{d^2}{dX^2} + \frac{1}{2}X^2\right]\psi_{\text{c.m.}} = E_{\text{c.m.}}\psi_{\text{c.m.}}\,.$$

Here, all energies have been expressed in units of $\hbar\omega_x$ and all lengths have been expressed in units of $l_{x,\text{c.m.}} = \sqrt{\hbar/(M\omega_x)}$ with $M = 2m$. The solution of that equation is given by the eigenenergies and eigenfunctions of the one-dimensional harmonic oscillator. The relative equation is given by

$$\left[-\frac{1}{2}\frac{d^2}{dx^2} + \frac{1}{2}x^2 + g_r\,\delta(x)\right]\psi_{\text{rel.}} = E_{\text{rel.}}\psi_{\text{rel.}}\,.$$

Here, all energies have been expressed in units of $\hbar\omega_x$ and all lengths have been expressed in units of $l_{x,\text{rel.}} = \sqrt{\hbar/(\mu\omega_x)}$ with $\mu = m/2$. The interaction strength g_r is now expressed in units of $\hbar\omega_x l_{x,\text{rel.}}$. It is related to g as follows

$$g = \widetilde{g}\hbar\omega_x l_x = \widetilde{g}_r \hbar\omega_x l_{x,\text{rel.}} \quad \Rightarrow \quad \widetilde{g}_r = \widetilde{g}\frac{l_x}{l_{x,\text{rel.}}}\,.$$

Here, $\widetilde{g}$ and $\widetilde{g}_r$ are the dimensionless interaction strengths. We omit the tilde symbol and obtain the relation

$$g_r = g/\sqrt{2} \tag{2.44}$$

since $l_{x,\text{rel.}} = \sqrt{2}\, l_x$. In the region $x \neq 0$, the δ potential is zero and the relative equation transforms to

$$\psi''_{\text{rel.}} - x^2\psi_{\text{rel.}} + 2E_{\text{rel.}}\psi_{\text{rel.}} = 0\,.$$

I solve this equation in appendix B. Due to the boundary condition $\psi_{\text{rel.}}(x) = 0$ for $|x| \to \infty$ we obtain the solution $\big[$see Eqs. (5.28) and (5.34)$\big]$

$$\psi_{\text{rel.}} = A\,U\Big(-E_{\text{rel.}};\sqrt{2}x\Big) = A\,D_{E_{\text{rel.}}-1/2}\left(\sqrt{2}x\right) = B\,U\left(-\frac{E_{\text{rel.}}}{2}+\frac{1}{4};\frac{1}{2};x^2\right)e^{-x^2/2} \tag{2.45}$$

where A and $B = A\,2^{E_{\text{rel.}}/2-1/4}$ are normalization constants. B is given by

$$B^2 = 2^{E_{\text{rel.}}+1/2}\pi^{-1/2}\frac{\Gamma(1/2-E_{\text{rel.}})}{\Psi(3/4-E_{\text{rel.}}/2)-\Psi(1/4-E_{\text{rel.}}/2)}\,. \tag{2.46}$$

$\big(B^2$ differs by a factor 2 from Eq. (5.63) since $\int_{-\infty}^{\infty} = 2\int_0^{\infty}$.$\big)$ It remains to determine $E_{\text{rel.}}$. The δ potential is equivalent to the boundary condition [83]

$$\lim_{\epsilon\to 0}\left(\left.\frac{d\psi_{\text{rel.}}}{dx}\right|_{\epsilon} - \left.\frac{d\psi_{\text{rel.}}}{dx}\right|_{-\epsilon}\right) = 2\,g_r\,\psi_{\text{rel.}}(0)\,. \tag{2.47}$$

Since $\psi_{\text{rel.}}(-x) = \psi_{\text{rel.}}(x)$ it follows that $\psi'_{\text{rel.}}(-\epsilon) = -\psi'_{\text{rel.}}(\epsilon)$ and the boundary condition becomes

$$\lim_{\epsilon\to 0}\left.\frac{d\psi_{\text{rel.}}}{dx}\right|_{\epsilon} = g_r\,\psi_{\text{rel.}}(0) \quad \Leftrightarrow \quad \frac{\psi'_{\text{rel.}}(0+)}{\psi_{\text{rel.}}(0)} = g_r\,.$$

Note the similarity to the boundary condition 5.41 in three dimensions! In Sec. 5.2 we will derive Eq. (5.40), which determines the energy as a function of the scattering length a_s, from the boundary condition 5.41. Thus, we obtain the energy of the relative motion $E_{\text{rel.}}$ simply by replacing $-1/a_s$ by the interaction strength g_r in Eq. (5.40):

$$-\,2\,\frac{\Gamma(3/4-E_{\text{rel.}}/2)}{\Gamma(1/4-E_{\text{rel.}}/2)} = g_r\,. \tag{2.48}$$

Finally, in order to compare with the numerical solution, we have to construct the total two-particle wave function:

$$\psi = \psi_{\text{c.m.}}\left(X\frac{l_x}{l_{x,\text{c.m.}}}\right)\psi_{\text{rel.}}\left(x\frac{l_x}{l_{x,\text{rel.}}}\right) = \psi_{\text{c.m.}}\left(\frac{x_1+x_2}{\sqrt{2}}\right)\psi_{\text{rel.}}\left(\frac{x_1-x_2}{\sqrt{2}}\right)$$

(given in units of l_x). I note, that one has to regard Eq. (2.44) for the comparison with the numerics.

Comparison with the numerical solution— Fig. 2.6 shows a comparison of the exact (black dashed) to the numerical solution (colored solid lines) for different interaction strengths g. The

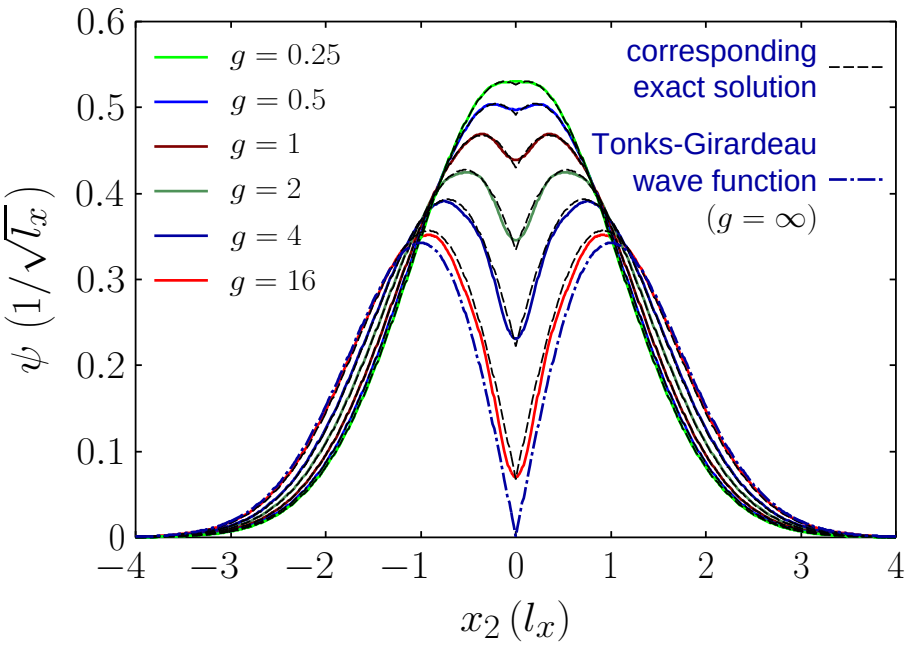

Figure 2.6: Exact (dashed) *vs.* numerical (solid) two-particle ground-state wave function. We fixed the coordinate of the first particle at $x_1 = 0$ and varied the coordinate x_2 of the second particle. Both solutions agree quite well apart from small differences around the cusp at coinciding particle positions $x_1 = x_2$. The wave functions at $g = 16$ nearly agree with the Tonks-Girardeau limiting solution (blue dash-dotted) at $g = \infty$. (The interaction strength g is given in units of $\hbar\omega_x l_x$.)

numerical wave functions are the result of an exact diagonalization of the Hamiltonian (2.5) within the restricted Hilbert space of the energetically lowest eigenfunctions of the noninteracting Hamiltonian, i. e., permutationally symmetric products of oscillator functions. The wave functions were obtained from the coefficients $(\ldots, c_N, \ldots)^T$ by means of the correlation function since for two particles the wave function is simply the square root of the correlation function, $\psi(\vec{r}, \vec{r}\,') = \sqrt{\langle\psi|\rho(\vec{r}, \vec{r}\,')|\psi\rangle}$. Thus, the comparison is also a test of that operator.

In Fig. 2.6 we fixed the coordinate of the first particle at $x_1 = 0$ and varied the coordinate x_2 of the second. One clearly sees the cusp in the wave function at the position $x_1 = x_2$ in accordance with the boundary condition (2.47). This cusp is not resolved in the numerical solution but in total both results agree quite well. It is not that surprising that we cannot resolve the cusp with a finite number of (smooth) harmonic oscillator functions. The accuracy of the numerical solution around the cusp does not become substantially better if we increase the energy cutoff from, e. g., $E_{\text{cutoff}} = 20\,\hbar\omega_x$ to $200\,\hbar\omega_x$ and thereby substantially increase the basis size (an effect similar to Gibbs phenomenon). Therefore, we expect the largest differences from the exact results for all quantities which are particularly sensitive to the wave function at equal particle positions $x_i = x_j$ like the local correlation function or the long-ranged tails of the momentum distribution.

Chapter 3

Evolution from a Bose-Einstein condensate to a Tonks-Girardeau gas

The main results of this chapter have been published in Ref. [2]. Parts have been published in my diploma thesis [1].

Subject of this chapter is a study of the interaction-driven evolution of a quasi-one-dimensional system of spinless hard-core bosons. First, in Sec. 3.1, I derive the effective Hamiltonian of spinless quasi-one-dimensional bosons. In Secs. 3.2 and 3.3 I discuss the two limiting regimes of weak and infinitely strong δ repulsion. In Sec. 3.4 I study the interaction-driven evolution of various ground-state properties. Besides the pair correlation function I will identify the momentum distribution as a reliable indicator for transitions of the system between three characteristic regimes, the Bose-Einstein-condenstate (BEC) regime, an intermediate regime with strong short-range correlations and the Tonks-Girardeau regime. I will quantify the interaction strength for the transitions by means of two characteristic features of the momentum distribution. In the last section 3.5 I will finally discuss the low-energy excitation spectrum of the boson system. Related studies on that subject have been performed by S. Zöllner *et al.* [41, 42] and by Y. Hao *et al.* [35].

3.1 Effective quasi-one-dimensional Hamiltonian

We consider a system of spin-polarized quasi-one-dimensional bosons, i. e., the axial level spacing $\hbar\omega_x$ and the interaction energy $E_{\text{int.},0}$ $\big[$estimated by Eq. (2.24)$\big]$ shall be much smaller than the transverse level spacings $\hbar\omega_y$ and $\hbar\omega_z$ and the N-particle spin function is given by $|1,1,\ldots,1\rangle$ or $|-1,-1,\ldots,-1\rangle$. In the experiment of Kinoshita *et al.* [21] for example we have $\omega_\perp/\omega_x \approx 2600$ $\big($with $\omega_\perp = \omega_y = \omega_z\big)$ and $\hbar\omega_\perp/E_{\text{int.},0} \approx 500$ (see the discussion in the end of Sec. 2.2) so that these conditions are rather well satisfied. But let me start the discussion with the complete Hamiltonian (2.4) of two particles

$$
\begin{aligned}
H = &\sum_{i=1}^{2}\left[-\frac{\hbar^2}{2m}\Delta_i + \frac{1}{2}m\Big(\omega_x^2 x_i^2 + \omega_y^2 y_i^2 + \omega_z^2 z_i^2\Big)\right]\otimes\mathbb{1}^{\otimes 2} \\
&-\sum_{i=1}^{2}\left[\frac{\mu_B B}{2}f_{z,i} + \frac{\mu_B^2 B^2}{2C_{\text{hfs}}}\left(\mathbb{1}^{\otimes 2} - \frac{1}{4}f_{z,i}^2\right)\right] + \delta(\vec{r}_1-\vec{r}_2)\Big(g_0\mathbb{1}^{\otimes 2} + g_2\vec{f}_1\cdot\vec{f}_2\Big).
\end{aligned}
$$

Let us assume that the two particles are initially in spin state $|1,1\rangle$. [1] This state is an eigenstate of the spin part of the above Hamiltonian since

$$\vec{f_1}\cdot\vec{f_2}\,|1,1\rangle = \left[f_z\otimes f_z + \frac{1}{2}\left(f_+\otimes f_- + f_-\otimes f_+\right)\right]|1,1\rangle = |1,1\rangle$$

and thus the spin-polarized state $|1,1\rangle$ is not coupled to states with other spin orientations by the spin-dependent interaction $g_2\delta(\vec{r}_1-\vec{r}_2)\vec{f}_1\cdot\vec{f}_2$. Since

$$\langle 1,1|\Big(g_0\mathbb{1}^{\otimes 2} + g_2\vec{f}_1\cdot\vec{f}_2\Big)|1,1\rangle = g_0+g_2 = \frac{4\pi\hbar^2 a_2}{m}$$

the effective spinless Hamiltonian (within the subspace $F_z=2$) is given by

$$\langle 1,1|H|1,1\rangle = \sum_{i=1}^{2}\left[-\frac{\hbar^2}{2m}\Delta_i + \frac{1}{2}m\Big(\omega_x^2x_i^2+\omega_y^2y_i^2+\omega_z^2z_i^2\Big)\right] + \frac{4\pi\hbar^2a_2}{m}\delta(\vec{r}_1-\vec{r}_2) + E_{Z,\text{offset}}$$

where the Zeeman energy

$$E_{Z,\text{offset}} = -2\left[\frac{\mu_B B}{2} + \frac{\mu_B^2B^2}{2C_{\text{hfs}}}\left(1-\frac{1}{4}\right)\right]$$

is a constant offset energy within this subspace. Now we assume that the two particles reside in the ground state of the transverse direction since the interaction energy is such small compared to the transverse level spacing

$$\psi_\perp = \psi_0(y_1)\psi_0(z_1)\psi_0(y_2)\psi_0(z_2)\,.$$

Here, ψ_0 is the ground state of the one-dimensional harmonic oscillator. We integrate over the transverse direction and obtain the effective Hamiltonian

$$\langle 1,1|\otimes\langle\psi_\perp|H|\psi_\perp\rangle\otimes|1,1\rangle = \sum_{i=1}^{2}\left(-\frac{\hbar^2}{2m}\frac{\partial^2}{\partial x_i^2}+\frac{1}{2}m\omega_x^2x_i^2\right) + g\delta(x_1-x_2) + E_{Z,\text{offset}} + E_{\perp,\text{offset}}$$

where the ground-state energy of the transverse motion is given by

$$E_{\perp,\text{offset}} = 2\left(\frac{1}{2}\hbar\omega_y + \frac{1}{2}\hbar\omega_z\right)$$

and where the effective one-dimensional interaction strength is given by

$$g = \frac{4\pi\hbar^2a_2}{m}\langle\psi_\perp|\delta(y_1-y_2)\delta(z_1-z_2)|\psi_\perp\rangle = \frac{4\pi\hbar^2a_2}{m}\,\frac{1}{l_yl_z}\,\frac{1}{2\pi} = 2\,\hbar\omega_\perp\,a_2\,. \tag{3.1}$$

Here we used $\int dy\psi_0^4(y)\int dz\psi_0^4(z) = 1/(2\pi l_y l_z)$ and $l_\perp = l_y = l_z = \sqrt{\hbar/(m\omega_\perp)}$. The effective Hamiltonian for the axial wave function ψ_{axial} is thus given by

$$H = \sum_{i=1}^{2}\left(-\frac{\hbar^2}{2m}\frac{\partial^2}{\partial x_i^2}+\frac{1}{2}m\omega^2x_i^2\right) + g\delta(x_1-x_2)\,.$$

[1] The discussion is analogous for the state $|-1,-1\rangle$.

Here I renamed the frequency $\omega = \omega_x$ and I neglected the constant offset energies. Generalization to N particles is straightforward

$$H = \sum_{i=1}^{N} \left(-\frac{\hbar^2}{2m} \frac{\partial^2}{\partial x_i^2} + \frac{1}{2} m\omega^2 x_i^2 \right) + g \sum_{i<j} \delta(x_i - x_j) \,. \tag{3.2}$$

Finally I note that the scattering length a_2 is affected by a tight transverse confinement. [2] It has been shown in Refs. [84, 85] that the effective scattering length $a_{2,\text{eff.}}$ is given by

$$a_{2,\text{eff.}} = \gamma \, a_2 \quad \text{with} \quad \gamma = \frac{1}{1 - 1.46 \, a_2 / \left(\sqrt{2} l_\perp\right)} \,.$$

However, for the transvere confinement considered here (see the frequencies of Ref. [21] in Table 2.1) the scattering length a_2 is only marginally modified since

$$1 < \gamma < 1.16 \quad \text{for} \quad 0 < \omega_\perp < 2\pi \times 70.7\,\text{kHz} \,.$$

3.2 Weakly interacting regime: Mean-field approximation

For vanishing interactions all the bosons occupy the ground state of the harmonic trap $\psi_0(x)$ and the many-particle wave function is given by $\psi(x_1, x_2, \ldots, x_N) = \prod_{i=1}^{N} \psi_0(x_i)$. Similarly, in the weakly interacting regime it is sufficiently accurate to assume that all the bosons condense into the same mean-field wave function $\psi_{\text{m.f.}}(x)$ so that the many-particle wave function is given by

$$\psi(x_1, x_2, \ldots, x_N) \approx \prod_{i=1}^{N} \psi_{\text{m.f.}}(x_i) \,. \tag{3.3}$$

However, the mean-field orbital is deformed due to the interaction between the bosons. The optimal shape of $\psi_{\text{m.f.}}(x)$ minimizes the total energy of the above state (3.3) with the Hamiltonian (3.2)

$$E\left(\psi_{\text{m.f.}}\right) = \int dx \left[N \psi_{\text{m.f.}}^*(x) \left(-\frac{\hbar^2}{2m} \frac{d^2}{dx^2} + \frac{1}{2} m\omega^2 x^2 \right) \psi_{\text{m.f.}}(x) + \frac{N(N-1)}{2} g \left|\psi_{\text{m.f.}}(x)\right|^4 \right].$$

The Gross-Pitaevskii equation is obtained from this energy functional by using a variational procedure [15, 16]

$$\left[-\frac{\hbar^2}{2m} \frac{d^2}{dx^2} + \frac{1}{2} m\omega^2 x^2 + (N-1) g \left|\psi_{\text{m.f.}}(x)\right|^2 \right] \psi_{\text{m.f.}}(x) = \mu \, \psi_{\text{m.f.}}(x) \tag{3.4}$$

where μ is the chemical potential. Eq. (3.4) is a nonlinear differential equation. Different from an ordinary single-particle Schrödinger equation there is an additional mean-field potential

$$V_{\text{m.f.}}(x) = (N-1) g \left|\psi_{\text{m.f.}}(x)\right|^2$$

[2] The three-dimensional scattering length a_s is usually determined from the phase shift δ_0 of the scattered wave in the limit of zero energy and zero confinement, where $\tan \delta_0 = -k a_s$. A tight confinement affects the behavior of the radial wave function at $r = R$ (where R is the range of the interaction potential), thus leading to a modification of the scattering length. [See Sec. 5.1 for the discussion of the short-ranged interaction between two particles in the trap-free case — in particular Eq. (5.17) for the definition of the scattering length and Eq. (5.20) for the relation between the scattering length and the phase shift. The influence of the confinement is discussed in Sec. 5.2. Note that all the quantities in that section are given in units of the oscillator length and the level spacing of the trap.]

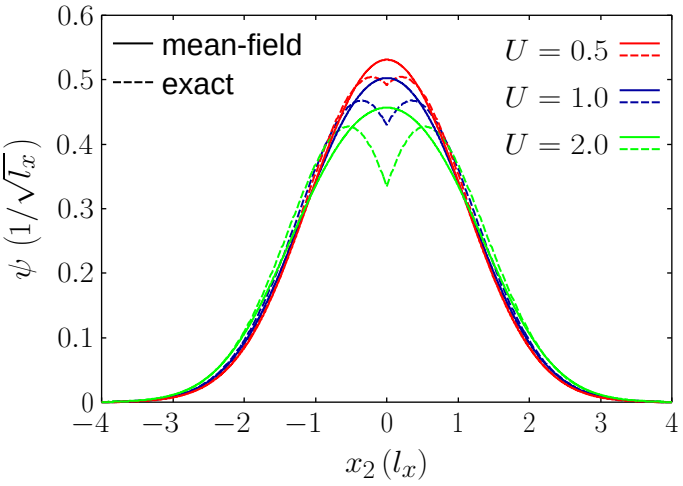

Figure 3.1: Exact $\left[\psi(0, x_2)\text{, dashed}\right]$ *vs.* mean-field $\left[\psi_{\text{m.f.}}(0)\psi_{\text{m.f.}}(x_2)\text{, solid}\right]$ two-particle wave function. The coordinate of the first particle is fixed at $x_1 = 0$. The interaction strength $U = g/l$ $(l = l_x)$ is given in $\hbar\omega$.

which is proportional to the particle density $\rho_{\text{m.f.}}(x) = N\left|\psi_{\text{m.f.}}(x)\right|^2$. Thus, the system favors lower particle densities, especially in the trap center, to reduce the interaction energy

$$E_{\text{int., m.f.}} = \frac{N(N-1)}{2}\, g \int dx \left|\psi_{\text{m.f.}}(x)\right|^4 .$$

The results of a numerical solution of the Gross-Pitaevskii equation (3.4) for two particles and different interaction strengths $U = g/l$ are shown as solid lines in Fig. 3.1. As can be seen, the system reacts to an increasing repulsion by a broadening and flattening of the mean-field wave function, since the effective potential $V_{\text{eff.}}(x) = m\omega^2 x^2/2 + V_{\text{m.f.}}(x)$ is shallower near the trap center due to the additional mean-field potential. In comparison with the exact two-particle wave function (dashed lines), the mean-field wave function does not exhibit short-range correlations, i. e., there is not such a rapid decrease of the mean-field wave function at short particle distances. For the smallest interaction strength shown in Fig. 3.1 $\left[U/(\hbar\omega) = 0.5\right]$, the short-range correlations are not significant and the mean-field solution is in total a good approximation of the exact wave function. Note that in typical experiments, performed in the mean-field regime, the interaction strength is even smaller, $U/(\hbar\omega) \ll 1$ (see the discussion of the different parameter regimes in the end of Sec. 2.2). For larger interaction strengths $U = 1$ or $2\,\hbar\omega$, the mean-field wave function more and more deviates from the exact solution at short particle distances. We conclude, that the mean-field wave function is a good approximation of the exact solution for small interaction strengths and large interparticle distances.

The main advantage of the mean-field ansatz is that many system properties can be easily calculated from a single-particle wave function: The N-particle density is given by

$$\rho_{\text{m.f.}}(x) = \psi^2_{\text{m.f.}}(x)\langle N|a^\dagger_{\text{m.f.}}a_{\text{m.f.}}|N\rangle = N\psi^2_{\text{m.f.}}(x)$$

where $|N\rangle$ denotes the wave function (3.3). Here $\left|\psi_{\text{m.f.}}(x)\right|^2 = \psi^2_{\text{m.f.}}(x)$ since the mean-field wave function of our system is real. The correlation function is given by

$$\rho_{\text{m.f.}}(x, x') = \frac{1}{2}\psi^2_{\text{m.f.}}(x)\psi^2_{\text{m.f.}}(x')\langle N|a^\dagger_{\text{m.f.}}a^\dagger_{\text{m.f.}}a_{\text{m.f.}}a_{\text{m.f.}}|N\rangle = \frac{N(N-1)}{2}\psi^2_{\text{m.f.}}(x)\psi^2_{\text{m.f.}}(x')$$

and thus it is proportional to the density when one particle coordinate is fixed. The kinetic energy is given by

$$E_{\text{kin., m.f.}} = N\frac{\hbar^2}{2m}\int dx \left[\frac{d\psi_{\text{m.f.}}(x)}{dx}\right]^2$$

and so forth ... Later in Sec. 3.4 I will determine the parameter regime where the mean-field approximation is sufficiently accurate.

3.3 Strongly interacting regime: Girardeau's Fermi-Bose mapping

Not only in the weakly interacting regime but also in the opposite limit of very strong repulsion there exists a simple method to analyze the system. Surprisingly it is even easier to calculate the exact many-particle wave function of the strongly interacting bosons than the mean-field wave function in the weakly interacting regime.

We are considering spinless one-dimensional bosons which interact via a δ potential. The Hamiltonian of that system is given by

$$H = \sum_{i=1}^{N}\left(-\frac{\hbar^2}{2m}\frac{\partial^2}{\partial x_i^2} + \frac{1}{2}m\omega^2 x_i^2\right) + g\sum_{i<j}\delta(x_i - x_j)\,.$$

(see the derivation of Eq. (3.2) in Sec. 3.1). One can derive from Eq. (2.47) that the interaction Hamiltonian $g\sum_{i<j}\delta(x_i - x_j)$ is equivalent to the boundary condition

$$\left(\frac{\partial}{\partial x_i} - \frac{\partial}{\partial x_j}\right)\psi|_{x_i=x_j+} - \left(\frac{\partial}{\partial x_i} - \frac{\partial}{\partial x_j}\right)\psi|_{x_i=x_j-} = \frac{2mg}{\hbar^2}\psi|_{x_i=x_j}\,, \tag{3.5}$$

i. e., ψ has cusps whenever two particles touch and the jumps in the derivative of ψ are $2mg/\hbar^2$. We are interested in the solution of the limiting case of infinite repulsion $g = \infty$. In that case it follows from the boundary condition (3.5) that the wave function has to be zero whenever two particle coordinates are equal

$$\psi(x_1, x_2, \ldots, x_N) = 0 \qquad \text{if } x_i = x_j\,.$$

Thus, we are searching for solutions of the Schrödinger equation of *noninteracting particles* which are zero on the surface $\{x_i = x_j\} \equiv \{(x_1, x_2, \ldots, x_N) \in \mathbb{R}^N, x_i = x_j\}$ and which are permutationally symmetric:

$$\psi \text{ solves} \quad \sum_{i=1}^{N}\left(-\frac{\hbar^2}{2m}\frac{\partial^2}{\partial x_i^2} + \frac{1}{2}m\omega^2 x_i^2\right)\psi = E\psi \quad \text{in } \mathbb{R}^N \setminus \{x_i = x_j\} \tag{3.6a}$$

$$\psi(x_1, x_2, \ldots, x_N) = 0 \quad \text{on the surface } \{x_i = x_j\} \tag{3.6b}$$

$$\psi \text{ has Bose symmetry (is permutationally symmetric).} \tag{3.6c}$$

Eq. (3.6a) and the boundary condition (3.6b) are readily fulfilled by the wave functions of noninteracting fermions $\psi^{(0)}_{\text{fermions}}(x_1, x_2, \ldots, x_N)$. These wave functions are given by the Slater determinant of the occupied single-particle orbitals. However, fermionic wave functions are antisymmetric under any permutations of particle coordinates. In order to construct a Bose wave function from the fermionic solution of (3.6a) we introduce the so-called "unit antisymmetric function"

$$A(x_1, x_2, \ldots, x_N) = \prod_{i<j}\text{sign}(x_i - x_j) \tag{3.7}$$

and construct the product [6]

$$\psi^{(\infty)}_{\text{bosons}} = A\psi^{(0)}_{\text{fermions}}\,. \tag{3.8}$$

This wave function now fulfills the Schrödinger equation (3.6a) and the boundary conditions (3.6b) and (3.6c) and thus it is the desired solution of spinless one-dimensional bosons with infinite δ repulsion. The unit antisymmetric function A is $+1$ or -1 in each sector of the configuration space $\mathbb{R}^N$

$$C_\pi = \left\{(x_1, x_2 \ldots, x_N) \in \mathbb{R}^N,\; x_{\pi(1)} < \cdots < x_{\pi(N)}\right\} \tag{3.9}$$

where π is an arbitrary permutation. To be more precisely: It is $+1$ if π is an even permutation and -1 if π is an odd permutation. A does nothing but to restore the Bose symmetry of the wave function and apart from that it does not alter the fermionic solution of (3.6a). Thus, in each sector C_π, the bosonic wave function $\psi^{(\infty)}_{\text{bosons}}$ is equal to the fermionic one $\psi^{(0)}_{\text{fermions}}$ apart from a ± 1 factor. It follows immediately from the Fermi-Bose map (3.8) that

$$\left[\psi^{(\infty)}_{\text{bosons}}\right]^2 = \left[\psi^{(0)}_{\text{fermions}}\right]^2$$

since $A^2 = 1$. Thus, all the properties of the spinless one-dimensional hard-core bosons which are calculated from the square of the wave function – such as the density, the correlation function and all the energy contributions – are equal to those of noninteracting fermions. In other words:

> *"One-dimensional hard-core bosons behave like noninteracting fermions."*

There are still differences which are remnants of the Bose symmetry of the wave function: I will show in the following section that the momentum distribution and the occupation of the single-particle orbitals is completely different from the fermionic one and exhibits typical bosonic features. However, Girardeau's simple idea turned out to be an extremely useful concept and it inspired other theorists to search for further exact solutions [7, 8, 9, 10] and new models [11, 12, 13] for one-dimensional systems.

Examples— Before I proceed I would like to construct explicitly the ground and the first excited state of two hard-core bosons in a harmonic trap. The discussion is visualized in Fig. 3.2. The ground state of two noninteracting fermions in a harmonic trap is given by

$$\psi^{(0)}_{\text{fermion gr.}}(x_1, x_2) \propto \begin{vmatrix} e^{-x_1^2/2} & x_1 e^{-x_1^2/2} \\ e^{-x_2^2/2} & x_2 e^{-x_2^2/2} \end{vmatrix} \propto (x_1 - x_2)\, e^{-(x_1^2+x_2^2)/2},$$

apart from a normalization constant. We multiply the fermion ground state with A and obtain the ground state of two hard-core bosons

$$\psi^{(\infty)}_{\text{boson gr.}}(x_1, x_2) \propto \text{sign}(x_1 - x_2)\,(x_1 - x_2)\, e^{-(x_1^2+x_2^2)/2} = |x_1 - x_2|\, e^{-(x_1^2+x_2^2)/2};$$

see Fig. 3.2(bottom row). This result for the boson ground state of the harmonic trap can be generalized to N particles [86]:

$$\psi^{(\infty)}_{\text{boson gr.}}(x_1, x_2, \ldots, x_N) \propto \prod_{i<j} |x_i - x_j| \prod_k e^{-x_k^2/2}. \tag{3.10}$$

We see in Fig. 3.2 that the Fermi wave functions have smooth zeros on the surface $\{x_i = x_j\}$. By contrast, the corresponding boson states have hard-core cusps (i. e. jumps in the first derivatives)

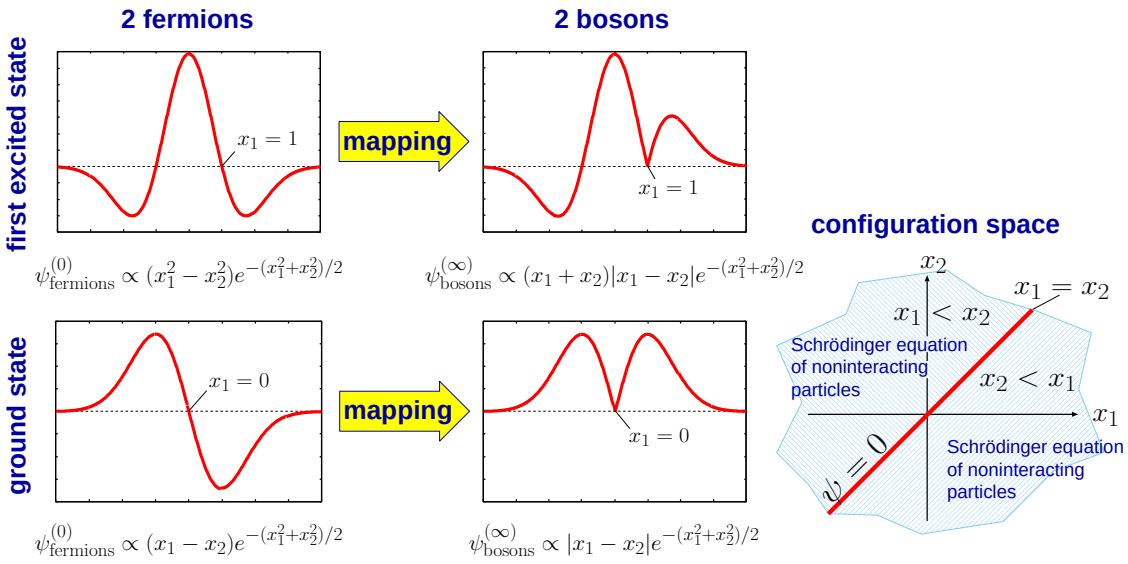

Figure 3.2: Sketch of Girardeau's Fermi-Bose map for two particles. *Bottom row:* ground state, *upper row:* first excited state, *right:* configuration space.

at the collision points $\{x_i = x_j\}$. One can show for a general trapping potential that the boson ground state is always given by the absolute value of the corresponding fermion ground state [6]

$$\psi^{(\infty)}_{\text{boson gr.}} = A\psi^{(0)}_{\text{fermion gr.}} = \left|\psi^{(0)}_{\text{fermion gr.}}\right|$$

since all the zeros of the Fermi ground state are located on the surface $\{x_i = x_j\}$ and there are no further zeros within the sectors C_π.

Let me now construct the first excited state. The first excited state of two noninteracting fermions in a harmonic trap is given by

$$\psi^{(0)}_{\text{fermion 1st}}(x_1, x_2) \propto \begin{vmatrix} e^{-x_1^2/2} & (2x_1^2 - 1)e^{-x_1^2/2} \\ e^{-x_2^2/2} & (2x_2^2 - 1)e^{-x_2^2/2} \end{vmatrix} \propto \left(x_1^2 - x_2^2\right) e^{-(x_1^2+x_2^2)/2} \, .$$

We multiply this state with the unit antisymmetric function A and obtain the first excited state of two hard-core bosons

$$\psi^{(\infty)}_{\text{boson 1st}}(x_1, x_2) \propto \text{sign}(x_1 - x_2)\left(x_1^2 - x_2^2\right) e^{-(x_1^2+x_2^2)/2} = (x_1 + x_2)\,|x_1 - x_2|\, e^{-(x_1^2+x_2^2)/2} \, .$$

We see that this state has interaction cusps on the "surface" $x_1 - x_2 = 0$ and additional smooth zeros on the "surface" $x_1 + x_2 = 0$ which runs through the sectors $x_1 < x_2$ and $x_2 < x_1$. Hence, the sign of the wave function of the first excited state changes not only on the sector boundaries ∂C_π but also within the sectors C_π. Anyway, one can generalize Eq. (3.10) according to

$$\psi^{(\infty)}_{\text{bosons}}(x_1, x_2, \ldots, x_N) \propto f_b(x_1, x_2, \ldots, x_N) \prod_{i<j} |x_i - x_j| \prod_k e^{-x_k^2/2} \tag{3.11}$$

with f_b being some permutationally symmetric polynomial. For the ground state we have $f_b = 1$ and for the first excited state we have $f_b = x_1 + x_2 + \ldots + x_N$. [3]

[3] I checked the relation (3.11) for the lowest excited states of the harmonic trap and different particle numbers by means of MATHEMATICA but I did not proof it.

Some ground-state properties— The N-particle ground-state density is given by

$$\rho(x) = \sum_{i=0}^{N-1} \psi_i^2(x)$$

where ψ_i is the ith eigenstate of the single-particle problem and the correlation function is given by [86]

$$\rho(x, x') = \sum_{0 \leqslant i < j \leqslant N-1} \left| \psi_i(x)\psi_j(x') - \psi_i(x')\psi_j(x) \right|^2 .$$

For the total energy in the harmonic trap we obtain

$$E_{\text{tot.}} = \sum_{i=0}^{N-1} \left(i + \frac{1}{2} \right) \hbar\omega = \frac{N^2}{2} \hbar\omega \, .$$

Kinetic and potential energy are equal in the harmonic trap and given by $E_{\text{kin.}} = E_{\text{pot.}} = E_{\text{tot.}}/2$. The interaction energy is zero like for noninteracting fermions despite the infinite repulsion between the bosons, since the wave function is zero at $\{x_i = x_j\}$.

3.4 Evolution of various ground-state properties

In this section I will study the interaction-driven crossover of few bosons from the mean-field to the Tonks-Girardeau regime. I performed calculations for up to seven particles but here I will concentrate on my results achieved for five bosons. I will show that one can discriminate between three regimes: the mean-field regime, an intermediate regime and the Tonks-Girardeau regime. Besides the pair correlation function I will identify the momentum distribution as a reliable indicator for transitions between these regimes.

Density: I start my discussion with the particle density $\rho(x)$ which is shown in Fig. 3.3. In the spinless one-dimensional system considered here the N-particle density is given by

$$\rho(x) = \left\langle \hat{\Psi}^\dagger(x) \hat{\Psi}(x) \right\rangle$$

where $\hat{\Psi}(x) = \sum_i \psi_i(x) a_i$ is the field operator $\big[a_i$ is the bosonic annihilation operator for a particle in the ith eigenstate ψ_i of the axial harmonic oscillator; the general formula for spinful bosons in three dimensions is given by Eq. (2.41)$\big]$. At small interaction strengths U the density reflects the conventional mean-field behavior (see Sec. 3.2) and $\rho(x) \approx \rho_{\text{m.f.}}(x) = N\psi_{\text{m.f.}}^2(x)$. In this regime all the bosons condense into the same single-particle wavefunction $\psi(x_1, x_2, \ldots, x_N) \approx \prod_{i=1}^{N} \psi_{\text{m.f.}}(x_i)$ and thus the many-boson system is well described by $\psi_{\text{m.f.}}(x)$ which solves the Gross-Pitaevskii equation. The system reacts to an increasing repulsive interaction with a density which becomes broader and flatter [30, 36, 35, 41, 39]. In the strong interaction regime density oscillations appear (see e. g. the curve at $U = 8\,\hbar\omega$ in Fig. 3.3) and with further increasing U the density of the bosons converges towards the density of five noninteracting fermions $\rho(x) \approx \rho_{\text{fermions}}(x) = \sum_{i=0}^{4} \psi_i^2(x)$, as predicted by Girardeau [6]. Both densities agree at $U = 20\,\hbar\omega$ indicating that the limit of infinite repulsion is practically reached. Thus, the density oscillations reflect the structure of the occupied orbitals in the harmonic trap. In contrast to Ref. [87] which predicts the oscillations to appear one after the other, when the repulsion between the bosons becomes stronger, I observe a simultaneous formation of five density maxima. These density oscillations are absent in mean-field calculations [88, 30]. However, for large particle numbers these oscillations die out and are barely visible.

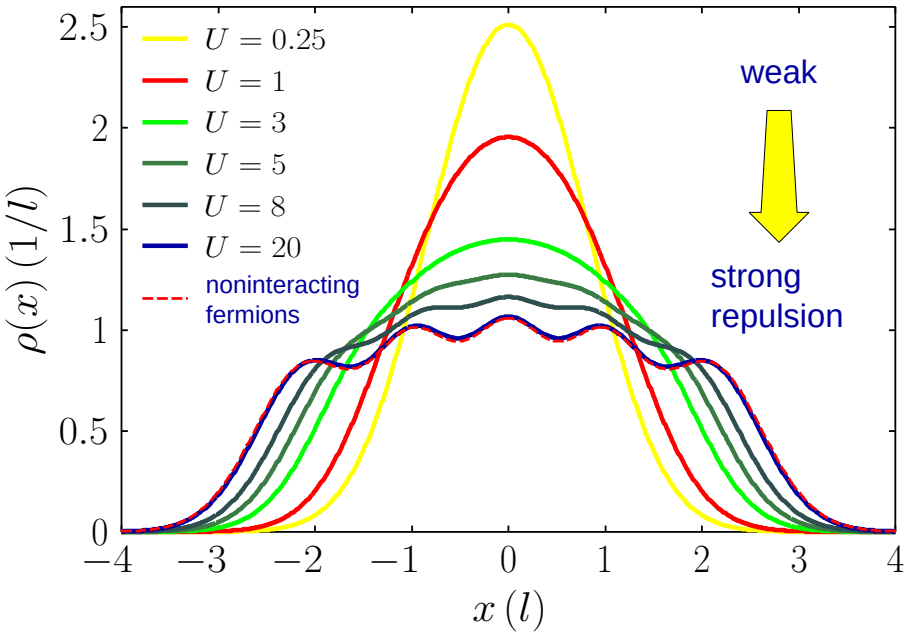

Figure 3.3: Particle density of five bosons for different interaction strengths U (given in units of $\hbar\omega$). The density becomes flatter and broader with increasing U. In the strong interaction regime oscillations appear. At $U = 20$ the density of the bosons agrees with the density of noninteracting fermions.

Pair correlation function: Additional insight into the evolution of the system with increasing repulsion can be obtained from the pair correlation function

$$\rho(x, x') = \frac{1}{2}\langle \hat{\Psi}^\dagger(x)\hat{\Psi}^\dagger(x')\hat{\Psi}(x')\hat{\Psi}(x)\rangle$$

which is depicted in Fig. 3.4(left) for different U. In the regime of weak interactions where the mean-field approximation is valid the correlation function resembles the particle density since $\rho(x, x') \approx N(N-1)/2\ \psi^2_{\text{m.f.}}(x)\psi^2_{\text{m.f.}}(x') \propto \rho_{\text{m.f.}}(x)\rho_{\text{m.f.}}(x')$. Thus, the system reacts to the increasing repulsion mainly by a flattening of the mean-field wave function $\psi_{\text{m.f.}}$ in the trap center in order to reduce the interaction energy

$$E_{\text{int.}} \approx E_{\text{int., m.f.}} = \frac{N(N-1)}{2}\, g \int dx\, \psi^4_{\text{m.f.}}(x)\,.$$

Significant short-range correlations appear around $U \approx 0.5\,\hbar\omega$; see the dip of $\rho(x, x')$ at $x' = 0$ in Fig. 3.4(left). This decrease of the wave function at short interparticle distances marks first deviations from the mean-field behavior. With further increasing U the overall correlation function becomes flatter and broader and the dip at $x = x'$ develops into a pronounced correlation hole. Finally at $U = 20\,\hbar\omega$ the correlation function of the bosons agrees rather good with that of five noninteracting fermions. As in the case of fermions the probability to find two bosons at the same position becomes zero. Thus, the infinite repulsion mimics Pauli's exclusion principle. Again, we observe minor oscillation with a wavelength which is of the order of the oscillator length.

I would like to note the rapid deformation of the correlation function in the (comparatively small) region $U = 0 \ldots 3\,\hbar\omega$. At $U = 3\,\hbar\omega$ the correlation function already attains a form which is typical for a Tonks-Girardeau gas: Flat long-range shoulders indicate the incompressibility of

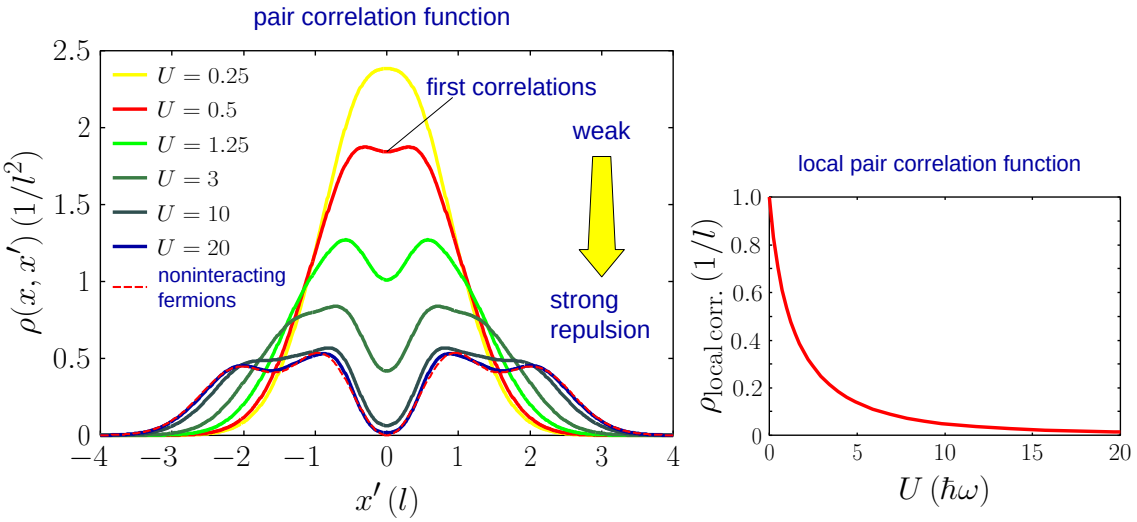

Figure 3.4: *Left:* Pair correlation function $\rho(x, x')$ of five bosons for different interaction strengths U (in units of $\hbar\omega$). One particle is fixed at $x = 0$. The distribution flattens and with increasing repulsion U it forms a correlation hole at coinciding particle positions $x = x'$. Note the rapid deformation of $\rho(x, x')$ in the region $U = 0 \ldots 3$ compared to the slow evolution above from $U = 3$. *Right:* Local pair correlation function $\rho_{\text{local corr.}} = \int dx \rho(x, x)$ as a function of U. I normalized the local pair correlation function such that $\rho_{\text{local corr.}}(0) = 1$ and thus it is one for noninteracting bosons.

a Fermi gas. By contrast, in the (large) region $U = 3 \ldots 20\,\hbar\omega$ the correlation function reacts comparatively slowly to the increasing repulsion. I note further that the *density* at $U = 3\,\hbar\omega$ still exhibits a mean-field shape; see Fig. 3.3).

In order to quantify the speed of change we additionally calculated the local pair correlation function

$$\rho_{\text{local corr.}} = \int dx\, \rho(x, x)$$

which is a measure for the probability to find two particles at the same position. Fig. 3.4(right) shows the result: In the region $U = 0 \ldots 3\,\hbar\omega$ the local pair correlation function decreases rapidly and $\rho_{\text{local corr.}}(3) \approx 1/5$. By contrast, above from $U = 3\,\hbar\omega$ the local pair correlation function converges rather slowly towards zero.

For the homogeneous system it has been found that the local pair correlation function decreases proportional to $1/\gamma^2$ where $\gamma = mg/[\hbar^2\rho(x)]$ [4] characterizes the interaction strength of the infinite system [32]. Similarly, we expect a decrease of $\rho_{\text{local corr.}} \propto 1/U^2$ for large U in our finite-size system. I was not able to extract the $1/U^2$ behavior of the local pair correlation function from my numerical calculations. The reason for that is discussed later in the end of this section.

However, apart from the comparison with the homogeneous system, another indication for the assumed $1/U^2$ behavior of the local pair correlation function comes from the analytical two-particle solution: In the two-particle case the pair correlation function is given by the square of

[4] In the homogeneous system the density is not spatially dependent and $\rho(x) = \rho =$ constant. In our finite-size system the density is spatially dependent and thus one often chooses the density at the trap center $\rho_0 = \rho(0)$ in order to calculate γ. For weak and intermediate interaction strengths $U = g/l$ the density at the trap center ρ_0 rapidly decreases as a function of U (see Fig. 3.3) and thus $\gamma \propto U/\rho_0(U)$. By contrast, for larger interaction strengths, ρ_0 is nearly constant, $\rho_0 \approx \rho_0(U = \infty)$, and thus $\gamma \propto U$.

the wave function, which can be expressed in terms of the center-of-mass and the relative-motion wave function $\psi = \psi_{\text{c.m.}}(X)\psi_{\text{rel.}}(x)$. The local pair correlation function is thus given by

$$\rho_{\text{local corr.}} = \underbrace{\left[\int_{-\infty}^{\infty} dx\, \psi_{\text{c.m.}}^2(x)\right]}_{=\text{const.}} \psi_{\text{rel.}}^2(0)\,.$$

In Sec. 2.9 we have determined the ground-state wave function of two interacting particles in a one-dimensional harmonic trap; see Eqs. (2.45), (2.46) and (2.48). We found a close relation between the one- and the three-dimensional two-particle solution. For example, one obtains the one-dimensional two-particle energy simply by replacing $-1/a_s$ by g_r in the three-dimensional equation (5.40). In Sec. 5.9 I calculate the lifetime of a three-dimensional molecule; see Eqs. (5.61), (5.62) and (5.65). The lifetime depends on the probability to find the two constituents of the molecule close to each other and Eq. (5.62) shows that this probability is approximately given by $\chi_{\text{rel.}}^2(0)$ [in three dimensions one often introduces the radial "wave function" $\chi_{\text{rel.}}(r) = r\,\psi_{\text{rel.}}(r)$]. By replacing $-1/a_s$ by g_r in Eq. (5.65) we thus obtain

$$\rho_{\text{local corr.}} \propto \psi_{\text{rel.}}^2(0) \propto -\frac{1}{g_r}\,\frac{1}{\Psi(3/4 - E_{\text{rel.}}/2) - \Psi(1/4 - E_{\text{rel.}}/2)}$$

(Ψ is the digamma function). In the limit of infinite repulsion ($g_r = \infty$) the energy of the relative motion converges towards $E_{\text{rel.}} = 3/2$ (the total energy is $E = N^2/2 = 2$ and the center-of-mass energy is $E_{\text{c.m.}} = 1/2$; all energies are given in units of $\hbar\omega$). A Taylor expansion of the right-hand side of the above equation around $E_{\text{rel.}} = 3/2$ gives the leading-order result

$$\rho_{\text{local corr.}} \propto -\frac{1}{g_r}\left(E_{\text{rel.}} - \frac{3}{2}\right).$$

Next, we perform a Taylor expansion of the left-hand side of Eq. (2.48) in order to express $E_{\text{rel.}}$ as a function of g_r and obtain

$$g_r = -\frac{2}{\sqrt{\pi}\left(E_{\text{rel.}} - \frac{3}{2}\right)} + \text{higher-order terms}\,. \tag{3.12}$$

Thus, in the regime of strong repulsion, the local pair correlation function of *two particles* decreases like $\rho_{\text{local corr.}} \propto 1/g_r^2 \propto 1/U^2$. I mention that it has been reported by Y. Hao *et al.* [35] that the local correlation function of $N \geqslant 2$ particles in a *finite-size hard-wall box* behaves similar to the homogeneous case [32]. It is thus highly probable that the local correlation function of $N > 2$ particles in a *harmonic trap* similarly decreases like $1/U^2$ for large repulsion.

Different energy contributions: Fig. 3.5 shows the evolution of various contributions to the total energy with increasing U. The interaction energy (green)

$$E_{\text{int.}} = \frac{U}{2}\int dx\, \left\langle \hat{\Psi}^\dagger(x)\hat{\Psi}^\dagger(x)\hat{\Psi}(x)\hat{\Psi}(x)\right\rangle = U\int dx\, \rho(x,x) = U\rho_{\text{local corr.}}$$

is directly related to the local pair correlation function. In Fig. 3.4(right) we have analyzed the evolution of $\rho_{\text{local corr.}}$ and seen that for small U it decays like $1 - f(U)$ where $f(U)$ is some rapidly increasing function. Thus, for small U, the interaction energy grows like $E_{\text{int.}} \propto U\big[1 - f(U)\big] \propto U$. For large U, however, it decreases like $E_{\text{int.}} \propto 1/U$ since the local correlation function decreases like $1/U^2$. Somewhere in between, at $U \approx 3\,\hbar\omega$ for five particles, the interaction energy reaches its maximum value. It is nearly constant in the region $U \approx 2 \ldots 4\,\hbar\omega$. We found the maximum

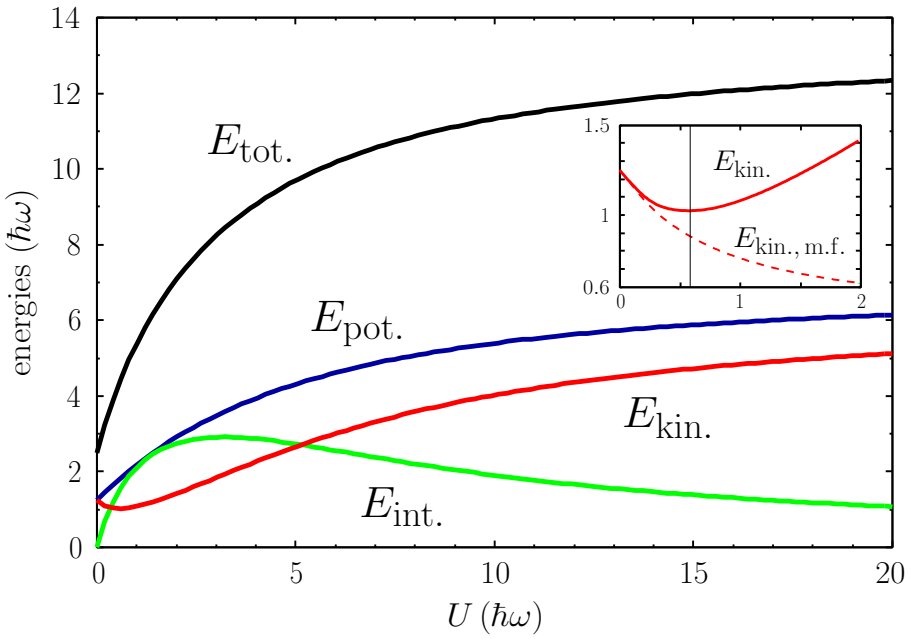

Figure 3.5: Evolution of various contributions to the total energy $E_{\text{tot.}}$ of five bosons with increasing interaction strength U. The energies evolve towards the accordant energies of noninteracting fermions. An interesting behavior is shown by the kinetic and the interaction energy. The interaction energy first grows $\propto U$, reaches a maximum and then decreases $\propto 1/U$ (for large U) since the short-range correlations decay like $1/U^2$. By contrast, the kinetic energy first decreases due to the flattening and broadening of the overall wave function ("density = wave function" in the mean-field regime). This effect is overcompensated by the development of short-range correlations which lead to an increase of the kinetic energy above from $U \approx 0.5\,\hbar\omega$. As can be seen the kinetic energy is rather sensitive to these short-range correlations. The minimum of the kinetic energy thus marks an upper limit of the mean-field regime.

of the interaction energy to be dependent on the number of particles: With increasing number of particles N its location $U_{\text{max.}}$ moves towards larger values of U.

The potential energy (the blue curve in Fig. 3.5) is given by

$$E_{\text{pot.}} = \frac{1}{2}m\omega^2 \int dx\, x^2 \underbrace{\langle \hat{\Psi}^\dagger(x)\hat{\Psi}(x)\rangle}_{=\rho(x)} = \frac{1}{2}m\omega^2\langle x^2\rangle$$

It grows continuously from $E_{\text{pot.}}^{(0)} = N/4\,\hbar\omega = 1.25\,\hbar\omega$ (for noninteracting bosons) to $E_{\text{pot.}}^{(\infty)} = N^2/4\,\hbar\omega = 6.25\,\hbar\omega$ in the Tonks-Girardeau limit. For larger U the increase of the potential energy and thus the broadening and flattening of the boson density slows down.

According to the above equation the potential energy is directly related to the width $w_x = 2\sqrt{\langle x^2\rangle}$ of the N-particle density which has been measured in Ref. [21]. In the Tonks-Girardeau limit the width of the boson system is given by $w_x^{(\infty)} = 2\sqrt{N^2/4}\,l = N\,l = 5\,l$. Thus, the mean interparticle distance $d_x = w_x/N = l$. This fact suggests to identify the maxima of the oscillations of the density with the positions of the individual particles [21] (see Fig. 3.3) since the separation of the oscsillation maxima is $\approx l$. By contrast, in the weakly interacting regime the width is given by $w_x^{(0)} = 2\sqrt{N/2}\,l = \sqrt{2N}\,l$ and thus the mean interparticle distance is $d_x = w_x/N = \sqrt{2/N}\,l \to 0$ for large N, i. e., the bosons sit on top of each other.

The total energy (black curve) behaves in a similar manner as the potential energy: It grows continuously from $E_{\text{tot.}}^{(0)} = N/2\,\hbar\omega = 2.5\,\hbar\omega$ for noninteracting bosons to $E_{\text{tot.}}^{(\infty)} = N^2/2\,\hbar\omega = 12.5\,\hbar\omega$ in the Tonks-Girardeau limit.

An interesting behavior is shown by the kinetic energy (the red curve in Fig. 3.5)

$$E_{\text{kin.}} = -\frac{\hbar^2}{2m}\int dx\,\big\langle \hat{\Psi}^\dagger(x)\,\frac{d^2}{dx^2}\,\hat{\Psi}(x)\big\rangle = \frac{1}{2m}\int dp\,p^2\,\underbrace{\big\langle \hat{\Pi}^\dagger(p)\hat{\Pi}(p)\big\rangle}_{=\rho(p)} = \frac{1}{2m}\big\langle p^2\big\rangle$$

which is related to the width $w_p = 2\sqrt{\langle p^2\rangle}$ of the momentum distribution $\rho(p) = \big\langle \hat{\Pi}^\dagger(p)\hat{\Pi}(p)\big\rangle$. Here I introduced the operator $\hat{\Pi}(p) = \frac{1}{\sqrt{2\pi\hbar}}\int dx\,\hat{\Psi}(x)e^{-\mathrm{i}px/\hbar}$ which annihilates a particle with momentum p. The kinetic energy first decreases within the small region $U = 0\ldots0.5\,\hbar\omega$, has a minimum at $U \approx 0.5\,\hbar\omega$ and grows rapidly for larger interaction strengths U. Like for the potential energy its limiting values are given by $E_{\text{kin.}}^{(0)} = N/4\,\hbar\omega = 1.25\,\hbar\omega$ (at $U = 0$) and by $E_{\text{kin.}}^{(\infty)} = N^2/4\,\hbar\omega = 6.25\,\hbar\omega$ in the Tonks-Girardeau limit.

Why does the kinetic energy first decrease for small interactions? In the mean-field region it is well approximated by

$$E_{\text{kin.}} \approx E_{\text{kin., m.f.}} = N\frac{\hbar^2}{2m}\int dx\left[\frac{d\psi_{\text{m.f.}}(x)}{dx}\right]^2 = \frac{\hbar^2}{2m}\int dx\left[\frac{d\sqrt{\rho_{\text{m.f.}}(x)}}{dx}\right]^2$$

and thus connected to the gradient of the particle density. Therefore, the flattening and broadening of the overall density ($\Rightarrow$ reduced gradient) leads to the initial decrease of the kinetic energy. The inset of Fig. 3.5 shows the mean-field kinetic energy (red dashed) which I extracted from the densities of Fig. 3.3 by means of the above equation. As can be seen $E_{\text{kin., m.f.}}$ decreases in the shown region $U = 0\ldots2\,\hbar\omega$.

However, the effect caused by the flattening of the density is in competition with the development of short-range correlations in the intermediate interaction regime above from $U \approx 0.5\,\hbar\omega$. The exact kinetic energy (in first quantization) is given by

$$E_{\text{kin.}} = N\frac{\hbar^2}{2m}\int dx_1\ldots dx_N\left[\frac{\partial}{\partial x_1}\psi_{\text{bosons}}(x_1\ldots x_N)\right]^2$$

and thus it is also sensitive to the rapid reduction of the boson wave function at short interparticle distances. We have seen in Fig. 3.4(left) that these short-range correlations become significant around $U \approx 0.5\,\hbar\omega$, i. e., exactly at that point when these correlations overcompensate the flattening of the overall wave function so that the kinetic energy starts to increase with U. Therefore, the minimum of the kinetic energy clearly marks the limit of the mean-field regime and the increasing importance of short-range correlations.

Further analysis of the momentum distribution: Fig. 3.6 shows selected momentum distributions at different U. The red dashed curve belongs to five noninteracting bosons. It is a Gaussian. The green dashed curve belongs to five noninteracting fermions. Due to Eq. (2.42) the momentum distribution of the fermions has the same form as the density and $\rho_{\text{fermions}}(p) = \sum_{i=0}^{N}\psi_i^2(p)$. Thus, the width of the fermion distribution is $w_p = N\,\hbar/l = 5\,\hbar/l$ and the Fermi edge is approximately located at $|p| = N/2\,\hbar/l = 2.5\,\hbar/l$. The black curve is the momentum distribution of five bosons with strong δ repulsion ($U = 20\,\hbar\omega$). It perfectly agrees with the momentum distribution of a Tonks-Girardeau gas calculated from the ground state in the trap (3.10) by means of a Monte-Carlo integration [89, 86].

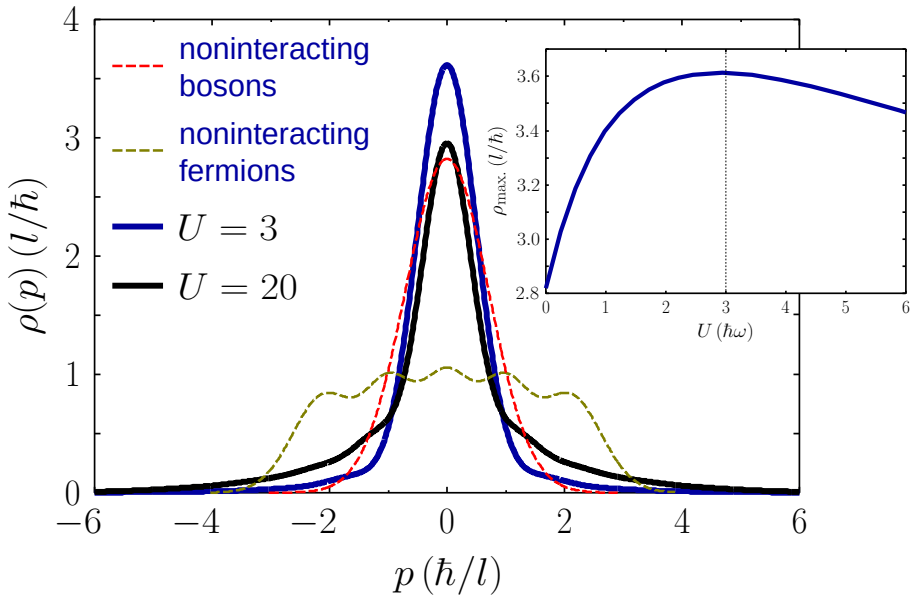

Figure 3.6: Momentum distributions of noninteracting bosons (red dashed), noninteracting fermions (green dashed), hard-core bosons in the Tonks-Girardeau limit (black) and strongly interacting bosons (blue). The distribution of the Tonks-Girardeau gas still exhibits typical bosonic features like the narrow and high central peak which is a remnant of the permutation symmetry of the wave function. The long-range high-momentum tails originate from the cusps in the wave function, i. e., the short-range correlations. The peak height $\rho_{\mathrm{max.}}$ of the distribution depends on the interaction strength U and the inset shows its evolution with increasing U. The maximum height of $\rho_{\mathrm{max.}}$ marks the limit of the Tonks-Girardeau regime (see text).

Note that the momentum distribution of the Tonks-Girardeau gas is completely different from that of noninteracting fermions. It has a pronounced zero-momentum peak (like for noninteracting bosons) which is a remnant of the Bose symmetry of the many-particle wave function and long-range tails which decay like $\rho(p) \propto 1/p^4$ for large momenta p [90, 91, 92]. T. Papenbrock found out that the peak height $\rho_{\mathrm{max.}} = \rho(0)$ is proportional to N [89]. Thus, the system of hard-core bosons mimics the macroscopic occupation of the zero-momentum state and in this aspect resembles a noninteracting Bose system. Another aspect, the "shoulders" of the distribution at $|p| \approx 1\,\hbar/l$, presumably originate from the Fridel-type oscillations of the density.

Note further that the momentum distribution of the hard-core bosons (black curve of Fig. 3.6) has the same width as the momentum distribution of the noninteracting fermions (green dashed). That is quite surprising since at first glance the black curve looks much narrower than the green dashed curve. But we have seen that the kinetic energy and thus the width of the momentum densities $w_p^{(\infty)} = N\,\hbar/l = 5\,\hbar/l$ are equal for hard-core bosons and noninteracting fermions.

But what is the origin of the high-momentum tails of the black distribution? We have seen in Fig. 3.2 and in Eq. 3.10 that the Tonks-Girardeau ground state has cusps at coinciding particle positions $x_i = x_j$. We need an infinite number of plain waves to approximate these cusps in the wave function and thus there must be a significant population of high-momentum states. Another argumentation goes as follows: The momentum distribution of the Tonks-Girardeau gas (black curve of Fig. 3.6) has the same width as the distribution of the noninteracting fermions (the green dashed curve). Below the Fermi edge $|p| < 2.5\,\hbar/l$ the hard-core bosons mainly populate the central peak (there is a comparatively large population of momentum states with $|p| < 1\,\hbar/l$)

and thus there must be a sufficiently strong population of high-momentum states above the Fermi edge in order to achieve the same width as for the noninteracting fermion distribution. I note that the high-momentum tails of the distribution are mainly responsible for the increase of the kinetic energy (or width of the momentum distribution) above from $U = 0.5\,\hbar\omega$ since the momentum density is weighted with p^2 in the expectation value $\langle p^2\rangle = \int dp\, p^2 \rho(p)$.

Another interesting aspect concerns the evolution of the height of the central peak. The blue curve in Fig. 3.6 is the momentum distribution of the bosons at $U = 3\,\hbar\omega$. As can be seen the peak height is larger than for noninteracting *and* hard-core bosons. The inset of Fig. 3.6 shows the evolution of the peak height which is largest around $U = 3\,\hbar\omega$. We found the location of this maximum to be independent of the number of particles. The height of the central peak at its maximum is approx. 30% larger than at small interaction strength ($U \approx 0$) and about 20% larger than at large interactions ($U = 20\,\hbar\omega$). This contrast increases with increasing particle number.

What are the two competing mechanisms which cause this behavior? The same effects which are responsible for the minimum of the kinetic energy at $U = 0.5\,\hbar\omega$! Due to the flattening and broadening of the particle density the central peak of the momentum distribution becomes narrower and higher. On the other hand, the formation of short-range correlations at $x = x'$ leads to an increasing population of high momentum states. This effect dominates above $U = 3\,\hbar\omega$, when the growth of the density width slows down thus leading to a redistribution from low- towards high-momentum states. At this point the height of the central peak has reached its maximum. This coincides with the transition behavior visible in the correlation function (see Fig. 3.4). Therefore, the maximum of the peak height marks the transition towards the Tonks-Girardeau regime.

Discrimination between the interaction regimes: Let me give a short summary of the most important results presented so far. Caused by the increasing repulsive interaction the overall boson wave function flattens, broadens and forms short-range correlations, which prevent the bosons from sitting on top of each other. Three interaction regimes can be distinguished: the mean-field and the Tonks-Girardeau regime and an intermediate regime in between. We found the momentum distribution of the boson system to be a reliable indicator for transitions between those three regimes. Its width is extremely sensitive to the formation of short-range correlations and thus the minimum width at $U = 0.5\,\hbar\omega$ clearly marks the limit of the mean-field regime. By contrast, the maximum of the peak height at $U = 3\,\hbar\omega$ marks the transition towards the Tonks-Girardeau regime. The evolution of both features of the momentum distribution is caused by two competing mechanisms, namely, the broadening and flattening of the overall wave function on the one hand and the formation of short-range correlations on the other hand.

Occupation of the single-particle states: I finally discuss the occupation number distribution $\langle n_i\rangle = \langle a_i^\dagger a_i\rangle$ of the harmonic oscillator states which is shown in Fig. 3.7. With increasing interaction strength U the bosons leave the ground state and occupy the excited states of the harmonic trap. At $U = 20\,\hbar\omega$ the distribution is similar to the distribution shown in [86] for $U = \infty$. However, we observe a stronger population of single-particle states with even parity compared to those with odd parity. This effect is most pronounced in mean-field calculations where occupations of odd parity orbitals are absent. Why? The mean-field ground state has even parity (see Fig 3.1), i. e., it is symmetric under horizontal flips, and thus the coefficients of the expansion $\psi_{\text{m.f.}}(x) = \sum_i c_i \psi_i(x)$ with $c_i = \int dx\, \psi_i(x)\psi_{\text{m.f.}}(x)$ are zero for states with odd parity (i. e. states with $i = 1, 3, 5, \ldots$). The comparatively stronger occupation of single-particle states with even parity can therefore be interpreted as another remnant of the mean-field regime. [5] M. Girardeau

[5] Despite the even parity of the *many-particle* ground state, there is nevertheless a significant population of odd-parity *single-particle* wave functions in that state. That is due to the fact that a Fock state $|N_0, N_1, N_2, \ldots\rangle$ (where N_i

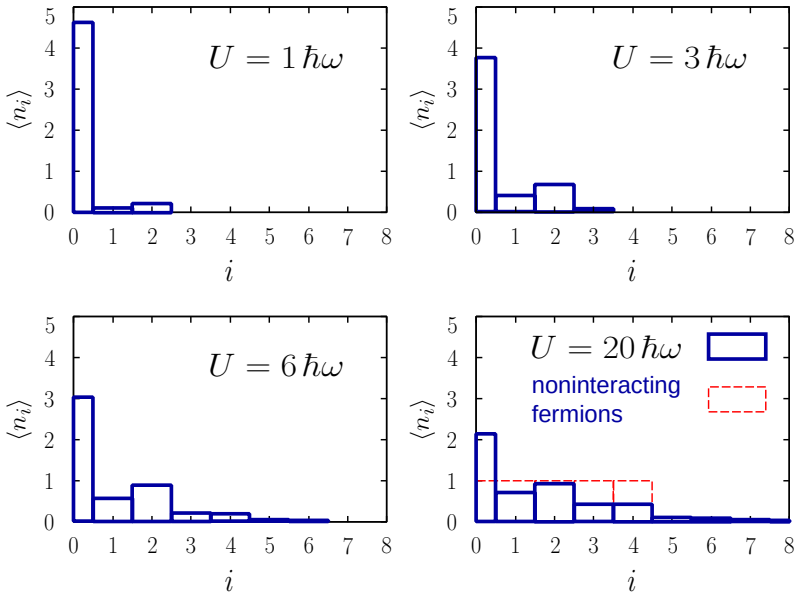

Figure 3.7: Occupation number distribution of the harmonic-oscillator eigenstates of five bosons for different interaction strengths U. With increasing interaction strength U the bosons leave the ground state and occupy excited states. Single-particle states with even parity are comparatively stronger populated than those with odd parity. Note the large population of the ground state in the Tonks-Girardeau limit $\big($given by $\langle n_0 \rangle = \sqrt{N} \gg 1\big)$ due to the permutation symmetry of the wave function and the significant population of high-energy states above the Fermi edge due to the cusps in the wave function at coinciding particle positions $x_i = x_j$.

et al. [86] and T. Papenbrock [89] found out that the population of the lowest *natural orbital* [6] is $\sqrt{N}$. My calculations are in agreement with a population of the *harmonic-oscillator* ground state of $\langle n_0 \rangle = \sqrt{N}$. Again, one sees in Fig. 3.7(bottom right) that the population of the harmonic-oscillator states is completely different for hard-core bosons and noninteracting fermions. The occupation of the harmonic-oscillator ground state is much larger than 1, due to the permutation symmetry of the wave function, and there is a significant population of high-energy states above the Fermi edge due to the cusps in the wave function at coinciding particle positions $x_i = x_j$.

Remarks on the accuracy of my calculations: I already discussed in Sec. 2.9, when I compared the resultant wave function of my numerical diagonalization with the exact analytical two-particle wave function (see Fig. 2.6), that the cusps in the wave function at $x_i = x_j$ are not resolved by our numerical approach although the overlap between both solutions is very close to one. That is no wonder since the singular δ potential does not match up very good with the smooth harmonic-oscillator states (leading to convergence problems similar to Gibbs phenomenon). I guess that the convergence would be significantly improved if the δ potential would be smeared out into a Gaussian of finite width. However, I think that I extensively proved in the previous discussion and in Sec. 2.9 that my calculations in general converged satisfactory. That is in agreement with the commonly known statement that the usual δ potential is unproblematic in one dimension.

Anyway, some results have been more accurately calculated using alternative methods, namely,

is the occupation number of the ith oscillator eigenstate $\psi_i\big)$ with an even-numbered population of odd-parity oscillator functions, $N_1 + N_3 + N_5 + \ldots =$ even, still has even parity in total; see Eq. (2.31).

[6] The "natural orbitals" are defined in Ref. [86] as the eigenfunctions of the reduced single-particle density matrix of the Tonks-Girardeau ground state.

all the properties which crucially depend on the shape of the wave function at $x_i = x_j$. To give some examples: The correlation functions of Fig. 3.4(left) have cusps at $x = x'$ for all nonzero and finite $0 < U < \infty$ $\big($not for $U = 0$ and not for $U = \infty\,!\big)$ as one can derive quickly from the exact two-particle solution of Sec. 2.9 and as has been shown for the infinite homogeneous system [37]. Secondly, I cannot extract a $1/U^2$ decay of the local pair correlation function for large U similar to the results of Ref. [32] but I also obtain the same qualitative behavior; as can be seen in Fig. 3.4(right). The same is true for the $1/p^4$ decay of the high-momentum tails of the distributions of Fig. 3.6.

I have performed calculations with different basis lengths in order to estimate the maximum deviations of the energies of Fig. 3.5 from its "true" values and in order to insure myself that my main statements concerning the momentum distribution are correct. From these calculations I obtained, e. g., the following limiting values of the energies at $U = 20\,\hbar\omega$: $E_{\text{tot., limit}} = 11.78\,\hbar\omega$, $E_{\text{pot., limit}} = 5.69\,\hbar\omega$, $E_{\text{kin., limit}} = 5.07\,\hbar\omega$ and $E_{\text{int., limit}} = 1.02\,\hbar\omega$ while the values of Fig. 3.5 are given by $E_{\text{tot., fig.}} = 12.32\,\hbar\omega$, $E_{\text{pot., fig.}} = 6.13\,\hbar\omega$, $E_{\text{kin., fig.}} = 5.10\,\hbar\omega$ and $E_{\text{int., fig.}} = 1.09\,\hbar\omega$. Thus, the deviation between these energies is 4.6% for the total energy, 7.7% for the potential energy, 0.6% for the kinetic energy and 7.2% for the interaction energy. Moreover, in order ensure myself that the limiting energies are in good agreement with the true energies, I cross-checked the method by means of the exact analytical two-particle solution from which the true energies can be determined with high precision.

More importantly I am confident that my statement holds true that the three interaction regimes can be distinguished by means of the momentum distribution since the underlying two competing mechanisms – the flattening and broadening of the overall wave function and the formation of short-range correlations – persist independent of the precise shape of the wave function at $x_i = x_j$. Again, I determined the minimum of the width and the maximum of the peak height of the momentum distribution independently from the exact analytical two-particle solution in order to cross-check my method. I cannot exclude that the limits of the mean-field regime at $U \approx 0.5\,\hbar\omega$ and of the Tonks-Girardeau regime at $U \approx 3\,\hbar\omega$ weakly depend on the number of particles N. However, for $2 - 7$ particles I could not see a dependency on the number of particles. Thus, I am sure that these values are at least valid for small particle numbers, but, to my knowledge, so far the quasi-one-dimensional strongly interacting regime has not been entered with large particle numbers ($N \sim 15 - 18$ in the experiment of Ref. [22] and ~ 54 in Ref. [21]).

3.5 Excitation spectrum

I close my discussion with a study of the excitation spectrum. First, a few remarks about the energy spectrum in the two limiting regimes of zero and infinite δ repulsion: Both spectra agree apart from the different ground-state energy. For noninteracting bosons the ground-state energy is $E_g^{(0)} = N/2\,\hbar\omega$ and the level spacing is $\Delta E = 1\,\hbar\omega$. The degeneracy of the lowest levels is given by

$$\text{degeneracy} = 1, 1, 2, 3, 5, 7, 10, 13, \ldots \tag{3.13}$$

for the ground state and the lowest seven excited states of five bosons since the lowest occupation number states are given by

$$|5\rangle \to |4,1\rangle \to |3,2\rangle,\ |4,0,1\rangle \to |2,3\rangle,\ |3,1,1\rangle,\ |4,0,0,1\rangle \to \ldots$$

$\big($here the ith position of a number state belongs to the $(i-1)$th single-particle state$\big)$. Since hard-core bosons behave like noninteracting fermions the ground-state energy is $E_g^{(\infty)} = N^2/2\,\hbar\omega$ and

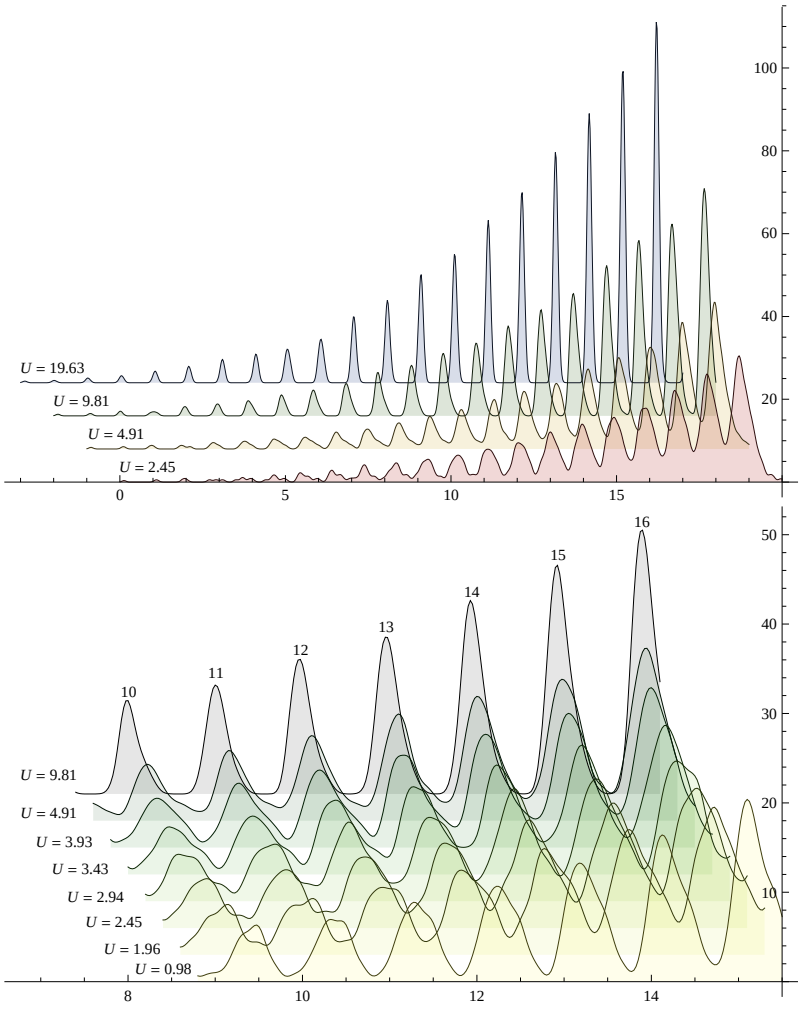

Figure 3.8: Density of states $\rho(E) = dN/dE$ for different interaction strengths U. The excitation energy $(E - E_g)$ above the ground state is plotted along the x-axis. The density of states $\rho(E)$ is plotted along the y-axis. *Top:* $\rho(E)$ in the region $(E - E_g) = 0 \ldots 20\,\hbar\omega$. *Bottom:* $\rho(E)$ in the region $(E - E_g) = 8.5 \ldots 15.5\,\hbar\omega$. (I thank Holger Niehus for the making of this figure.)

the level spacing is $\Delta E = 1\,\hbar\omega$ in the limit of infinite δ repulsion. The degeneracy equals that of noninteracting *bosons* since the lowest fermion states are given by

$$|1,1,1,1,1\rangle \to |1,1,1,1,0,1\rangle \to |1,1,1,1,0,0,1\rangle,\ |1,1,1,0,1,1\rangle$$
$$\to |1,1,1,1,0,0,0,1\rangle,\ |1,1,1,0,1,0,1\rangle,\ |1,1,0,1,1,1,1\rangle \to \ldots\ .$$

Fig. 3.8 shows the density of states $\rho(E) = dN/dE$, i. e., the number of energy levels within the interval $E \ldots E + dE$. What is shown? The excitation energy $(E - E_g)$ above the ground state is plotted along the x-axis, i. e., I always subtracted the ground-state energy so that $\rho(E_g)$ is located at $E = 0$. The density of states $\rho(E)$ is plotted along the y-axis.

The upper picture shall give an overview. It shows the density of states $\rho(E)$ for excitation energies in the region $(E - E_g) = 0 \ldots 20\,\hbar\omega$. The backmost density $\rho(E)$ of the upper picture at $U = 19.63\,\hbar\omega$ belongs to the Tonks-Girardeau gas. Thus, we see sharp δ-like peaks with a separation of $\Delta E = 1\,\hbar\omega$. The height of these peaks grows according to Eq. (3.13). The same structure would

be observed for noninteracting bosons at $U = 0$. In between these limiting regimes we observe a substantial broadening of the peaks but the center of these peaks is still located at $0, 1, 2, \ldots$. The height of the peaks decreases due to the broadening of the peaks, since they consist of the same number of states. I observe the largest broadening of the peaks for an interaction strength of $U = 2.45\,\hbar\omega$. Below and above this point the peaks become narrower and higher when moving from $U = 2.45\,\hbar\omega$ towards $U = 0$ or in the other direction from $U = 2.45\,\hbar\omega$ towards $U = \infty$. This can be clearly seen in the upper picture of Fig. 3.8: The broadest and flattest peaks belong to the density of states at $U = 2.45\,\hbar\omega$ and with increasing U the peaks become narrower and higher; compare with the density of states at $U = 4.91, 9.81$ and $19.63\,\hbar\omega$.

The lower picture of Fig. 3.8 shows the density of states in the region $(E - E_g) \approx 8.5 \ldots 15.5\,\hbar\omega$, i. e., the $10 - 16$th excited level. Here I show more densities $\rho(E)$ around the critical interaction strength $U \approx 2.45\,\hbar\omega$. One sees in the bottom picture of Fig. 3.8 that the peak height is lowest for $U \approx 2.45\,\hbar\omega$ and that it is substantially higher for $U = 0.98$ or $9.81\,\hbar\omega$.

To summarize the result: For zero $(U = 0)$ and infinite δ repulsion $(U = \infty)$ we observe the same energy structure and each energy level is degenerate according to Eq. (3.13). Each multiplet has a finite width w_E for nonzero and finite interaction strengths $0 < U < \infty$. The width w_E of the multiplets is largest for $U \approx 2.5\,\hbar\omega$. This critical point coincides quite well with the limit of the Tonks-Girardeau regime at $U \approx 3\,\hbar\omega$ which we have determined in the previous section from the ground-state behavior. However, despite the broadening of the energy levels (i. e., the broadening of the δ-like peaks) for intermediate repulsions the energy levels are clearly separated from each other for all interaction strengths and the spacing between the levels is always $\Delta E = 1\,\hbar\omega$.

Chapter 4

The spinor Tonks-Girardeau gas

The main results of this chapter have been published in Ref. [4].

Subject of this chapter is a study of spinful one-dimensional bosons with strong δ repulsion. In the first section 4.1, I will derive an exact analytical solution for infinite δ repulsion. This solution is not only valid for spin-1 bosons but for particles with arbitrary permutation symmetry (bosons and fermions) and arbitrary spin. Moreover, it is applicable to Fermi-Fermi and Bose-Bose mixtures. An analytical formula for the spin densities will be given in Sec. 4.3. Derivation of that formula has been given to me by Klaus Fredenhagen [93]. I show the derivation of that formula in appendix A. In Sec. 4.4 I will present selected momentum distributions of the degenerate ground states. These distributions have been obtained from the numerical calculations. In Sec. 4.2 I will finally discuss the structure of the ground-state multiplet for large but finite repulsion. Here I will compare the numerical results to the exact limiting solutions. Similar results have been found recently for mixtures of two different atomic species [69], two-level atoms [70, 71] and spin-$1/2$ fermions[94].

4.1 Analytical solution for hard-core particles with spin

We are searching for the solution of quasi-one-dimensional spin-1 bosons with infinite δ repulsion at zero magnetic field. The Hamiltonian of such a system is given by

$$H = \sum_{i=1}^{N} \left(-\frac{\hbar^2}{2m}\frac{\partial^2}{\partial x_i^2} + \frac{1}{2}m\omega^2 x_i^2 \right) \mathbb{1}^{\otimes N} + \sum_{i<j} \delta(x_i - x_j)\Big(g_0 \mathbb{1}^{\otimes N} + \cancel{g_2 \vec{f}_i \cdot \vec{f}_j} \Big). \tag{4.1}$$

[See Sec. 3.1 for the derivation of a quasi-one-dimensional Hamiltonian from Eq. (2.5).] Here, g_0 is infinite and the value of g_2 is arbitrary. The spin-dependent interaction can be neglected since the wave function is already zero at equal particle positions $x_i = x_j$. Thus, there is no coupling between the spin and the motional degrees of freedom in the limit of infinite repulsion, i. e., the Hamiltonian is diagonal in spin space. It follows that we can restrict ourselves to the solution of the spinless Hamiltonian

$$H = \sum_{i=1}^{N} \left(-\frac{\hbar^2}{2m}\frac{\partial^2}{\partial x_i^2} + \frac{1}{2}m\omega^2 x_i^2 \right) + g_0 \sum_{i<j} \delta(x_i - x_j)\,, \tag{4.2}$$

since we obtain a valid solution of the spinful Hamiltonian (4.1) simply by multiplying an eigenfunction of the spinless Hamiltonian (4.2) with an arbitrary N-particle spin function. If,

e. g., $\psi(x_1, x_2, \ldots, x_N)$ is an eigenfunction of (4.2) then all the 3^N spinful wave functions $\psi(x_1, x_2, \ldots, x_N)|m_1, m_2, \ldots, m_N\rangle$ with $m_1, m_2, \ldots, m_N = 0, \pm 1$ are automatically eigenfunctions of the Hamiltonian (4.1).

So what is the difference to the spinless problem of section 3.3? In the case of spinless bosons the wave function has to be symmetric under any permutation π of the particle coordinates:

$$\psi(x_1, x_2, \ldots, x_N) = \psi\big(x_{\pi(1)}, x_{\pi(2)}, \ldots, x_{\pi(N)}\big).$$

Here, by contrast, the wave function has to be symmetric under any permutation of the combined space-spin indices (x_i, m_i) and it follows that all the single components of the vector-valued wave function are interrelated to each other by the prescription

$$\psi_{m_1,\ldots,m_N}(x_1, \ldots, x_N) = \psi_{m_{\pi(1)},\ldots,m_{\pi(N)}}\big(x_{\pi(1)}, \ldots, x_{\pi(N)}\big).$$

This relation holds true for *any* permutation π if the vector-valued wave function $|\psi\rangle$ describes spinful bosons. That is a big difference to the spinless case, since now it is not excluded that the motional wave functions of the individual spin components $\psi_{m_1,m_2,\ldots,m_N}(x_1, x_2, \ldots, x_N)$ can be nonsymmetric, i. e., it could be that

$$\psi_{m_1,\ldots,m_N}(x_1, \ldots, x_N) \neq \psi_{m_1,\ldots,m_N}\big(x_{\pi(1)}, \ldots, x_{\pi(N)}\big)\,!$$

Consider, e. g., two bosons with spin $f = 1$. Their two-particle (nine-component vector-valued) wave function is given by

$$\psi(x_1, x_2) = \sum_{m_1,m_2=-1,0,1} \psi_{m_1,m_2}(x_1, x_2)|m_1, m_2\rangle\,.$$

This wave function shall be symmetric under the exchange of the space-spin indices of the first and the second particle $(x_1, m_1) \leftrightarrow (x_2, m_2)$ since we are considering bosons and it follows for all of its components

$$\psi_{m_1,m_2}(x_1, x_2) = \psi_{m_2,m_1}(x_2, x_1)\,.$$

So, it follows that the wave-function components $\psi_{1,1}(x_1, x_2)$, $\psi_{0,0}(x_1, x_2)$ and $\psi_{-1,-1}(x_1, x_2)$ are symmetric under the exchange of the coordinates x_1 and x_2. All the other wave-function components $\psi_{1,0}(x_1, x_2)$, $\psi_{1,-1}(x_1, x_2)$, $\psi_{0,1}(x_1, x_2)$, $\psi_{0,-1}(x_1, x_2)$, $\psi_{-1,1}(x_1, x_2)$ and $\psi_{-1,0}(x_1, x_2)$ can, however, be nonsymmetric. They are mutually related to each other, e. g., by the prescription $\psi_{1,0}(x_1, x_2) = \psi_{0,1}(x_2, x_1)$ but both wave-function components can be nonsymmetric under the exchange of x_1 and x_2, i. e., it is not excluded that $\psi_{1,0}(x_1, x_2) \neq \psi_{1,0}(x_2, x_1)$ and $\psi_{0,1}(x_1, x_2) \neq \psi_{0,1}(x_2, x_1)$.

In order to find the bosonic eigenfunctions of the spinful Hamiltonian (4.1), we therefore construct in a first step all the eigenfunctions of the spinless Hamiltonian (4.2). These solutions do not need to be permutationally symmetric or antisymmetric. Thus, they describe distinguishable spinless particles with infinite δ repulsion. Similar to Eq. (3.6) the following set of equations and boundary conditions has to be solved:

$$\psi \text{ solves} \quad \sum_{i=1}^{N}\left(-\frac{\hbar^2}{2m}\frac{\partial^2}{\partial x_i^2} + \frac{1}{2}m\omega^2 x_i^2\right)\psi = E\psi \quad \text{in } \mathbb{R}^N \setminus \{x_i = x_j\} \tag{4.3a}$$

$$\psi(x_1, x_2, \ldots, x_N) = 0 \quad \text{on the surface } \{x_i = x_j\} \tag{4.3b}$$

$$\psi \text{ does not need to obey any exchange symmetry!} \tag{4.3c}$$

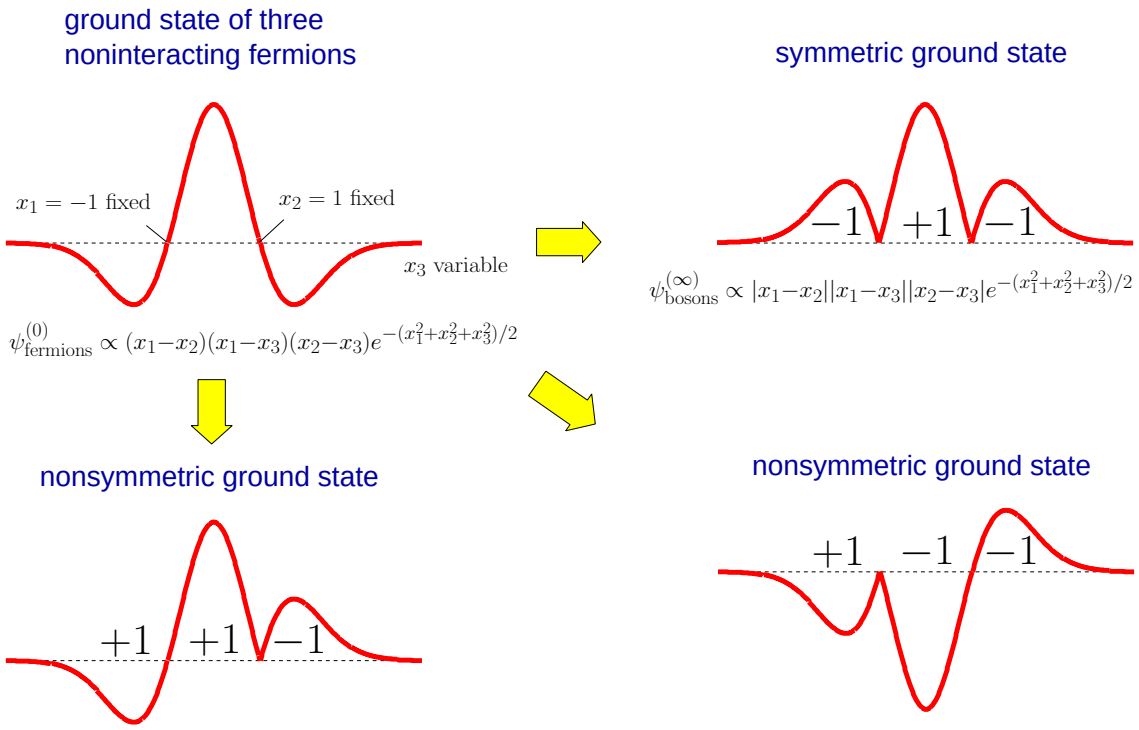

Figure 4.1: Construction of nonsymmetric ground states from the ground-state Slater determinant of three fermions. Since no permutation symmetry is required one can assign ± 1 values at will to each sector C_π of the configuration space $\mathbb{R}^N$. By means of this procedure one can construct $2^{N!}$ ground states of distinguishable particles since the configuration space $\mathbb{R}^N$ decomposes into $N!$ different sectors C_π and in each sector we can choose for $+1$ or -1. But these states are not orthonormal and even linearly dependent.

So, while in Sec. 3.3 we have constructed a bosonic wave function from a Slater determinant, we are now trying to construct wave functions of distinguishable particles from a Slater determinant.

What possibilities do we have to construct nonsymmetric wave functions from a given Slater determinant? In Sec. 3.3 we have multiplied the Slater determinant with the "unit antisymmetric function" (3.7) in order to construct a wave function which is permutationally symmetric under any exchange of particle coordinates. I discussed in Sec. 3.3 that the "unit antisymmetric function" A is $+1$ in all the sectors C_π [see Eq. (3.9) for the definition], where the order of the coordinates $x_{\pi(1)} < \cdots < x_{\pi(N)}$ is given by an even permutation π and -1 if π is odd. One first idea is therefore to multiply the Slater determinant with ± 1 signs at will in each sector C_π in order to construct all the valid wave functions if no permutation symmetry is required [69]. This idea is illustrated in Fig. 4.1:

Starting from the ground-state Slater determinant one can multiply in each sector with ± 1 values at will and thereby flip vertically the corresponding part of the wave function (if multiplied with -1) or leave it unaffected (if multiplied with $+1$). By means of this procedure one can construct $2^{N!}$ ground states of distinguishable particles, since the configuration space $\mathbb{R}^N$ decomposes into $N!$ different sectors C_π and in each sector one can choose for a $+1$ or -1 sign. A big disadvantage of this method is that the ground states constructed in that way are not orthonormal. Moreover, it turns out that most of these ground states are linear superpositions of the others.

A basis for spinless, distinguishable hard-core particles: In order to construct an orthonormal

basis of the space of nonsymmetric ground states we try the ansatz:

$$\langle x_1, \ldots, x_N|\pi\rangle \equiv \begin{cases} \sqrt{N!}\, A\, \psi^{(0)}_{\text{fermion gr.}} & \text{if } x_{\pi(1)} < \cdots < x_{\pi(N)} \\ 0 & \text{otherwise}\,, \end{cases} \tag{4.4}$$

i. e., we take the boson ground state $\psi^{(\infty)}_{\text{boson gr.}} = A\,\psi^{(0)}_{\text{fermion gr.}}$, restrict that wave function to the region C_π and multiply with the prefactor $\sqrt{N!}$ in order to normalize it. These states are orthogonal by construction, since each state $\psi_\pi(x_1, \ldots, x_N) = \langle x_1, \ldots, x_N|\pi\rangle$ is nonzero only in the corresponding region C_π and there is no overlap between different regions C_π and $C_{\pi'}$. Further, they are normalized, since

$$\begin{aligned} \langle\pi|\pi\rangle &= N! \int_{x_{\pi(1)}<\ldots<x_{\pi(N)}} dx_1 \ldots dx_N \cancel{A^2} \left[\psi^{(0)}_{\text{fermion gr.}}(x_1, \ldots, x_N)\right]^2 \\ &= \int_{\mathbb{R}^N} dx_1 \ldots dx_N \left[\psi^{(0)}_{\text{fermion gr.}}(x_1, \ldots, x_N)\right]^2 = 1\,. \end{aligned}$$

In the second step of the calculation I extended the integration from the region C_π to the whole configuration space $\mathbb{R}^N$ and I used the symmetry of the square of the Fermi ground state

$$\left[\psi^{(0)}_{\text{fermion gr.}}\big(x_{\pi(1)}, \ldots, x_{\pi(N)}\big)\right]^2 = \left[\psi^{(0)}_{\text{fermion gr.}}(x_1, \ldots, x_N)\right]^2.$$

I note that all the wave functions (4.4) have the same ground-state energy $E_g = N^2/2\,\hbar\omega$ so that the space of ground states is $N!$ times degenerate $\big($there are $N!$ different permutations of N different items and thus $N!$ disjoint regions $C_\pi\big)$. Moreover, the result (4.4) for the ground state can be generalized to an arbitrary Slater determinant $\psi^{(0)}_{i\text{th fermion st.}}(x_1, x_2, \ldots, x_N)$ and is thus also valid for the excited states, i. e., one can construct $N!$ nonsymmetric orthonormal states from the ith Slater determinant of the noninteracting fermions. Correspondingly, the energies of these states are given by the energy of that Slater determinant $E_i = E\left[\psi^{(0)}_{i\text{th fermion st.}}\right]$.

The wave functions (4.4) look a bit strange but they are a valid solution of the set of equations (4.3): Each wave function $\psi_\pi(x_1, \ldots, x_N) = \langle x_1, \ldots, x_N|\pi\rangle$ is a solution of the Schrödinger equation (4.3a) in the region C_π, since it is proportional to the ground state of noninteracting fermions. Outside the region C_π it is zero and thus trivially solves (4.3a). Moreover, $\psi_\pi(x_1, \ldots, x_N)$ is zero on the surface $\{x_i = x_j\}$ as required by the boundary condition (4.3b).

Let us look at the two-particle ground states of Fig. 4.2 to become more familiar with these solutions: As discussed in Sec. 3.3 the fermion and boson ground states are given by

$$\psi^{(0)}_{\text{fermion gr.}} \propto (x_1 - x_2)\, e^{-(x_1^2+x_2^2)/2} \quad \text{and} \quad \psi^{(\infty)}_{\text{boson gr.}} \propto |x_1 - x_2|\, e^{-(x_1^2+x_2^2)/2}\,,$$

respectively. Since there are no symmetry restrictions we can superimpose both solutions. The sum of both solutions is the nonsymmetric basis state

$$\psi^{(0)}_{\text{fermion gr.}} + \psi^{(\infty)}_{\text{boson gr.}} = |\pi_{12}\rangle = \begin{cases} \sqrt{2!}\,\psi^{(\infty)}_{\text{boson gr.}} & \text{if } x_2 < x_1 \\ 0 & \text{if } x_1 < x_2\,, \end{cases}$$

where $\pi_{12}(1) = 2$, $\pi_{12}(2) = 1$ exchanges the two indices. The difference of both solutions results in the nonsymmetric basis state

$$\psi^{(0)}_{\text{fermion gr.}} - \psi^{(\infty)}_{\text{boson gr.}} = |\text{id}\rangle = \begin{cases} \sqrt{2!}\,\psi^{(\infty)}_{\text{boson gr.}} & \text{if } x_1 < x_2 \\ 0 & \text{if } x_2 < x_1\,, \end{cases}$$

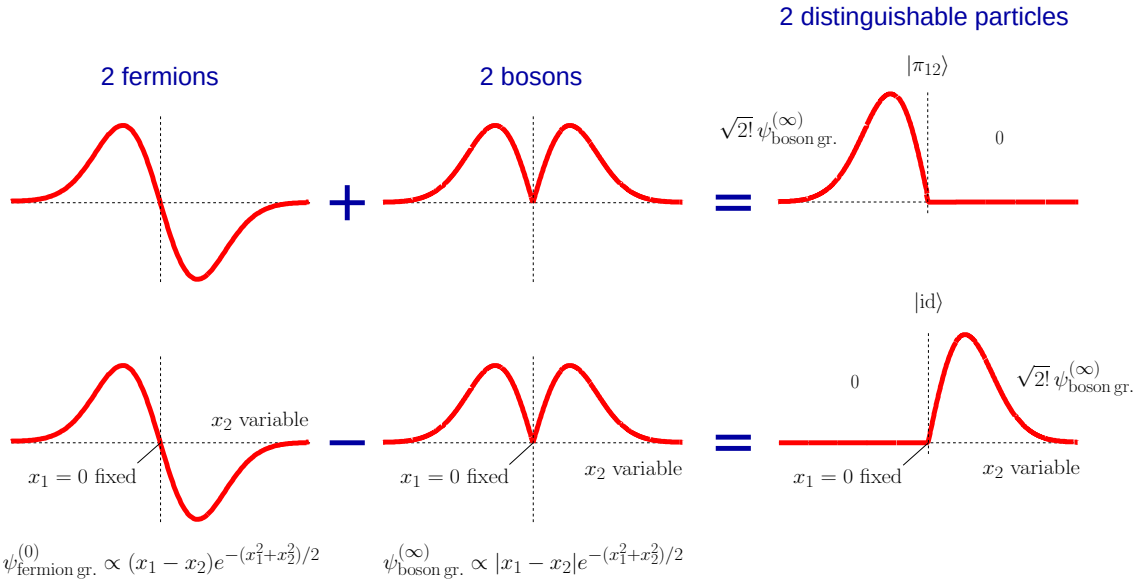

Figure 4.2: Construction of nonsymmetric spinless wave functions of two distinguishable particles. The states $|\pi_{12}\rangle$ and $|\mathrm{id}\rangle$ form a basis of the twofold degenerate space of ground states. The nonsymmetric basis states are superpositions of the fermion and the boson ground states.

where $\mathrm{id}(1) = 1$, $\mathrm{id}(2) = 2$ is the identical permutation. Both solutions describe distinguishable particles since they are nonsymmetric. There are no further basis states since the configuration space $\mathbb{R}^2$ can only be decomposed into the two disjoint regions $C_{\mathrm{id}} = \{(x_1, x_2) \in \mathbb{R}^2, x_1 < x_2\}$ and $C_{\pi_{12}} = \{(x_1, x_2) \in \mathbb{R}^2, x_2 < x_1\}$. Thus the space of ground states is twofold degenerate.

Analytical solution for spinful hard-core particles: Actually, the main work has already been done, namely, to construct nonsymmetric motional wave functions which account for the infinite δ repulsion. The wave functions (4.4) for distinguishable particles solve the Hamiltonian (4.2). As discussed before, we need only to multiply one of the spinless solutions with an arbitrary many-particle spin function $|\chi\rangle$ (e. g. $|\chi\rangle = |m_1, m_2, \ldots, m_N\rangle$ or any superposition of these states) in order to obtain a (spinful) solution of the Hamiltonian (4.1):

$$\left|\psi^{(\infty)}_{\text{spinful particle gr.}}\right\rangle = |\pi\rangle \otimes |\chi\rangle\,.$$

However, these solutions are nonsymmetric and thus describe distinguishable hard-core particles with spin. In order to describe bosons one has to symmetrize this nonsymmetric wave function:

$$\left|\psi^{(\infty)}_{\text{spinful boson gr.}}\right\rangle = \sqrt{N!}\,P_S\left(|\pi\rangle \otimes |\chi\rangle\right). \tag{4.5}$$

Here, I introduced the projection into the subspace of the permutationally symmetric wave functions

$$P_S = \frac{1}{N!}\sum_{\pi \epsilon S_N} U(\pi)\,.$$

S_N is the symmetric group, i. e., the set of all bijective functions from $\{1, 2, \ldots, N\}$ to $\{1, 2, \ldots, N\}$, or, in other words, the set of all permutations of the numbers $1, 2, \ldots, N$. $U(\pi)$ is the permutation operator which exchanges particle indices according to the permutation

$$\pi = \begin{pmatrix} 1 & 2 & \ldots & N \\ \pi(1) & \pi(2) & \ldots & \pi(N) \end{pmatrix}$$

with $\pi(i) \in \{1, 2, \ldots, N\}$ and $\pi(i) \neq \pi(j)$. $U(\pi)$ acts as follows on an arbitrary state $\big|\alpha_1, \alpha_2, \ldots, \alpha_N\big\rangle$ $\big($where α_i are some quantum numbers of the same kind$\big)$ [95]:

$$\begin{aligned} U(\pi)\big|\alpha_1, \alpha_2, \ldots, \alpha_N\big\rangle &= U(\pi)\big|\alpha_1\big\rangle_1 \otimes \big|\alpha_2\big\rangle_2 \otimes \ldots \otimes \big|\alpha_N\big\rangle_N \\ &= \big|\alpha_1\big\rangle_{\pi(1)} \otimes \big|\alpha_2\big\rangle_{\pi(2)} \otimes \ldots \otimes \big|\alpha_N\big\rangle_{\pi(N)} \\ &= \big|\alpha_{\pi^{-1}(1)}\big\rangle_1 \otimes \big|\alpha_{\pi^{-1}(2)}\big\rangle_2 \otimes \ldots \otimes \big|\alpha_{\pi^{-1}(N)}\big\rangle_N \\ &= \big|\alpha_{\pi^{-1}(1)}, \alpha_{\pi^{-1}(2)}, \ldots, \alpha_{\pi^{-1}(N)}\big\rangle\,. \end{aligned} \tag{4.6}$$

Since $U(\pi)$ is unitary [95]

$$U^\dagger(\pi) = U^{-1}(\pi) = U\big(\pi^{-1}\big)$$

it follows that

$$\big\langle\alpha_1, \alpha_2, \ldots, \alpha_N\big|U(\pi) = \Big[U\big(\pi^{-1}\big)\big|\alpha_1, \alpha_2, \ldots, \alpha_N\big\rangle\Big]^\dagger = \big\langle\alpha_{\pi(1)}, \alpha_{\pi(2)}, \ldots, \alpha_{\pi(N)}\big|\,.$$

Thus, the amplitude of some wave function $U(\pi)|\psi\rangle$ at position $\big|x_1, x_2, \ldots, x_N\big\rangle$ is given by [95]

$$\big\langle x_1, x_2, \ldots, x_N\big|U(\pi)\big|\psi\big\rangle = \big\langle x_{\pi(1)}, x_{\pi(2)}, \ldots, x_{\pi(N)}\big|\psi\big\rangle = \psi\big(x_{\pi(1)}, x_{\pi(2)}, \ldots, x_{\pi(N)}\big)\,. \tag{4.7}$$

Using the above relations (4.6), (4.7) and Eq. (4.4) we obtain the following formula for the action of the permutation operator $U(\pi)$ on the ground state $|\pi'\rangle \otimes |m_1, m_2, \ldots, m_N\rangle$:

$$U(\pi)\big|\pi'\big\rangle \otimes \big|m_1, m_2, \ldots, m_N\big\rangle = \big|\pi \circ \pi'\big\rangle \otimes \big|m_{\pi^{-1}(1)}, m_{\pi^{-1}(2)}, \ldots, m_{\pi^{-1}(N)}\big\rangle \tag{4.8}$$

where $\pi \circ \pi'$ is the composition of the permutations π and π'. Now we have collected all the calculation rules which we need to understand Eq. (4.5).

Since one can choose between $N!$ different orbital wave functions $|\pi\rangle$ and 3^N different spin functions $|m_1, m_2, \ldots, m_N\rangle$ $\big($with $m_i = -1, 0, 1\big)$, one might think that the ground state of the hard-core bosons is $N! \times 3^N$ times degenerate. But that is not the case. Instead, it turns out that most of the states constructed by the prescription (4.5) are linearly dependent. If we choose, e. g., the product wave function $|\pi\rangle \otimes |1, 1, \ldots, 1\rangle$ then we obtain by means of Eqs. (4.5) and (4.8) the boson ground state

$$\big|\psi^{(\infty)}_{\text{spinful boson gr.}}\big\rangle = \frac{1}{\sqrt{N!}} \sum_{\pi' \epsilon S_N} |\pi' \circ \pi\rangle \otimes |1, 1, \ldots, 1\rangle\,.$$

Using Eq. (4.4) we see that

$$\sum_{\pi' \epsilon S_N} |\pi' \circ \pi\rangle = \sum_{\pi'' \circ \pi^{-1} \epsilon S_N} \big|\pi''\big\rangle = \sum_{\pi'' \epsilon S_N} \big|\pi''\big\rangle = \sqrt{N!}\, A\, \psi^{(0)}_{\text{fermion gr.}} = \sqrt{N!}\, \psi^{(\infty)}_{\text{boson gr.}}\,.$$

In the first step I substituted $\pi'' = \pi' \circ \pi \;\Rightarrow\; \pi'' \circ \pi^{-1} = \pi' \circ \pi \circ \pi^{-1} \;\Rightarrow\; \pi'' \circ \pi^{-1} = \pi'$ and in the second step I changed the order of the summation. In Eq. (4.4) we have decomposed the (spinless) wave function $A\, \psi^{(0)}_{\text{fermion gr.}}$ along the boundaries of the sectors C_π in order to obtain a basis for spinless distinguishable particles. Thus, we get back the original state $A\, \psi^{(0)}_{\text{fermion gr.}}$ if we sum up all the components $\sum_{\pi \epsilon S_N} |\pi\rangle$. In the last step I used Girardeau's Fermi-Bose map (3.8) for spinless particles. We finally obtain

$$\big|\psi^{(\infty)}_{\text{spinful boson gr.}}\big\rangle = \psi^{(\infty)}_{\text{boson gr.}} \otimes |1, 1, \ldots, 1\rangle \tag{4.9}$$

$\big($where $\psi^{(\infty)}_{\text{boson gr.}}$ is the spinless boson ground state$\big)$. We see that the final result (4.9) does not depend on the choice of the orbital wave function $|\pi\rangle$ and thus all the $N!$ initial states $\big\{|\pi\rangle \otimes |1,1,\ldots,1\rangle,\ \text{with } \pi \in S_N\big\}$ lead to the same boson state (4.9). So, what remains to do is to find a construction scheme for a basis of the space of ground states with Bose symmetry.

Map for bosons: Such a basis can be directly constructed from an *arbitrary* basis of the N-particle spin space by means of the unitary map

$$W = \sqrt{N!}\, P_S\, |\text{id}\rangle \otimes \mathbb{1}_{\text{spin}} \qquad (4.10)$$

where id is the identical permutation and where $\mathbb{1}_{\text{spin}}$ is the identity in spin space. So, when we apply the map W to an arbitrary spin function $|\chi\rangle$ then we obtain the boson ground state

$$\big|\psi^{(\infty)}_{\text{spinful boson gr.}}\big\rangle = W|\chi\rangle = \sqrt{N!}\, P_S \Big(|\text{id}\rangle \otimes |\chi\rangle\Big)\,.$$

In the following I will proof the most important properties of the map W. First, ***W* is linear** since the tensor product is bilinear and since P_S is linear.

***W* preserves the scalar product:** The scalar product of two boson ground states $W|\chi\rangle$ and $W|\chi'\rangle$ is given by

$$\langle\chi|W^\dagger W|\chi'\rangle = N!\langle\chi| \otimes \langle\text{id}|P_S|\text{id}\rangle \otimes |\chi'\rangle = \sum_{\pi\in S_N} \langle\chi| \otimes \langle\text{id}|\pi\rangle \otimes \big[U(\pi)|\chi'\rangle\big] = \langle\chi|\chi'\rangle\,.$$

In the second step I used that P_S is self-adjoined $P_S^\dagger = P_S$ and a projection operator $P_S^2 = P_S$, and in the last step I used the orthonormality of the nonsymmetric orbitals $\langle\text{id}|\pi\rangle = \delta_{\text{id},\pi}$. Thus, if the two spin states $|\chi\rangle$ and $|\chi'\rangle$ are orthogonal then the two boson ground states $W|\chi\rangle$ and $W|\chi'\rangle$ are also orthogonal, and if the spin state $|\chi\rangle$ is normalized then the boson ground state $W|\chi\rangle$ is also normalized. It follows that ***W* is** also **injective**.

***W* is surjective:** An arbitrary boson ground state $|\psi\rangle$ is a superposition of the states (4.5)

$$|\psi\rangle = \sum_{\pi\, m_1\ldots m_N} c_{\pi m_1\ldots m_N} \Big(\sqrt{N!}\, P_S\, |\pi\rangle \otimes |m_1, m_2, \ldots, m_N\rangle\Big)\,.$$

By using $|\pi\rangle \otimes |m_1, m_2, \ldots, m_N\rangle = U(\pi)|\text{id}\rangle \otimes \big|m_{\pi(1)}, m_{\pi(2)}, \ldots, m_{\pi(N)}\big\rangle$ and $P_S U(\pi) = P_S$ we obtain

$$|\psi\rangle = \sqrt{N!}\, P_S\, |\text{id}\rangle \otimes \Bigg(\underbrace{\sum_{\pi\, m_1\ldots m_N} c_{\pi m_1\ldots m_N} \big|m_{\pi(1)}, m_{\pi(2)}, \ldots, m_{\pi(N)}\big\rangle}_{=|\phi\rangle}\Bigg) = W|\phi\rangle\,.$$

Here we used the bilinearity of the tensor product and the linearity of P_S. Thus, for any boson ground state $|\psi\rangle$ there exists a spin function $|\phi\rangle$ with $|\psi\rangle = W|\phi\rangle$.

Therefore, the map W from the spin space into the space of boson ground states is linear, **bijective** and it preserves the scalar product — and thus it is unitary. Due to the bijectivity of the map W we can immediately determine the degeneracy of the boson ground state, which is given by the dimension of the spin space.

Another useful feature is that ***W* commutes with the *z*-component and the square of the total spin**, $F_z = \sum_{i=1}^N f_{z,i}$ and $\vec{F}^2 = \left(\sum_{i=1}^N \vec{f}_i\right)^2$, i. e.,

$$\left(\mathbb{1}_{\text{pos.}} \otimes F_z\right) W = W F_z \quad \text{and} \quad \left(\mathbb{1}_{\text{pos.}} \otimes \vec{F}^2\right) W = W \vec{F}^2$$

$\left(\mathbb{1}_{\text{pos.}}\right.$ is the identity in position space$\left.\right)$. The proof uses the fact that $\left(\mathbb{1}_{\text{pos.}} \otimes F_z\right)$ and $\left(\mathbb{1}_{\text{pos.}} \otimes \vec{F}^2\right)$ are symmetric under any exchange of particle indices so that they commute with P_S:

$$\begin{aligned}&\left(\mathbb{1}_{\text{pos.}} \otimes F_z\right) W = \sqrt{N!}\, P_S \left(\mathbb{1}_{\text{pos.}} \otimes F_z\right) |\text{id}\rangle \otimes \mathbb{1}_{\text{spin}} = \sqrt{N!}\, P_S\, |\text{id}\rangle \otimes F_z \\ &= \left[\sqrt{N!}\, P_S\, |\text{id}\rangle \otimes \mathbb{1}_{\text{spin}}\right] F_z = W F_z\end{aligned}$$

$\left(\text{and analog for } \vec{F}^2\right)$. Therefore, if the spin function $|\chi\rangle$ is an F_z and $\vec{F}^2$ eigenfunction with the eigenvalues F and M_F then the boson ground state $W|\chi\rangle$ is also an $\left(\mathbb{1}_{\text{pos.}} \otimes F_z\right)$ and $\left(\mathbb{1}_{\text{pos.}} \otimes \vec{F}^2\right)$ eigenfunction with the same eigenvalues F and M_F.

Construction of a basis of the space of ground states: A basis of the space of ground states can be directly constructed from an arbitrary basis of the N-particle spin space. One may, for example, choose the spin functions $|m_1, m_2, \ldots, m_N\rangle$ $(m_i = -1, 0, 1)$ as a basis of the N-particle spin space in order to construct the basis wave functions $W|m_1, m_2, \ldots, m_N\rangle$ of the space of boson ground states. In other situations it might be better to choose a basis of spin functions which are simultaneously eigenfunctions of F_z and $\vec{F}^2$.

Map for fermions: It is obvious that one obtains a solution with Fermi symmetry if one replaces P_S by P_A in Eq. (4.10)

$$W' = \sqrt{N!}\, P_A\, |\text{id}\rangle \otimes \mathbb{1}_{\text{spin}} \tag{4.11}$$

where

$$P_A = \frac{1}{N!} \sum_{\pi \epsilon S_N} \text{sign}(\pi) U(\pi)$$

is the projection into the subspace of the permutationally antisymmetric wave functions. The function sign(π) is $+1$ if π is even and -1 if π is an odd permutation. The previously discussed properties of W hold also for W' since similarly $P_A^\dagger = P_A$ and $P_A^2 = P_A$ but $P_A U(\pi) = \text{sign}(\pi) P_A$ (but that difference is not relevant in the proof of the surjectivity).

The map W' allows for the direct construction of a ground state of spinful hard-core fermions from an arbitrary spin function. I note that two fermions do not feel the δ interaction if they are in the same single-particle spin state, but they feel it if they occupy different spin states.

The map works with arbitrary spin functions: The previous discussion was not restricted to specific single-particle spin functions. So, in principle, Eqs. (4.10) and (4.11) work for bosons or fermions with spin $1/2$, 1, $3/2$, 2, $\ldots$. Thus, since spin-$1/2$ bosons [1] (or spin-$1/2$ fermions) with a fixed z-component of the total spin F_z can be mapped to Bose-Bose mixtures (or Fermi-Fermi mixtures) and vice versa, formulas (4.10) and (4.11) can also be used to describe these mixtures of hard-core particles [69].

Equivalence of spin-$1/2$ *systems and mixtures*— A many-particle state of a mixture of a- and b-bosons is represented by the Fock state $|N_{0a}, N_{0b}, N_{1a}, N_{1b}, \ldots\rangle$, where $N_{ia/b}$ is the number of

[1] In Ref. [46] ^{87}Rb in spin states $|\uparrow\rangle \equiv |f = 2, m = 1\rangle$ and $|\downarrow\rangle \equiv |f = 1, m = -1\rangle$ has been used to realize isospin-$1/2$ Bose systems.

a/b-bosons which occupy the ith oscillator eigenstate ψ_i. Here, I consider the case that the a- and b-bosons have (nearly) equal masses, which could be realized by choosing different isotopes of an alkali element. The Hamiltonian of such a Bose-Bose mixture is given by [43]

$$H_{\text{mix.}} = \sum_{\alpha=a,b} \int dx\, \hat{\Psi}^\dagger_\alpha(x) \left[-\frac{\hbar^2}{2m} \frac{d^2}{dx^2} + \frac{1}{2} m\omega^2 x^2 \right] \hat{\Psi}_\alpha(x) + \sum_{\alpha=a,b} \frac{g_\alpha}{2} \int dx\, \hat{\Psi}^\dagger_\alpha(x) \hat{\Psi}^\dagger_\alpha(x) \hat{\Psi}_\alpha(x) \hat{\Psi}_\alpha(x) + g_{ab} \int dx\, \hat{\Psi}^\dagger_a(x) \hat{\Psi}^\dagger_b(x) \hat{\Psi}_b(x) \hat{\Psi}_a(x)\,,$$

where g_α ($\alpha = a, b$) and g_{ab} are the intra- and interatomic interaction strengths. The Hamiltonian can also be written in the form

$$H_{\text{mix.}} = \sum_{\alpha=a,b} \int dx\, \hat{\Psi}^\dagger_\alpha(x) \left[-\frac{\hbar^2}{2m} \frac{d^2}{dx^2} + \frac{1}{2} m\omega^2 x^2 \right] \hat{\Psi}_\alpha(x) + \sum_{\alpha,\beta,\gamma,\delta=a,b} \frac{g_{\alpha\beta\gamma\delta}}{2} \int dx\, \hat{\Psi}^\dagger_\alpha(x) \hat{\Psi}^\dagger_\beta(x) \hat{\Psi}_\gamma(x) \hat{\Psi}_\delta(x)$$

with $g_{aaaa} \equiv g_a$, $g_{bbbb} \equiv g_b$, $g_{abab} = g_{abba} = g_{baab} = g_{baba} \equiv g_{ab}/2$ and $g_{\alpha\beta\gamma\delta} \equiv 0$ otherwise. Similarly, a many-particle state of spin-$1/2$ bosons is represented by the Fock state $|N_{0\uparrow}, N_{0\downarrow}, N_{1\uparrow}, N_{1\downarrow}, \ldots\rangle$, where $N_{i\uparrow}$ ($N_{i\downarrow}$) is the occupation number of the eigenstate $\psi_i|\uparrow\rangle$ ($\psi_i|\downarrow\rangle$) with ψ_i being the ith oscillator eigenstate and with the spin function $|\uparrow\rangle$ ($|\downarrow\rangle$). The Hamiltonian of such a spin system is given by [52]

$$H_{\text{spin}} = \sum_{\alpha=\uparrow,\downarrow} \int dx\, \hat{\Psi}^\dagger_\alpha(x) \left[-\frac{\hbar^2}{2m} \frac{d^2}{dx^2} + \frac{1}{2} m\omega^2 x^2 \right] \hat{\Psi}_\alpha(x) + \sum_{\alpha,\beta,\gamma,\delta=\uparrow,\downarrow} \frac{g_{\alpha\beta\gamma\delta}}{2} \int dx\, \hat{\Psi}^\dagger_\alpha(x) \hat{\Psi}^\dagger_\beta(x) \hat{\Psi}_\gamma(x) \hat{\Psi}_\delta(x)\,.$$

Thus, by replacing a- and b- by $\uparrow$- and $\downarrow$-labels, we obtain the Fock states and the Hamiltonian of a spin-$1/2$ system from those of a Bose-Bose mixture. If the number of a- and b-bosons is given by $N_a = \sum_i N_{ia}$ and $N_b = \sum_i N_{ib}$, then the magnetization of the corresponding spin-$1/2$ Bose system is given by $F_z = N_a - N_b$.

Excited states: As discussed before, one can use an arbitrary Slater determinant of the spinless noninteracting fermions $\psi^{(0)}_{i\text{th fermion st.}}$ instead of the ground state in Eq. (4.4). This means that one can similarly decompose the ith eigenstate of the spinless noninteracting fermions $\psi^{(0)}_{i\text{th fermion st.}}$ along the boundaries of the sectors C_π and thereby obtain $N!$ nonsymmetric orbitals $|\pi_i\rangle$. Therefore, one can similarly construct a map W_i (or W_i') by using the ith eigenfunction of the spinless noninteracting fermions

$$W_i = \sqrt{N!}\, P_S\, |\text{id}_i\rangle \otimes \mathbb{1}_{\text{spin}}$$

where $\langle x_1, x_2, \ldots, x_N|\text{id}_i\rangle = \sqrt{N!}\, A\, \psi^{(0)}_{i\text{th fermion st.}}$ if $x_1 < x_2 < \ldots < x_N$ and zero otherwise (for W_i' one has to use P_A instead). By applying W_i to an arbitrary spin function $|\chi\rangle$,

$$W_i|\chi\rangle = \sqrt{N!}\, P_S \left(|\text{id}_i\rangle \otimes |\chi\rangle \right), \tag{4.12}$$

one obtains similarly a state of spinful bosons with an excited motional energy E_i $\big($where E_i is the energy of the spinless noninteracting fermion state $\psi^{(0)}_{i\text{th fermion st.}}\big)$.

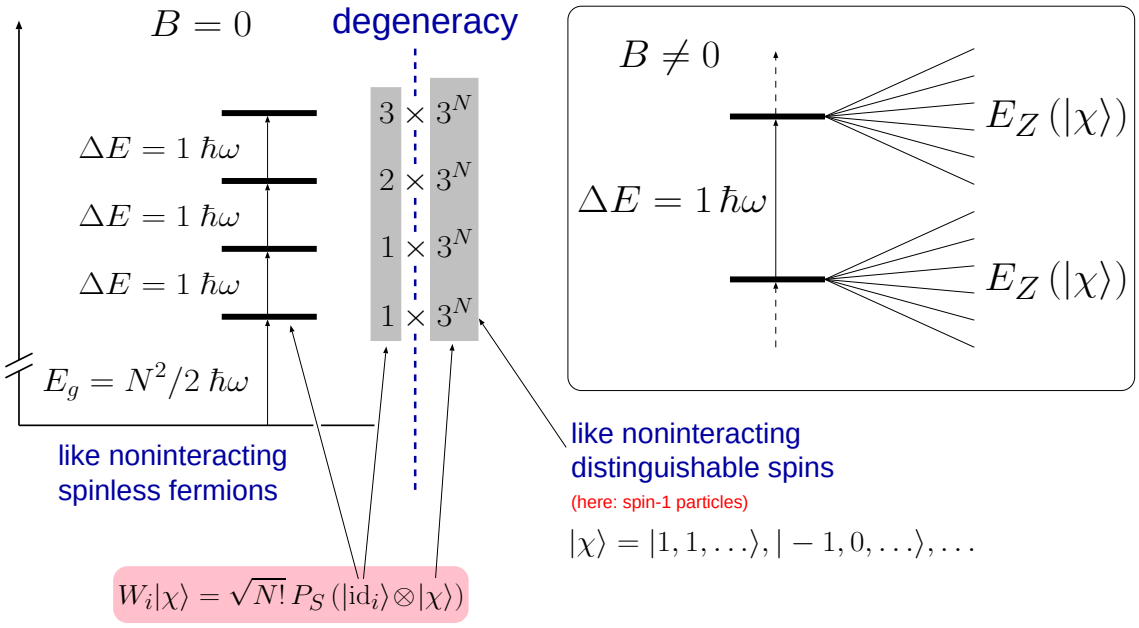

Figure 4.3: Energy spectrum of spin-1 bosons. At zero magnetic field the ground-state energy and the level spacing equal those of noninteracting spinless fermions. The degeneracy of each level equals the degeneracy of the corresponding level of the noninteracting spinless fermions multiplied by the dimension of the spin space. Here, we consider spin-1 particles and thus the dimension of the spin space is 3^N. The degenerate levels split up when a magnetic field is applied. The energy shift of the boson wave function $W_i|\chi\rangle$ is given by the Zeeman energy of its spin function $E_Z(|\chi\rangle)$.

Consequences: In the previous text I constructed the wave functions of spinful hard-core particles (bosons and fermions) from the wave functions of noninteracting spinless fermions and from the wave functions of noninteracting distinguishable spins. The consequences of the mapping functions Eqs. (4.10) and (4.11) can thus be summarized as follows:

> *"One-dimensional hard-core particles (bosons or fermions) with spin degrees of freedom behave like noninteracting spinless fermions and noninteracting distinguishable spins."*

Energy spectrum: The dual behavior of one-dimensional hard-core particles with spin is especially reflected in the energy spectrum and the (spin) densities (which I will show later in Sec. 4.3). In Fig. 4.3 the energy spectrum of spin-1 hard-core bosons is shown as an example. A direct consequence of the mapping (4.10) and its generalization to the excited states (4.12) is that the energy of the boson state $W_i|\chi\rangle$ is given by the sum of the motional energy of the spinless noninteracting fermions $E_i = E\left[\psi^{(0)}_{i\text{th fermion st.}}\right]$ and the Zeeman energy $E_Z\left[|\chi\rangle\right]$ of the spin function $|\chi\rangle$,

$$E\left[W_i|\chi\rangle\right] = E\left[\psi^{(0)}_{i\text{th fermion st.}}\right] + E_Z\left[|\chi\rangle\right]. \tag{4.13}$$

Thus, at zero magnetic field $B = 0$, we observe the same energy eigenvalues as for the spinless one-dimensional noninteracting fermions since $E_Z\left[|\chi\rangle\right] = 0$, i. e., the ground-state energy is

$E_g = N^2/2\,\hbar\omega$ and the level spacing is $\Delta E = 1\,\hbar\omega$, as shown in Fig. 4.3(left). However, the degeneracy of the energy levels is much larger: The second consequence of the mappings (4.10) and (4.12) is that the degeneracy is given by the product of the degeneracy of the corresponding level of the noninteracting fermions and the dimension of the N-particle spin space. Thus, the degeneracy of each level is 3^N times larger than for the spinless noninteracting fermions since we consider spin-1 particles in Fig. 4.3(left).

When a magnetic field is applied along the z-axis the spin functions $|\chi\rangle$ must also be eigenstates of the Zeeman Hamiltonian V_Z. $\big($It is then automatically guaranteed that the boson state $W_i|\chi\rangle$ is also an eigenstate of V_Z since W commutes with V_Z.$\big)$ An eigenbasis of V_Z may, for example, be given by the spin functions $|m_1, m_2, \ldots, m_N\rangle$ $\big($with $m_i = -1, 0, 1\big)$. Thus, the energy levels E_i split up according to Eq. (4.13) and the Zeeman shift of each boson state $W_i|m_1, m_2, \ldots, m_N\rangle$ is given by the Zeeman shift of the spin function $E_Z\big(|m_1, m_2, \ldots, m_N\rangle\big)$; see Fig. 4.3(right).

4.2 Large but finite repulsion

In the limit of infinite repulsion $U_0 = \infty$ (and at zero magnetic field) the ground state of N spin-1 bosons is 3^N times degenerate. Any superposition

$$\sum_{m_1,\ldots,m_N} c_{m_1,\ldots,m_N} W|m_1, m_2, \ldots, m_N\rangle$$

with *arbitrary* coefficients $c_{m_1,\ldots,m_N}$ $\big($apart from the constraint $\sum_{m_1,\ldots,m_N}\big|c_{m_1,\ldots,m_N}\big|^2 = 1\big)$ is a valid boson ground state. When the spin-independent interaction U_0 is made large but finite the degenerate ground-state level splits up into a quasidegenerate multiplet. The eigenstates of this multiplet are still well approximated by the limiting solutions. However, the coefficients $c_{m_1,\ldots,m_N}$ of the corresponding limiting solutions are no longer arbitrary but they are determined by the spin-independent and spin-dependent interactions.

In the following I will first show in Fig. 4.4 that the wave functions of a realistic system (with large but finite interactions) are well approximated by the Tonks-Girardeau limiting solutions — if one has once found the right superposition of basis spin functions $|m_1, m_2, \ldots, m_N\rangle$. Later in Fig. 4.5, I will discuss the splitting of the ground-state multiplet of three spin-1 bosons in the $F_z = 0$ subspace. These findings are not only valid for three particles and Fig. 4.6 summarizes our observations made for $2 - 5$ spin-1 bosons.

Approximation of a realistic wave function by its limiting solution: In the experiment of Kinoshita *et al.* [21] an effective one-dimensional interaction strength of $U \lesssim 15.4\,\hbar\omega$ has been achieved. That is deep within the strongly interacting regime, where the realistic wave function is well approximated by the Tonks-Girardeau limiting solution. This has already been discussed in Sec. 3.4 and in connection with Fig. 2.6, where the evolution of a (spinless bosonic) two-particle wave function with increasing repulsion is shown. One sees in Fig. 2.6 that the wave function of the strongly interacting bosons nearly agrees with the limiting Tonks-Girardeau wave function for interaction strengths above $U \gtrsim 16\,\hbar\omega$.

Similarly, we expect that the real wave function of the spin-1 bosons is well approximated by its limiting solution if the spin-independent repulsion U_0 is sufficiently strong. Fig. 4.4 shows a cut through the nonzero spin-components of a particular three-boson ground state $\big(x_2 = -0.8\,l$ and $x_3 = 0.8\,l$ are fixed and x_1 is variable$\big)$. The red solid line of Fig. 4.4 corresponds to the exact limiting solution and the blue dashed line has been obtained from a numerical diagonalization of the Hamiltonian (4.1) for a large but finite repulsion U_0. As can be seen, the agreement between both solutions is rather good.

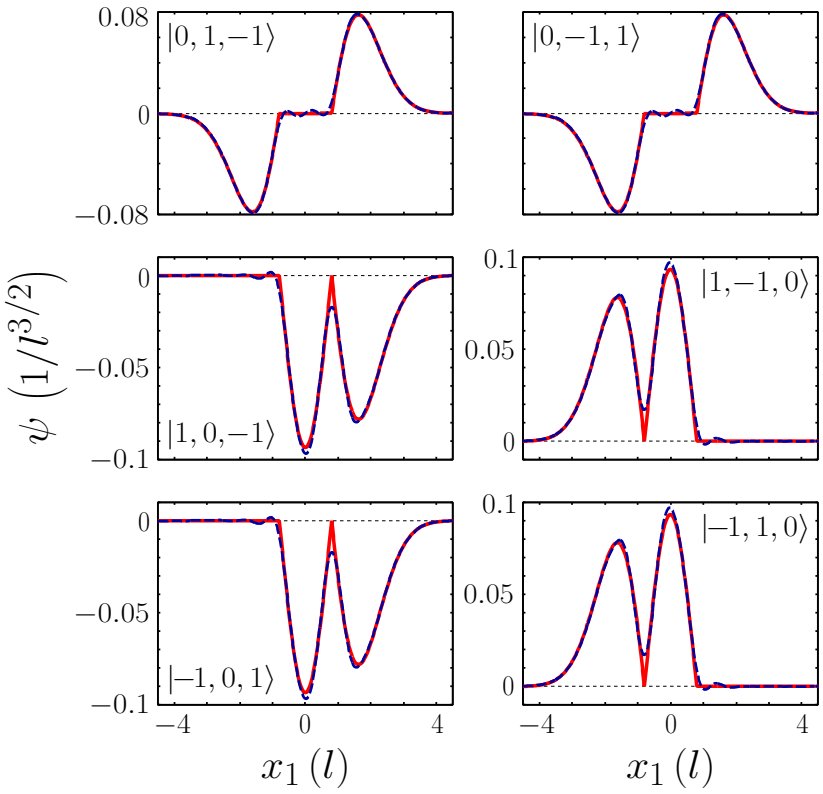

Figure 4.4: Cut through the nonzero spin-components of a bosonic 3-particle state. The second and the third coordinate are fixed at $x_2 = -0.8\,l$ and $x_3 = 0.8\,l$. Shown is the exact wave function in the limit of infinite δ-repulsion (red solid line) and the solution of a numerical diagonalizion of the Hamiltonian in the limit of large but finite repulsion (blue dashed line).

I note that both wave functions of Fig. 4.4 deviate from the real solution of (4.1) when U_0 is large but finite. Similar to the spinless two-boson wave function of Fig. 2.6, the first derivative of the exact wave function is discontinuous at $x_1 = x_2 = -0.8\,l$ and $x_1 = x_3 = 0.8\,l$. The numerical solution, by contrast, is rounded and shows minor oscillations around these points, since it is obtained from a superposition of a finite number of smooth oscillator wave functions. This behavior is not a feature of the realistic wave function at large but finite interactions but a result of our approximative method. However, a true feature of the numerical solution is the observation that in the case of a finite repulsion the cusps in the wave function are located at a finite height, i. e., the wave function is not zero at these points as in the limiting case of infinite repulsion $\big($see, e. g., the behavior of the blue dashed wave function at $x_1 = -0.8\,l$ in the spin component $|-1, 1, 0\rangle\big)$. We conclude that the numerical wave function of Fig. 4.4 resembles the true solution apart from some minor oscillations and the rounding of the cusps at the collision points $x_1 = x_2$ and $x_1 = x_3$ — but the finite height of the cusps is a true feature of the real wave function since the interaction strength is finite. By contrast, the Tonks-Girardeau limiting solution is zero at the collision points.

Energy structure of the ground-state multiplet: Fig. 4.5 shows the energies of three spin-1 bosons in the ground-state multiplet in the subspace $F_z = 0$ together with the corresponding limiting eigenfunctions. The energies have been obtained from a numerical diagonalization of the Hamiltonian (4.1) for a strong spin-independent repulsion ($U_0 = 20\,\hbar\omega$) and a small ferromagnetic spin-dependent interaction strength ($U_2 = -U_0/2000$). The wave functions of Fig. 4.5 are the limiting Tonks-Girardeau solutions of the numerical eigenfunctions.

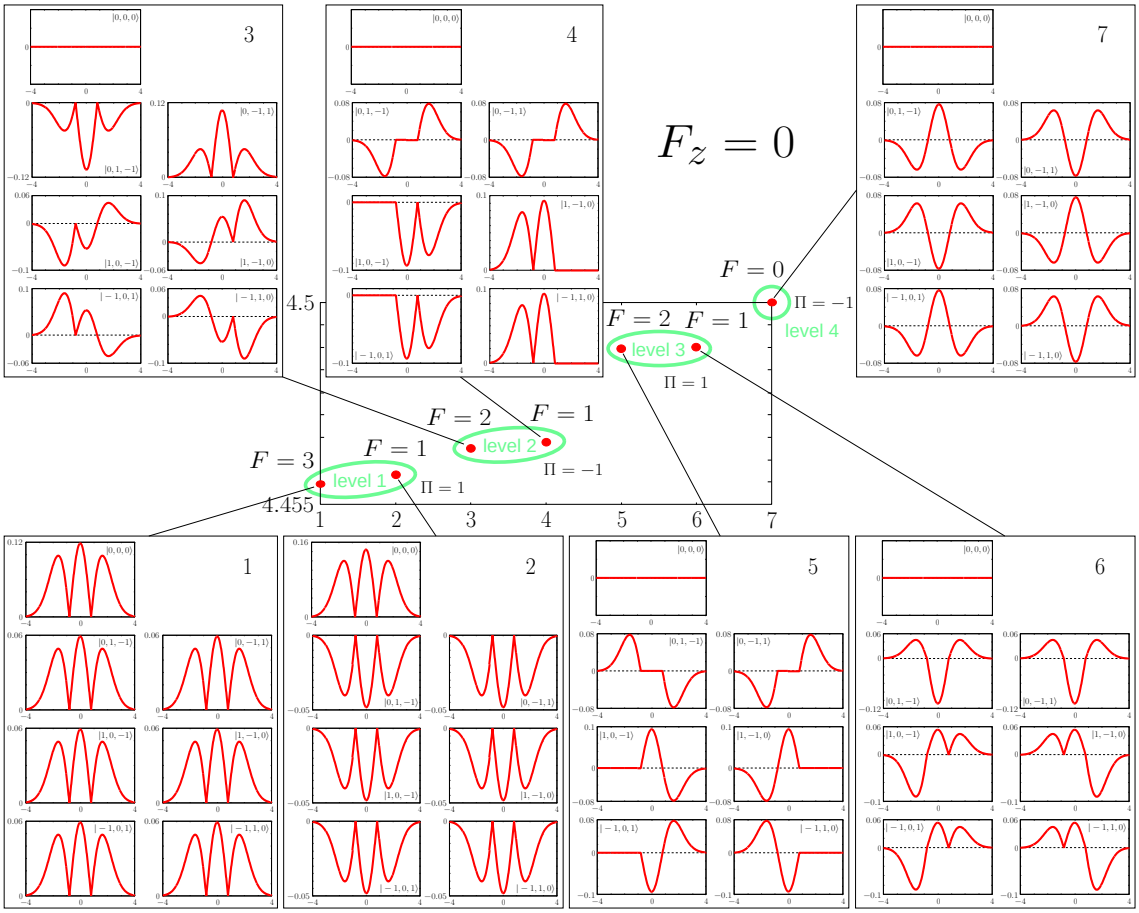

Figure 4.5: Energy structure of the ground-state multiplet of three spin-1 bosons in the subspace $F_z = 0$. The spin-independent interaction $U_0 = 20\,\hbar\omega$ is large and the spin-dependent interaction $U_2 = -U_0/2000$ is weak and ferromagnetic. Note the small splitting of the ground-state multiplet, which is much smaller than the spacing from the first excited multiplet: $(4.5 - 4.455)\hbar\omega = 0.045\,\hbar\omega \ll 1\,\hbar\omega$. The energy eigenvalues have been obtained from a numerical diagonalization of the Hamiltonian. The corresponding limiting solutions of the eigenfunctions are also shown. The 4th eigenstate is the example wave function of Fig. 4.4.

The states are ordered by energy (1: lowest, ..., 7: largest energy). In the $F_z = 0$ subspace the ground-state multiplet consists of 7 boson wave functions since a basis of the corresponding spin space is, e. g., given by the states $|0,0,0\rangle$, $|1,0,-1\rangle$, $|1,-1,0\rangle$, $|0,1,-1\rangle$, $|0,-1,1\rangle$, $|-1,1,0\rangle$ and $|-1,0,1\rangle$. For infinite repulsion $U_0 = \infty$ all the seven states acquire the same energy $E_g = N^2/2\,\hbar\omega = 4.5\,\hbar\omega$. For a large but finite repulsion only the 7th state has exactly that energy and the energies of the other states are slightly lower. Note that the splitting of the multiplet is much smaller than the spacing from the first excited multiplet: $(4.5 - 4.455)\hbar\omega = 0.045\,\hbar\omega \ll 1\,\hbar\omega$. With increasing repulsion the states $1-6$ approach the limiting energy from below.

The 7th state is not affected by the δ repulsion. For all values of U_0 it has the same energy $4.5\,\hbar\omega$. The spin function of that state is antisymmetric under any permutation of two particles

$$|\chi_7\rangle = \frac{1}{\sqrt{6}}\Big(|0,1,-1\rangle + |1,-1,0\rangle + |-1,0,1\rangle - |0,-1,1\rangle - |-1,1,0\rangle - |1,0,-1\rangle\Big) = \sqrt{3!}P_A|0,1,-1\rangle.$$

Likewise the motional wave function of the corresponding boson ground state is permutationally

antisymmetric as well

$$W|\chi_7\rangle = \left(\sqrt{3!}P_A|\mathrm{id}\rangle\right) \otimes \left(\sqrt{3!}P_A|0,1,-1\rangle\right) = \psi^{(0)}_{\text{fermion gr.}} \otimes \left(\sqrt{3!}P_A|0,1,-1\rangle\right), \tag{4.14}$$

i. e., the orbital function is given by the ground-state Slater determinant of three noninteracting fermions

$$\psi^{(0)}_{\text{fermion gr.}} \propto (x_1 - x_2)(x_1 - x_3)(x_2 - x_3)e^{-(x_1^2+x_2^2+x_3^2)/2},$$

which is zero at $\{x_i = x_j\}$ and hence the particles in that state do not feel the δ interaction potential. I note finally that the 7th state is an $\vec{F}^2$ and parity eigenstate $(F = 0, \Pi = -1)$.

By contrast, the 1st and the 2nd state of Fig. 4.5 (which form the 1st level of the multiplet) have permutationally symmetric motional wave functions and they are strongly influenced by the increasing δ repulsion. One can build two linearly independent symmetric spin functions from the above states: The state $|0,0,0\rangle$, which is already symmetric, and the state $\sqrt{3!}\,P_S|1,0,-1\rangle$. For $U_2 = 0$ (when the spin-dependent interaction is switched off) both boson ground states $W|0,0,0\rangle$ and $W\sqrt{3!}\,P_S|1,0,-1\rangle$ are energetically degenerate and the system can be in arbitrary superpositions of these states, which need not to be $\vec{F}^2$ eigenstates. The degeneracy is lifted, when U_2 is switched on and both states become $\vec{F}^2$ eigenstates. One state has total spin $F = 3$ and is approximately given by the limiting solution

$$W|\chi_1\rangle = W|\chi_{F=3}\rangle = W\left(\sqrt{\frac{2}{5}}|0,0,0\rangle + \sqrt{\frac{3}{5}}\,\sqrt{3!}\,P_S|1,0,-1\rangle\right) \tag{4.15}$$

and the other state has total spin $F = 1$ and is approximately given by

$$W|\chi_2\rangle = W|\chi_{F=1}\rangle = W\left(\sqrt{\frac{3}{5}}|0,0,0\rangle - \sqrt{\frac{2}{5}}\,\sqrt{3!}\,P_S|1,0,-1\rangle\right). \tag{4.16}$$

These states can also be written as $W|\chi_{1/2}\rangle = \psi^{(\infty)}_{\text{boson gr.}} \otimes |\chi_{1/2}\rangle$, i. e., the orbital wave function is given by the permutationally symmetric spinless Tonks-Girardeau wave function

$$\psi^{(\infty)}_{\text{boson gr.}} \propto |x_1 - x_2||x_1 - x_3||x_2 - x_3|e^{-(x_1^2+x_2^2+x_3^2)/2}. \tag{4.17}$$

The states $W|\chi_{1/2}\rangle$ of the first level are strongestly influenced by the δ interaction, since for a motional wave function with Bose symmetry the probability is highest to find two particles at the same position. Both states have evolved from the noninteracting ground-states $\psi^{(0)}_{\text{boson gr.}} \otimes |\chi_{1/2}\rangle$ with $\psi^{(0)}_{\text{boson gr.}} \propto e^{-(x_1^2+x_2^2+x_3^2)/2}$.

Additionally, the energy of the states of the lowest level, which are approximated by $W|\chi_{F=3}\rangle$ and $W|\chi_{F=1}\rangle$, depends on the sign of the spin-dependent interaction U_2. We found for two particles $\left[\text{see Eq. (2.3)}\right]$ that the interaction Hamiltonian can be written as

$$V_{\text{int.}} = \delta(\vec{r}_1 - \vec{r}_2)\left[(g_0 - 2g_2)\mathbb{1}^{\otimes 2} + (g_2/2)\vec{F}^2\right] \tag{4.18}$$

$\left(U_{0/2} = g_{0/2}/l\right)$. [2] The first term of the interaction (4.18) has already deformed the motional wave function of both states which is now approximately given by (4.17). The second term has two effects: Firstly, both states become $\vec{F}^2$ eigenstates and, secondly, their energy is shifted by the

[2] I note that for $N \geqslant 3$ particles the spin-dependent interaction is not simply proportional to $\vec{F}^2$ as in the two-particle case. Otherwise all the eigenstates of Fig. 4.5 with same F would have the same energy. However, still $\left[H_{\text{int.}}, \vec{F}^2\right] = 0$.

spin-dependent interaction term. Here, g_2 is negative and thus the energy of the state $W|\chi_{F=3}\rangle$ is more lowered than the energy of the state $W|\chi_{F=1}\rangle$. I note finally that both states of level 1 have parity $\Pi = 1$.

So far we have discussed the two limiting cases of the ground-state multiplet of Fig. 4.5: The two states of level 1, which have the lowest energy within the multiplet and which have permutationally symmetric orbital wave functions, and the 7th state, which has the highest energy and a permutationally antisymmetric orbital wave function. I now turn to the states in between which form the levels 2 and 3. One first notices that the motional wave functions of different spin-components of one single state can look completely different from each other $\big($compare, for example, the $|0,1,-1\rangle$- and the $|1,0,-1\rangle$-component of the 5th state of Fig. 4.5$\big)$. And, secondly, one sees that all the motional wave functions of the single spin-components of the states $3-6$ are nonsymmetric.

$\big[$By contrast, the states of level 1 have the same orbital wave functions in all the components $|0,1,-1\rangle$, $|0,-1,1\rangle$, $|1,0,-1\rangle$, $|1,-1,0\rangle$, $|-1,0,1\rangle$ and $|-1,1,0\rangle$. These components deviate only by ± 1 and a scaling factor from the orbital wave function of the $|0,0,0\rangle$-component. Secondly, the orbital wave functions look permutationally symmetric, since they are symmetric around the collision points: for example $\psi(x_1 = x_2 - \delta x_2, x_2, x_3) \approx \psi(x_1 = x_2 + \delta x_2, x_2, x_3)$. Likewise, the 7th state has the same orbital wave function in all the components $|0,1,-1\rangle$, $|0,-1,1\rangle$, $|1,0,-1\rangle$, $|1,-1,0\rangle$, $|-1,0,1\rangle$ and $|-1,1,0\rangle$ apart from the sign of the permutation sign(π). The orbital wave function of the 7th state looks permutationally antisymmetric since it is antisymmetric around the collision points: $\psi(x_1 = x_2 - \delta x_2, x_2, x_3) \approx -\psi(x_1 = x_2 + \delta x_2, x_2, x_3)$.$\big]$

We have already seen that the spin functions of the ground states of level 1 are permutationally symmetric $\big[$see Eqs. (4.15) and (4.16)$\big]$ and that the spin function of the 7th state is permutationally antisymmetric $\big[$see Eq. (4.14)$\big]$. The spin functions of the states $3-6$, by contrast, are nonsymmetric:

$$W|\chi_3\rangle = \frac{W}{2\sqrt{3}}\Big(|0,1,-1\rangle - |0,-1,1\rangle + 2\,|1,0,-1\rangle - 2\,|-1,0,1\rangle + |1,-1,0\rangle - |-1,1,0\rangle\Big)$$

$$W|\chi_4\rangle = \frac{W}{2}\Big(|0,1,-1\rangle + |0,-1,1\rangle - |1,-1,0\rangle - |-1,1,0\rangle\Big)$$

$$W|\chi_5\rangle = \frac{W}{2}\Big(|0,1,-1\rangle - |0,-1,1\rangle - |1,-1,0\rangle + |-1,1,0\rangle\Big)$$

$$W|\chi_6\rangle = \frac{W}{2\sqrt{3}}\Big(-|0,1,-1\rangle - |0,-1,1\rangle + 2\,|1,0,-1\rangle + 2\,|-1,0,1\rangle - |1,-1,0\rangle - |-1,1,0\rangle\Big).$$

$\big[$These states are at the same time $\vec{F}^2$ and parity eigenstates and the corresponding eigenvalues are given by: $(W|\chi_3\rangle : F = 2, \Pi = -1)$; $(W|\chi_4\rangle : F = 1, \Pi = -1)$; $(W|\chi_5\rangle : F = 2, \Pi = 1)$; $(W|\chi_6\rangle : F = 1, \Pi = 1)$.$\big]$

We see in Fig. 4.5 that the boson states $W|\chi_3\rangle$ and $W|\chi_4\rangle$ are grouped together in level 2 while the states $W|\chi_5\rangle$ and $W|\chi_6\rangle$ form level 3. Again, we observe that the states of the same level are energetically degenerate when U_2 is switched off. An infinitesimal perturbation $(U_2 \neq 0)$ has the effect that all the ground states of the multiplet become $\vec{F}^2$ eigenstates. Here, the 3rd (5th) state has total spin $F = 2$ and the 4th (6th) state has total spin $F = 1$. Because $U_2 < 0$ and due to Eq. (4.18) the energy of the state with largest F is lowered by the largest amount since the spin-dependent interaction energy E_{spin} is proportional to U_2 and $F(F+1)$, $E_{\text{spin}} \propto U_2\, F(F+1)$.

We studied the level structure of the ground-state multiplet in more detail and made the following further observations: The seven states of the multiplet are grouped together in 4 levels

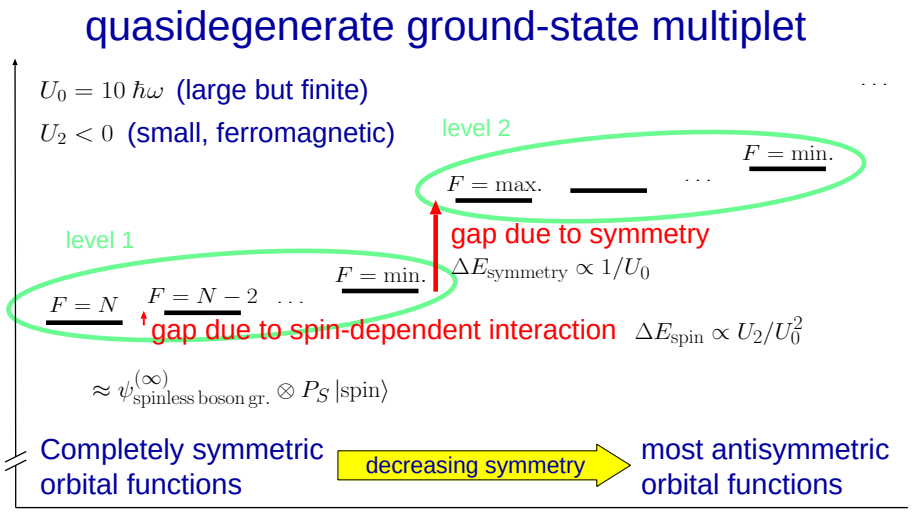

Figure 4.6: Sketch of the energy structure of the ground-state multiplet of $2-5$ particles. The ground-state multiplet splits up into several levels when the δ repulsion is made large but finite. Comparatively large gaps due to the different symmetry of the motional wave functions separate the different levels from each other. These "symmetry gaps" depend only on the strength of the spin-independent interaction $\Delta E_{\text{symmetry}} \propto 1/U_0$. The splitting within the levels is furthermore determined by the spin-dependent interaction strength and $\Delta E_{\text{spin}} \propto U_2/U_0^2$. With increasing level index the motional wave functions of the ground states become more and more permutationally antisymmetric.

(see Fig. 4.5). The symmetry of the motional wave functions decreases with increasing level index (level 1: permutationally symmetric motional wave functions, ... increasing antisymmetry ..., level 4: permutationally antisymmetric motional wave function). The energy gaps between different levels are comparatively large and solely determined by the spin-independent interaction strength $\Delta E_{\text{symmetry}} \propto 1/U_0$. [A similar energy structure has been discussed in Ref. [69] for a two-component system by means of the two-particle solution; see Eqs. (2.45), (2.46) and (2.48). From a Taylor expansion of the left-hand side of Eq. (2.48) one obtains Eq. (3.12). Thus, the energy gap $\Delta E = E - 3/2 \propto 1/g_r = 1/U$.] The comparatively small energy gaps within the single levels depend also on the spin-dependent interaction strength U_2 and they are given by $\Delta E_{\text{spin}} \propto U_2/U_0^2$ since the local correlation function $\rho_{\text{local corr.}} = \int dx \rho(x,x)$ is proportional to $1/U_0^2$ in the limit of strong repulsion [32] and since $\Delta E_{\text{spin}} = U_2\,\rho_{\text{local corr.}}$.

Generalization to other particle numbers: We made similar observations for $2-5$ particles and I believe that the general structure of the ground-state multiplet is independent of the number of particles N. Fig. 4.6 summarizes the results: The ground-state multiplet decomposes into several levels. All the states of level 1 have permutationally symmetric motional wave functions — in agreement with Ref. [96]. The states of different levels are separated from each other by "symmetry gaps". The spacing between the levels solely depends on the spin-independent interaction strength $\Delta E_{\text{symmetry}} \propto 1/U_0$. The comparatively small gaps within the single levels depend moreover on the spin-dependent interaction strength $\Delta E_{\text{spin}} \propto U_2/U_0^2$. The symmetry of the motional wave functions decreases with increasing level index, i. e., the states of the energetically highest level have the most antisymmetric motional wave functions. (Note that one can not build completely permutationally antisymmetric spin functions for more than three spin-1 particles since, for example, $P_A|1,1,0,-1\rangle = 0$.) Each state of the ground-state multiplet can be approximated

by a superposition of the basis states $W|m_1, m_2, \ldots, m_N\rangle$ and the corresponding coefficients $c_{m_1,\ldots,m_N}$ are determined by the interaction Hamiltonian. So far we find these coefficients from the comparison with the numerical solutions (which we have done so far only for three particles).

4.3 Spin densities of the ground states

We found in Sec. 4.1 that hard-core particles with spin behave *at the same time* like noninteracting spinless fermions *and* noninteracting distinguishable spins. The dual nature of the particles became clearly visible in the energy spectrum (see Fig. 4.3). A similar behavior is shown by the (spin) densities of the system. I will show in the following that the total density of all the degenerate ground states always equals that of noninteracting spinless fermions. The spin densities, by contrast, depend sensitively on the superposition of the spin function and equal those of a chain of localized particles with the spin orientations given by the spin function; see Fig. 4.7.

First, I will derive the first-quantized form of the spin density. The operator of the probability to find particle 1 in spin state m is given by

$$\begin{aligned}|m\rangle\langle m|_1 &= |m\rangle\langle m| \otimes \mathbb{1}^{\otimes(N-1)} = \sum_{m_2,\ldots,m_N} |m, m_2, \ldots, m_N\rangle\langle m, m_2, \ldots, m_N| \\ &= \sum_{m_1,m_2,\ldots,m_N} \delta_{m\,m_1} |m_1, m_2, \ldots, m_N\rangle\langle m_1, m_2, \ldots, m_N| \,.\end{aligned}$$

Here, $\mathbb{1}$ is the identity matrix of the single-particle spin space. This operator is of course not permutationally symmetric and we cannot measure whether particle 1 is in spin state m since the particles are indistinguishable. We can only measure whether *one* particle is in spin state m and the corresponding symmetrized operator is given by

$$\sum_{i=1}^{N} |m\rangle\langle m|_i = \sum_{i=1}^{N} \sum_{m_1,\ldots,m_N} \delta_{m\,m_i} |m_1, \ldots, m_N\rangle\langle m_1, \ldots, m_N| \,.$$

Likewise we construct the projection operator of finding one particle at position x

$$\sum_{i=1}^{N} |x\rangle\langle x|_i = \sum_{i=1}^{N} \int_{\mathbb{R}^N} dx_1 \ldots dx_N \, \delta(x - x_i) |x_1, \ldots, x_N\rangle\langle x_1, \ldots, x_N| \,.$$

The spin density is the probability to find one particle in spin state m at position x. The corresponding operator is therefore the projection

$$\begin{aligned}\rho_m(x) &= \sum_{i=1}^{N} |x\,m\rangle\langle x\,m|_i \\ &= \sum_{i=1}^{N} \sum_{m_1,\ldots,m_N} \int_{\mathbb{R}^N} dx_1 \ldots dx_N \, \delta_{m\,m_i} \, \delta(x - x_i) \\ &\quad \times |x_1, \ldots, x_N\rangle \otimes |m_1, \ldots, m_N\rangle\langle m_1, \ldots, m_N| \otimes \langle x_1, \ldots, x_N| \,. \qquad (4.19)\end{aligned}$$

We want to calculate the spin density of a ground state $W|\chi\rangle$ which is given by the expectation value

$$\langle \rho_m(x) \rangle = \langle \chi | W^\dagger \rho_m(x) W | \chi \rangle = N! \langle \chi | \otimes \langle \mathrm{id} | \, P_S^\dagger \, \rho_m(x) \, P_S \, | \mathrm{id} \rangle \otimes | \chi \rangle \,.$$

$P_S = P_S^\dagger$ is self-adjoined, it commutes with any permutationally symmetric operator $\big[$and thus also with $\rho_m(x)\big]$ and it is a projection operator $P_S^2 = P_S$. We thus obtain

$$\langle \rho_m(x) \rangle = \sum_{\pi \in S_N} \langle \chi | \otimes \langle \mathrm{id} | \rho_m(x) | \pi \rangle \otimes \Big[U(\pi) | \chi \rangle \Big] = \langle \chi | \otimes \langle \mathrm{id} | \rho_m(x) | \mathrm{id} \rangle \otimes | \chi \rangle \,, \tag{4.20}$$

since $\langle \mathrm{id} | \rho_m(x) | \pi \rangle = \delta_{\mathrm{id},\pi} \langle \mathrm{id} | \rho_m(x) | \mathrm{id} \rangle$. By inserting Eq. (4.19) into Eq. (4.20) we obtain the expectation value of the spin density in state $W|\chi\rangle$

$$\begin{aligned} \langle \rho_m(x) \rangle = \sum_i & \underbrace{\left(\sum_{m_1,\ldots,m_N} \delta_{m\, m_i} \big| \langle m_1, \ldots, m_N | \chi \rangle \big|^2 \right)}_{=: p_i(m)} \\ & \times \underbrace{\left(\int dx_1 \ldots dx_N \, \delta(x - x_i) \big| \langle x_1, \ldots, x_N | \mathrm{id} \rangle \big|^2 \right)}_{=: \rho^{(i)}(x)} . \end{aligned} \tag{4.21}$$

Here, we have defined the probability $p_i(m)$ to find the ith particle of the system in spin state m and the probability density $\rho^{(i)}(x)$ to find the ith particle of the system, restricted to the standard sector C_{id}, at point x. Thus, we obtain the following formula for the spin density

$$\langle \rho_m(x) \rangle = \sum_i p_i(m) \rho^{(i)}(x) \,. \tag{4.22}$$

An explicit calculation of the probability density $\rho^{(i)}(x)$ (which I will derive in appendix A) yields the following formula

$$\rho^{(i)}(x) = \frac{d}{dx} \left[\sum_{k=0}^{N-i} \frac{(-1)^{N-i}(N-k-1)!}{(i-1)!(N-k-i)!\, k!} \, \frac{\partial^k}{\partial \lambda^k} \det\Big[B(x) - \lambda \mathbb{1} \Big] \Big|_{\lambda=0} \right], \tag{4.23}$$

where the $N \times N$-matrix $B(x)$ has entries $\beta_{ij}(x) = \int_{-\infty}^{x} dx' \psi_i(x') \psi_j(x')$ with the single-particle eigenfunctions of the spinless problem ψ_i $\big(\mathbb{1}$ is the $N \times N$ identity matrix$\big)$.

I note that formula (4.22) is independent of the spin and the statistics of the hard-core particles $\big($it can be applied to spin-$1/2, 1, 3/2, \ldots$ bosons or fermions$\big)$. Formula (4.23) is independent of the confining potential and also applicable to the excited states $\big($simply use the corresponding $B_i(x)$ matrix of the excited state $W_i|\chi\rangle$ and the single-particle eigenfunctions of the confining potential which has to be studied$\big)$. In the following I will apply the formula to the ground states of spin-1 hard-core bosons, which are confined in a one-dimensional harmonic trap.

Spin densities of spin-1 bosons: Fig. 4.7 shows the spin densities of selected ground states of 8 spin-1 hard-core bosons in a harmonic trap. The spin density has 3 components which correspond to $m = -1, 0, 1$. The single components are drawn as a blue dashed (ρ_1), red solid (ρ_0) and a green dotted line (ρ_{-1}). In Fig. 4.7(a) and (b) we have also plotted the densities $\rho^{(i)}(x)$ of the particles $i = 1 - 8$. Note that $\rho^{(i)}(x)$ is not a measurable observable! However, it will serve as a very useful quantity in order to develop an intuitive understanding of Eq. (4.22). Despite the quite complicated form of Eq. (4.23) the densities $\rho^{(i)}(x)$ of the particles $i = 1 - 8$ look rather simple $\big[$see Fig. 4.7(a) and (b)$\big]$, namely, like Gaussians which are located in a row along the x-axis, one after the other, at $\langle x_1 \rangle \approx -3.5\, l$, $\langle x_2 \rangle \approx -2.5\, l, \ldots, \langle x_8 \rangle \approx 3.5\, l$ $\big[$with $\langle x_i \rangle = \int dx\, x \rho^{(i)}(x)\big]$. One might, therefore, develop the intuitive picture of particles, which are

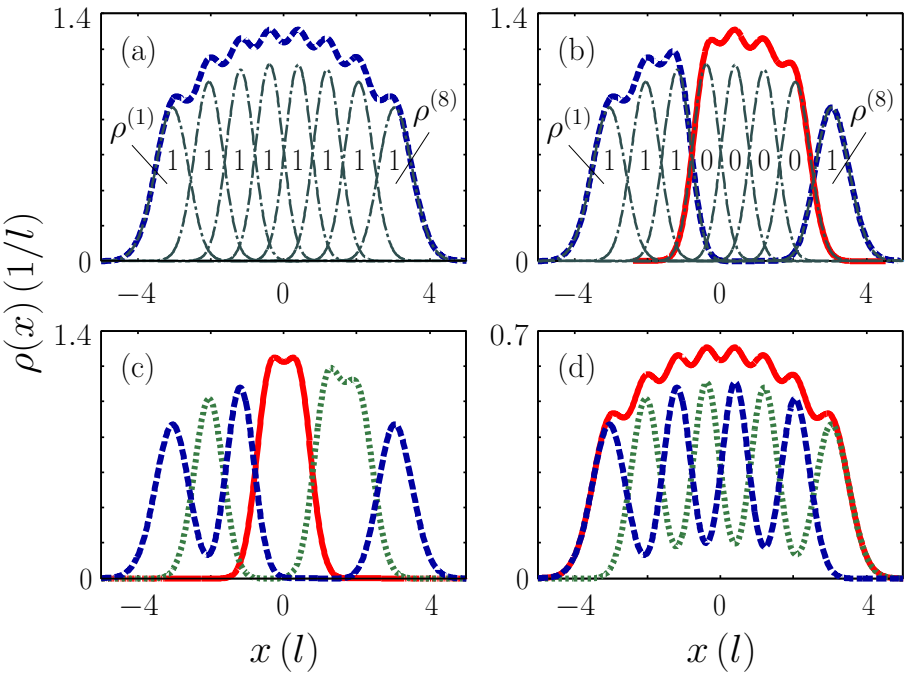

Figure 4.7: Spin densities of 8 spin-1 bosons in different ground states (see text). Shown are the densities $\rho^{(i)}$ (gray dash-dotted line, see text), and the components ρ_0 (red solid line), ρ_1 (blue dashed line) and ρ_{-1} (green dotted line) of the spin density. The spin densities resemble chains of localized spins.

aligned in a row along the x-axis, by interpreting the square root of the densities $\rho^{(i)}(x)$ as the wave packets of imaginary particles, $\psi^{(i)}(x) \equiv \sqrt{\rho^{(i)}(x)}$ [21] with the spin orientations given by $\vec{u}^{\,(i)} \equiv \left(\sqrt{p_i(-1)}, \sqrt{p_i(0)}, \sqrt{p_i(1)}\right)^T$ (the unit vector $\vec{u}^{\,(i)}$ has length one). Thus, we obtain the spin density $\rho_m(x)$ as follows: We draw the density $\rho^{(i)}(x)$ of the localized particle i as done in Fig. 4.7(a) and (b), we multiply $\rho^{(i)}(x)$ by $p_i(m)$ in order to obtain the spin density of particle i, $\rho_m^{(i)}(x) \equiv p_i(m)\rho^{(i)}(x)$, and in the final step we sum up the spin densities of all the eight particles $\rho_m(x) = \sum_i \rho_m^{(i)}(x)$ — that is precisely the meaning of Eq. (4.22).

Fig. 4.7(a) shows the spin density of the spin-polarized state $W|\chi_+\rangle = W|1,1,\ldots\rangle$. In the spin-polarized case all the probabilities $p_i(1) = 1$; see the definition of $p_i(m)$ in Eq. (4.21). Therefore, Eq. (4.22) reduces to

$$\rho_1(x) = \sum_i \rho^{(i)}(x) = \rho_{\text{fermion gr.}}(x) = \sum_{i=0}^{7} \psi_i^2(x)\,,$$

which is the usual density of a spinless Tonks-Girardeau gas. Fig. 4.7(b) shows the spin density of the ground state $W|1,1,1,0,0,0,0,1\rangle$. Similarly we obtain $p_i(1) = 1$ for $i = 1,2,3$ and 8, and $p_i(0) = 1$ for $i = 4-7$. Thus, the spin density $\rho_1(x)$ of that state is given by $\rho_1(x) = \rho^{(1)}(x) + \rho^{(2)}(x) + \rho^{(3)}(x) + \rho^{(8)}(x)$ and $\rho_0(x)$ is given by $\rho_0(x) = \sum_{i=4}^{7} \rho^{(i)}(x)$, i. e., we add the particle densities $\rho^{(1)}(x) - \rho^{(3)}(x)$ and $\rho^{(8)}(x)$ to the component $\rho_1(x)$ and the particle densities $\rho^{(4)}(x) - \rho^{(7)}(x)$ to the component $\rho_0(x)$ of the spin density. Finally, Figs. 4.7(c) and (d) show the spin densities of the ground state $W|1,-1,1,0,0,-1,-1,1\rangle$ and the superposition state $W\left(|0,0,\ldots\rangle + |1,-1,1,-1,\ldots\rangle\right)/\sqrt{2}$ respectively. We see in Figs. 4.7(b–d) that the spin densities of the hard-core bosons can strongly vary on a rather short length scale, given by the mean

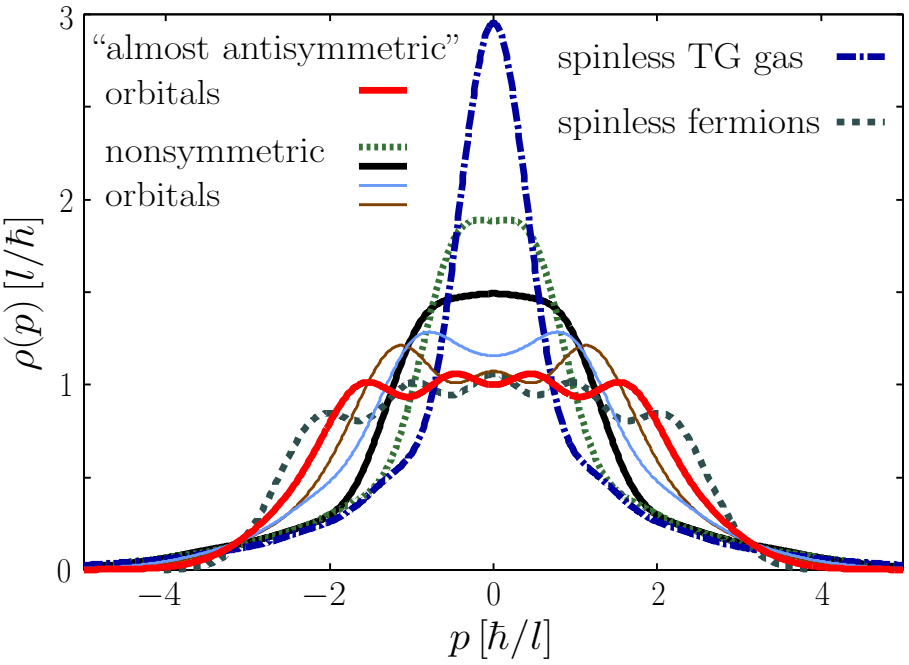

Figure 4.8: Momentum distributions of 5 spin-1 bosons in different ground states. The gray dashed line shows for comparison the momentum distribution of 5 noninteracting fermions. The shape of the momentum distribution depends on the symmetry of the orbital wave function.

interparticle spacing $\approx l$ — different from the total density, which shows only minor oscillations on this length scale, which are washed out for $N \to \infty$. I finally note that the total density of all the degenerate ground states is always equal to that of spinless noninteracting fermions

$$\rho(x) = \sum_{m=-1,0,1} \rho_m(x) = \sum_i \rho^{(i)}(x) = \rho_{\text{fermion gr.}}(x)\,.$$

To summarize — we have seen that the (spin) densities combine properties of spinless noninteracting fermions and distinguishable noninteracting spins. The spin densities resemble chains of localized (and thus distinguishable) spins and the total densities of all the degenerate ground states are always equal to the density of spinless noninteracting fermions. Different from the spinless case, the spin densities can strongly vary on the length scale of the mean interparticle spacing $\approx l$.

4.4 Momentum distributions of the ground states

One of the most important experimentally accessible quantities is the momentum distribution of the spinor bosons, given by

$$\rho(p) = \sum_i \int dp_1 \ldots dp_N \sum_{m_1,\ldots,m_N} \delta(p - p_i)|\psi_{m_1,\ldots,m_N}(p_1,\ldots,p_N)|^2.$$

Fig. 4.8 shows selected momentum distributions of 5 spin-1 bosons in their degenerate ground states, obtained from a numerical diagonalization of (4.1). For comparison we have also plotted the momentum distribution of 5 noninteracting fermions (gray dashed line). It turns out that the shape of the momentum distribution depends on the symmetry of the spin function so that different

ground states can have completely different momentum distributions. This has to be contrasted with the total density, which was completely independent of the spin function and equal for each ground state. States with a completely symmetric spin function $|\chi_s\rangle$ have a completely symmetric orbital function, $W|\chi_s\rangle = \psi^{(\infty)}_{\text{boson gr.}}(x_1, \ldots, x_N)|\chi_s\rangle$, which is given by the usual spinless Tonks-Girardeau wave function. The momentum distribution of these states is equal to that of a spinless Tonks-Girardeau gas (blue dash-dotted line), which exhibits a pronounced zero-momentum peak and long-range, high-momentum tails [90, 92]. The other extreme case is given by a flat and broad momentum distribution, which resembles the fermionic one (red solid line). In the case of 2 and 3 spin-1 bosons, some spin functions $|\chi_a\rangle$ can be completely antisymmetric and thus the corresponding ground state is given by $W|\chi_a\rangle = \psi^{(0)}_{\text{fermion gr.}}(x_1, \ldots, x_N)|\chi_a\rangle$ so that its momentum distribution is equal to that of spinless fermions. One cannot construct completely antisymmetric spin functions with more than 3 spin-1 particles. However, it is possible to construct nonsymmetric spin functions, which are "almost antisymmetric" (see Young's Tableaux [97]), resulting in momentum distributions which are almost fermionic. We believe, due to group theoretical arguments [97], that this broadening and flattening of some momentum distributions saturates for large N. However, as one sees in Fig. 4.8, some spinful bosons aquire Fermi-like momentum distributions depending on the symmetry of their spin function. That is quite different from the spinless case, where the momentum distribution clearly exhibits bosonic features. The opposite observation is made for spinful fermions. Here, the ground states with "almost antisymmetric" spin functions have momentum distributions which resemble those of spinless hard-core bosons. The relationship between the symmetry of the motional wave function of a ground state and the shape of its momentum distribution is sketched in Fig. 4.9. I finally note that all the momentum distributions of Fig. 4.8 have the same width $w_p = 2\sqrt{\langle p^2 \rangle} = 5\,\hbar/l$ since the kinetic energy $E_{\text{kin.}} \propto \langle p^2 \rangle$ is independent of the spin function and equal to that of noninteracting spinless fermions.

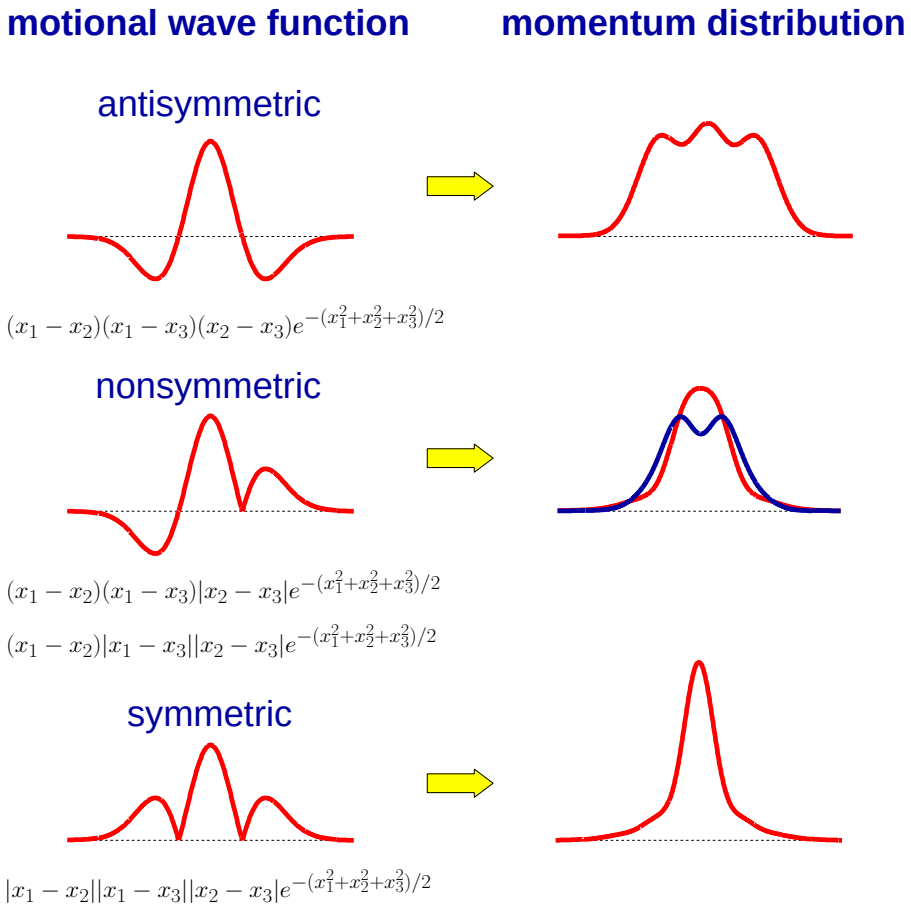

Figure 4.9: Relationship between the symmetry of the orbital wave function of a ground state and the shape of its momentum distribution (three particles). A state with a completely antisymmetric orbital function has a momentum distribution which equals that of spinless noninteracting fermions (upper row). In the other extreme case of a state with a completely symmetric orbital wave function the momentum distribution equals that of spinless hard-core bosons (lower row). A remnant of the Bose symmetry of that orbital function is the typical pronounced zero-momentum peak while the high-momentum tails are related to the cusps in the wave function at $\{x_i = x_j\}$. By gradually replacing absolute values by brackets in the spinless Tonks-Girardeau wave function we obtain more an more antisymmetric orbital functions (middle row) resulting in momentum distributions which combine Bose- and Fermi-like features.

Chapter 5

Ultracold heteronuclear Feshbach molecules

The main results of Secs. 5.6 – 5.9 have been published in Ref. [3].

The aim of this chapter is a theoretical description of the experiment of C. Ospelkaus *et al.* [72] on the formation of ultracold Feshbach molecules from two different atomic elements. In Secs. 5.1 – 5.4 I present simple models for the interaction between ultracold atoms. These models are used to become familiar with some of the most important concepts, namely the scattering length, the phase shift, the pseudopotential approximation and Feshbach resonances. In Sec. 5.6 I describe the exact-diagonalization algorithm used to calculate the low-energy spectrum and the corresponding wave functions of two interacting atoms at a single site of an optical lattice. In the following sections 5.7 – 5.9 I compare our results to the experimental data and calculate the transfer efficiency of the rf association and the lifetime of the Feshbach molecules. Related theoretical work has been published by J. F. Bertelsen and K. Mølmer [98, 99].

5.1 S-wave scattering in free space

Let us consider two atoms in free space (i. e. no external potential) which interact via a spherically symmetric box potential

$$V_{\text{box}}(r) = \begin{cases} V & \text{if } r \leqslant R \\ 0 & \text{if } r > R. \end{cases} \tag{5.1}$$

We are searching for the solution of the radial equation

$$\left[-\frac{\hbar^2}{2\mu} \frac{1}{r} \frac{d^2}{dr^2} r + V_{\text{box}}(r) - E \right] \psi(r) = 0.$$

The equation consists of the kinetic energy of the radial motion, the potential energy of the box and the energy of the relative motion. We restrict our discussion to particles with relative angular momentum zero ($l = 0$), i. e., the centrifugal barrier is zero. By substituting

$$\chi(r) \equiv r\, \psi(r)$$

the radial equation transforms to

$$\frac{d^2\chi(r)}{dr^2} + \frac{2\mu}{\hbar^2} \big[E - V_{\text{box}}(r) \big] \chi(r) = 0\,. \tag{5.2}$$

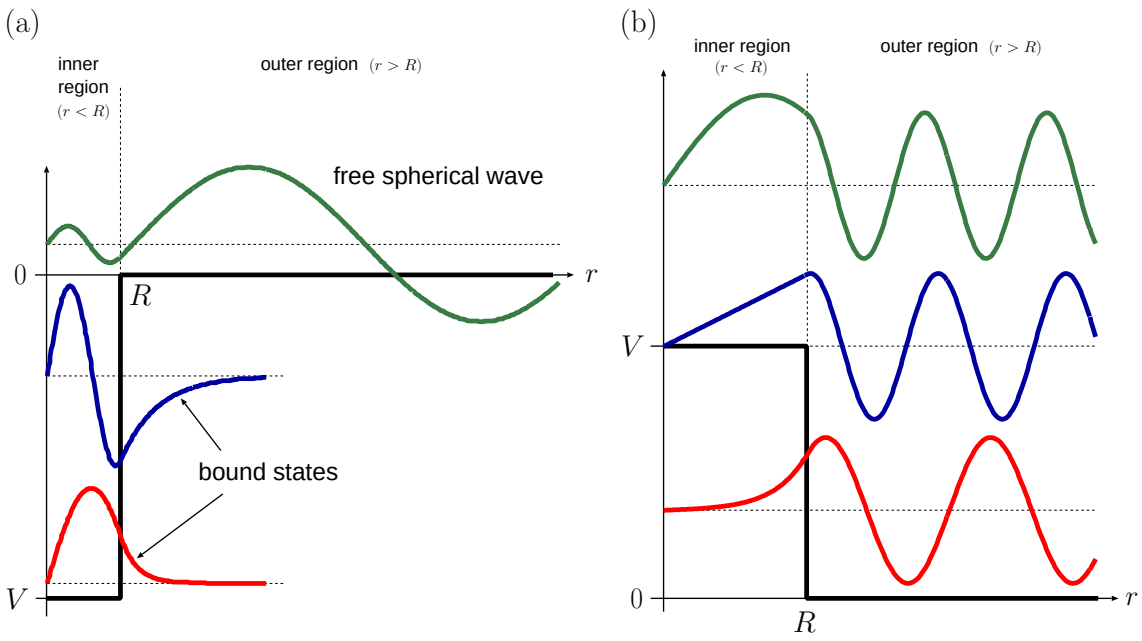

Figure 5.1: Radial wave functions $\chi(r)$ of an attractive (a) and a repulsive (b) spherically symmetric box potential. Attractive interaction (a): In the inner region $\chi_{\text{in}} \propto \sin(Kr)$. The larger the wave number $K \propto \sqrt{E-V}$ the faster the oscillation. In the outer region $\chi_{\text{out}} \propto e^{-\rho r}$ $(E < 0)$ or $\chi_{\text{out}} \propto \sin(kr)$ $(E > 0)$. The energy spectrum is discrete for $E < 0$ leading to a finite number of molecular bound states. For $E > 0$ the energy spectrum is continuous: The free spherical waves can have every energy $E > 0$. Repulsive interaction (b): In the inner region $\chi_{\text{in}} \propto \sinh(K'r)$ $(E < V)$ or $\chi_{\text{in}} \propto \sin(Kr)$ $(E > V)$. In the borderline case $E = V$ the inner wave function is just a straight line $\chi_{\text{in}} \propto r$. In the outer region $\chi_{\text{out}} \propto \sin(kr)$.

The probability $\rho(\vec{r}) = |\psi(r)|^2 |Y_{lm}(\theta,\phi)|^2$ to find the relative particle at position $\vec{r}$ shall be finite everywhere (Y_{lm} are spherical harmonics). Therefore, it is a reasonable constraint that the wave function $\psi(r)$ is finite everywhere too, in particular at the origin: $\psi(0) =$ finite. Thus, the wave function $\chi(r)$ has to obey the boundary condition $\chi(0) = 0$ [78]. We introduce some abbreviations

$$\epsilon \equiv \frac{2\mu E}{\hbar^2}, \qquad \theta \equiv \frac{2\mu V}{\hbar^2}, \qquad k \equiv \sqrt{\epsilon}, \qquad \rho \equiv \sqrt{-\epsilon},$$
$$K \equiv \sqrt{\epsilon - \theta}, \qquad K' \equiv \sqrt{\theta - \epsilon} = \mathrm{i}K. \tag{5.3}$$

Firstly we want to solve Eq. (5.2) in the inner region $(r \leqslant R)$. We consider the case $\epsilon > \theta$. Then, Eq. (5.2) becomes

$$\chi''(r) + K^2 \chi(r) = 0.$$

Two linearly independent solutions of this equation are the sine and the cosine function

$$\sin(Kr) \quad \text{and} \quad \cos(Kr).$$

But due to the boundary condition $\chi(0) = 0$ only the sine function is a possible solution of the inner region

$$\chi_{\text{in}}(r) = A \sin(Kr) \qquad (\epsilon > \theta)$$

(A is a constant). Similarly we obtain

$$\chi_{\text{in}}(r) = A \sinh(K'r) \qquad (\epsilon < \theta)$$

in the case $\epsilon < \theta$ since $\sin(\mathbb{i}x) = \mathbb{i}\sinh(x)$. We now turn to the outer region ($r > R$). In the case $\epsilon < 0$ Eq. (5.2) becomes

$$\chi''(r) - \rho^2\chi(r) = 0.$$

Two linearly independent solutions of this equation are

$$e^{\rho r} \quad \text{and} \quad e^{-\rho r}.$$

But since $e^{\rho r}$ blows up as $r \to \infty$ the only possible solution of the outer region is given by

$$\chi_{\text{out}}(r) = Be^{-\rho r} \qquad (\epsilon < 0)$$

(B is a constant). In the case $\epsilon > 0$ Eq. (5.2) becomes

$$\chi''(r) + k^2\chi(r) = 0.$$

Two possible linearly independent solutions of this equation are

$$\sin(kr) \quad \text{and} \quad \cos(kr).$$

There are no further constrains: The point $r = 0$ does not belong to the interval $[R, \infty)$ and, since $\sin(kr)$ and $\cos(kr)$ belong to the continuous energy spectrum, the wave function does not need to be normalizable. Thus, any superposition of these functions is a solution of the outer region. Let us choose the two constants B (amplitude) and δ_0 (phase shift) to construct the solution

$$\chi_{\text{out}}(r) = B\big[\cos\delta_0 \sin(kr) + \sin\delta_0 \cos(kr)\big] = B\sin(kr + \delta_0).$$

Molecules: The different solutions are now merged at $r = R$. In the case $\theta < \epsilon < 0$ we may obtain molecular bound states

$$\chi_{\text{bound}}(r) = \begin{cases} \chi_{\text{in}}(r) = A\sin(Kr) & \text{if } r \leqslant R \\ \chi_{\text{out}}(r) = Be^{-\rho r} & \text{if } r \geqslant R. \end{cases} \tag{5.4}$$

The possible energies of the bound states are determined by the continuity of the logarithmic derivative at $r = R$

$$\beta_0 \equiv \frac{\chi'_{\text{in}}(R)}{\chi_{\text{in}}(R)} = \frac{\chi'_{\text{out}}(R)}{\chi_{\text{out}}(R)} \tag{5.5}$$

Using (5.4) we obtain

$$\frac{K\cos(KR)}{\sin(KR)} = -\frac{\rho e^{-\rho R}}{e^{-\rho R}}.$$

The possible eigenenergies are thus given by the zeros of the "energy function"

$$F(\epsilon) \equiv \tan\left(\sqrt{\epsilon - \theta}R\right) + \sqrt{\frac{\epsilon - \theta}{(-\epsilon)}} = 0. \tag{5.6}$$

The constant B is determined by the continuity of χ at R

$$\chi_{\text{in}}(R) = \chi_{\text{out}}(R) \quad \Rightarrow \quad B = A\sin(KR)e^{\rho R}. \tag{5.7}$$

Finally the constant A is determined by the normalization condition

$$A = \int_0^\infty dr\chi^2(r). \tag{5.8}$$

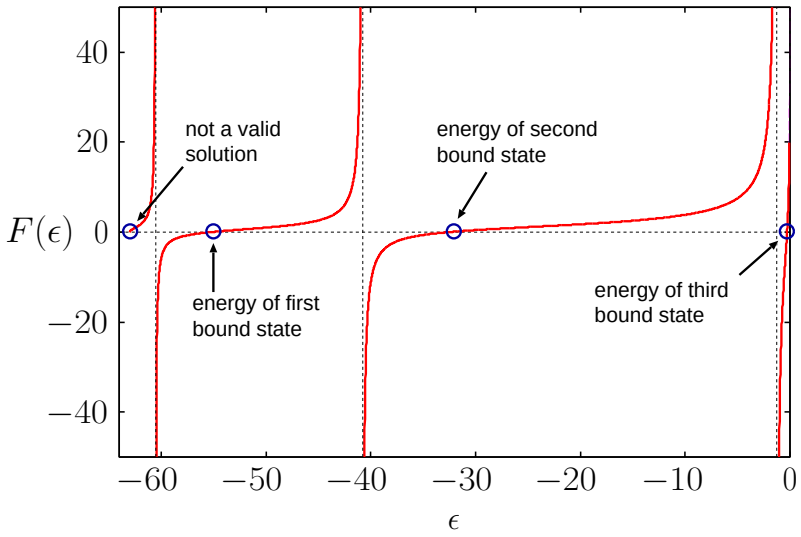

Figure 5.2: "Energy function" $F(\epsilon)$ for parameters $R = 1$ and $\theta = -63$. The energy eigenvalues are the zeros of $F(\epsilon)$. These are located at $\epsilon_1 = -55.3$, $\epsilon_2 = -32.6$ and $\epsilon_3 = -0.27$. The zero at $\epsilon = \theta = -63$ is not a valid solution since it belongs to the wave function $\chi_{\text{bound}}(r) = 0$. The zeros are located between the singularities of $F(\epsilon)$. These are located at $\epsilon_{\text{sing.}}(n) = \theta + \left[(2n-1)\frac{\pi}{2R}\right]^2$ with $n = 1, 2, \ldots, n_{\text{bound}}$ (n_{bound} total number of bound states).

Two examples of molecular bound states are depicted in Fig. 5.1(a). The corresponding eigenenergies have been determined numerically by solving Eq. (5.6) by means of MATHEMATICA. An example plot of the "energy function" is given in Fig. 5.2. We see that the zeros are located between the singularities of $F(\epsilon)$. These singularities can be determined easily:

$$
\begin{aligned}
& F(\epsilon) = \pm\infty \quad \Rightarrow \quad \tan\left(\sqrt{\epsilon-\theta}R\right) = \pm\infty \\
& \Rightarrow \ \sqrt{\epsilon-\theta}R = (2n-1)\frac{\pi}{2} \quad (n = 1, 2, 3, \ldots) \\
& \Rightarrow \ \epsilon_{\text{sing.}}(n) = \theta + \left[(2n-1)\frac{\pi}{2R}\right]^2 \quad (n = 1, 2, 3, \ldots, n_{\text{bound}})
\end{aligned}
$$

where n_{bound} is the total number of bound states. This number can be calculated as follows: We assume that the energy of the least bound state is approximately zero ($\epsilon = 0-$). Then, we obtain from the "energy function"

$$
\begin{aligned}
& \frac{1}{F(\epsilon=0)} = 0 \quad \Rightarrow \quad \cot\left(\sqrt{-\theta}R\right) = 0 \\
& \Rightarrow \ \sqrt{-\theta}R = (2n-1)\frac{\pi}{2} \quad (n = 1, 2, 3, \ldots) \\
& \Rightarrow \ n_{\text{bound}} = \left\lfloor \frac{\sqrt{-\theta}R}{\pi} + \frac{1}{2} \right\rfloor
\end{aligned}
\tag{5.9}
$$

where $\lfloor x \rfloor$ is the greatest integer less than or equal to x. Therefore, if the box is too shallow and too narrow, it might be possible that there exists no bound state at all.

Strongly bound molecules— For strongly bound molecules ($\epsilon \ll 0$) the box potential is practically infinitely high. Thus the molecular wave function is given by $\chi_{\text{bound}} = A\sin(Kr)$ for $r \leqslant R$ and zero otherwise. From the boundary condition $\chi_{\text{bound}}(R) \approx 0$ we obtain $KR \approx n\pi$ and thus

$\epsilon \approx \theta + n^2(\pi/R)^2$ — the well-known result of a particles in a one-dimensional infinite square well. The wave function is therefore approximately given by $\chi_{\text{bound}} \approx A\sin\big[n\pi(r/R)\big]$. Thus, the inner wave function of the nth strongly bound molecule shows $n/2$ sine oscillations [compare with the blue and green wave function of Fig. 5.5(a)]. The mean distance between the atoms is $\langle r\rangle = \int dr\, r\, \chi^2_{\text{bound}} \approx R/2$.

Weakly bound molecules— For weakly bound molecules ($\epsilon \lesssim 0$) the outer wave function is approximately given by $\chi_{\text{out}} = Be^{-\sqrt{-\epsilon}\,r} \approx B(1-\sqrt{-\epsilon}\,r)$. We have seen in the derivation of Eq. (5.9) that in this case $K \approx \sqrt{-\theta} \approx (2n_{\text{bound}}-1)\pi/(2R)$ so that the inner wave function is given by $\chi_{\text{in}} \approx A\sin\big[(2n_{\text{bound}}-1)(\pi/2)(r/R)\big]$. Thus, the inner wave function of the weakly bound molecule shows $(2n_{\text{bound}}-1)/4$ sine oscillations [compare with the red wave function of Fig. 5.5(a)]. The mean distance between the atoms $\langle r\rangle$ approaches $+\infty$ when ϵ approaches zero since then the outer wave function becomes a constant $\chi_{\text{out}} \approx B$.

Free spherical waves: We now turn to the case $\epsilon > 0$ where the solutions are free spherical waves. In the case $\epsilon > \theta$ we obtain for the wave function

$$\chi_{\text{free}}(r) = \begin{cases} \chi_{\text{in}}(r) = A\sin(Kr) & \text{if } r \leqslant R \\ \chi_{\text{out}}(r) = B\sin(kr+\delta_0) & \text{if } r \geqslant R \end{cases} \qquad (\epsilon > \theta). \tag{5.10}$$

The phase shift δ_0 can be calculated from the logarithmic derivative at R: Using the inner wave function we obtain

$$\beta_0 = \frac{\chi'_{\text{in}}(R)}{\chi_{\text{in}}(R)} = K\cot(KR) \qquad (\epsilon > \theta). \tag{5.11}$$

From the outer solution we obtain

$$\beta_0 = \frac{\chi'_{\text{out}}(R)}{\chi_{\text{out}}(R)} = \frac{k\big[\cos\delta_0\cos(kR) - \sin\delta_0\sin(kR)\big]}{\cos\delta_0\sin(kR) + \sin\delta_0\cos(kR)} = k\frac{\cos(kR) - \tan\delta_0\sin(kR)}{\sin(kR) + \tan\delta_0\cos(kR)}.$$

Thus, the phase shift is given by

$$\delta_0 = \arctan\left[\frac{k\cos(kR) - \beta_0\sin(kR)}{k\sin(kR) + \beta_0\cos(kR)}\right]. \tag{5.12}$$

The constant A can be deduced from the continuity of χ at R

$$\chi_{\text{in}}(R) = \chi_{\text{out}}(R) \quad \Rightarrow \quad A = \frac{B\sin(kR+\delta_0)}{\sin(KR)} \qquad (\epsilon > \theta). \tag{5.13}$$

The remaining constant B can be chosen at will since the free spherical waves are not normalizable. I choose $B = 1$.

The case $\epsilon < \theta$ is very similar since $\sin(\mathbb{i}x) = \mathbb{i}\sinh(x)$ and $\cos(\mathbb{i}x) = \cosh(x)$: Simply replace $\sin(Kr)$ by $\sinh(K'r)$ in Eq. (5.10) to obtain the wave function

$$\chi_{\text{free}}(r) = \begin{cases} \chi_{\text{in}}(r) = A\sinh(K'r) & \text{if } r \leqslant R \\ \chi_{\text{out}}(r) = B\sin(kr+\delta_0) & \text{if } r \geqslant R \end{cases} \qquad (\epsilon < \theta), \tag{5.14}$$

replace $K\cot(KR)$ by $K'\coth(K'R)$ in (5.11) to obtain the logarithmic derivative

$$\beta_0 = K'\coth(K'R) \qquad (\epsilon < \theta) \tag{5.15}$$

and replace $\sin(KR)$ by $\sinh(K'R)$ in (5.13) to obtain the constant A

$$A = \frac{B\sin(kR+\delta_0)}{\sinh(K'R)} \qquad (\epsilon < \theta). \tag{5.16}$$

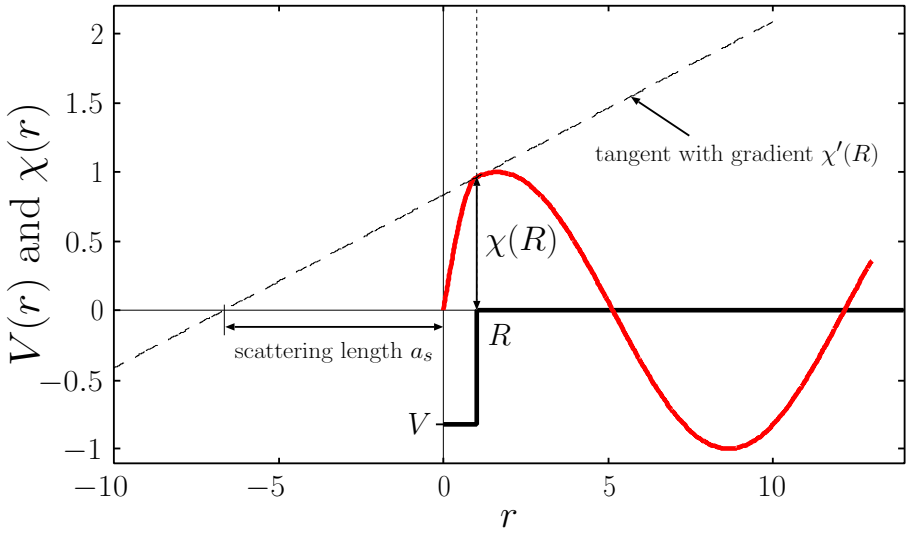

Figure 5.3: Definition of the scattering length. The picture shows an attractive potential $V(r)$ (black thick solid line), a radial wave function $\chi(r)$ (red thick solid line) and the tangent of χ at R. We define the scattering length a_s as the intersection of the tangent of χ at R with the r-axis.

Also in this case the phase shift is given by Eq. (5.12) (since in both cases the outer wave function $\chi_{\text{out}}(r)$ is the same) but now one has to use Eq. (5.15) for the logarithmic derivative β_0 (since the inner solutions are different). Again we choose $B = 1$.

Hard sphere— In the extreme case of a hard sphere ($V = \infty$) it follows from Eqs. (5.3), (5.12), (5.15) and (5.16) that $K' = \infty$, $A = 0$, $\beta_0 = \infty$ and $\delta_0 = -kR$. Thus the wave function is simply $\chi_{\text{free}}(r) = \sin\big[k(r-R)\big]$ if $r \geqslant R$ and zero if $r \leqslant R$.

Examples of free spherical waves are depicted in Fig. 5.1(a) and (b). For $\epsilon < \theta$ the wave function grows exponentially in the inner region, $\chi_{\text{free}} \propto \sinh(K'r)$, with $K' \propto \sqrt{V-E}$. In the borderline case $\epsilon = \theta$ the wave function is just a straight line and $\chi_{\text{free}} \propto r$. For $\epsilon > \theta$ the wave function shows an oscillatory behavior, $\chi_{\text{free}} \propto \sin(Kr)$, with $K \propto \sqrt{E-V}$. In the outer region the wave function $\chi_{\text{free}} \propto \sin(kr)$ oscillates with $k \propto \sqrt{E}$.

Scattering length: Let me now introduce the concept of the scattering length. We define the scattering length a_s as the intersection of the tangent of χ at R with the r-axis, [1] see Fig. 5.3 (this definition can be applied to any potential with a finite range R). As can be seen in Fig. 5.3 the following relation holds

$$\frac{\chi(R)}{R-a_s} = \chi'(R) \quad \Leftrightarrow \quad a_s = R - \frac{\chi(R)}{\chi'(R)} = R - \frac{1}{\beta_0}. \tag{5.17}$$

In the extreme case of a hard sphere $\big[V = \infty$; see Fig. 5.4(a)$\big]$ the scattering length is simply given by the radius of the hard sphere

$$a_s = R \qquad \text{(hard sphere)}$$

since $\beta_0 = \infty$. In the case of a soft sphere $\big[0 < E \leqslant V = $ finite; see Figs. 5.4(b) and (c)$\big]$ it follows from Eqs. (5.17) and (5.15) that the scattering length is given by

$$a_s = R - \frac{1}{K'}\tanh(K'R) \qquad (0 < E \leqslant V). \tag{5.18}$$

[1] See pp. 413-414 of Ref. [97].

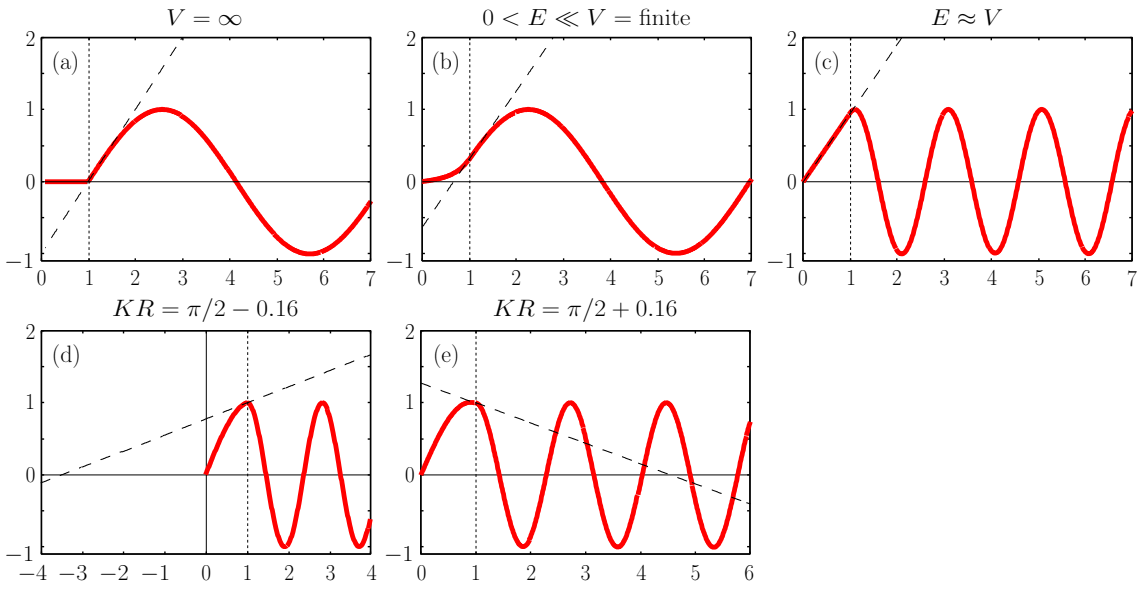

Figure 5.4: Scattering length of several wave functions. The pictures show a wave function $\chi(r)$ (red thick solid line) and its tangent at R (black thin dashed line). The radius of the box potential is $R = 1$. The scattering length a_s is the intersection of the tangent of χ at R with the r-axis. (a) $a_s = R$, (b) $a_s = 0.66R$, (c) $a_s = 0$, (d) $a_s = -3.5R$ and (e) $a_s = 4.5R$.

Thus, if $K'R \ll 1$ the scattering length is $a_s \approx 0$ since $\tanh(x) \approx x$ for small x. On the other hand, if $K'R \gg 1$ the scattering length is $a_s \approx R - 1/K'$ since $\tanh(x) \approx 1$ for large x. Therefore, in the case of a soft sphere, the following inequality holds:

$$0 \leqslant a_s < R \qquad (\text{for } 0 < E \leqslant V = \text{finite}).$$

In the case $E > V$ the scattering length has to be calculated from Eqs. (5.17) and (5.11)

$$a_s = R - \frac{1}{K}\tan(KR) \qquad (E > V). \tag{5.19}$$

Therefore the scattering length varies from $-\infty$ to $+\infty$ depending on KR. In particular a_s jumps from $-\infty$ to $+\infty$ if $KR \to (2n-1)\pi/2$ $(n = 1, 2, \ldots)$; see Figs. 5.4(d) and (e).

Relation between scattering length and phase shift— In the case of a hard sphere $a_s = R$ and $\delta_0 = -kR$ leading to $\delta_0 = -ka_s$. In general we can connect the scattering length with the phase shift by inserting the logarithmic derivative of the outer solution $\beta_0 = \chi'_{\text{out}}(R)/\chi_{\text{out}}(R)$ into Eq. (5.17)

$$a_s = R - \frac{1}{k}\tan(kR + \delta_0). \tag{5.20}$$

For $k \approx 0$ and $R \ll a_s$ we obtain $\tan\delta_0 = -ka_s$.

Some borderline cases— Strongly bound molecules: Similar to the case of the hard sphere the wave function is approximately zero at R since $\chi_{\text{in}} \approx A\sin\big[n\pi(r/R)\big]$. Therefore, the scattering length is $a_s \approx R$ (more precisely $a_s \gtrsim R$); see the tangents of the blue and the green wave function in Fig. 5.5(a). Weakly bound molecules: The outer wave function is approximately given by $\chi_{\text{out}} \approx B(1 - \sqrt{-\epsilon}r)$. Therefore, a_s approaches $+\infty$ when ϵ approaches zero; see Figs. 5.5(a-c). Low-energy free waves: The outer wave function is approximately given by $\chi_{\text{out}} \approx B\cos\big[k(r-R)\big]$. Thus, at $r = R$, the gradient of χ_{out} is zero and $|a_s| = \infty$. More precisely $a_s = -\infty$; see Fig. 5.5(d).

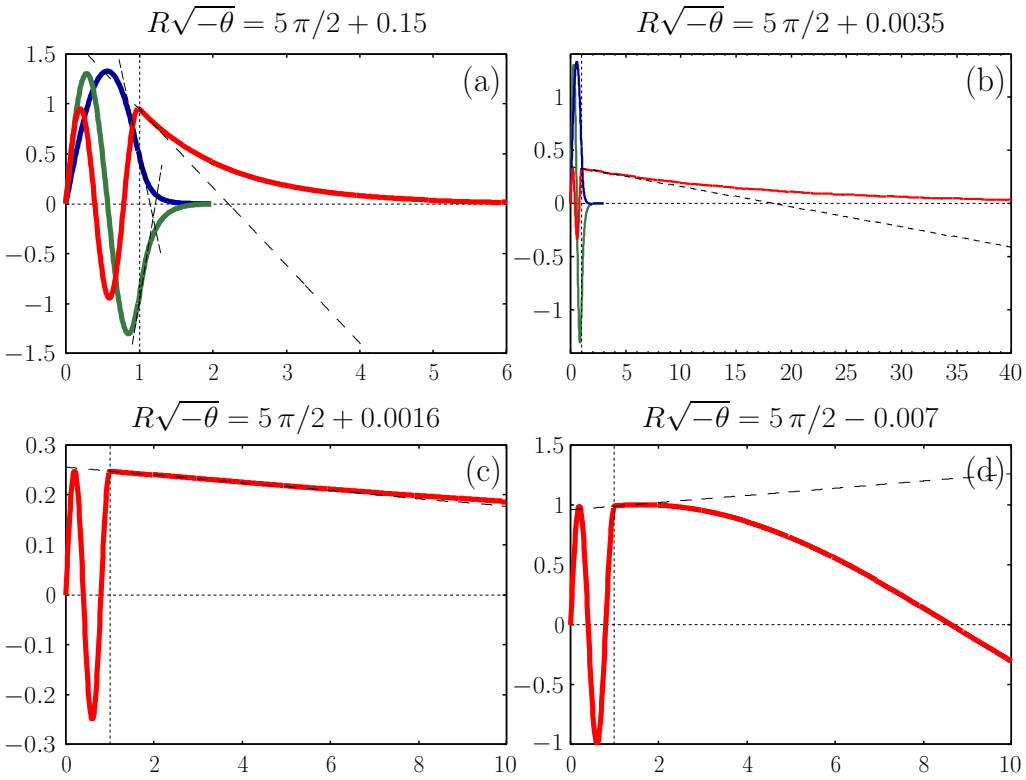

Figure 5.5: (a) Three molecular bound states. Blue: molecule in the lowest vibrational state, green: molecule in the first excited vibrational state, red: least bound state (with highest vibrational energy). (b) The extent of the weakly bound molecule tends to infinity when the binding energy approaches zero. (c) $a_s = +\infty$ for a least bound state with $E = 0-$ and (d) $a_s = -\infty$ for a low-energy free wave with $E = 0+$.

Weakly bound molecules: We have seen that the binding energy of the least bound state approaches zero if $\sqrt{-\theta}R = (2n-1)\pi/2$ [see the derivation of Eq. (5.9)]. In Figs. 5.5(a) and (b) I have chosen the parameters of the attractive box potential according to $\sqrt{-\theta}R \gtrsim 5\,\pi/2$ so that three bound states occur. The blue line is the wave function of the strongest bound molecule which is in the lowest vibrational state. The green line belongs to a molecule which is in the first excited vibrational state and the red line belongs to a molecule which is in the second excited vibrational state. The blue and the green wave function have large binding energies and they are located within the box potential ($\langle r\rangle \approx 0.6R$). By contrast the red wave function has an extremely small binding energy and the mean distance between the atoms is large ($\langle r\rangle \approx 9.2R$ in the top right figure). The probability to find the two atoms within the radius R is extremely small.

We can relate the scattering length to the binding energy of the least bound state. Using the logarithmic derivative of the outer wave function (5.4) we obtain from Eq. (5.17)

$$a_s = R + \frac{1}{\rho} \;\Leftrightarrow\; \rho = \frac{1}{a_s - R} \quad \Rightarrow \quad E_b \equiv -E = \frac{\hbar^2\rho^2}{2\mu} = \frac{\hbar^2}{2\mu(a_s-R)^2} \approx \frac{\hbar^2}{2\mu a_s^2} \tag{5.21}$$

for large scattering lengths $a_s \gg R$. Further, a_s is related to the distance $\langle r\rangle$ between the atoms. As can be seen in Fig. 5.5(b), for a weakly bound molecule, the probability to find the particles

within a sphere with radius R is negligible compared to the probability to find them outside,

$$\int_0^R dr\chi^2 \approx 0 \quad \text{and} \quad \int_R^\infty dr\chi^2 \approx 1\,.$$

Since $\chi_{\text{out}} = Be^{-\rho r}$ we obtain

$$1 \approx \int_R^\infty dr\chi_{\text{out}}^2 = B^2 \int_R^\infty dr e^{-2\rho r} \quad \Rightarrow \quad B^2 = 2\rho e^{2\rho R}$$

and the mean distance $\langle r\rangle$ is given by

$$\langle r\rangle \approx \int_R^\infty dr\, r\, \chi_{\text{out}}^2 = B^2 \int_R^\infty dr\, r\, e^{-2\rho r} = R + \frac{1}{2\rho} = \frac{R+a_s}{2}. \tag{5.22}$$

Figs. 5.5(c) and (d) show the evolution from a weakly bound state to a low-energy free wave when the attractive potential is made shallower. As can be seen $a_s = +\infty$ when the energy of the least bound state is infinitesimal small, $E = 0-$, and $a_s = -\infty$ for a free wave with $E = 0+$.

Delta potential: The usual repulsive δ potential has no influence on the scattered wave. To see this we consider the potential $\delta_R = 3/(4\pi R^3)$ if $r \leqslant R$ and zero if $r \geqslant R$. The scattered wave shall have a low fixed energy E. For small enough R we have $0 < E < 3/(4\pi R^3)$ so that $0 < a_s < R$. Thus, $a_s \to 0$ if $R \to 0$. Further, $\delta_0 \to 0$ if $a_s \to 0$ and $R \to 0$; see Eq. (5.20).

5.2 S-wave scattering in a harmonic trap

We consider two atoms which interact via the box potential (5.1). Additionally the atoms are confined by a harmonic oscillator potential. The angular momentum of the relative motion shall be zero ($l = 0$). The radial dimensionless equation of the relative motion reads

$$\left[-\frac{1}{2r}\frac{d^2}{dr^2}r + V_{\text{box}}(r) + \frac{1}{2}r^2 - E\right]\psi(r) = 0.$$

Here, all lengths have been expressed in units of the oscillator length $l_{\text{osc}} = \sqrt{\hbar/(\mu\omega)}$ and all energies have been expressed in units of $\hbar\omega$. Again, we substitute $\chi = r\psi$ and obtain the equation

$$\chi'' - r^2\chi + 2\big[E - V_{\text{box}}\big]\chi = 0. \tag{5.23}$$

Two linearly independent solutions of this equation are given by

$$y_1\big[-(E - V_{\text{box}}); \sqrt{2}r\big], \qquad y_2\big[-(E - V_{\text{box}}); \sqrt{2}r\big]/\sqrt{2}$$

where the parabolic cylinder functions y_1 and y_2 [2] are given by

$$y_1(a;z) = {}_1F_1\left[\frac{a}{2}+\frac{1}{4};\frac{1}{2};\frac{z^2}{2}\right]e^{-z^2/4}, \qquad y_2(a;z) = z\,{}_1F_1\left[\frac{a}{2}+\frac{3}{4};\frac{3}{2};\frac{z^2}{2}\right]e^{-z^2/4}. \tag{5.24}$$

The function ${}_1F_1(a;b;z)$ is the confluent hypergeometric function of the first kind [3]

$${}_1F_1(a;b;z) = 1 + \frac{a}{b}z + \frac{a(a+1)}{b(b+1)}\frac{z^2}{2} + \ldots + \frac{a\ldots(a+n-1)}{b\ldots(b+n-1)}\frac{z^n}{n!} + \ldots \tag{5.25}$$

[2] Entries 19.2.1 and 19.2.3 of Ref. [100] / Wikipedia / Wolfram *MathWorld*.

[3] Entry 13.1.2 of Ref. [100] / Wikipedia / Wolfram *MathWorld*.

which is implemented as "Hypergeometric1F1" in MATHEMATICA. A derivation of the solutions y_1 and y_2 by means of a polynomial ansatz is given in appendix B.

In the inner region $r \leqslant R$ we have to satisfy the boundary condition $\chi(0) = 0$. Since $y_1(a;0) = 1$ and $y_2(a;0) = 0$ the solution of the inner region is given by ($V_{\text{box}} = V$)

$$\chi_{\text{in}}(r) = A\, y_2\big[-(E-V); \sqrt{2}r\big].$$

In the outer region $r \geqslant R$ we have to fulfill the boundary condition $\chi(\infty) = 0$. For this reason we construct another pair of linearly independent solutions of Eq. (5.23) [4]

$$\begin{aligned} U(a;z) &= \cos\big[\pi(a/2+1/4)\big]Y_1(a;z) - \sin\big[\pi(a/2+1/4)\big]Y_2(a;z), \\ V(a;z) &= \frac{1}{\Gamma(1/2-a)}\Big\{\sin\big[\pi(a/2+1/4)\big]Y_1(a;z) + \cos\big[\pi(a/2+1/4)\big]Y_2(a;z)\Big\} \end{aligned} \tag{5.26}$$

with

$$Y_1(a;z) = \frac{\Gamma(1/4-a/2)}{\sqrt{\pi}\,2^{a/2+1/4}}\, y_1(a;z), \qquad Y_2(a;z) = \frac{\Gamma(3/4-a/2)}{\sqrt{\pi}\,2^{a/2-1/4}}\, y_2(a;z). \tag{5.27}$$

The behavior of these functions at $r = \infty$ is known: [5] $V(a;z)$ diverges and $U(a;z)$ approaches zero for large values of r. Thus, the solution of the outer region is given by ($V_{\text{box}} = 0$)

$$\chi_{\text{out}}(r) = B\, U\big[-E; \sqrt{2}r\big]. \tag{5.28}$$

The discrete energies follow from the logarithmic derivative at R

$$\frac{y_2'\big[-(E-V); \sqrt{2}R\big]}{y_2\big[-(E-V); \sqrt{2}R\big]} = \frac{U'\big[-E; \sqrt{2}R\big]}{U\big[-E; \sqrt{2}R\big]}, \tag{5.29}$$

the constant B follows from the continuity at R

$$\chi_{\text{in}}(R) = \chi_{\text{out}}(R) \quad \Rightarrow \quad B = A\frac{y_2\big[-(E-V); \sqrt{2}R\big]}{U\big[-E; \sqrt{2}R\big]}$$

and the constant A follows from the normalization condition.

Discussion— As an example Fig. 5.6 shows the evolution of two wave functions with decreasing box depth and Fig. 5.7 shows the corresponding energies and the scattering length of the molecule.

Fig. 5.6(a): For the chosen box depth of $V = -1485\,\hbar\omega$ we have three molecular bound states. Shown is the least bound molecule (red) which is in the second excited (internal) vibrational state. Therefore we see a fast oscillation within the inner region $r \leqslant R$ and a fast exponential decrease in the outer region $r \leqslant R$. Similarly the next excited state (blue) rapidly oscillates in the inner region. In the outer region it perfectly agrees with the ground state of the harmonic trap (yellow dashed). Thus, the phase shift δ_0 and the scattering length a_s of this state are zero.

Fig. 5.6(b): The molecule (red) is now only weakly bound and the distance between the atoms is twice as large as in (a). The next excited state (blue) now resembles the ground state of the harmonic trap (blue dashed line) which is slightly shifted rightwards along the r-axis ($\Rightarrow$ small negative phase shift). The scattering length is small and positive and approximately given by the intersection of the blue wave function with the r-axis at $r \approx 0.35\, l_{\text{osc}}$.

[4] Entries 19.3.1, 19.3.2, 19.3.3 and 19.3.4 of Ref. [100] / Wikipedia / Wolfram *MathWorld*.

[5] Entries 19.8.1 and 19.8.2 of Ref. [100] / Wikipedia / Wolfram *MathWorld*.

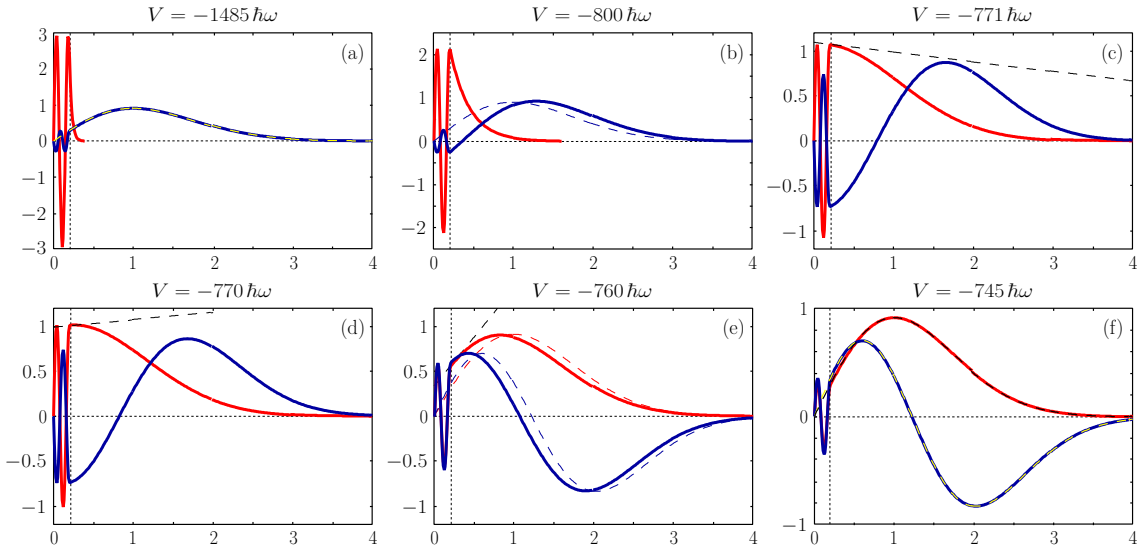

Figure 5.6: Evolution of two wave functions with decreasing depth of the box potential. I have chosen $R = 0.2\,l_{\text{osc}}$ for all pictures. (a) The box depth is $V = -1485\,\hbar\omega$. Red is the molecule, blue is the wave function with the next highest energy and yellow dashed is the ground state of the harmonic trap $\left(\chi \propto re^{-r^2/2}\right.$ since $\chi = r\psi$ and $\left.\psi \propto e^{-r^2/2}\right)$. The molecule is strongly bound. The distance between the atoms $\langle r\rangle \gtrsim R/2$. The blue wave function perfectly agrees with the ground state of the harmonic trap in the outer region apart from some fast oscillations in the inner region. Scattering length a_s and phase shift δ_0 are zero. (b) The scattering length is $a_s \approx 0.35\,l_{\text{osc}}$ and the phase shift is small and negative $\delta_0 \approx -ka_s$. The outer blue wave function looks like the ground state of the harmonic trap (blue dashed) which is shifted rightwards along the r-axis. The molecule is weakly bound and $\langle r\rangle \gtrsim R$. (c) $V = -771\,\hbar\omega$, $a_s \approx 10\,l_{\text{osc}}$, $\delta_0 \approx -\pi/2$ and $\langle r\rangle \approx 3.5R$. (d) $V = -770\,\hbar\omega$, $a_s \approx -12\,l_{\text{osc}}$, $\delta_0 \approx +\pi/2$. (e) $V = -760\,\hbar\omega$, $a_s \approx -0.3\,l_{\text{osc}}$, $\delta_0 \approx -ka_s$ small and positive and $\langle r\rangle \approx 5R \approx 1\,l_{\text{osc}}$. Red dashed is the ground state and blue dashed is the next excited state of the harmonic trap. The outer red (blue) wave function looks like the ground (next excited) state of the harmonic trap which is shifted leftwards along the r-axis. (f) $\langle r\rangle \approx 1.13\,l_{\text{osc}}$. The red (blue) wave function now perfectly agrees with the ground (next excited) state of the harmonic trap. Again, $a_s = 0$ and $\delta_0 = 0$. (a-f) With decreasing box depth the molecule (ground state) evolves towards the ground (next excited) state of the trap.

Fig. 5.6(c): With decreasing box depth the molecule becomes more and more loosely bound. The scattering length increases up to a maximum value of $a_s = +\infty$; see the tangent of the molecular wave function (black dashed line). Likewise the mean distance $\langle r\rangle$ between the atoms is much larger than R. However, $\langle r\rangle$ does not converge towards infinity according to Eq. (5.22) due to the external trapping potential.

Fig. 5.6(d): Similar to the free-space case [see Fig. 5.5] the molecule becomes an unbound pair of atoms when the scattering length switches from plus to minus infinity. It seems to be a reasonable definition of the transition point. However, there is no dicontinuous change of the wave function at this transition point. The wave functions of Figs. 5.6(c) and (d) look almost equal. Only the gradient of the wave function at R changes slightly from $0-$ to $0+$ leading to an abrupt jump of intersection of the tangent of the wave function at R with the r-axis. Likewise the phase shift δ_0 jumps from $-\pi/2$ to $+\pi/2$. However, since $\sin(x - \pi/2) = -\sin(x + \pi/2) = -\cos(x)$ and since the minus sign is absorbed by the global phase of the normalization constant, there is no visible influence on the wave function.

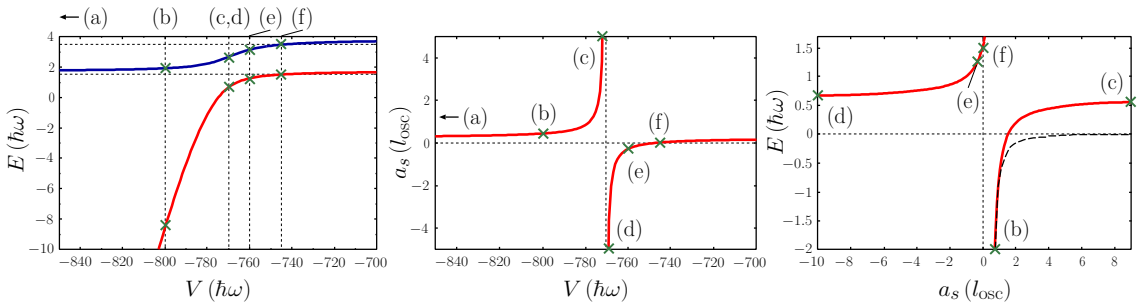

Figure 5.7: *Left:* Evolution of the energy of the weakly bound molecule (red) and the ground state of the harmonic trap (blue) with decreasing depth of the attractive box potential. The green crosses mark the corresponding wave functions of Fig. 5.6. *Middle:* Evolution of the scattering length of the molecule with decreasing box depth. *Right:* Energy of the molecule (red) as a function of the scattering length. Black dashed is an estimate of the molecular energy according to $E = -\hbar^2/\left[2\mu(a_s - R)^2\right]$ which is exact in free space [see Eq. (5.21)].

With further decreasing trap depth the red wave function, which was formerly a bound molecule, evolves more and more into a wave function which is very similar to the ground state of the harmonic oscillator apart from the fast oscillations in the inner region. In Fig. 5.6(e) the red wave function has already a large overlap with the ground state of the trap (red dashed line). It is only shifted a little bit leftwards along the r-axis compared to the ground state of the trap (small positive phase shift). Likewise the blue wave function resembles the next excited state (blue dashed) of the trap. Thus, the phase shift is small and positive.

The phase shift becomes even zero for $V = -745\,\hbar\omega$; see Fig. 5.6(f). At this point also the scattering length is again zero; see the middle picture of Fig 5.7. Now, the red and the blue wave function perfectly agree with the ground (next excited) state of the harmonic trap in the outer region. Thus, one can say, that the least bound molecule (ground state of the trap) continuously evolves into the ground (next excited) state of the trap when the depth of the box potential is made shallower.

The transition behavior is also visible in the evolution of the energies; see Fig. 5.7(left). Red is the energy of the molecule and blue is the energy of the ground state of the trap. In a rotationally symmetric harmonic trap the energy eigenvalues are given by $E = (2n + l + 3/2)\hbar\omega$ where $n = 0, 1, \ldots$ is the principal quantum number and $l = 0, 1, \ldots$ is the relative angular momentum. The ground-state energy is $E_0 = 3/2\,\hbar\omega$ and the energy of the next excited state with $l = 0$ is $E_2 = 7/2\,\hbar\omega$ [this is the second excited state since the state $(n, l) = (0, 1)$ has a lower energy]. When the box is made shallower from $V = -1485$ to $-780\,\hbar\omega$ the energy of the molecule (red) grows rapidly from $E = -576$ to $-1\,\hbar\omega$. This increase dramatically slows down in the region $V = -780 \ldots -745\,\hbar\omega$. At $V = -745\,\hbar\omega$ the energy of the former molecule exactly coincides with the energy of the ground state of the trap $E_0 = 3/2\,\hbar\omega$. At this point the scattering length is zero and the former molecule exactly coincides with the ground state of the trap in the outer region. Above $V = -745\,\hbar\omega$, in the region $V = -745 \ldots -500\,\hbar\omega$, the energy of the former molecule is nearly unaffected by large changes of the box depth, it increases only from $E = 1.5$ to $1.7\,\hbar\omega$. Likewise the energy of the oscillator ground state (blue) evolves from $E_0 = 3/2\,\hbar\omega$ to $E_2 = 7/2\,\hbar\omega$. The change of the energy mainly occures in the small region $V = -790 \ldots -750\,\hbar\omega$ and is fastest around $V = -770\,\hbar\omega$ where the scattering length jumps from plus to minus infinity. Remarkably the energy of this state (and all the other harmonic oscillator states) is nearly unaffected by the large changes of the trap depth below $V = -790\,\hbar\omega$ and above $V = -750\,\hbar\omega$. This is also true

for the wave function (see the change of the scattering length in the middle picture of Fig. 5.7).

Finally, Fig. 5.7(right) shows the energy of the molecule (red) as a function of the scattering length which are connected through $E(V(a_s))$. Black dashed is the free-space energy of the molecule according to Eq. (5.21). Both curves agree well for small positive scattering lengths since a tightly bound molecule is nearly unaffected by an additional external trap.

Comparison with the solution of Busch et al.: Firstly, I will show that the outer wave function (5.28) is equal to the solution of Busch *et al.* [75]. Eq. (17) of Ref. [75] reads

$$\psi_{\text{Busch}}(r) = \frac{1}{2}\pi^{-3/2} A e^{-r^2/2}\Gamma(-\nu) U\left(-\nu; \frac{3}{2}; r^2\right) \tag{5.30}$$

where A is a normalization constant, $\Gamma(z)$ is the gamma function and

$$U(a,b,z) = \frac{\pi}{\sin(\pi b)}\left[\frac{{}_1F_1(a;b;z)}{\Gamma(1+a-b)\Gamma(b)} - z^{1-b}\frac{{}_1F_1(1+a-b;2-b;z)}{\Gamma(a)\Gamma(2-b)}\right] \tag{5.31}$$

is the confluent hypergeometric function of the second kind [6] which is implemented as "HypergeometricU" in MATHEMATICA. The index ν is related to the energy according to $E = 2\nu + 3/2$. I define the normalization constant $B' \equiv 1/2\pi^{-3/2} A\Gamma(-\nu)$. Thus, we have to show that

$$\chi_{\text{out}}(r) = B\, U\left[-E; \sqrt{2}r\right] = r\psi_{\text{Busch}}(r) = B'\, r\, U\left(-\frac{E}{2} + \frac{3}{4}; \frac{3}{2}; r^2\right) e^{-r^2/2}. \tag{5.32}$$

One finds [7]

$$U(a;z) = D_{-a-1/2}(z) \tag{5.33}$$

and [8]

$$D_\nu(z) = 2^{\nu/2} e^{-z^2/4} U\left(-\frac{\nu}{2}; \frac{1}{2}; \frac{z^2}{2}\right).$$

Using these relations we obtain from Eq. (5.28)

$$\chi_{\text{out}}(r) = B\, D_{E-1/2}(\sqrt{2}r) = B'\, U\left(-\frac{E}{2} + \frac{1}{4}; \frac{1}{2}; r^2\right) e^{-r^2/2} \tag{5.34}$$

with $B' = B\, 2^{E/2-1/4}$. One finds [9]

$$U(a;b;z) = z^{1-b} U(1+a-b; 2-b; z).$$

Using this relation with $a = -E/2 + 1/4$, $b = 1/2$ and $z = r^2$ we finally obtain the right-hand side of Eq. (5.32). Thus, we may use Eq. (5.28), the right-hand side of Eq. (5.32) or Eq. (5.34) for the outer wave function $\chi_{\text{out}}(r)$. However, the energy of our system (box potential with radius R) is still different from the energy of the system of Busch *et al.* [75] (regularized δ potential) and in the inner region ($r \leqslant R$) the wave function $\chi_{\text{in}}(r)$ strongly deviates from Eq. (5.34).

It arises the question, whether the energy of our system becomes equal to the energy of the system of Busch *et al.*, when the radius of the box becomes infinitesimal small, $R \to 0$, since then both wave functions agree for all r. Eq. (16) of Ref. [75] reads

$$\sqrt{2}\,\frac{\Gamma(-E/2+3/4)}{\Gamma(-E/2+1/4)} = \frac{1}{a_s} \tag{5.35}$$

[6] Entry 13.1.3 of Ref. [100] / Wikipedia / Wolfram *MathWorld*.
[7] Entry 19.3.7 of Ref. [100] / Wolfram *MathWorld*.
[8] Entry 19.240 of Ref. [101] / Wolfram *MathWorld*.
[9] Entry 13.1.29 of Ref. [100].

which determines the energy as a function of the scattering length. By contrast the energy of our system is determined by Eq. (5.29) and thus a function of V and R.

We have seen in Fig. 5.7 that both, the energy and the scattering length, are functions of the box depth. Both quantities change dramatically with V around a characteristic value (here $V \approx -770\,\hbar\omega$) when a weakly bound state evolves into the ground state of the trap. Thus, E and a_s are directly connected with each other through $E(V(a_s))$ and we can plot the energy as a function of the scattering length; see Fig. 5.7(right). Can we directly calculate E as a function of a_s without making use of the box depth V? We remember that the energy is determined by the boundary condition that the logarithmic derivatives of the inner and outer solutions must agree at $r = R$ $\big[$Eq. (5.5)$\big]$. Further, we remember that the scattering length is also determined by the logarithmic derivative at R $\big[$Eq. (5.17)$\big]$. Using Eq. (5.17) and the outer wave function (5.28) we obtain

$$\sqrt{2}\,\frac{U'(-E;\sqrt{2}R)}{U(-E;\sqrt{2}R)} = \frac{1}{R-a_s} \tag{5.36}$$

which determines the energy as a function of a_s and R. I would like to note that this formula is much more useful for practical purposes than Eq. (5.29) since in practice the precise shape of the interaction potential is often unknown and definitely not given by a simple box. Eq. (5.36) does not make use of the precise shape of $V_{\text{int.}}(r)$. The only parameters which remain of $V_{\text{int.}}(r)$ are the range of the interaction potential R (which might be, e. g., the van der Waals length scale) and the scattering length a_s. Both quantities are experimentally accessible.

We would expect that the energy becomes even independent of R when the range of the interaction potential becomes much smaller than the oscillator length of the relative motion $l_{\text{osc}} = \sqrt{\hbar/(\mu\omega)}$. This is indeed the case. In the following I will show that in this case Eq. (5.36) is equal to Eq. (5.35). For $R = 0$ Eq. (5.36) reads

$$\frac{1}{-a_s} = \sqrt{2}\,\frac{U'(-E;0)}{U(-E;0)}. \tag{5.37}$$

We see from Eqs. (5.24) and (5.25) that

$$y_1(a;0) = 1, \quad y_1'(a;0) = 0, \quad y_2(a;0) = 0 \quad \text{and} \quad y_2'(a;0) = 1.$$

Using these relations and Eqs. (5.26) and (5.27) we obtain

$$U(-E;0) = \cos\Big(\frac{\pi}{4} - E\frac{\pi}{2}\Big)\,\frac{\Gamma(1/4+E/2)}{\sqrt{\pi}2^{1/4-E/2}} \tag{5.38}$$

and

$$U'(-E;0) = -\sin\Big(\frac{\pi}{4} - E\frac{\pi}{2}\Big)\,\frac{\Gamma(3/4+E/2)}{\sqrt{\pi}2^{-1/4-E/2}}$$

so that the above equation becomes

$$\frac{1}{a_s} = 2\,\tan\Big(\frac{\pi}{4} - E\frac{\pi}{2}\Big)\,\frac{\Gamma(3/4+E/2)}{\Gamma(1/4+E/2)}.$$

Now I use Euler's reflection formula for the gamma function [10]

$$\Gamma(z)\Gamma(1-z) = \frac{\pi}{\sin(\pi z)}.$$

[10] Entry 6.1.17 of Ref. [100] / Wikipedia / Wolfram *MathWorld*.

It follows

$$\Gamma\left(\frac{1}{4}+\frac{E}{2}\right)=\frac{\pi}{\sin\left(\frac{\pi}{4}+E\frac{\pi}{2}\right)\Gamma\left(\frac{3}{4}-\frac{E}{2}\right)} \tag{5.39}$$

and

$$\Gamma\left(\frac{3}{4}+\frac{E}{2}\right)=\frac{\pi}{\sin\left(\frac{3\pi}{4}+E\frac{\pi}{2}\right)\Gamma\left(\frac{1}{4}-\frac{E}{2}\right)}=\frac{\pi}{\cos\left(\frac{\pi}{4}+E\frac{\pi}{2}\right)\Gamma\left(\frac{1}{4}-\frac{E}{2}\right)}.$$

Using these relations we obtain

$$\frac{1}{a_s}=2\,\tan\left(\frac{\pi}{4}-E\frac{\pi}{2}\right)\tan\left(\frac{\pi}{4}+E\frac{\pi}{2}\right)\frac{\Gamma(3/4-E/2)}{\Gamma(1/4-E/2)}$$

which is equal to

$$2\,\frac{\Gamma(3/4-E/2)}{\Gamma(1/4-E/2)}=\frac{1}{a_s} \tag{5.40}$$

since $\tan(\pi/4-x)\tan(\pi/4+x)=1$. Eqs. (5.35) and (5.40) differ only by a factor of $\sqrt{2}$. But this is only due to the unconventional definition of the relative and center-of-mass coordinates used in Ref. [75]. Both results agree when the usual definitions of the relative and center-of-mass coordinates are used. Therefore the regularized δ potential is equivalent to the boundary condition

$$\frac{\chi'_{\text{out}}(0)}{\chi_{\text{out}}(0)}=-\frac{1}{a_s} \tag{5.41}$$

on the logarithmic derivative of the outer wave function at the origin [98, 99]. Thus, the boundary condition (5.41) replaces the usual boundary condition at the origin, $\chi(0)=0$, which has to be used in connection with regular interaction potentials.

5.3 Regularized delta potential

In many problems the mean distance $\langle r\rangle$ between the particles is much larger than the range R of the interaction; see, e. g., the wave functions of Fig. 5.6 apart from the strongly bound molecule in (a). Then the probability to find the particles within the range R is negligible compared to the probability to find them outside $\int_0^R dr\chi_{\text{in}}^2 \ll \int_R^\infty dr\chi_{\text{out}}^2$. Therefore, slight modifications of the inner wave function (replace χ_{in} by $\widetilde{\chi}_{\text{in}}$) have practically no impact on the properties of the system if still $\int_0^R dr\widetilde{\chi}_{\text{in}}^2 \ll \int_R^\infty dr\chi_{\text{out}}^2$.

This is shown in Fig 5.8. The real inner wave function (red dashed line) and the real outer wave function (red solid line) are a magnification of the "oscillator ground state" of Fig. 5.6(e). As can be seen $\int_0^R dr\chi_{\text{in}}^2 \ll \int_R^\infty dr\chi_{\text{out}}^2$. One can, e. g., simply replace the inner wave function χ_{in} by the outer wave function $\widetilde{\chi}_{\text{in}}=\chi_{\text{out}}$ (blue line), i. e., one simply extends the outer wave function into the inner region $[0,R]$. Still $\int_0^R dr\widetilde{\chi}_{\text{in}}^2 \ll \int_R^\infty dr\chi_{\text{out}}^2$ and (nearly) all the properties of the system are correctly described by this modified wave function. The only problem which arises from this slight modification is that the probability to find the particle at the origin becomes infinite: $\chi_{\text{out}}(0)=\text{const.} \Rightarrow \psi_{\text{out}}(0)=\chi_{\text{out}}(0)/0=\infty$. However, as long as we don't ask for $\rho(0)=|\psi_{\text{out}}(0)|^2$ the essential physics of the system is well described. As has been shown in the last section the extended wave function has to obey the boundary condition (5.41) at the origin which is equal to Eqs. (5.37) and (5.40) in a harmonic trap.

Now I wish to reintegrate the boundary condition (5.41) into the Schrödinger equation. That is, I have to reintegrate an interaction potential into the Schrödinger equation such that the outer

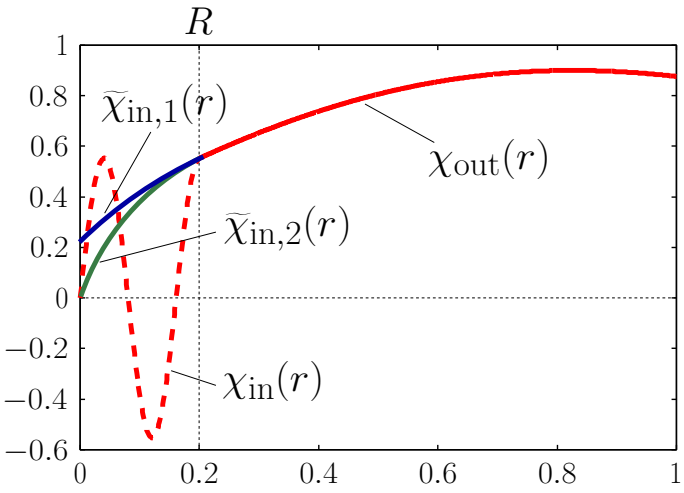

Figure 5.8: "Oscillator ground state" of Fig. 5.6(e) in the region $0 \leqslant r \leqslant 1$. Red is the outer and red dashed is the inner wave function. Since the probability to find the particles within the range R is negligible compared to the probability to find them outside, $\int_0^R dr\chi_{\text{in}}^2 \ll \int_R^\infty dr\chi_{\text{out}}^2$, a modification of the inner wave function ($\chi_{\text{in}} \to \widetilde{\chi}_{\text{in}}$) has no influence on the properties of the system. $\widetilde{\chi}_{\text{in},1} \equiv \chi_{\text{out}}(r)$: The outer wave function has been extended into the inner region. $\widetilde{\chi}_{\text{in},2}$: The inner wave function has been modified according to Eq. (5.42).

wave function obeys the boundary condition (5.41). Since I can choose nearly arbitrary inner wave functions $\widetilde{\chi}_{\text{in}}$ I can construct an interaction potential which is much easier than realistic interaction potentials. I discuss the procedure firstly for free particles.

Free space— The outer wave function solves the Schrödinger equation of noninteracting particles and is given by $\psi_{\text{out}}(r) = (B/r)\,\sin(kr + \delta_0)$ (free spherical wave) or $\psi_{\text{out}}(r) = (B/r)\,e^{-\rho r}$ (molecule). For the inner wave function I choose $\psi_{\text{in}}(r) = (A/R)\big[3/2 - 1/2\,(r/R)^2\big]$:

$$\psi(r) = \begin{cases} \psi_{\text{in}}(r) = \dfrac{A}{R}\left[\dfrac{3}{2} - \dfrac{1}{2}\left(\dfrac{r}{R}\right)^2\right] & \text{if } r \leqslant R \\ \psi_{\text{out}}(r) = \dfrac{B}{r}\sin(kr+\delta_0) \;\text{ or }\; \psi_{\text{out}}(r) = \dfrac{B}{r}e^{-\rho r} & \text{if } r \geqslant R\,. \end{cases} \tag{5.42}$$

The inner wave function $\chi_{\text{in}}(r) = r\,\psi_{\text{in}}(r) = (A/R)\big[(3/2)\,r - 1/2\,(r^3/R^2)\big]$ is shown in Fig 5.8 (green line). We wish the wave function to be continuous at R. Then we can express the constant A by means of the outer wave function

$$\psi_{\text{in}}(R) = \frac{A}{R} = \psi_{\text{out}}(R) \quad \Rightarrow \quad A = R\,\psi_{\text{out}}(R).$$

Let's act with the Laplacian on $\psi(r)$. In the inner region we obtain

$$\Delta\psi_{\text{in}} = \frac{1}{r}\frac{d^2}{dr^2}(r\,\psi_{\text{in}}) = -\frac{3A}{R^3} = -4\pi\delta_R(r)\big[R\,\psi_{\text{out}}(R)\big]$$

with $\delta_R(r) \equiv 1\big/\big[(4/3)\pi R^3\big]$ if $r \leqslant R$ and $\delta_R(r) \equiv 0$ if $r > R$. In the outer region we get in both cases

$$\Delta\psi_{\text{out}} = -k^2\,\psi_{\text{out}} = -\epsilon\,\psi_{\text{out}} \quad \text{or} \quad \Delta\psi_{\text{out}} = \rho^2\,\psi_{\text{out}} = -\epsilon\,\psi_{\text{out}}.$$

Thus we obtain, when acting with the kinetic energy operator on the wave function,

$$-\frac{\hbar^2}{2\mu}\Delta\psi(r) = E\,\psi_{\text{out}}(r) + \frac{4\pi\hbar^2}{2\mu}\delta_R(r)\big[R\,\psi_{\text{out}}(R)\big].$$

Now we include the boundary condition (5.17) into the equation. We use

$$\frac{1}{R-a_s} = \left.\frac{\big[r\,\psi_{\text{out}}(r)\big]'}{r\,\psi_{\text{out}}(r)}\right|_{r=R} \quad \Rightarrow \quad R\,\psi_{\text{out}}(R) = (R-a_s)\frac{\partial}{\partial r}\big[r\,\psi_{\text{out}}(r)\big]\Big|_{r=R}$$

and obtain

$$-\frac{\hbar^2}{2\mu}\Delta\psi(r) + \frac{2\pi\hbar^2(a_s-R)}{\mu}\delta_R(r)\frac{\partial}{\partial r}\big[r\,\psi_{\text{out}}(r)\big]\Big|_{r=R} = E\,\psi_{\text{out}}(r).$$

In the limit $R \to 0$ this equation becomes

$$\left[-\frac{\hbar^2}{2\mu}\Delta + \frac{2\pi\hbar^2 a_s}{\mu}\delta(\vec{r})\frac{\partial}{\partial r}\,r\right]\psi(r) = E\,\psi(r)$$

$\big[$since $\delta_R(r) \to \delta(\vec{r})$ for $R \to 0\big]$ where the operator

$$V_{\text{int.}}(r) = \frac{2\pi\hbar^2 a_s}{\mu}\delta(\vec{r})\frac{\partial}{\partial r}\,r \tag{5.43}$$

is the desired pseudopotential which reintegrates the boundary condition (5.41) into the Schrödinger equation of the noninteracting particles.

Harmonic trap— The derivation is almost equal to the free-space case since we did not use the specific shape of the free-space solutions. Again, we choose the inner wave function of Eq. (5.42). The outer wave function is now given by $\psi_{\text{out}}(r) = (B/r)\,U\big[-E;\sqrt{2}r\big]$. Again A is given by $A = R\,\psi_{\text{out}}(R)$. Now we slightly modify the Hamiltonian of the inner region

$$H_0^{(R)} \equiv \begin{cases} H_0^{(\text{in})} = -\dfrac{\hbar^2}{2\mu}\Delta & \text{if } r \leqslant R \\ H_0^{(\text{out})} = -\dfrac{\hbar^2}{2\mu}\Delta + \dfrac{1}{2}\mu\omega^2 r^2 & \text{if } r > R\,. \end{cases}$$

We act with this Hamiltonian on the wave function and obtain

$$H_0^{(R)}\psi(r) = E\psi_{\text{out}}(r) + \frac{2\pi\hbar^2}{\mu}\delta_R(r)\big[R\,\psi_{\text{out}}(R)\big].$$

Now we replace $R\,\psi_{\text{out}}(R)$ by $(R-a_s)\big[r\,\psi(r)\big]'\big|_{r=R}$ and thereby integrate the boundary condition (5.17) into the above equation

$$H_0^{(R)}\psi(r) + \frac{2\pi\hbar^2(a_s-R)}{\mu}\delta_R(r)\frac{\partial}{\partial r}\big[r\,\psi_{\text{out}}(r)\big]\Big|_{r=R} = E\psi_{\text{out}}(r).$$

In the limit $R \to 0$ the Hamiltonian $H_0^{(R)}$ is solely given by $H_0^{(\text{out})}$ and the above equation becomes

$$\left[-\frac{\hbar^2}{2\mu}\Delta + \frac{1}{2}\mu\omega^2 r^2 + \frac{2\pi\hbar^2 a_s}{\mu}\delta(\vec{r})\frac{\partial}{\partial r}\,r\right]\psi(r) = E\,\psi(r)\,.$$

Summary— Let me summarize the main steps of the pseudopotential method (for cold atoms). Outside the range R of the true (short-ranged) interaction potential $V_{\text{int.}}(r)$ the outer wave function $\psi_{\text{out}}(r)$ is only determined by the Schrödinger equation of noninteracting particles and the boundary condition $\big[r\,\psi_{\text{out}}(r)\big]'/\big[r\,\psi_{\text{out}}(r)\big]\big|_{r=R} = 1/(R-a_s)$. Thus, the whole impact of the true

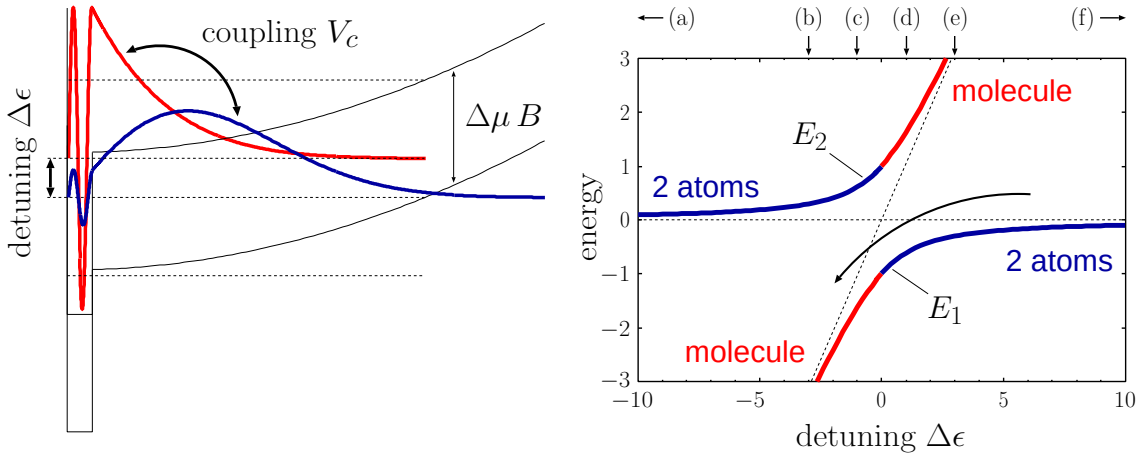

Figure 5.9: *Left:* Sketch of a simple Feshbach-resonance model. Red is the wave function of the molecule ($\chi \propto e^{-\rho r}$) and blue is the wave function of the noninteracting atoms ($\chi \propto r e^{-r^2/2}$). The molecule and the noninteracting atoms shall have different magnetic moments $\mu_m \neq \mu_a$. By applying a homogeneous magnetic field B one can shift the energy of the atoms relative to the energy of the molecule. The shift is given by $\Delta E_{\text{mag.}} = \Delta\mu\, B$ with $\Delta\mu = \mu_a - \mu_m$. For a certain value $B = B_0$ the energy of the molecule exactly agrees with the energy of the atoms and the detuning becomes zero $\Delta\epsilon = 0$ (B_0 is the center of the Feshbach resonance). Around B_0 the wave functions of the molecule and the two atoms strongly mix up, provided there is some additional coupling V_c between the two states. *Right:* Energies of the two eigenstates as a function of the detuning $\Delta\epsilon$ for fixed coupling $V_c = -1$. The labels (a-f) correspond to Figs. 5.10(a-f).

interaction potential reduces to a boundary condition on the outer wave function which depends only on two parameters of $V_{\text{int.}}(r)$, namely its range R and the scattering length a_s. When the mean distance $\langle r \rangle$ between the particles is much larger than R the probability to find both particles within R is negligible compared to the probability to find them outside, $\int_0^R dr (r\,\psi_{\text{in}})^2 \ll \int_R^\infty dr (r\,\psi_{\text{out}})^2$. Then, one can replace the inner wave function ψ_{in} by ψ_{out} so that the wave function is solely given by $\psi = \psi_{\text{out}}$ for all $r \in [0, \infty)$. After this small modification (see the blue line in Fig. 5.8) still $\int_0^R dr (r\,\psi)^2 \ll \int_R^\infty dr (r\,\psi)^2$. The extended outer wave function is determined by the Schrödinger equation of noninteracting particles and the boundary condition $\big[r\,\psi(r)\big]'/(r\,\psi(r)\big|_{r=0} = -1/a_s$. This boundary condition can be included *exactly* into the Schrödinger equation of the noninteracting particles by means of the regularized δ potential (5.43). Thus, if $\langle r \rangle \gg R$, the true interaction potential can be replaced by the regularized δ potential. The extended outer wave functions have a (harmless integrable) $1/r$ singularity at $r = 0$ and thus the probability $\rho(0) = |\psi(0)|^2 = \infty$. However, apart from this deficiency the essential physics is well described by the extended outer wave functions. [11]

5.4 Feshbach resonance

Simple model— A Feshbach resonance occurs if the energy of the least bound state is close to the energy of the noninteracting atoms. Additionally we need some coupling between both states. Consider Fig. 5.9(left): Red is the relative wave function of the least bound molecule $\chi_{\text{mol.}} \propto e^{-\rho r}$ and blue is the relative wave function of the noninteracting atoms $\chi_{\text{atoms}} \propto r e^{-r^2/2}$. The molecule

[11] See also the discussion in Sec. 2.5 "The Bethe-Peierls model" (pp. 26-29) of Ref. [102] and references therein.

and the two atoms have different magnetic moments $\mu_m \neq \mu_a$ so that an external magnetic field B shifts the energy of both states relative to each other according to $\Delta E_{\text{mag.}} = \Delta\mu\, B$ with $\Delta\mu = \mu_a - \mu_m$. For a certain value of B the energy of the molecule exactly agrees with the energy of the atoms and the detuning becomes zero $\Delta\epsilon = 0$. This value $B = B_0$ is the center of the Feshbach resonance. Around B_0 the wave functions of the molecule and the two atoms strongly mix up if there is an additional coupling V_c between the two states.

The mixing of the two states can be modeled by a simple 2×2 matrix

$$H_{\text{F.}} = \begin{pmatrix} 0 & V_c \\ V_c & \Delta\epsilon \end{pmatrix}. \tag{5.44}$$

The eigenenergies of this Hamiltonian are

$$E_1 = (\Delta\epsilon/2) - \sqrt{V_c^2 + (\Delta\epsilon/2)^2}, \qquad E_2 = (\Delta\epsilon/2) + \sqrt{V_c^2 + (\Delta\epsilon/2)^2}$$

and the corresponding eigenvectors are given by

$$\chi_1 = N_1 \left[\chi_{\text{mol.}} - \frac{\Delta\epsilon + \sqrt{(2V_c)^2 + (\Delta\epsilon)^2}}{2V_c} \chi_{\text{atoms}} \right]$$
$$\chi_2 = N_2 \left[\chi_{\text{mol.}} - \frac{\Delta\epsilon - \sqrt{(2V_c)^2 + (\Delta\epsilon)^2}}{2V_c} \chi_{\text{atoms}} \right]$$

where N_1 and N_2 are normalization constants. E_1 and E_2 are plotted in Fig. 5.9(right) as a function of $\Delta\epsilon$ for fixed coupling $V_c = -1$. In the limit $\Delta\epsilon = -\infty$ the coupling V_c is negligible so that $H_{\text{F.}}$ is approximately diagonal and $E_1 = \Delta\epsilon$, $E_2 = 0$, $\chi_1 = \chi_{\text{mol.}}$ and $\chi_2 = \chi_{\text{atoms}}$. In the opposite limit $\Delta\epsilon = +\infty$ we obtain $E_1 = 0$, $E_2 = \Delta\epsilon$, $\chi_1 = \chi_{\text{atoms}}$ and $\chi_2 = \chi_{\text{mol.}}$. Therefore, by changing $\Delta\epsilon$ adiabatically from a positive to a negative value, two noninteracting atoms evolve continuously into a weakly bound molecule [follow the arrow in Fig. 5.9(right)]. Exactly at $\Delta\epsilon = 0$ the energies are given by $E_1 = -|V_c|$, $E_2 = +|V_c|$ and the corresponding eigenvectors are $\chi_1 = (\chi_{\text{mol.}} - \chi_{\text{atoms}})/\sqrt{2}$ and $\chi_2 = (\chi_{\text{mol.}} + \chi_{\text{atoms}})/\sqrt{2}$.

Relation between scattering length and detuning— Fig. 5.10 shows several superpositions of a molecular wave function $\chi_{\text{mol.}}$ and a wave function of two atoms χ_{atoms} for a fixed coupling $V_c = -1$ and variable detuning $\Delta\epsilon$. In this example I have chosen a box depth of $V = -780\,\hbar\omega$ for the least bound molecule and $V = -745\,\hbar\omega$ for the two atoms so that the outer wave function of the two atoms exactly coincides with the ground state of the harmonic trap ($\Rightarrow a_s = 0$). The shape of $\chi_{\text{mol.}}$ and χ_{atoms} was fixed for all values of $\Delta\epsilon$.

Fig. 5.10(a): For $\Delta\epsilon = -100$ there is no mixing between the two wave functions and $\chi_1 = \chi_{\text{mol.}}$ (red) and $\chi_2 = \chi_{\text{atoms}}$ (blue).

Fig. 5.10(b): For $\Delta\epsilon = -3$ the superposition wave functions are given by $\chi_1 \approx 0.29\,\chi_{\text{atoms}} + 0.96\,\chi_{\text{mol.}}$ (red) and $\chi_2 \approx 0.96\,\chi_{\text{atoms}} - 0.29\,\chi_{\text{mol.}}$ (blue). This leads to a broadening of the molecular wave function (red) and a smaller binding energy $E_b = -E_1$ [for the corresponding binding energy see Fig. 5.9(right)]. Likewise the two atoms (blue) move a little bit apart from each other and their energy E_2 increases. I note that the blue superposition wave function χ_2 looks very similar to the blue wave function of Fig. 5.6(b). Therefore, I have varied the box depth V such that the overlap between the resulting ground state of the trap and the blue superposition wave function was maximized. The resulting blue dashed wave function belongs to a box depth of $V_{\text{opt.}} = -820\,\hbar\omega$. It has a small positive scattering length $a_s \approx 0.3\,l_{\text{osc}}$ and its overlap with the blue superposition state is nearly one. The red dashed wave function is the least bound molecule

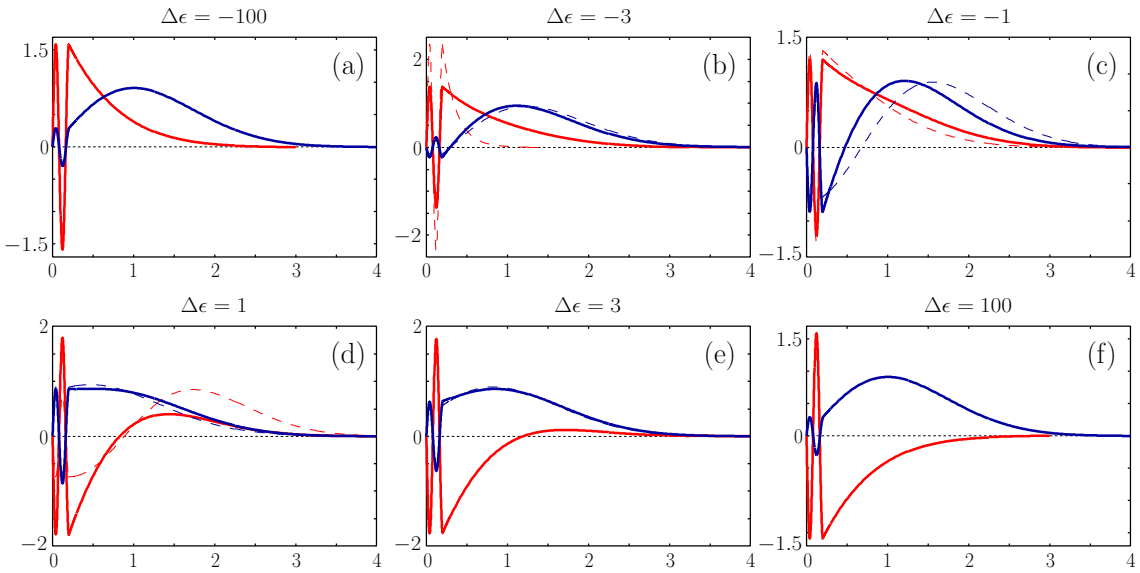

Figure 5.10: Evolution of the superposition wave functions χ_1 and χ_2 (see text) with the detuning $\Delta\epsilon$ ($V_c = -1 =$ fixed). The superposition with more than 50% admixture of $\chi_{\text{mol.}}$ is drawn as a red solid line and the superposition with more than 50% admixture of χ_{atoms} is drawn as a blue solid line. One can adjust the wave functions of Sec. 5.2 (given by the red and the blue dashed lines) to the superposition wave functions χ_1 and χ_2 by choosing an optimal trap depth $V_{\text{opt.}}$ for each detuning $\Delta\epsilon$. Such a fit works quite good for the molecule if $\Delta\epsilon < 0$ and $|\Delta\epsilon|$ not too large (i. e. $a_s > 0$ not too small), see the red curve of Fig. (c). For the repulsively interacting atoms [blue curves of Figs. (b) and (c)] and the attractively interacting atoms [blue curves of Figs. (d) and (e)] the fit works for all values of $\Delta\epsilon$.

of the same box $V_{\text{opt.}} = -820\,\hbar\omega$. As can be seen the overlap between the red dashed and the red wave function is much smaller (overlap ≈ 0.76).

Fig. 5.10(c): For $\Delta\epsilon = -1$ the superposition wave functions are given by $\chi_1 \approx 0.53\,\chi_{\text{atoms}} + 0.85\,\chi_{\text{mol.}}$ (red) and $\chi_2 \approx 0.85\,\chi_{\text{atoms}} - 0.53\,\chi_{\text{mol.}}$ (blue). Again we vary the box depth V such that a maximum overlap with the corresponding least bound molecule (red dashed) and the ground state of the trap (blue dashed) is achieved. The optimum box depth is now given by $V_{\text{opt.}} = -775\,\hbar\omega$ leading to an overlap of 0.99 between the red and the red dashed wave function and an overlap of 0.91 between the blue and the blue dashed wave function. The scattering lengths of the red and the blue dashed wave functions are large and positive since we are close to the critical box depth $V \approx -771 \ldots -770\,\hbar\omega$ where the scattering length diverges [compare with Fig. 5.6(c)].

Fig. 5.10(d): For $\Delta\epsilon = +1$ the superposition wave functions are given by $\chi_1 \approx 0.85\,\chi_{\text{atoms}} + 0.53\,\chi_{\text{mol.}}$ (blue) and $\chi_2 \approx -0.53\,\chi_{\text{atoms}} + 0.85\,\chi_{\text{mol.}}$ (red). The optimum box depth is $V_{\text{opt.}} = -768\,\hbar\omega$ and thus the scattering lengths of the dashed wave functions are large and negative [compare with Fig. 5.6(d)]. The overlap between the blue wave functions is approximately one and it is ≈ 0.74 between the red wave functions.

Fig. 5.10(e): For $\Delta\epsilon = +3$ the superposition wave functions are given by $\chi_1 \approx 0.96\,\chi_{\text{atoms}} + 0.29\,\chi_{\text{mol.}}$ (blue) and $\chi_2 \approx -0.29\,\chi_{\text{atoms}} + 0.96\,\chi_{\text{mol.}}$ (red). The optimum box depth is $V_{\text{opt.}} = -760\,\hbar\omega$ and thus the scattering length of the blue dashed wave function is $a_s \approx -0.3\,l_{\text{osc}}$ [compare with Fig. 5.6(e)]. The overlap between the blue wave functions is nearly one.

Fig. 5.10(f): For $\Delta\epsilon = +100$ there is no mixing between the two wave functions and $\chi_1 = \chi_{\text{atoms}}$

(blue) and $\chi_2 = \chi_{\text{mol.}}$ (red).

Relation between scattering length and magnetic field— We conclude that the scattering length of the optimally adjusted (dashed) wave functions depends on the detuning $a_s = a_s(V_{\text{opt.}}(\Delta\epsilon))$. And since the detuning depends on the strength of the magnetic field B there is also a functional relation between a_s and B. This functional relation is given by [103]

$$a_s(B) = a_{\text{bg}} \left(1 - \frac{\Delta B}{B - B_0}\right) \tag{5.45}$$

where a_{bg} is the non-resonant background scattering length, ΔB the magnetic field width of the resonance and B_0 the resonance center position. [12]

5.5 A short description of the experiment

I now turn to a short description of the experiment of C. Ospelkaus *et al.* [72]. More details are given in the Ph.D. theses of Christian [73] and Silke Ospelkaus [74]. In a first step, an ultracold (quantum-degenerate) mixture of ^{40}K atoms in the $|f = 9/2, m_f = 9/2\rangle$ spin state and ^{87}Rb in the $|f = 2, m_f = 2\rangle$ spin state was achieved by means of radio-frequency (rf) induced sympathetic cooling in a magnetic trap. [*Evaporative cooling of the bosonic ^{87}Rb atoms:* The ^{87}Rb atoms are enclosed in a harmonic potential with a finite height. The barrier of the potential is slightly lowered for a short period so that the high-energy atoms can escape from the trap. Thereby the mean kinetic energy of the remaining atoms is lowered. The remaining atoms scatter with each other which leads to a thermalization at a lower temperature. The cycle is repeated until quantum degeneracy is achieved. *Sympathetic cooling of the fermionic ^{40}K atoms:* A pure sample of ^{40}K atoms does not thermalize since fermions cannot occupy the same position in space due to the Pauli exclusion principle and thus they do not feel the δ interaction potential. In a mixture, the fermionic ^{40}K atoms can scatter with the bosonic ^{87}Rb atoms so that a cooling of the ^{87}Rb sample simultaneously cools the ^{40}K sample.]

Afterwards the mixture was transferred into a (shallow) optical dipole trap with final trap frequencies for ^{87}Rb of $2\pi \times 50\,$Hz. In the optical dipole trap, ^{87}Rb atoms were transferred from $|2, 2\rangle$ to $|1, 1\rangle$ by a microwave sweep at 20 G and any remaining atoms in the upper hyperfine $|f = 2, m_f\rangle$ states were removed by a resonant light pulse. Next, the ^{40}K atoms were transferred into the $|9/2, -7/2\rangle$ state by performing an rf sweep at the same magnetic field with almost 100% efficiency. With the mixture in the ^{87}Rb$|1, 1\rangle \otimes ^{40}K|9/2, -7/2\rangle$ state, the magnetic field was ramped up to final field values at the Feshbach resonance occurring around 547 G [104]. Note that the prepared state is not Feshbach-resonant at the magnetic field values which have been studied, and that a final transfer of ^{40}K into the $|9/2, -9/2\rangle$ state was necessary to access the resonantly interacting state. This was precisely the transition which has been used to measure the energy spectrum as outlined further below.

In a next step, a 3D optical lattice was ramped up at a wavelength of $\lambda = 1030\,$nm, where the trapping potential for both species is related according to $V_{\text{K}} = 0.86\, V_{\text{Rb}}$. Due to the different masses of the two species, the trapping frequencies are $\omega_{\text{K}} = \sqrt{87/40 \cdot 0.86}\,\omega_{\text{Rb}} \simeq 1.37\,\omega_{\text{Rb}}$ in the harmonic approximation. The lattice was formed by three retroreflected laser beams. In order to get a maximum of lattice sites occupied by one boson and one fermion, the best trade-off has been to limit the particle number at this stage to a few ten thousand.

[12] See Sec. 2.4 "A two-channel model" (pp. 22-26) of Ref. [102] for a derivation of Eq. (5.45).

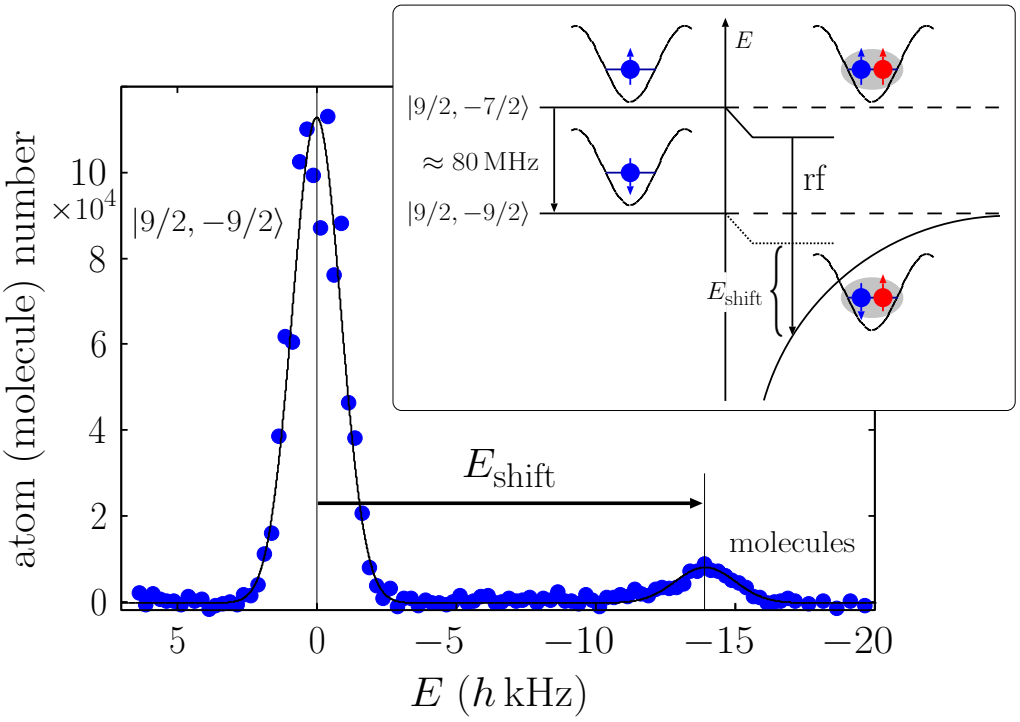

Figure 5.11: Rf spectroscopy of ^{40}K–^{87}Rb in a 3D optical lattice on the ^{40}K $|9/2,-7/2\rangle \rightarrow |9/2,-9/2\rangle$ transition (see inset) at a lattice depth of $V_{\mathrm{Rb}} = 27.5\, E_{r,\mathrm{Rb}}$ and a magnetic field of 547.13 G, where the interaction is attractive. The spectrum is plotted as a function of detuning from the undisturbed atomic resonance frequency and clearly shows the large atomic peak at zero detuning. The peak at -13.9 kHz is due to association of ^{87}Rb$|1,1\rangle \otimes^{40}$K$|9/2,-7/2\rangle$ atom pairs into a bound state.

In the optical lattice, the binding energy of pairs of one ^{87}Rb and one ^{40}K atom at a single lattice site was studied by rf spectroscopy (see inset of Fig. 5.11). The idea for the measurement was to drive an rf transition between the two atomic sublevels of ^{40}K one of which is characterized by the presence of the Feshbach resonance and exhibits a large variation of the scattering length as a function of magnetic field according to Eq. (5.45). The other level involved in the rf transition is characterized by a non-resonant scattering length independent of magnetic field over the experimentally studied field range. Here, the ^{40}K $|9/2,-7/2\rangle \rightarrow |9/2,-9/2\rangle$ transition was used where the Feshbach-resonant state is the final ^{87}Rb$|1,1\rangle \otimes^{40}$K$|9/2,-9/2\rangle$ state.

A sample spectrum of this transition for the mixture in the optical lattice is shown in Fig. 5.11. The figure shows two peaks: One of them occurs at the frequency corresponding to the undisturbed ^{40}K $|9/2,-7/2\rangle \rightarrow |9/2,-9/2\rangle$ Zeeman transition frequency at lattice sites occupied by a single ^{40}K fermion. This peak was used for the calibration of the magnetic field across the Feshbach resonance using the Breit-Rabi formula for ^{40}K [73]. For 57 measurements on 11 consecutive days a mean deviation from the magnetic field calibration of 2.7 mG at magnetic fields around 547 G has been found, corresponding to a field reproducibility of 5×10^{-6}. There was an additional uncertainty on the absolute value of the magnetic field due to the specified reference frequency source accuracy for the rf synthesizer of 1×10^{-5}, resulting in an uncertainty of the measured magnetic fields of 12 mG.

The second peak at a negative detuning of -13.9 kHz is the result of interactions between ^{40}K and ^{87}Rb at lattice sites where one heteronuclear atom pair is present. There are two different energy

shifts causing the observed separation of the peaks: One is the constant, small energy shift of the initial $^{87}\mathrm{Rb}|1,1\rangle \otimes ^{40}\mathrm{K}|9/2,-7/2\rangle$ state which is independent of B, and the important, magnetic field sensitive collisional shift which stems from the strong Feshbach-resonant interactions in the $^{87}\mathrm{Rb}|1,1\rangle \otimes ^{40}\mathrm{K}|9/2,-9/2\rangle$ final state (inset of Fig. 5.11). In the specific example, the binding energy of the final state increases the transition frequency as seen in Fig. 5.11.

In order to perform spectroscopy on the aforementioned transition, pulses with a gaussian amplitude envelope ($1/e^2$ full width of 400 μs and total pulse length of 800 μs) have been used, resulting in an rf $1/e^2$ half linewidth of 1.7 kHz. The pulse power was chosen such as to achieve full transfer on the single atom transition, i. e. rf pulse parameters including power are identical for all magnetic fields.

5.6 Modeling of two interacting atoms at a single optical lattice site

Two interacting atoms in a harmonic trap: The Schrödinger equation of two atoms which interact via a regularized δ potential and which are confined in a harmonic potential is given by

$$\left[\sum_{i=1,2}\left(-\frac{\hbar^2}{2m_i}\Delta_i+\frac{1}{2}m_i\omega^2 r_i^2\right)+\frac{2\pi\hbar^2 a_s}{\mu}\delta(\vec{r})\frac{\partial}{\partial r}r\right]\psi(\vec{r}_1,\vec{r}_2)=E\psi(\vec{r}_1,\vec{r}_2).$$

Here, m_i is the mass and $\vec{r}_i$ is the position of atom i, ω is the angular frequency of the trap, a_s is the s-wave scattering length, $\mu = m_1 m_2/M$ is the reduced mass, $M = m_1 + m_2$ is the total mass, $\vec{r} = \vec{r}_1 - \vec{r}_2$ is the relative position and $r = |\vec{r}_1 - \vec{r}_2|$ is the distance between the atoms. The first term consists of the kinetic and the potential energy of atom i and the second term is the regularized δ potential which we have introduced in Sec. 5.3 in order to model the short-ranged interaction between ultracold atoms. We introduce center-of-mass and relative coordinates

$$\vec{R}=(m_1\vec{r}_1+m_2\vec{r}_2)/M,\quad \vec{r}=\vec{r}_1-\vec{r}_2\quad\Leftrightarrow\quad \vec{r}_1=\vec{R}+m_2\vec{r}/M,\quad \vec{r}_2=\vec{R}-m_1\vec{r}/M.$$

By inserting these relations into the above Schrödinger equation, we obtain

$$\left[-\frac{\hbar^2}{2M}\Delta_{\text{c.m.}}+\frac{1}{2}M\omega^2R^2-\frac{\hbar^2}{2\mu}\Delta_{\text{rel}}+\frac{1}{2}\mu\omega^2r^2+\frac{2\pi\hbar^2a_s}{\mu}\delta(\vec{r})\frac{\partial}{\partial r}r\right]\psi(\vec{R},\vec{r})=E\psi(\vec{R},\vec{r}).$$

We are looking for solutions that are separable into products

$$\psi(\vec{R},\vec{r})=\psi_{\text{c.m.}}(\vec{R})\psi_{\text{rel}}(\vec{r}).$$

Putting this into the above equation, we obtain two separate equations for the center-of-mass and the relative motion

$$\left[-\frac{\hbar^2}{2M}\Delta_{\text{c.m.}}+\frac{1}{2}M\omega^2R^2\right]\psi_{\text{c.m.}}(\vec{R})=E_{\text{c.m.}}\psi_{\text{c.m.}}(\vec{R}),$$

$$\left[-\frac{\hbar^2}{2\mu}\Delta_{\text{rel}}+\frac{1}{2}\mu\omega^2r^2+\frac{2\pi\hbar^2a_s}{\mu}\delta(\vec{r})\frac{\partial}{\partial r}r\right]\psi_{\text{rel}}(\vec{r})=E_{\text{rel}}\psi_{\text{rel}}(\vec{r})$$

$\big($with $E = E_{\text{c.m.}} + E_{\text{rel}}\big)$ which can be solved independent of each other. We express all lengths of the center-of-mass and the relative motion in units of $l_{\text{c.m.}} = \sqrt{\hbar/(M\omega)}$ and $l_{\text{rel}} = \sqrt{\hbar/(\mu\omega)}$

respectively, and we express all energies in units of $\hbar\omega$. The dimensionless Schrödinger equations of the center-of-mass and the relative motion read

$$\left[-\frac{1}{2}\widetilde{\Delta}_{\text{c.m.}}+\frac{1}{2}\widetilde{R}^2\right]\widetilde{\psi}_{\text{c.m.}}=\widetilde{E}_{\text{c.m.}}\widetilde{\psi}_{\text{c.m.}},\quad \left[-\frac{1}{2}\widetilde{\Delta}_{\text{rel}}+\frac{1}{2}\widetilde{r}^2+2\pi\widetilde{a}_s\widetilde{\delta}(\widetilde{\vec{r}})\frac{\partial}{\partial\widetilde{r}}\widetilde{r}\right]\widetilde{\psi}_{\text{rel}}=\widetilde{E}_{\text{rel}}\widetilde{\psi}_{\text{rel}}.$$

[Here, we have separated each quantity into a dimensionless quantity (which we mark by a tilde symbol) and its unit: $\Delta_{\text{c.m.}}=\widetilde{\Delta}_{\text{c.m.}}/l_{\text{c.m.}}^2$, $R=\widetilde{R}\,l_{\text{c.m.}}$, $\psi_{\text{c.m.}}=\widetilde{\psi}_{\text{c.m.}}/l_{\text{c.m.}}^{3/2}$, $E_{\text{c.m.}}=\widetilde{E}_{\text{c.m.}}\,\hbar\omega$, $\Delta_{\text{rel}}=\widetilde{\Delta}_{\text{rel}}/l_{\text{rel}}^2$, $r=\widetilde{r}\,l_{\text{rel}}$, $\psi_{\text{rel}}=\widetilde{\psi}_{\text{rel}}/l_{\text{rel}}^{3/2}$ and $E_{\text{rel}}=\widetilde{E}_{\text{rel}}\,\hbar\omega$. In particular the scattering length and the δ function are given by $a_s=\widetilde{a}_s\,l_{\text{rel}}$ and $\delta=\widetilde{\delta}/l_{\text{rel}}^3$. One can easily show that the dimensionless equations are equivalent to the original ones. We keep these relations in mind but throughout the following text I will always omit the tilde symbol.]

Center-of-mass equation— The Schrödinger equation of a particle in a 3D rotationally symmetric harmonic oscillator has to be solved. The spectrum is given by

$$E_{\text{c.m.}}=2N+L+\frac{3}{2} \tag{5.46}$$

with $N,L=0,1,2,\ldots$. The associated eigenfunctions are given by

$$\psi_{\text{c.m.}}=\mathfrak{R}_{NL}(R)Y_{LM}(\Theta,\Phi)$$

with $M=-L,-L+1,\ldots,L-1,L$. $Y_{LM}(\Theta,\Phi)$ are spherical harmonics (implemented as "SphericalHarmonicY" in MATHEMATICA) and the radial eigenfunctions are given by

$$\mathfrak{R}_{NL}(R)=A_{NL}\,R^L\,\mathfrak{L}_N^{L+1/2}(R^2)\,e^{-R^2/2} \tag{5.47}$$

with the normalization constant $A_{NL}=\sqrt{(2N!)/\Gamma(N+L+3/2)}$ and the generalized Laguerre polynomials $\mathfrak{L}_a^b$ (implemented as "LaguerreL" in MATHEMATICA). Alternatively one may also use the confluent hypergeometric function of the first kind since [13]

$$\mathfrak{L}_a^b(z)=\frac{(a+b)!}{a!b!}{}_1F_1(-a;b+1;z).$$

The solution of the radial equation by means of a polynomial ansatz is given in Vol. 2 of Ref. [78].

Relative equation— Two cases have to be considered. In the case of nonzero relative angular momentum ($l\neq 0$) we obtain again the solutions of a 3D rotationally symmetric harmonic oscillator (but now in units of $\hbar\omega_{\text{rel}}$ and l_{rel}) since the $l\neq 0$ wave functions do not feel the δ potential at the origin. The energy spectrum is given by

$$E_{\text{rel}}=2n+l+\frac{3}{2}\qquad(l\neq 0) \tag{5.48}$$

with $n=0,1,2,\ldots$ and $l=1,2,\ldots$. The associated eigenfunctions are given by

$$\psi_{\text{rel}}=\mathfrak{R}_{nl}(r)Y_{lm}(\theta,\phi)\qquad(l\neq 0)$$

with $m=-l,-l+1,\ldots,l-1,l$ and

$$\mathfrak{R}_{nl}(r)=A_{nl}\,r^l\,\mathfrak{L}_n^{l+1/2}(r^2)\,e^{-r^2/2}\qquad(l\neq 0) \tag{5.49}$$

[13] Eq. (13.128) of Ref. [105] / Wolfram *MathWorld*.

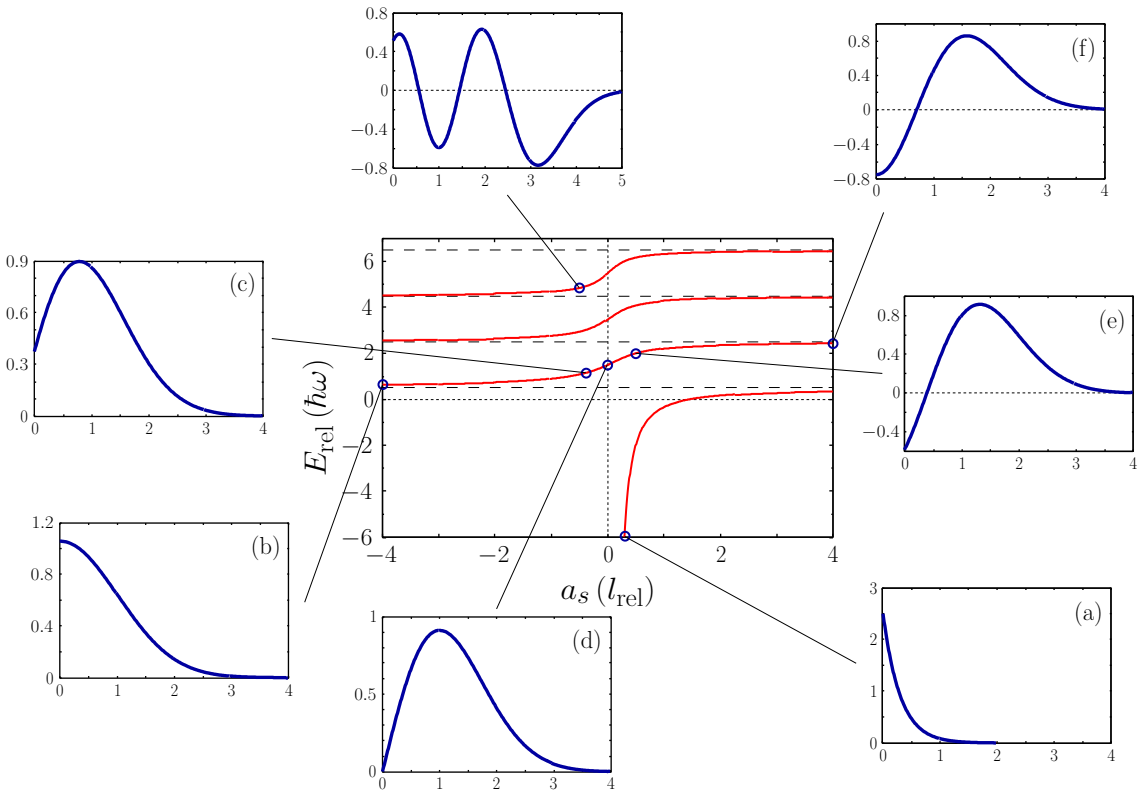

Figure 5.12: Energy spectrum (red) and eigenfunctions $\chi_{\rm rel} = r\,\psi_{\rm rel}$ (blue) of the $l = 0$ states. Note the similarity to the wave functions of Fig. 5.6 outside the range R and to the energy spectrum of the molecule of Fig. 5.7(right).

where $A_{nl} = \sqrt{(2n!)/\Gamma(n+l+3/2)}$ is again a normalization constant. In the case of zero angular momentum ($l = 0$) the solutions have already been derived in Sec. 5.2. The energy spectrum is determined by the equation

$$2\,\frac{\Gamma(3/4 - E_{\rm rel}/2)}{\Gamma(1/4 - E_{\rm rel}/2)} = \frac{1}{a_s} \qquad (l = 0). \tag{5.50}$$

It is convenient to define a non-integer effective harmonic oscillator quantum number ν by $E_{\rm rel} = 2\nu + 3/2$. The associated eigenfunctions are given by

$$\psi_{\rm rel} = \Re_\nu(r) = A_\nu\; U\left(-\nu; \frac{3}{2}; r^2\right) e^{-r^2/2} \qquad (l = 0) \tag{5.51}$$

where A_ν is a normalization constant which we determine numerically (here, the spherical harmonic $Y_{00} = 1/(2\sqrt{\pi})$ has been included into A_ν).

Energy spectrum (red) and associated wave functions (blue) of the $l = 0$ states are plotted in Fig. 5.12. As has been discussed in Sec. 5.2, these wave functions agree with the solutions of a realistic interaction potential outside the range R; see Fig. 5.6.

Let us move along the energy spectrum starting from the ground state of the noninteracting atoms [wave function (d), energy $E_{\rm rel} = 3/2\,\hbar\omega$]. If we increase the scattering length a_s from zero to $+\infty$, the wave function continuously transforms into the wave function (f) via (e). These wave functions belong to repulsively interacting atoms. At $a_s = +\infty$ these repulsively interacting

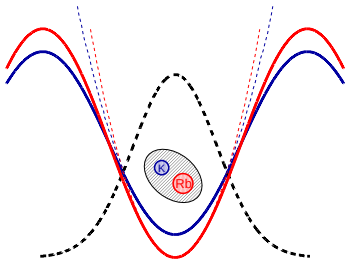

Figure 5.13: One ^{40}K and one ^{87}Rb atom at a single site of an optical lattice. The atoms have different masses $m_{\mathrm{K}}/m_{\mathrm{Rb}} \approx 0.46$ and they feel different lattice depths $V_{\mathrm{K}}/V_{\mathrm{Rb}} \approx 0.86$. We are interested in the ground-state properties of the system. Around the minimum, each lattice site is well approximated by a harmonic oscillator potential. To achieve higher accuracy, we include anharmonic corrections up to eighth order.

atoms acquire a positive "binding energy" of $+1\,\hbar\omega$. The limit $|a_s| = \infty$ is often referred to as the unitary limit. In this limit, E_{rel} and ψ_{rel} become independent of a_s since then $1/(a_s = \infty) = 0$ and the parameter a_s is absent in Eq. (5.50).

Now we move into the opposite direction from (d) via (c) to the state (b) by lowering the scattering length a_s from zero to $-\infty$. These wave functions belong to attractively interacting atoms. Again, in the unitary limit at $a_s = -\infty$, the atoms acquire a negative "binding energy" of $-1\,\hbar\omega$.

Now we jump from $a_s = -\infty$ to $a_s = +\infty$ and arrive at the lowest branch of the energy spectrum which belongs to the molecule. Note, that neither the wave function nor the energy change discontinuously when a_s jumps from $-\infty$ to $+\infty$. This is clear if we remember the definition of the scattering length: a_s is the intersection of the tangent of χ_{rel} at $r = 0$ with the r-axis. Thus, the abrupt change of a_s is due to an infinitesimal change of $\chi'_{\mathrm{rel}}(0)$ from $0+$ to $0-$. Note further, that this change can be achieved by an infinitesimal change of the depth of a realistic interaction potential [Figs. 5.6 and 5.7(middle)] or by a small change of the magnetic field B in the vicinity of a Feshbach resonance [Figs. 5.9(right) and 5.10].

We follow the energy of the lower branch by decreasing the scattering length from $a_s = +\infty$ to $a_s = 0+$. At $a_s = +0.3\,l_{\mathrm{rel}}$ we arrive at the wave function (a) of Fig. 5.12. As discussed in Sec. 5.1, for small a_s, the energy of the molecule tends to $-\infty$ according to $E_{\mathrm{rel}} = -\hbar^2/(2\mu a_s^2)$ [see Eq. (5.21)] and the size of the molecule decreases proportionally to $a_s/2$ [see Eq. (5.22)].

Two interacting atoms at a single site of an optical lattice: We now turn to the description of two ultracold atoms at a single site of an optical lattice. We consider the situation of Fig. 5.13: The two atoms (^{40}K and ^{87}Rb) have different masses and they experience different lattice potentials, i. e., the two atomic species feel different lattice depths. The Schrödinger equation of our system is given by

$$\left[\sum_{i=1,2}\left(-\frac{\hbar^2}{2m_i}\Delta_i + V_{\mathrm{lattice},i}(\vec{r}_i)\right) + \frac{2\pi\hbar^2 a_s}{\mu}\delta(\vec{r})\frac{\partial}{\partial r}r\right]\psi(\vec{r}_1,\vec{r}_2) = E\psi(\vec{r}_1,\vec{r}_2). \tag{5.52}$$

The lattice was formed by three retroreflected laser beams. The resulting effective lattice potential is a superposition of three orthogonal one-dimensional lattices [106]

$$V_{\mathrm{lattice},i}(\vec{r}) = V_i\left[\sin^2(kx) + \sin^2(ky) + \sin^2(kz)\right]. \tag{5.53}$$

Here, V_i is the depth of the lattice felt by atom i, and $k = 2\pi/\lambda$ is the wave number (λ is the wavelength). The experiment has been performed in the Mott insulator regime. Thus, we can

neglect tunneling and we can restrict to the description of one atom pair at a single lattice site. In order to make use of the known solution of two interacting atoms in a harmonic oscillator, we perform a taylor expansion of the $\sin^2$ function around the origin:

$$\sin^2(kx) = k^2x^2 - \frac{k^4}{3}x^4 + \frac{2k^6}{45}x^6 - \dots .$$

By inserting this expansion into Eq. (5.53) we obtain

$$V_{\text{lattice},i} = V_i\left[k^2r^2 - \frac{k^4}{3}\left(x^4+y^4+z^4\right) + \frac{2k^6}{45}\left(x^6+y^6+z^6\right) - \dots\right] \tag{5.54}$$

with $r^2 = x^2+y^2+z^2$. The first term of Eq. (5.54) gives rise to the harmonic approximation through $\omega_i = \sqrt{2V_ik^2/m_i}$, and the remainder gives rise to the anharmonic corrections $V_{\text{corr.}}$. By inserting Eq. (5.54) into Eq. (5.52) we obtain

$$\left[\sum_{i=1,2}\left(-\frac{\hbar^2}{2m_i}\Delta_i + \frac{1}{2}m_i\omega_i^2r_i^2\right) + \frac{2\pi\hbar^2a_s}{\mu}\delta(\vec{r})\frac{\partial}{\partial r}r + V_{\text{corr.}}(\vec{r}_1,\vec{r}_2)\right]\psi(\vec{r}_1,\vec{r}_2) = E\psi(\vec{r}_1,\vec{r}_2)$$

where $V_{\text{corr.}}$ contains the higher-order terms of $(V_{\text{lattice},1}+V_{\text{lattice},2})$. Again, we introduce center-of-mass and relative coordinates and transform the above Schrödinger equation according to

$$\begin{aligned}\Big[&-\frac{\hbar^2}{2M}\Delta_{\text{c.m.}} + \frac{1}{2}M\omega_{\text{c.m.}}^2R^2 - \frac{\hbar^2}{2\mu}\Delta_{\text{rel}} + \frac{1}{2}\mu\omega_{\text{rel}}^2r^2 + \frac{2\pi\hbar^2a_s}{\mu}\delta(\vec{r})\frac{\partial}{\partial r}r\\ &+\mu\Delta\omega^2\vec{r}\cdot\vec{R} + V_{\text{corr.}}(\vec{R},\vec{r})\Big]\psi(\vec{R},\vec{r}) = E\psi(\vec{R},\vec{r})\end{aligned} \tag{5.55}$$

where we have defined the frequencies

$$\omega_{\text{c.m.}} \equiv \sqrt{\frac{m_1\omega_1^2+m_2\omega_2^2}{m_1+m_2}}, \qquad \omega_{\text{rel}} \equiv \sqrt{\frac{m_2\omega_1^2+m_1\omega_2^2}{m_1+m_2}}, \quad \text{and} \quad \Delta\omega \equiv \sqrt{\omega_1^2-\omega_2^2}\,. \tag{5.56}$$

In the previous case both particles felt the same trap frequency $\omega = \omega_1 = \omega_2$ and thus $\omega_{\text{c.m.}} = \omega_{\text{rel}} = \omega$ and $\Delta\omega = 0$. In this case, however, both atoms feel different trap frequencies $\omega_1 \neq \omega_2$ and thus $\omega_{\text{c.m.}} \neq \omega_{\text{rel}}$ and $\Delta\omega \neq 0$. Therefore, the first effect of the different trap frequencies $\omega_1 \neq \omega_2$ is that not only the length scales $l_{\text{c.m.}} = \sqrt{\hbar/(M\omega_{\text{c.m.}})}$ and $l_{\text{rel}} = \sqrt{\hbar/(\mu\omega_{\text{rel}})}$ but also the energy scales $\hbar\omega_{\text{c.m.}}$ and $\hbar\omega_{\text{rel}}$ of the center-of-mass and the relative motion are different. The second effect of the different trap frequencies $\omega_1 \neq \omega_2$ is that the center-of-mass and the relative motion are coupled through $\mu\Delta\omega^2\vec{r}\cdot\vec{R}$. Moreover, the center-of-mass and the relative motion are coupled due to the anharmonic corrections $V_{\text{corr.}}(\vec{R},\vec{r})$. Since the problem is no longer separable, there exists no exact analytical solution of Eq. (5.55). Therefore, we perform a numerically exact diagonalization of the Hamiltonian $H = H_{\text{c.m.}} + H_{\text{rel}} + H_{\text{couple}}$ of Eq. (5.55) by using the energetically lowest eigenfunctions of the decoupled problem $H_0 = H_{\text{c.m.}} + H_{\text{rel}}$. We expect convergence with rather small matrices since the main contribution to the total energy of the lowest states (especially the strong interaction) is already included in the diagonal part of H.

Exact diagonalization of the Hamiltonian— The basis functions of the diagonalization are given by the eigenfunctions of the decoupled problem $H_0 = H_{\text{c.m.}} + H_{\text{rel}}$ [see Eqs. (5.47), (5.49) and (5.51); note that the interaction is already included in H_0]

$$\left\langle\vec{R},\vec{r}\,\middle|N,L,M,n,l,m;a_s\right\rangle = \mathfrak{R}_{NL}(R)Y_{LM}(\Theta,\Phi)\begin{cases}\mathfrak{R}_{\nu(a_s,n)}(r) & \text{if } l=0\\ \mathfrak{R}_{nl}(r)Y_{lm}(\theta,\phi) & \text{if } l\neq 0\,.\end{cases}$$

The non-integer index $\nu(a_s, n)$ is constructed as follows: Look at the energy spectrum of Fig. 5.12. We assign the index $n = 0$ to the ground state, the index $n = 1$ to the first excited state and so on. If $a_s > 0$ and $n = 0$, we relate the index ν to the energy of the molecule. The energy of the molecule $E_{\text{rel}}(a_s)$ is determined numerically from Eq. (5.50). MATHEMATICA needs three numbers to find the solution: E_{min}, E_{start} and E_{max}. We conclude from Fig. 5.12 that for the molecule one set of possible numbers is given by $(E_{\text{min}}, E_{\text{start}}, E_{\text{max}}) = (-\infty, -10, 0.5)$ $\big[$for E_{start} we can choose any value of the interval $(-\infty, 0.5)\big]$. From the relative energy E_{rel} the index ν is calculated through $\nu = E_{\text{rel}}/2 - 3/4$. Let me visualize the functional relation $\nu(a_s > 0, n = 0)$:

$$(a_s > 0, n = 0) \rightarrow (E_{\text{min}}, E_{\text{start}}, E_{\text{max}}) = (-\infty, -10, 0.5) \rightarrow E_{\text{rel}} \rightarrow \nu.$$

In the other cases, $a_s > 0$ and $n = 1, 2, 3, \ldots$, a possible set of numbers is given by

$$(E_{\text{min}}, E_{\text{start}}, E_{\text{max}}) = \left(2n - \frac{1}{2}, 2n, 2n + \frac{1}{2}\right)$$

so that the functional relation $\nu(a_s > 0, n = 1, 2, 3, \ldots)$ is given by

$$(a_s > 0, n = 1, 2, 3, \ldots) \rightarrow (E_{\text{min}}, E_{\text{start}}, E_{\text{max}}) = \left(2n - \frac{1}{2}, 2n, 2n + \frac{1}{2}\right) \rightarrow E_{\text{rel}} \rightarrow \nu.$$

Now we turn to the left side of the energy spectrum, $a_s \leqslant 0$. For all indices $n = 0, 1, 2, \ldots$, the functional relation $\nu(a_s \leqslant 0, n = 0, 1, 2, \ldots)$ is given by

$$(a_s \leqslant 0, n = 0, 1, 2, \ldots) \rightarrow (E_{\text{min}}, E_{\text{start}}, E_{\text{max}}) = \left(2n + \frac{1}{2}, 2n + 1, 2n + \frac{3}{2}\right) \rightarrow E_{\text{rel}} \rightarrow \nu.$$

As basis we have chosen the states $|N, L, M, n, l, m; a_s\rangle$ with lowest principal quantum numbers $\Pi \equiv 2N + L + 2n + l = 0, 1, ..., \Pi_{\text{max}}$, where N, L, M and n, l, m are the quantum numbers of the eigenfunctions of the rotationally symmetric harmonic oscillator of center-of-mass and relative motion, respectively. We typically used $\Pi_{\text{max}} = 7$ leading to a total number of 258 basis states. We have found that adding another level of the uncoupled problem to the basis set leads to additional changes in the energy smaller than $\approx 10^{-3}\,\hbar\omega_{\text{rel}}$. Furthermore, we exploited the fact that the total angular momentum $L_z = \hbar(M + m)$ of the low-energy eigenfunctions is approximately conserved despite the cubic symmetry of the optical lattice. Again, we found that including $L_z \neq 0$ basis states lowers the energy by only $\approx 3 \times 10^{-3}\,\hbar\omega_{\text{rel}}$. [14]

The matrix of the decoupled Hamiltonian $H_0 = H_{\text{c.m.}} + H_{\text{rel}}$ is diagonal and the diagonal elements are given by

$$\langle i|H_0|i\rangle = \left(2N + L + \frac{3}{2}\right)(\omega_{\text{c.m.}}/\omega_{\text{rel}}) + \begin{cases} 2\nu + 3/2 & \text{if } l = 0 \\ 2n + l + 3/2 & \text{if } l \neq 0\,. \end{cases}$$

Here, $|i\rangle = |N, L, M, n, l, m; a_s\rangle$ and $\langle i|H_0|i\rangle$ is given in units of $\hbar\omega_{\text{rel}}$. The matrix elements of the dipole Hamiltonian $H_{\text{dipole}} = \mu\Delta\omega^2\vec{r}\cdot\vec{R}$ are given by

$$\langle i|H_{\text{dipole}}|j\rangle = C_{\text{dipole}}\Big(\langle i|xX|j\rangle + \langle i|yY|j\rangle + \langle i|zZ|j\rangle\Big)$$

[14] I note that we neglect many low-energy basis states $|N, L, 0, 0, 0, 0\rangle$ with $2N + L > \Pi_{\text{max}}$ when the scattering length is small and positive $a_s \gtrsim 0$. These molecule states with highly excited center-of-mass energy have nevertheless low total energy since the energy of the relative motion is large and negative. We have included the states $|N, L, 0, 0, 0, 0\rangle$ with $2N + L \leq \Pi_{\text{max}}$ to allow for the flattening of the center-of-mass wave function due to the anharmonicity of the lattice site potential. But we have neglected the states with $2N + L > \Pi_{\text{max}}$ since they are only weakly coupled to the states $|0, 0, 0, 0, 0, 0\rangle$ (molecule) and $|0, 0, 0, n = 1, 0, 0\rangle$ (repulsively interacting atoms of the decoupled problem).

where the coupling constant C_{dipole} is calculated according to

$$C_{\text{dipole}} = \mu\Delta\omega^2 l_{\text{rel}} l_{\text{c.m.}} = \widetilde{\Delta\omega}^2\, \widetilde{l}_{\text{c.m.}}\, \mu l_{\text{rel}}^2 \omega_{\text{rel}}^2 = \widetilde{\Delta\omega}^2\, \widetilde{l}_{\text{c.m.}}\, \hbar\omega_{\text{rel}}$$

with $\widetilde{l}_{\text{c.m.}} = l_{\text{c.m.}}/l_{\text{rel}}$ and $\widetilde{\Delta\omega} = \Delta\omega/\omega_{\text{rel}}$. The integrals $\langle i|xX|j\rangle, \ldots$ are calculated further below.

Let me first calculate the energy and length scales for a typical set of experimental parameters: A typical lattice depth, felt by the ^{87}Rb atoms, was chosen to be $V_{\text{Rb}} = 40.5\, E_{r,\text{Rb}}$ where $E_{r,\text{Rb}} = \hbar^2k^2/(2m_{\text{Rb}}) = \text{h}^2/(2m_{\text{Rb}}\lambda^2)$ is the ^{87}Rb recoil energy. For $\lambda = 1.03\,\mu$m we obtain $E_{r,\text{Rb}} \approx 2.16\,h$kHz and $V_{\text{Rb}} \approx 86.6\,h$kHz (see appendix D for the masses of ^{87}Rb and ^{40}K). The lattice depth of ^{40}K was a little bit shallower, $V_{\text{K}} = 0.86\, V_{\text{Rb}} \approx 74.8\,h$kHz. In the harmonic approximation of one lattice well, the angular trap frequencies are given by $\omega_{\text{Rb}} = \sqrt{2V_{\text{Rb}}k^2/m_{\text{Rb}}} = 4\pi\sqrt{40.5}\, E_{r,\text{Rb}}/\text{h} \approx 2\pi \times 27.4\,\text{kHz}$ and $\omega_{\text{K}} \approx \sqrt{87/40 \cdot 0.86}\,\omega_{\text{Rb}} \simeq 1.37\,\omega_{\text{Rb}} \approx 2\pi \times 37.5\,\text{kHz}$. A comparison of these frequencies with the accordant lattice depths $V_{\text{Rb}}/(\hbar\omega_{\text{Rb}}) = 86.6/27.4 \approx 3.2$ and $V_{\text{K}}/(\hbar\omega_{\text{K}}) = 74.8/37.5 \approx 2$ shows that, for the ^{87}Rb atom, the lattice depth is larger than the energy of the first excited state, while, for the ^{40}K atom, the lattice depth is larger than the ground-state energy of the harmonic oscillator. According to Eq. (5.56) the angular frequencies of the relative and the center-of-mass motion are given by

$$\omega_{\text{rel}} \approx 2\pi \times \sqrt{\frac{87 \cdot 37.5^2 + 40 \cdot 27.4^2}{40 + 87}}\,\text{kHz} \approx 2\pi \times 34.6\,\text{kHz}$$

and

$$\omega_{\text{c.m.}} \approx 2\pi \times \sqrt{\frac{87 \cdot 27.4^2 + 40 \cdot 37.5^2}{40 + 87}}\,\text{kHz} \simeq 0.89\,\omega_{\text{rel}}\,.$$

The frequency difference $\Delta\omega$ is given by

$$\Delta\omega \approx \sqrt{1.37^2 - 1}(27.4/34.6)\,\omega_{\text{rel}} \simeq 0.74\,\omega_{\text{rel}}\,.$$

The oscillator lengths of the relative and the center-of-mass motion are given by

$$l_{\text{rel}} = \sqrt{\frac{\hbar}{\mu\omega_{\text{rel}}}} \approx \sqrt{\frac{1.055 \cdot 10^{-34}(40+87)}{40 \cdot 87 \cdot 1.66 \cdot 10^{-27} \cdot 2\pi \cdot 34.6 \cdot 10^3}}\,\text{m} \approx 103\,\text{nm}$$

and

$$l_{\text{c.m.}} = \sqrt{\frac{\hbar}{M\omega_{\text{c.m.}}}} \approx \sqrt{\frac{87 \cdot 40}{(87+40)^2 \cdot 0.89}}\, l_{\text{rel}} \simeq 0.49\, l_{\text{rel}}\,.$$

The dipole coupling constant is therefore given by

$$C_{\text{dipole}} \approx 0.74^2 \cdot 0.49\,\hbar\omega_{\text{rel}} \simeq 0.27\,\hbar\omega_{\text{rel}}\,.$$

Now we turn to the calculation of the integrals $\langle i|xX|j\rangle, \ldots$. The dimensionless dipole integrals $\langle i|xX|j\rangle, \ldots$ have been calculated in spherical coordinates

$$\begin{aligned}\langle i|xX|j\rangle \;=\; &\langle N, L|R|N', L'\rangle \langle L, M|\sin\Theta\cos\Phi|L', M'\rangle \times \\ &\langle n, l; a_s|r|n', l'; a_s\rangle \langle l, m|\sin\theta\cos\phi|l', m'\rangle\end{aligned}$$

with similar expressions for $\langle i|yY|j\rangle$ and $\langle i|zZ|j\rangle$ (spherical coordinates: $x = r\sin\theta\cos\phi$, $y = r\sin\theta\sin\phi$ and $z = r\cos\theta$). The integrals $\langle N, L|R|N', L'\rangle$, $\langle L, M|\sin\Theta\cos\Phi|L', M'\rangle$, $\langle n, l \neq 0; a_s|r|n', l' \neq 0; a_s\rangle$ and $\langle l, m|\sin\theta\cos\phi|l', m'\rangle$ have been calculated analytically by means

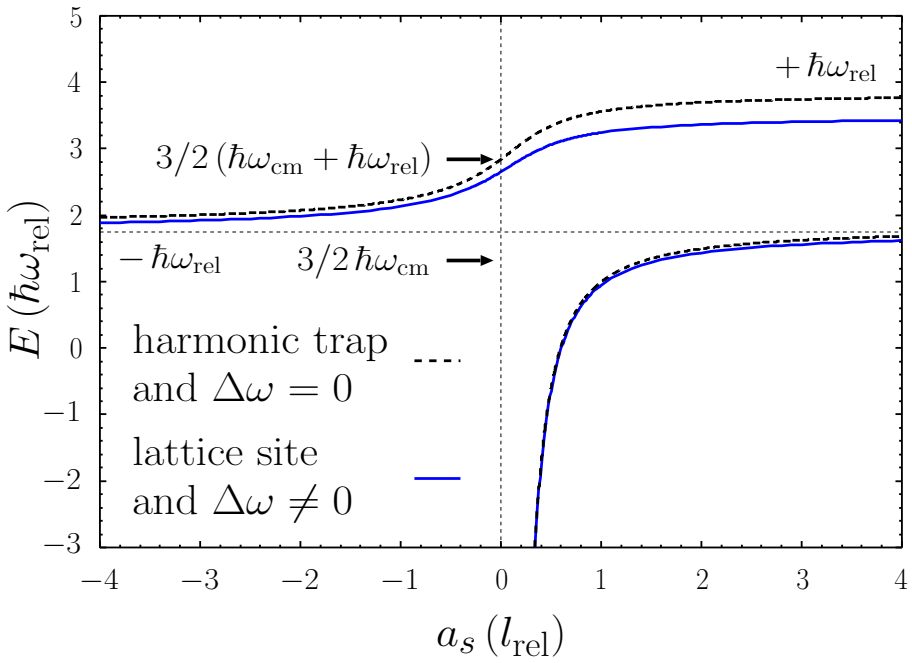

Figure 5.14: Energy eigenvalues of ^{40}K and ^{87}Rb as a function of the scattering length without (black dashed line) and with coupling terms (blue solid line) due to the anharmonicity and the unequal trap frequencies of the lattice for parameters: $V_{\rm Rb} = 40.5\,E_{r,\rm Rb}$, $V_{\rm K} = 0.86\,V_{\rm Rb}$ and $\lambda = 1030\,$nm. The deviation between the idealized model and the full solution is substantial in particular for the upper branch.

of the "Integrate" function of MATHEMATICA. Only the integrals $\langle n, l = 0; a_s|r|n', l' \neq 0; a_s\rangle$ or $\langle n, l \neq 0; a_s|r|n', l' = 0; a_s\rangle$ have been calculated numerically by means of the "NIntegrate" function of MATHEMATICA. Analytic formulas for the radial integrals are given in Ref. [98]. We did not care about further simplifications since the calculation of the comparatively small Hamiltonian matrix was sufficiently fast anyway. However, it turns out that the dipole Hamiltonian $H_{\rm dipole}$ does not contribute to the diagonal elements of H. Therefore, the energy shift, caused by $H_{\rm dipole}$, was comparatively small in the deep optical lattice with $V_{\rm Rb} = 40.5\,E_{r,\rm Rb}$.

Now we consider the calculation of the matrix elements of the anharmonic corrections $\langle i|V_{\rm corr.}|j\rangle$. Since $x_1 = X + ax$ and $x_2 = X - bx$ with $a \equiv m_2/M$ and $b \equiv m_1/M$, the x-dependent part of the anharmonic corrections $V^{(x)}_{\rm corr.}$ transforms to

$$V^{(x)}_{\rm corr.} = -\frac{k^4}{3}(V_1x_1^4 + V_2x_2^4) + \ldots = -\frac{V_1+V_2}{3}k^4X^4 - \frac{4(V_1a - V_2b)}{3}k^4xX^3$$
$$-2(V_1a^2 + V_2b^2)k^4x^2X^2 - \frac{4(V_1a^3 - V_2b^3)}{3}k^4x^3X - \frac{V_1a^4 + V_2b^4}{3}k^4x^4 + \ldots .$$

Corresponding expressions are obtained for the y- and z-direction, $V^{(y)}_{\rm corr.}$ and $V^{(z)}_{\rm corr.}$. The transformation of the anharmonic corrections into center-of-mass and relative coordinates has been done automatically by means of the algebraic-formula-manipulation functions "Expand" and "Collect" of MATHEMATICA. Again, the calculation of the matrix elements of the anharmonic corrections has been performed in spherical coordinates. In the numerical implementation, we have tested for convergence with terms up to eighth order. We found that including eighth-order corrections improve the accuracy of the calculation by only $\approx 3 \times 10^{-3}\,\hbar\omega_{\rm rel}$.

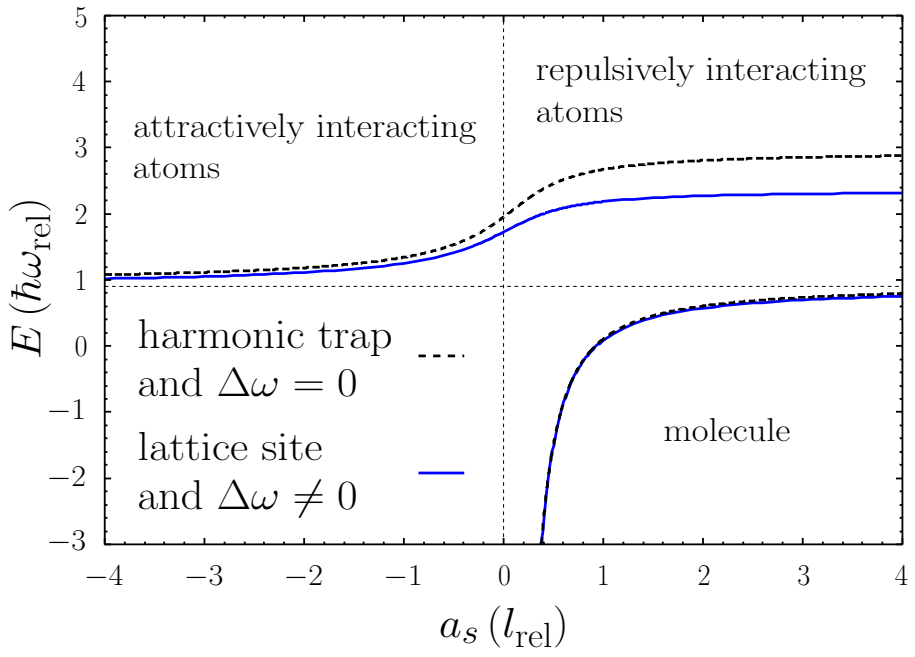

Figure 5.15: Low-energy spectrum of the states with a center-of-mass energy $3/2\,\hbar\omega_{\text{c.m.}}$ for ^{6}Li and ^{133}Cs and the lattice parameters $V_{\text{Li}} = V_{\text{Cs}} = 10\,\hbar^2k^2/2\mu$ and $\lambda = 1\,\mu$m. The energy is much more lowered compared to the case of ^{40}K and ^{87}Rb since the mass of the ^{6}Li atom is much smaller than the mass of the ^{133}Cs atom.

Once the Hamiltonian matrix has been calculated, we diagonalize it numerically by means of the function "Eigensystem" of MATHEMATICA. The resulting eigenvectors $\left(c_{(0,0,0,0,0,0)}, \ldots\right)$ are the coefficients of the expansion

$$|\psi\rangle = \sum_{N,L,M,n,l,m} c_{(N,L,M,n,l,m)} |N, L, M, n, l, m; a_s\rangle$$

and the corresponding eigenvalues $E_{|\psi\rangle}$ are the desired eigenenergies of the interacting atoms at a single lattice site. The wave function $|\psi_0\rangle$ with the lowest energy E_0 belongs to the molecule if $a_s > 0$ and to the attractively interacting atoms if $a_s \leqslant 0$, respectively. For $a_s \gtrsim 0$, there are many molecular wave functions with a highly excited center-of-mass energy. To determine the wave function of the repulsively interacting atoms, we search for the state with $\left|c_{(0,0,0,1,0,0)}\right| \geqslant 0.5$.

Energy spectrum— Fig. 5.14 shows the resulting energy spectrum (blue solid line) compared to the uncoupled solution (black dashed line), calculated for ^{40}K and ^{87}Rb with the experimental parameters of Ref. [72]: $V_{\text{Rb}} = 40.5\,E_{r,\text{Rb}}$, $V_{\text{K}} = 0.86\,V_{\text{Rb}}$, and $\lambda = 1030\,$nm. In the case of heteronuclear atom pairs it is useful to express the lattice depth in units of $E_{r,\text{rel}} = \hbar^2k^2/2\mu$, which is the kinetic energy given to a particle with reduced mass μ by a photon of momentum $\hbar k$. Then, $V_{\text{Rb}} = 40.5\,E_{r,\text{Rb}} = 12.6\,E_{r,\text{rel}}$. As can be seen from the figure, the deviation between the idealized model, where the coupling term has been neglected, and the full solution is substantial. The difference is most pronounced in the repulsively interacting pair branch ($0.34\,\hbar\omega_{\text{rel}} \approx 20\%$ of the level spacing) and becomes smaller as we enter the attractively-interacting-atom part of the spectrum. The molecular branch is relatively unaffected by the coupling term H_{couple}. This is natural because as we approach $a \to +0$, the role of the external confinement decreases since the molecule becomes smaller.

The influence of the coupling term H_{couple} is even stronger if we consider molecules with large

atom pair	E_0	ΔE_{dipole}	$\Delta E_{\text{corr.}}$	ΔE
^{40}K and ^{87}Rb	3.74	-0.12 (29%)	-0.27 (71%)	-0.39
^{6}Li and ^{133}Cs	2.88	-0.35 (62%)	-0.22 (38%)	-0.57
^{6}Li and ^{87}Rb	2.99	-0.36 (61%)	-0.22 (39%)	-0.58
^{6}Li and ^{40}K	3.24	-0.31 (58%)	-0.24 (42%)	-0.55
^{6}Li and ^{7}Li	3.92	-0.01 (2%)	-0.29 (98%)	-0.30

Table 5.1: Influence of the individual coupling terms H_{dipole} and $V_{\text{corr.}}$ on the total energy of several atom pairs. The energies are given in units of $\hbar\omega_{\text{rel}}$. All values are calculated at $a_s = 4\,l_{\text{rel}}$ for lattice depths of $V_1 = V_2 = 10\,E_{r,\text{rel}}$ and a wavelength of $\lambda = 1\,\mu$m. $E_0 = E_{\text{c.m.}} + E_{\text{rel}}$ is the energy of the uncoupled Hamiltonian. Including H_{dipole} into the Hamiltonian reduces the energy by ΔE_{dipole} and including $H_{\text{dipole}} + V_{\text{corr.}}$ reduces the energy further by $\Delta E_{\text{corr.}}$. The value in brackets is the percentage contribution of the individual coupling terms to the total change of the energy ΔE.

mass ratios as in the case of ^{6}Li and ^{133}Cs, see Fig. 5.15. We have chosen the lattice parameters $V_{\text{Li}} = V_{\text{Cs}} = 10\,E_{r,\text{rel}}$ and $\lambda = 1\,\mu$m. Here, the energy of the repulsively interacting atoms is lowered by up to $\approx 0.6\,\hbar\omega_{\text{rel}}$.

Table 5.1 shows the effect of the individual coupling terms H_{dipole} and $V_{\text{corr.}}$ on the energy of several atom pairs. The energies have been calculated for repulsively interacting atoms at $a_s = 4\,l_{\text{rel}}$ which is the largest scattering length shown in Figs. 5.14 and 5.15. All the energies of Table 5.1 are given in units of the level spacing of the relative motion $\hbar\omega_{\text{rel}}$. Adding the coupling term H_{dipole} contributes up to 62% to the total change ΔE for ^{6}Li and ^{133}Cs. The strong influence of H_{dipole} stems from the large mass ratio which results in extremely different trap frequencies ω_{Li} and ω_{Cs}. By contrast, the energy of ^{6}Li and ^{7}Li atoms is nearly not affected by H_{dipole} since the trap frequencies are almost equal.

5.7 Experimental vs. theoretical spectrum. Resonance position

Next, we compare the calculated energy spectrum of Fig. 5.14 to the measured binding energy of Ref. [72]. From rf spectra as in Fig. 5.11, the separation between the single atom and the two-particle ("molecular") peak has been determined with high precision (typical uncertainty of 250 Hz). From the separation of the two peaks the binding energy has been extracted up to a constant offset due to nonzero background scattering lengths. At the same time, the atomic peak was used for a precise magnetic field calibration as described in Sec. 5.5. Spectra as in Fig. 5.11 have been recorded for magnetic field values across the whole resonance and yield the energy spectrum as a function of magnetic field.

Fig. 5.16 shows the measured energy shift across the resonance at a lattice depth of $40.5\,E_{r,\text{Rb}}$ as a function of magnetic field. The energy shift is obtained from Fig. 5.14 by subtracting the motional energy of the initial $^{87}\text{Rb}|1,1\rangle \otimes {}^{40}\text{K}|9/2,-7/2\rangle$ state: $E_{\text{shift}} = E - E(a_{-7/2} = -175\,a_B)$. [15] In addition, Figs. 5.16 and 5.14 are connected through Eq. (5.45). One branch of the spectrum is characterized by the presence of a positive "binding energy", the repulsively interacting pair branch. In Fig. 5.14, we have seen that this branch continuously transforms into attractively in-

[15] For the scattering length in the initial $^{87}\text{Rb}|1,1\rangle \otimes {}^{40}\text{K}|9/2,-7/2\rangle$ state in the considered magnetic field range $544\,\text{G} < B < 549\,\text{G}$ we take the value $-175 a_B$ [107].

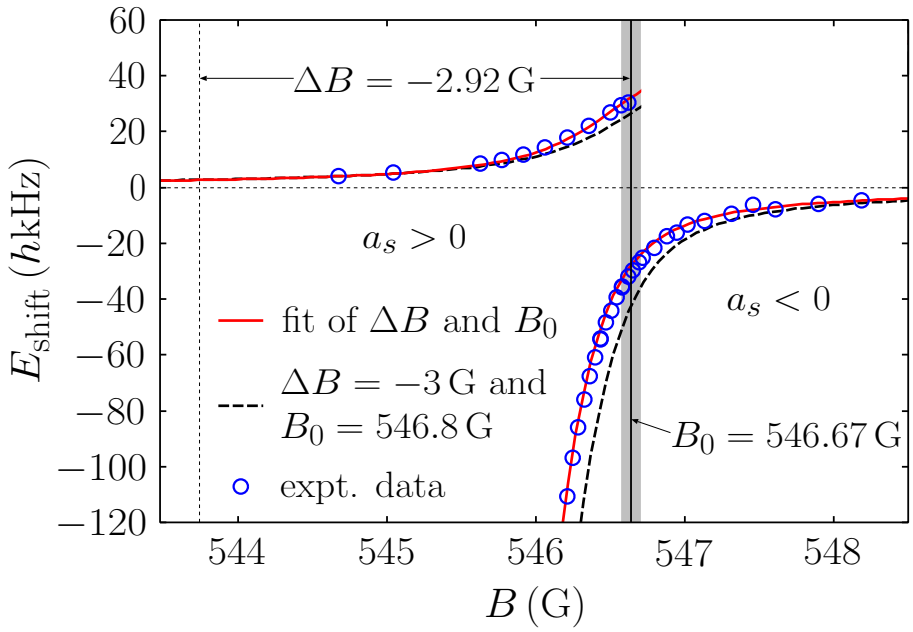

Figure 5.16: Experimentally observed energy spectrum of K–Rb at a lattice depth of $40.5\,E_{r,\mathrm{Rb}}$ together with theory without free parameters (black dashed line) and a least squares fit for the resonance parameters B_0 and ΔB (red solid line).

teracting atoms as a function of a_s. As a function of magnetic field, however, and as a result of Eq. (5.45), we observe this transition as a jump from the left-hand side of Fig. 5.16, where the interaction is weak and repulsive, to the right-hand side of Fig. 5.16, where the interaction is weak and attractive. Here, we find attractively interacting atoms which decay into free atom pairs if the external confinement of the optical lattice is removed.

Whereas in Fig. 5.14, the attractively interacting atoms branch and the molecule branch are only asymptotically equal in the limit $|a_s| \to \infty$, the singularity on resonance in Eq. (5.45) transforms this into a continuous crossover across the center of the resonance position as a function of magnetic field and as seen in Fig. 5.16. These molecules are stable even in the absence of the optical lattice potential.

In order to compare the numerically calculated energy spectrum $E(a_s)$ (blue solid line of Fig. 5.14) to the experimental data $E(B)$ of Fig. 5.16, we transform the scattering length a_s into the magnetic field strength B via Eq. (5.45). By using parameters from the literature: $a_{\mathrm{bg}} = -185\,a_B$, $\Delta B = -3\,\mathrm{G}$ [108] and $B_0 = 546.8\,\mathrm{G}$ [104], we obtain the black dashed curve in Fig. 5.16. As can be seen, the difference between the theoretical prediction and the experimental data can be overcome by a shift of the black dashed curve along the magnetic field axis. We attribute this shift to an insufficient knowledge of the resonance center position B_0.

We therefore fit our theoretical calculations to the experimental data in order to improve the estimate for the resonance center position B_0. As independent fit parameters we choose B_0 and ΔB, while a_{bg} is fixed. The latter parameter cannot be determined independently from the measurements due to its strong correlations with ΔB. This is due to the fact that in the vicinity of the resonance center position B_0 the first term of Eq. (5.45) is negligible so that only the product $a_{\mathrm{bg}}\Delta B$ can be determined precisely from the fit. We therefore set $a_{\mathrm{bg}} = -185\,a_B$ [108] and use ΔB and B_0 as free fit parameters, with the caveat that only the value obtained for B_0 is to be considered precise. In Fig. 5.16, the result of the least squares fit is displayed as a red solid line. Note

that the reliability of the fitting procedure sensitively depends on an accurate calculation of the energy spectrum $E(a_s)$ which includes an exact treatment of the anharmonicity and the different trap frequencies of the two atoms.

The least squares fit results in the following values of the resonance parameters $\Delta B = -2.92\,\mathrm{G}$ and $B_0 = 546.669\,\mathrm{G}$. The fit results in an uncertainty of 2 mG on B_0. The value of B_0 sensitively depends on the scattering length of the initial state $a_{-7/2}$. Assuming an uncertainty of $a_{-7/2}$ of 10% results in an uncertainty on B_0 of 20 mG. Another possible source of systematic uncertainties may be the lattice depth calibration. The lattice depth has been calibrated by parametric excitation from the first to the third band of the lattice and is estimated to have an uncertainty of 5%. Repeating the fit procedure with $\pm 5\%$ variations on the lattice depth calibration, we obtain a corresponding systematic uncertainty on B_0 of 7 mG. A third source of systematic uncertainties finally stems from the finite basis and an imprecise approximation of the lattice site potential. Here, we included corrections up to eighth order and generated basis states of the lowest eight energy levels of the uncoupled Hamiltonian. This improved the value of B_0 by 2 mG compared to a calculation with up to sixth order corrections and basis states of lowest seven energy levels. Adding the systematic uncertainty of the magnetic field calibration of 12 mG (see Sec. 5.5), we finally obtain

$$B_0 = 546.669(24)_{\mathrm{syst}}(2)_{\mathrm{stat}}\,\mathrm{G}$$

under the assumption that the pseudopotential treatment is valid in the present experimental situation. [16]

5.8 Efficiency of radio-frequency (rf) association

Not only the binding energy but also the two-atom (molecule) wave function changes dramatically in the vicinity of a Feshbach resonance; see Figs. 5.10 and 5.12. This change of the wave function is, e. g., reflected in the efficiency of the rf association process, i. e., the ratio N_f/N_i where N_i and N_f are the number of atoms in the initial $^{87}\mathrm{Rb}|1,1\rangle \otimes {}^{40}\mathrm{K}|9/2,-7/2\rangle$ and final $^{87}\mathrm{Rb}|1,1\rangle \otimes {}^{40}\mathrm{K}|9/2,-9/2\rangle$ states respectively. In the vicinity of the Feshbach resonance a strong dependency of the transfer efficiency N_f/N_i on the magnetic field strength B has been observed as can be seen in Fig. 5.17.

Let me recapitulate the rf association process (see Sec. 5.5 and inset of Fig. 5.11): In the beginning the two atoms are in state $\psi_i(\vec{r}_1,\vec{r}_2)|1,1\rangle \otimes |9/2,-7/2\rangle$ where ψ_i is the initial motional wave function. In this state the atoms interact only weakly via the small negative scattering length $a_{-7/2} = -175\,a_B$ ($\approx -0.1\,l_{\mathrm{rel}}$) leading to a small deformation of the two-atom wave function compared to the noninteracting case. An rf pulse with a frequency of $\omega \approx 2\pi \times 80\,\mathrm{MHz}$ and an amplitude of $\omega_{\mathrm{rf,\,max}} = 2\pi \times 1250\,\mathrm{Hz}$ [73] switches the spin of the ^{40}K atom from $|9/2,-7/2\rangle$ to $|9/2,-9/2\rangle$. In the final state $\psi_f(\vec{r}_1,\vec{r}_2)|1,1\rangle \otimes |9/2,-9/2\rangle$ the atoms interact strongly via $a_s(B)$ leading to a large deformation of the final motional wave function ψ_f.

[16] We expect the pseudopotential model to be fairly accurate for the experimental parameters of Ref. [72]. Indeed, even for large scattering lengths, this model is expected to become exact in the zero-range limit [102], that is when $1/k_{\mathrm{typ}} \gg \max(\beta_6, |r_e^0|)$. Here, k_{typ} is the typical wave number of the relative motion of the two atoms, $\beta_6 = (2\mu C_6/\hbar^2)^{1/4}$ is the van der Waals length scale and $r_e^0 \equiv -\hbar^2/(\mu a_{\mathrm{bg}} \Delta B \partial E_{\mathrm{res}}/\partial B)$, $\partial E_{\mathrm{res}}/\partial B$ being the magnetic moment of the closed channel with respect to the two-atom open channel. For K-Rb in their ground state, $\beta_6 = 7.6\,\mathrm{nm}$ [109]. Using $\partial E_{\mathrm{res}}/\partial B = k_B 144\,\mu\mathrm{K/G}$ [107], we get $r_e^0 = -4.6\,\mathrm{nm}$. It remains to estimate k_{typ}. In the molecule regime, we have $1/k_{\mathrm{typ}} \sim a_s > 47\,\mathrm{nm}$. In the other regimes (attractively and repulsively interacting atoms), we have $1/k_{\mathrm{typ}} \sim l_{\mathrm{rel}}$. In the harmonic approximation for the experimental lattice depth, $l_{\mathrm{rel}} = 103\,\mathrm{nm}$. Thus, the above inequality is fairly well satisfied.

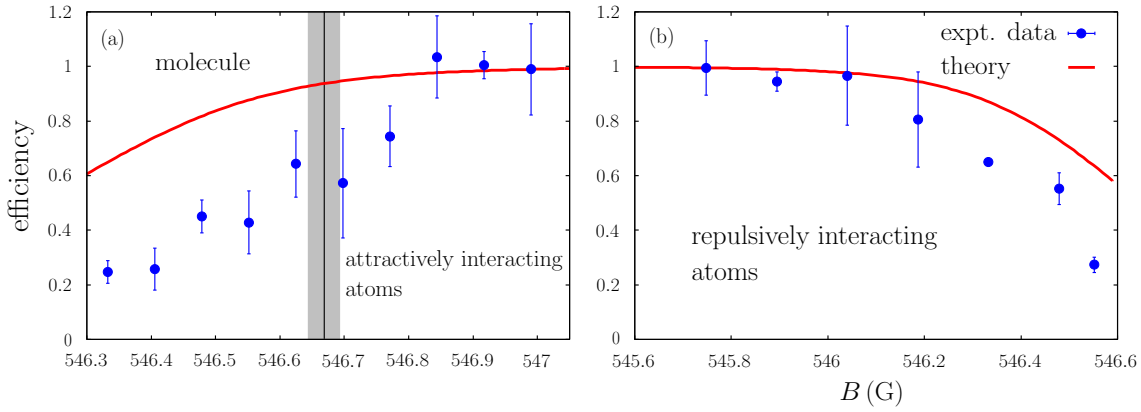

Figure 5.17: Transfer efficiency of rf association as observed in the experiment and estimated from a Rabi model, both for (a) attractively interacting atoms and molecules, and for (b) repulsively interacting pairs. The experimental data contain a global factor which has been chosen such that the value of the outermost right (a) [left (b)] data point is one (see text).

As long as the initial and final wave functions are similar, the molecules are produced with nearly 100% efficiency, i. e., the final number of molecules equals the initial number of atom pairs. We have seen in Fig. 5.12 that the wave function of the tightly bound molecules (and the strongly repulsive atoms) is very dissimilar from the initial wave function of the nearly noninteracting atoms. In that case the efficiency of the rf association rapidly drops down, i. e., the initial number of atom pairs is much larger than the final number of molecules which have been produced by the rf pulse. In the following I will show that the transfer efficieny depends on the overlap between the initial and final motional two-atom wave functions $\langle\psi_i|\psi_f\rangle$.

We can describe the rf association process by a Rabi model (see appendix C for a detailed discussion): The atoms are initially in state $|1\rangle \equiv (\psi_i, 0)^T$ and afterwards in state $|2\rangle \equiv (0, \psi_f)^T$. In the rotating frame, the spin Hamiltonian is given by (see the derivation of Eq. C.2)

$$H_{\text{spin}} = \frac{\hbar}{2}\begin{pmatrix} +\Delta\omega & -\omega_{\text{rf}}(t) \\ -\omega_{\text{rf}}(t) & -\Delta\omega \end{pmatrix}.$$

Here, $\Delta\omega \equiv \omega - \omega_0 - \omega_{\text{shift}}$ is the detuning, $\omega_0 \propto B_0$ is proportional to the applied static magnetic field and ω_{shift} is proportional to the separation distance between the atomic and the molecular peak $E_{\text{shift}} = \hbar\omega_{\text{shift}}$ (see Fig. 5.11). The rf amplitude $\omega_{\text{rf}}(t)$ is time-dependent with Gaussian shape. In the present experimental situation we can savely apply the rotating wave approximation since $|\omega_{\text{rf, max}}/\omega| \lesssim 10^{-3} \ll 1$; see Fig. C.2. By integrating out the spatial degrees of freedom,

$$(H_{\text{rf}})_{11} \equiv \langle 1|H_{\text{spin}}|1\rangle = \int d\vec{R}d\vec{r}\,(\psi_i, 0)\frac{\hbar}{2}\begin{pmatrix} +\Delta\omega & -\omega_{\text{rf}}(t) \\ -\omega_{\text{rf}}(t) & -\Delta\omega \end{pmatrix}\begin{pmatrix} \psi_i \\ 0 \end{pmatrix} = \frac{\hbar}{2}\Delta\omega \underbrace{\int d\vec{R}d\vec{r}\,\psi_i^2}_{=1},$$

$$(H_{\text{rf}})_{12} = \int d\vec{R}d\vec{r}\,(\psi_i, 0)\frac{\hbar}{2}\begin{pmatrix} +\Delta\omega & -\omega_{\text{rf}}(t) \\ -\omega_{\text{rf}}(t) & -\Delta\omega \end{pmatrix}\begin{pmatrix} 0 \\ \psi_f \end{pmatrix} = -\frac{\hbar}{2}\omega_{\text{rf}}(t) \underbrace{\int d\vec{R}d\vec{r}\,\psi_i\psi_f}_{=\langle\psi_i|\psi_f\rangle}$$

$$\Rightarrow\ (H_{\text{rf}})_{12} = (H_{\text{rf}})_{21} = -\frac{\hbar}{2}\omega_{\text{rf}}(t)\langle\psi_i|\psi_f\rangle,$$

$$(H_{\text{rf}})_{22} = -\frac{\hbar}{2}\Delta\omega \qquad \text{(analog)}$$

we obtain the effective Hamiltonian

$$H_{\rm rf} = \frac{\hbar}{2}\begin{pmatrix} +\Delta\omega & -\omega_{\rm rf}(t)\langle\psi_i|\psi_f\rangle \\ -\omega_{\rm rf}(t)\langle\psi_i|\psi_f\rangle & -\Delta\omega \end{pmatrix}. \tag{5.57}$$

As can be seen, the off-diagonal elements of Hamiltonian (5.57) are not only proportional to the rf amplitude $\omega_{\rm rf}(t)$, but also to the overlap integral $\langle\psi_i|\psi_f\rangle$. Therefore, the transfer probability between states $|1\rangle$ and $|2\rangle$ corresponds to Rabi flopping with a Rabi frequency reduced by the overlap integral of ψ_i and ψ_f compared to the pure atomic transition.

Exactly on the molecular resonance, we have $\omega = \omega_0 + \omega_{\rm shift}$ $(\rightarrow \Delta\omega = 0)$. The on-resonant result for the transfer probability (efficiency) is thus given by [see Eq. (C.7)]

$$N_f/N_i = P_{1\rightarrow 2} = \sin^2\left[\frac{1}{2}\langle\psi_i|\psi_f\rangle\int_0^t \omega_{\rm rf}(t')dt'\right] \tag{5.58}$$

which is unity for a transfer between atomic states, where $\psi_i = \psi_f$, when setting the area under the $\omega_{\rm rf}(t)$ curve to $\int_0^t \omega_{\rm rf}(t')dt' = \pi$. For transfer into the molecular state, the probability decreases as a function of the wave function overlap integral since the molecular final orbital wave function becomes more and more dissimilar from the initial two-body atomic wave function.

In the experiment, the molecules were associated using rf pulses designed to induce a π pulse for the noninteracting atoms: $\int_0^t \omega_{\rm rf}(t')\,dt' = \pi$. This π pulse has been kept fixed over the entire range of magnetic field values investigated. The experimental association efficiency is determined from the height of the molecular peak (see Fig. 5.11) as a function of magnetic field for constant pulse parameters and $\omega = \omega_0 + \omega_{\rm shift}$ $(\rightarrow \Delta\omega = 0)$ as in the theory above.

Figs. 5.17(a) and 5.17(b) show a comparison between the conversion efficiency as extracted from the experimental data and the theoretical estimate from equation (5.58). Theory and experiment show the general trend of dropping association efficiency with increasing binding energy when the initial and final wave functions become more and more dissimilar. In this context, we define the experimental conversion efficiency as the ratio of the number of molecules created and the initial lattice sites which are occupied by exactly one K and one Rb atom. Note that only on these lattice sites molecules can be created. For the comparison of experimental and theoretical transfer efficiency, the experimental data have been scaled by a global factor to reproduce a conversion efficiency of 1 far off the Feshbach resonance where initial and final two-body wave function are equal. This is necessary, because the initial lattice sites occupied by one K and one Rb atom have not been determined experimentally.

While the experiments presented here were performed at constant rf pulse parameters, it should be possible from the above arguments to increase either pulse power or duration or both of the rf pulse to account for the reduced wave function overlap and thereby always obtain an efficiency of 1. In particular, it should be possible to drive Rabi oscillations between atoms and molecules in a very similar way as recently demonstrated [110].

The comparison indicates that in the case of association efficiency a better quantitative agreement might require a two-level Feshbach-resonance model like that of Sec. 5.4. [17] This is in contrast to the analysis of binding energies and lifetimes (see below), where the good quantitiative agreement shows that here the δ interaction approximation and the single-channel model of the Feshbach resonance capture the essential physics. Testing the Rabi oscillation hypothesis for molecules with rf might provide further insight.

[17] Using the superposition wave functions of Fig. 5.10 instead would possibly give better results. However, for that purpose I need to know the parameters $\Delta\epsilon(B)$ and V_c of the Hamiltonian matrix (5.44) as well as the scattering length of the molecular wave function.

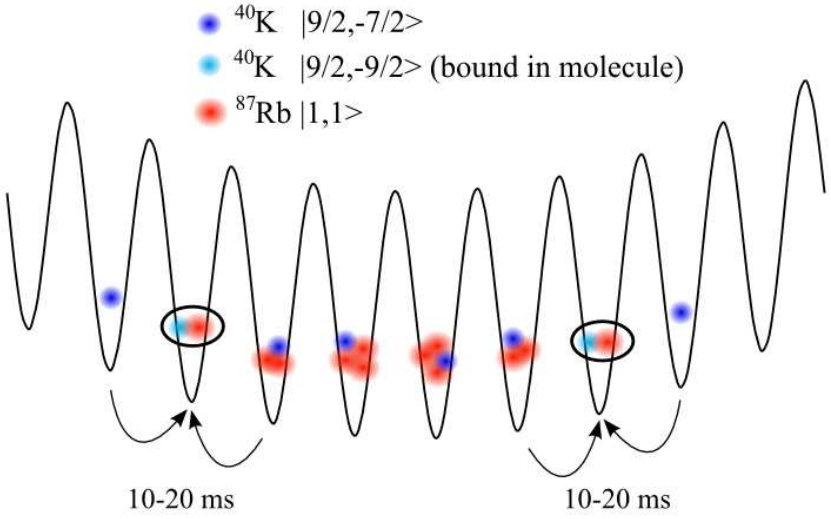

Figure 5.18: Sketch of expected lattice occupation. The arrows illustrate tunneling of remaining fermionic ^{40}K atoms to the "molecular" shell where they can undergo inelastic three-body collisions with a ^{40}K-^{87}Rb molecule.

5.9 Lifetime

Molecule formation at atomic Feshbach resonances results in dimers which are very weakly bound. These dimers can scatter inelastically with other molecules and atoms which limits their lifetimes. As far as collisions between molecules are concerned, the fermionic character of the molecule should become more evident the deeper the molecule is bound, thus resulting in suppression of collisions. As far as collisions with residual atoms are concerned, we expect that inelastic collisions with fermionic atoms in the same spin state as the fermionic component of the molecule, i. e. in the $|9/2, -9/2\rangle$ state, are suppressed due to the Pauli exclusion principle close to the resonance, when the atomic character of the molecule's constituents is still significant [111, 112]. For collisions with bosonic atoms and fermionic atoms in a different internal state, we do not expect any Pauli-blocking enhanced lifetime, since the residual atom can in principle come arbitrarily near to the molecule's constituents.

In our situation, where the molecules are created through rf association, residual fermionic atoms remain in a different spin state, either in $|9/2, -7/2\rangle$ or $|9/2, -5/2\rangle$ (for the latter case, and for a description of the experimental procedure, see Ref. [72]). These residual fermionic atoms as well as the remaining bosonic atoms may therefore limit the stability of the molecular sample.

Molecule creation in the optical lattice introduces a second aspect concerning the lifetime: lattice occupation and tunneling probabilities. In Fig. 5.18, we have sketched the expected occupation in the optical lattice. Prior to molecule creation, we expect slightly less than unity filling for the fermionic component. As far as the bosons are concerned, we expect a central occupation number between 3 and 5, surrounded by shells of decreasing occupation number. In the rf association process, molecules are only created in the shell where we have one fermion and one boson per lattice site. In the outermost region of the lattice, we have lattice sites with only one fermion which are responsible for the "atomic" peak in the rf spectroscopy signal. After the rf association process in the "molecular" shell, bosons from neighboring sites as well as fermions remaining in a different spin state can tunnel to the "molecular" shell and provoke inelastic three-body loss. In

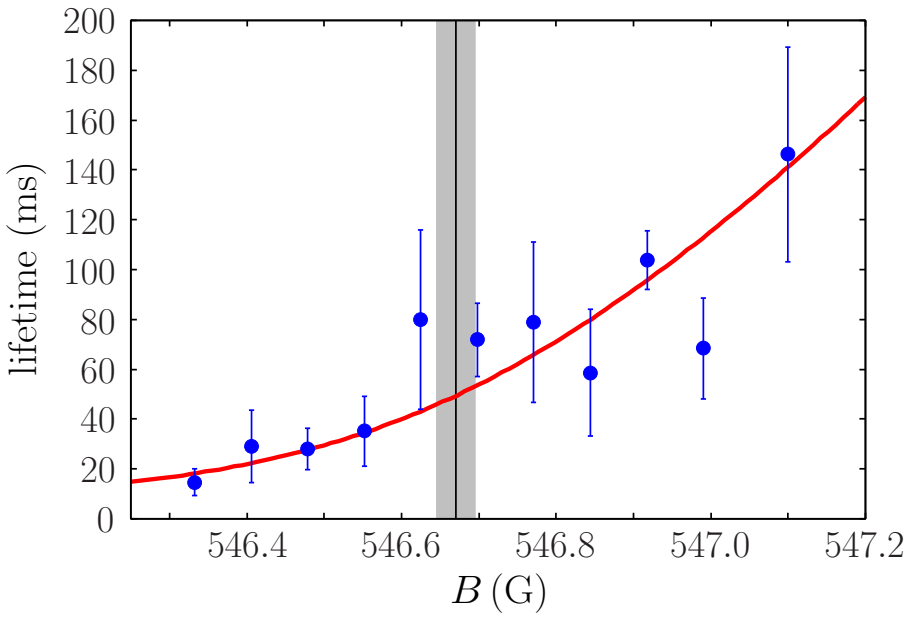

Figure 5.19: Lifetime of heteronuclear ^{40}K-^{87}Rb molecules in the optical lattice. The Lifetime is limited due to residual atoms which can tunnel to lattice sites with molecules and provoke inelastic three-body loss. The theoretical prediction uses the pseudopotential wave function and contains a global factor which was adjusted to the experimental data.

our experimental situation, this is more probable for the remaining fermionic atoms, since they are lighter and have a smaller tunneling time (10 to 20 ms for the lattice depths discussed here). For the highest binding energies observed in the experiment, we find a limiting lifetime of 10 to 20 ms as seen in Fig. 5.19, which is consistent with the assumption that in this case, three-body loss is highly probable once tunneling of a distinguishable residual fermion has occured. Still, for the more weakly bound molecules and in particular for attractively interacting atoms, we observe high lifetimes of 120 ms, raising the question of the magnetic field dependence of the lifetime.

We can understand this magnetic field dependence using the pseudopotential model by introducing a product wave function for the combined wave function of the resonantly interacting atom pair and a residual fermionic atom after tunneling to a molecular site. We write this three-body wave function as

$$\psi(\vec{r},\vec{R},\vec{r}_3) = \psi_{\text{mol.}}(\vec{r},\vec{R})\psi_3(\vec{r}_3) \tag{5.59}$$

where $\psi_{\text{mol.}}$ is the result of the pseudopotential calculation for the molecule and ψ_3 is the ground-state wave function of the residual atom at the same lattice site. Note that this treatment assumes weak interactions between the residual atom and the molecule (the interaction between the residual atom and the molecule's constituents is on the order of the background scattering length). From solution (5.59) of the pseudopotential model, the dependence of the loss rate on the scattering length can be obtained close to the resonance [111, 112]: the loss rate Γ is proportional to the probability $\mathcal{P}$ of finding the three atoms within a small sphere of radius σ, where they can undergo three-body recombination. This probability is expected to become larger for more deeply bound molecules, since two of the three atoms are already at a close distance. Up to a global factor, $\mathcal{P}$ is independent of the value chosen for σ, provided $\sigma \ll l_{\text{rel.}}$, and also $\sigma \ll a_s$ in the molecule

regime. More quantitatively, we calculate this probability according to

$$\mathcal{P} = \int_{\substack{|\vec{r}|<\sigma \\ |\vec{r}_3-\vec{R}|<\sigma}} d\vec{r}\, d\vec{R}\, d\vec{r}_3 \left|\psi_{\text{mol.}}(\vec{r},\vec{R})\right|^2 \left|\psi_3(\vec{r}_3)\right|^2. \tag{5.60}$$

The magnetic field dependence of the loss rate is given through $\Gamma \propto \mathcal{P}$, and the lifetime is proportional to $1/\Gamma$.

In the harmonic trap the molecular wave function separates into a relative and a center-of-mass wave function $\psi_{\text{mol.}}(\vec{r},\vec{R}) = \psi_{\text{c.m.}}(\vec{R})\psi_{\text{rel.}}(\vec{r})$ and Eq. (5.60) becomes

$$\mathcal{P} = \underbrace{\int_{|\vec{r}_3-\vec{R}|<\sigma} d\vec{R}\, d\vec{r}_3 \left|\psi_{\text{c.m.}}(\vec{R})\right|^2 \left|\psi_3(\vec{r}_3)\right|^2}_{=C} \int_{|\vec{r}|<\sigma} d\vec{r} \left|\psi_{\text{rel.}}(\vec{r})\right|^2 \tag{5.61}$$

where C is a constant which is independent of a_s. The second integral is proportional to

$$\begin{aligned}\int_{|\vec{r}|<\sigma} d\vec{r} \left|\psi_{\text{rel.}}(\vec{r})\right|^2 &\propto \int_0^\sigma dr\, \chi_{\text{rel.}}(r)^2 \overset{(5.34)}{=} A^2 \int_0^\sigma dr\, U^2\left(-\frac{E}{2}+\frac{1}{4};\frac{1}{2};r^2\right) e^{-r^2} \\ &\approx A^2\, \sigma\, U^2\left(-\frac{E}{2}+\frac{1}{4};\frac{1}{2};0\right) \quad \text{for } \sigma \approx 0\end{aligned} \tag{5.62}$$

where A is a normalization constant. In order to calculate A^2 we use the relation [18]

$$\int_0^\infty dz\, D_\nu^2(z) = \sqrt{\pi} 2^{-3/2} \frac{\Psi(1/2-\nu/2) - \Psi(-\nu/2)}{\Gamma(-\nu)}$$

where $\Psi(x) \equiv \Gamma'(x)/\Gamma(x)$ is the digamma function. From the normalization condition we obtain

$$\begin{aligned} 1 &= \int_0^\infty dr\, \chi_{\text{rel.}}(r)^2 \overset{(5.34)}{=} A^2\, 2^{-E+1/2} \int_0^\infty dr\, D_{E-1/2}\left(\sqrt{2}r\right)^2 \\ &= A^2\, 2^{-E+1/2}\, \sqrt{\pi}\, \frac{\Psi(3/4-E/2) - \Psi(1/4-E/2)}{4\,\Gamma(1/2-E)} \\ \Leftrightarrow\ A^2 &= 2^E 2^{3/2} \pi^{-1/2} \frac{\Gamma(1/2-E)}{\Psi(3/4-E/2) - \Psi(1/4-E/2)}. \end{aligned} \tag{5.63}$$

Now we calculate $U^2(-E/2+1/4;1/2;0)$. We obtain

$$\begin{aligned} U^2\left(-\frac{E}{2}+\frac{1}{4};\frac{1}{2};0\right) &\overset{(5.34)}{=} 2^{-E+1/2} D_{E-1/2}^2(0) \overset{(5.33)}{=} 2^{-E+1/2} U^2(-E;0) \\ &\overset{(5.38)}{=} \frac{1}{\pi} \cos^2\left(\frac{\pi}{4} - E\frac{\pi}{2}\right) \Gamma^2\left(\frac{1}{4}+\frac{E}{2}\right) \\ &\overset{(5.39)}{=} \cos^2\left(\frac{\pi}{4} - E\frac{\pi}{2}\right) \frac{\pi}{\sin^2\left(\frac{\pi}{4}+E\frac{\pi}{2}\right) \Gamma^2\left(\frac{3}{4}-\frac{E}{2}\right)} \\ &= \frac{\pi}{\Gamma^2(3/4-E/2)}. \end{aligned} \tag{5.64}$$

In the last step we have used $\sin(\pi/2+x) = \cos(x) = \cos(-x)$. It follows from Eqs. (5.61–5.64):

$$\mathcal{P} = C'\, 2^E\, \frac{\Gamma(1/2-E)}{\Gamma^2(3/4-E/2)}\, \frac{1}{\Psi(3/4-E/2) - \Psi(1/4-E/2)}$$

[18] Entry 7.711.3 of Ref. [101] / Wolfram *MathWorld*.

where C' is a constant. Since [19]

$$\Gamma(2z) = (2\pi)^{-1/2} 2^{2z-1/2} \Gamma(z)\Gamma(z+1/2)$$

we get

$$\Gamma(1/2 - E) = (2\pi)^{-1/2} 2^{-E} \Gamma(1/4 - E/2)\Gamma(3/4 - E/2)$$

so that we finally obtain

$$\begin{aligned} \mathcal{P} &= C'' \frac{\Gamma(1/4 - E/2)}{\Gamma(3/4 - E/2)} \frac{1}{\Psi(3/4 - E/2) - \Psi(1/4 - E/2)} \\ &\overset{(5.40)}{=} C''' \frac{a_s}{\Psi(3/4 - E/2) - \Psi(1/4 - E/2)}. \end{aligned} \tag{5.65}$$

Again, C'' and C''' are constants which are independent of a_s. [20] Eq. (5.65) holds for the harmonic approximation of one lattice site. However, we found no visible deviation from a numerical integration of Eq. (5.60) using the eigenfunctions of the complete Hamiltonian (5.55). This is in agreement with the fact that local properties are insensitive to the geometry of the trap.

The lifetime obtained from the calculation is shown in Fig. 5.19 as a red solid line, scaled by a global factor to allow comparison to the experiment. As can be seen, the theoretical prediction explains the magnetic field dependence of the lifetime rather well. From an experimental point of view, we can therefore expect that removal of the remaining atoms using a resonant light pulse will significantly increase the lifetime of the molecules in the optical lattice.

[19] Entry 6.1.18 of Ref. [100] / Wolfram *MathWorld*.

[20] Eq. (5.65) was derived by Félix Werner [113, 114].

Chapter 6

Conclusions and outlook

In the previous chapters I studied one-dimensional boson systems of ultracold atoms with special emphasis on the Tonks-Girardeau limit of strong interactions and ultracold heteronuclear Feshbach molecules.

In chapter 2 I explained in detail the exact-diagonalization approach for bosons with spin-dependent contact interactions since this approach was used throughout this thesis and since this method is relatively new in the field of ultracold atoms.

In chapter 3 I studied the interaction-driven evolution of a one-dimensional spin-polarized few boson system from a Bose-Einstein condensate to a Tonks-Girardeau gas. I analyzed the transition behavior of the particle density, the pair correlation function, the different contributions to the total energy, the momentum and the occupation number distribution as well as the low-energy excitation spectrum of these systems. I found an interesting behavior of the momentum distribution with increasing interaction strength. The high zero-momentum peak of the momentum distribution was traced back to the Bose symmetry of the many-particle wave function and the high-momentum tails were related to the short-range correlations between the particles.

In particular I found that the width of the momentum distribution first decreases, reaches a minimum value at $U = 0.5\,\hbar\omega$ and increases above this value with increasing repulsion between the bosons. The height of the zero-momentum peak by contrast first increases, reaches its maximum value at $U = 3\,\hbar\omega$ and decreases above this value with increasing interaction strength. The reason for that behavior is in both cases an interplay between two effects, namely the broadening and flattening of the overal wave function and the development of short-range correlations. I used the above mentioned features of the momentum distribution to discriminate between three interaction regimes, namely the BEC, an intermediate and the Tonks-Girardeau regime.

In chapter 4 I analyzed the ground-state properties of a Tonks-Girardeau gas with spin degrees of freedom. First we generalized Girardeau's Fermi-Bose map for spinless bosons to arbitrary particles (bosons of fermions) with arbitrary spin. A generalization to these important systems was surprisingly not given elsewhere before. Our solution is not only valid for bosons with integer spin or fermions with half-integer spin but also for isospin-$1/2$ bosons and thus it is also applicable to Bose-Bose mixtures which have been recently discussed in Ref. [69]. Furthermore our solution shows that one-dimensional bosons and fermions have the same energy spectra and spin densities in the regime of an infinitely strong δ repulsion between the particles.

We used the exact limiting wave functions to approximate the wave functions of spin-1 bosons with large *but finite* interactions and we discussed the energy structure of the ground-state multiplet. It would be desirable to extend this approximative scheme to arbitrary particle numbers in a future

project. Further, we found a closed formula for the spin densities of one-dimensional particles, which is valid for arbitrary particle numbers and (spin-independent) trapping potentials. These spin densities resemble a chain of localized spins.

Again, the momentum distribution of these systems showed an interesting behavior. I found that its form strongly depends on the spin configuration of the one-dimensional system. For example in some spin configurations the momentum distribution of a boson system exhibits clear fermionic features. Unfortunately I was only able to calculate these momentum distributions numerically for up to 5 spin-1 bosons. It would be desirable to develop other (numerical) methods which allow for the calculation of the momentum distribution of larger systems – similar to the approach of T. Papenbrock [89], who performed calculations of the momentum distribution for up to 160 spinless bosons.

I am sure that it will be possible in the future to precisely manipulate and prepare these quasi-one-dimensional systems with strong interactions since the first steps into this direction have recently been done [25]. Our approach might be a useful complementation to other theoretical approaches in order to develop a microscopic understanding of such systems. In a next step it would be interesting to study the dynamics of one-dimensional spin systems with strong interactions based on our approach.

In chapter 5 I studied the formation of heteronuclear molecules from two different atomic species in a deep three-dimensional optical lattice by means of rf association in the vicinity of a magnetic field Feshbach resonance. We developed an exact-diagonalization approach to account for the coupling of center-of-mass and relative motion of the two-atom wave function due to the anharmonic corrections of the lattice sites and the different masses of the two atoms. This method might also be useful for other mixtures of different atomic species.

In particular we determined the location of the magnetic field Feshbach resonance, we developed a model of the rf association process and we explained the magnetic field dependence of the lifetime of the molecules. We compared our results to the experiment of C. Ospelkaus *et al.* [72] which was an important key experiment towards the production of ultracold polar molecules in the internal vibrational ground state which has been achieved only recently [115, 116]. These polar molecules might soon enable the realization of quantum gases with long-range interactions.

Appendix A

Particle densities

In this appendix, I will derive Eq. (4.23) for the probability density $\rho^{(i)}(x)$ to find the ith particle of the system, restricted to the standard sector C_{id}, at point x

$$\rho^{(i)}(x) = \frac{d}{dx}\left[\sum_{k=0}^{N-i} \frac{(-1)^{N-i}(N-k-1)!}{(i-1)!(N-k-i)!\,k!}\,\frac{\partial^k}{\partial\lambda^k}\det\Big[B(x)-\lambda\mathbb{1}\Big]\Big|_{\lambda=0}\right]. \tag{A.1}$$

The derivation of this formula has been given to me by Klaus Fredenhagen [93]. The probability density of the ith particle $\rho^{(i)}(x)$ has been defined in Eq. (4.21) according to

$$\rho^{(i)}(x) = \int dx_1 \ldots dx_N\, \delta(x-x_i)\big|\langle x_1,\ldots,x_N|\text{id}\rangle\big|^2 .$$

Using the definition of the wave function $\langle x_1,\ldots,x_N|\text{id}\rangle$, Eq. (4.4), we obtain

$$\rho^{(i)}(x) = N!\int_{x_1<x_2<\ldots<x_N} dx_1\ldots dx_N\,\delta(x-x_i)\Big[\psi^{(0)}_{\text{fermion gr.}}(x_1,x_2,\ldots,x_N)\Big]^2 .$$

Note that the integration is restricted to the standard sector C_{id}. We carry out the integration over the δ function and obtain the expression

$$\begin{aligned}\rho^{(i)}(x) = N!\int_{x_1<\ldots<x_{i-1}<x<x_{i+1}<\ldots<x_N} & dx_1\ldots dx_{i-1}dx_{i+1}\ldots dx_N \\ &\times\Big[\psi^{(0)}_{\text{fermion gr.}}(x_1,\ldots,x_{i-1},x,x_{i+1},\ldots,x_N)\Big]^2 .\end{aligned}$$

Now we extend the region of integration to the domain $\{x_1,\ldots,x_{i-1}<x<x_{i+1},\ldots,x_N\}$: We use the fact that the square of the fermion ground state is totally symmetric and

$$\begin{aligned}&\{x_1,\ldots,x_{i-1}<x<x_{i+1},\ldots,x_N\} = \\ &\qquad\bigcup_{\pi,\pi'}\{x_{\pi(1)}<\ldots<x_{\pi(i-1)}<x<x_{\pi'(i+1)}<\ldots<x_{\pi'(N)}\},\end{aligned}$$

where π and π' run over all permutations on the sets $\{1,2,\ldots,i-1\}$ and $\{i+1,i+2,\ldots,N\}$, respectively. The number of different sets $\{x_{\pi(1)}<\ldots<x_{\pi(i-1)}<x<x_{\pi'(i+1)}<\ldots<x_{\pi'(N)}\}$ is $(i-1)!(N-i)!$ and all of these sets have the same size. Thus, we have to devide the integral by

the combinatorial factor $(i-1)!(N-i)!$, when we extend the region of integration to the domain $\{x_1,\ldots,x_{i-1}<x<x_{i+1},\ldots,x_N\}$:

$$\rho^{(i)}(x) = \frac{N!}{(i-1)!(N-i)!}\int_{-\infty}^{x}dx_1\ldots\int_{-\infty}^{x}dx_{i-1}\int_{x}^{\infty}dx_{i+1}\ldots\int_{x}^{\infty}dx_N \times\left[\psi^{(0)}_{\text{fermion gr.}}(x_1,\ldots,x_{i-1},x,x_{i+1},\ldots,x_N)\right]^2 .$$

The ground-state Slater determinant of noninteracting fermions is given by

$$\psi^{(0)}_{\text{fermion gr.}}(x_1,\ldots,x_N) = \frac{1}{\sqrt{N!}}\sum_{\pi\in S_N}\text{sign}(\pi)\prod_{i=1}^{N}\psi_{\pi(i)}(x_i) .$$

Here, I denoted the N energetically lowest states of the single-particle problem by $\psi_1,\psi_2,\ldots,\psi_N$. We obtain

$$\rho^{(i)}(x) = \frac{1}{(i-1)!(N-i)!}\int_{-\infty}^{x}dx_1\ldots\int_{-\infty}^{x}dx_{i-1}\int_{x}^{\infty}dx_{i+1}\ldots\int_{x}^{\infty}dx_N \times\sum_{\pi,\pi'}\text{sign}(\pi\circ\pi')\psi_{\pi(1)}(x_1)\psi_{\pi'(1)}(x_1)\ldots\psi_{\pi(i)}(x)\psi_{\pi'(i)}(x)\ldots\psi_{\pi(N)}(x_N)\psi_{\pi'(N)}(x_N) .$$

Now we introduce the integrals

$$\beta_{ij}(x) = \int_{-\infty}^{x}dx'\psi_i(x')\psi_j(x') = \delta_{ij} - \int_{x}^{\infty}dx'\psi_i(x')\psi_j(x')$$

and use the fact that $\beta'_{ij}(x) = \psi_i(x)\psi_j(x)$. We obtain

$$\rho^{(i)}(x) = \frac{1}{(i-1)!(N-i)!}\sum_{\pi,\pi'}\text{sign}(\pi\circ\pi')\left[\prod_{j=1}^{i-1}\beta_{\pi(j)\pi'(j)}(x)\right] \times\beta'_{\pi(i)\pi'(i)}(x)\left[\prod_{j=i+1}^{N}\left[\delta_{\pi(j)\pi'(j)}-\beta_{\pi(j)\pi'(j)}(x)\right]\right].$$

In the next step we change the order of the summation: We define the permutation $\pi''\equiv\pi'\circ\pi^{-1}$ ($\Rightarrow\ \pi'=\pi''\circ\pi$) and sum over π and π''

$$\rho^{(i)}(x) = \frac{1}{(i-1)!(N-i)!}\sum_{\pi,\pi''}\text{sign}(\pi'')\left[\prod_{j=1}^{i-1}\beta_{\pi(j)\pi''\circ\pi(j)}(x)\right] \times\beta'_{\pi(i)\pi''\circ\pi(i)}(x)\left[\prod_{j=i+1}^{N}\left[\delta_{\pi(j)\pi''\circ\pi(j)}-\beta_{\pi(j)\pi''\circ\pi(j)}(x)\right]\right].$$

Here we used $\text{sign}(\pi\circ\pi''\circ\pi)=\text{sign}(\pi'')$. Now we exploit the fact that the order of the factors within the first and the last product is irrelevant, by which means many terms of the sum over π are equal. In order to unite these terms we replace the sum over π by the sum over all decompositions of $\underline{N}\equiv\{1,\ldots,N\}$ into the three disjoint subsets $I=\{\pi(1),\ldots,\pi(i-1)\}$, $J=\{\pi(i)\}$ and $L=\{\pi(i+1),\ldots,\pi(N)\}$, i. e., we sum over $I+J+L=\underline{N}$. Since the order, in which the

elements within the sets I and L are listed, is irrelevant, we have to multiply with the combinatorial factor $(i-1)!(N-i)!$ and obtain

$$\rho^{(i)}(x) = \sum_{I+J+L=\underline{N}} \sum_{\pi''} \text{sign}(\pi'') \prod_{j\in I} \beta_{j\pi''(j)}(x) \prod_{j\in J} \beta'_{j\pi''(j)}(x) \prod_{j\in L} \Big[\delta_{j\pi''(j)} - \beta_{j\pi''(j)}(x)\Big] \,. \quad \text{(A.2)}$$

In the next step we want to multiply out the last product. To this end we sum over all decompositions of L into the two disjoint subsets $K = \{j \in L \text{ with } \pi''(j) = j\}$ and $M = L \setminus K$ $\big($i. e. K is an arbitrary subset of all those elements of L which are mapped onto themselves by $\pi''\big)$. The result is given by

$$\prod_{j\in L} \Big[\delta_{j\pi''(j)} - \beta_{j\pi''(j)}(x)\Big] = (-1)^{|L|} \sum_{M+K=L} (-1)^{|K|} \prod_{j\in M} \beta_{j\pi''(j)}(x) \,. \quad \text{(A.3)}$$

I discuss two examples to become more familiar with that equation. *First example*— $L = \{2,4\}$ and $\pi''(2) = 2$, $\pi''(4) = 4$. The left-hand side of Eq. (A.3) becomes

$$\prod_{j\in\{2,4\}} \Big[\delta_{j\pi''(j)} - \beta_{j\pi''(j)}(x)\Big] = \Big[\delta_{22} - \beta_{22}(x)\Big]\Big[\delta_{44} - \beta_{44}(x)\Big] = 1 - \beta_{22}(x) - \beta_{44}(x) + \beta_{22}(x)\beta_{44}(x) \,.$$

There are 4 possible decompositions of L $\big($in all the 4 cases $|L| = 2\big)$:

$$\begin{aligned}
&K = L,\ M = \emptyset,\ |K| = 2 \ \Rightarrow\ \text{1st summand} = (-1)^2(-1)^2\, 1 = 1 \\
&K = \{4\},\ M = \{2\},\ |K| = 1 \ \Rightarrow\ \text{2nd summand} = (-1)^2(-1)^1\beta_{22}(x) = -\beta_{22}(x) \\
&K = \{2\},\ M = \{4\},\ |K| = 1 \ \Rightarrow\ \text{3rd summand} = (-1)^2(-1)^1\beta_{44}(x) = -\beta_{44}(x) \\
&K = \emptyset,\ M = L,\ |K| = 0 \ \Rightarrow\ \text{4th summand} = (-1)^2(-1)^0\beta_{22}(x)\beta_{44}(x) = \beta_{22}(x)\beta_{44}(x) \,.
\end{aligned}$$

Second example— $L = \{2,4\}$ and $\pi''(2) = 2$, $\pi''(4) = 5$. The left-hand side of Eq. (A.3) becomes

$$\prod_{j\in\{2,4\}} \Big[\delta_{j\pi''(j)} - \beta_{j\pi''(j)}(x)\Big] = \Big[\delta_{22} - \beta_{22}(x)\Big]\Big[\delta_{45} - \beta_{45}(x)\Big] = -\beta_{45}(x) + \beta_{22}(x)\beta_{45}(x) \,.$$

There are 2 possible decompositions of L $\big($in all the 2 cases $|L| = 2\big)$:

$$\begin{aligned}
&K = \{2\},\ M = \{4\},\ |K| = 1 \ \Rightarrow\ \text{1st summand} = (-1)^2(-1)^1\beta_{45}(x) = -\beta_{45}(x) \\
&K = \emptyset,\ M = L,\ |K| = 0 \ \Rightarrow\ \text{2nd summand} = (-1)^2(-1)^0\beta_{22}(x)\beta_{45}(x) = \beta_{22}(x)\beta_{45}(x) \,.
\end{aligned}$$

Thus, Eq. (A.3) seems to work properly. Upon combining Eqs. (A.2) and (A.3) and by noting that $|L| = N - i$ we obtain

$$\rho^{(i)}(x) = (-1)^{N-i} \sum_{I+J+M+K=\underline{N}} (-1)^{|K|} \sum_{\pi''} \text{sign}(\pi'') \prod_{j\in I} \beta_{j\pi''(j)}(x) \prod_{j\in J} \beta'_{j\pi''(j)}(x) \prod_{j\in M} \beta_{j\pi''(j)}(x) \,. \quad \text{(A.4)}$$

Now we unite the sets I and M into the set $I + M = P$ and we sum over all decompositions of $\underline{N}$ into the three disjoint subsets P, J and K, i. e., we sum over $P + J + K = \underline{N}$. Different pairs of sets (I_1, M_1) and (I_2, M_2) can lead to the same set P. *Example*— $P = \{1,2,3,4,5\} = \{1,2,3\} + \{4,5\} = \{1,2,4\} + \{3,5\}$. The number of different decompositions of P into two

disjoint subsets I and M is given by the combinatorial factor $|P|!/(|I|!|M|!)$. By using $|I| = i-1$, $|M| = |L| - |K| = N - i - |K|$ and $|P| = |I| + |M| = N - |K| - 1$ we obtain

$$\rho^{(i)}(x) = \sum_{P+J+K=\underline{N}} \frac{(-1)^{N-i}(N-|K|-1)!}{(i-1)!(N-|K|-i)!}\,(-1)^{|K|} \sum_{\pi\in S_{\underline{N}\setminus K}} \mathrm{sign}(\pi) \prod_{j\in P} \beta_{j\pi(j)}(x) \prod_{j\in J} \beta'_{j\pi(j)}(x)\,. \tag{A.5}$$

Note that we also replaced the inner sum over $\pi'' \in S_N$ in Eq. (A.4) by a sum over $\pi \in S_{\underline{N}\setminus K}$ in Eq. (A.5) and thus $\mathrm{sign}(\pi'')$ and $\mathrm{sign}(\pi)$ might differ from each other. But they are equal, since we have excluded only those elements of $\underline{N}$ which are mapped onto themselves. *Example*— $\underline{N} = \{1,2,3,4,5\}$ and $\big(\pi''(1),\pi''(2),\pi''(3),\pi''(4),\pi''(5)\big) = \big(3,2,5,4,1\big)$. K might be given by $K = \emptyset$ $\big[\pi = \pi''\big]$, $K = \{2\}$ $\big[\big(\pi(1),\pi(3),\pi(4),\pi(5)\big) = \big(3,5,4,1\big)\big]$, $\{K = 4\}$ $\big[\big(\pi(1),\pi(2),\pi(3),\pi(5)\big) = \big(3,2,5,1\big)\big]$ or $K = \{2,4\}$ $\big[\big(\pi(1),\pi(3),\pi(5)\big) = \big(3,5,1\big)\big]$. But in all the four cases we obtain $\mathrm{sign}(\pi) = \mathrm{sign}(\pi'')$. Next, we perform the sum over all decompositions of $R = P + J$ with one-element sets J. Using Leibniz' rule

$$\sum_{P+J=R} \prod_{j\in P} \beta_{j\pi(j)}(x) \prod_{j\in J} \beta'_{j\pi(j)}(x) = \frac{d}{dx}\left[\prod_{j\in R} \beta_{j\pi(j)}(x)\right]$$

we obtain from Eq. (A.5)

$$\rho^{(i)}(x) = \frac{d}{dx}\left[\sum_{R+K=\underline{N}} \frac{(-1)^{N-i}(N-|K|-1)!}{(i-1)!(N-|K|-i)!}\,(-1)^{|K|} \sum_{\pi\in S_R} \mathrm{sign}(\pi) \prod_{j\in R} \beta_{j\pi(j)}(x)\right].$$

Now we successively sum up all the decompositions of $R + K = \underline{N}$ with $|K| = 0, 1, \ldots,$ $|L| = N - i$ $\big(K$ is a subset of $L\big)$

$$\rho^{(i)}(x) = \frac{d}{dx}\left[\sum_{k=0}^{N-i} \frac{(-1)^{N-i}(N-k-1)!}{(i-1)!(N-k-i)!}\,(-1)^{k} \sum_{R+K=\underline{N},|K|=k} \sum_{\pi\in S_R} \mathrm{sign}(\pi) \prod_{j\in R} \beta_{j\pi(j)}(x)\right]. \tag{A.6}$$

From a comparison of Eq. (A.6) with Eq. (A.1) we see that it remains to show that

$$k!\,(-1)^k \sum_{R+K=\underline{N},|K|=k} \sum_{\pi\in S_R} \mathrm{sign}(\pi) \prod_{j\in R} \beta_{j\pi(j)}(x) = \frac{\partial^k}{\partial\lambda^k} \det\Big[B(x) - \lambda\mathbb{1}\Big]\Big|_{\lambda=0}\,. \tag{A.7}$$

The determinant of the $N \times N$ matrix $\big[B(x) - \lambda\mathbb{1}\big]$ with elements $\big[\beta_{ij}(x) - \lambda\delta_{ij}\big]$ is given by

$$\det\big[B(x) - \lambda\mathbb{1}\big] = \sum_{\pi\in S_N} \mathrm{sign}(\pi) \prod_{j\in\underline{N}} \Big[\beta_{j\pi(j)}(x) - \lambda\delta_{j\pi(j)}\Big]\,. \tag{A.8}$$

We can apply formula (A.3) to the product

$$\begin{aligned}
&\prod_{j\in\underline{N}} \Big[\beta_{j\pi(j)}(x) - \lambda\delta_{j\pi(j)}\Big] = (-\lambda)^N \prod_{j\in\underline{N}} \Big[\delta_{j\pi(j)} - \beta_{j\pi(j)}(x)/\lambda\Big] \\
&= (-\lambda)^N (-1)^N \sum_{R+K=\underline{N}} (-1)^{|K|} \prod_{j\in R} \beta_{j\pi(j)}(x)/\lambda \\
&= \sum_{R+K=\underline{N}} (-\lambda)^{|K|} \prod_{j\in R} \beta_{j\pi(j)}(x)\,.
\end{aligned} \tag{A.9}$$

Here, $K = \{j \in \underline{N} \text{ with } \pi(j) = j\}$, $R = \underline{N} \setminus K$ and we used $\lambda^N/\lambda^{|R|} = \lambda^N/\lambda^{N-|K|} = \lambda^{|K|}$. After inserting the result of Eq. (A.9) into Eq. (A.8) we obtain

$$\begin{aligned}\det\big[B(x) - \lambda\mathbb{1}\big] &= \sum_{\pi\in S_N} \operatorname{sign}(\pi) \sum_{R+K=\underline{N}} (-\lambda)^{|K|} \prod_{j\in R} \beta_{j\pi(j)}(x) \\ &= \sum_{R+K=\underline{N}} (-\lambda)^{|K|} \sum_{\pi\in S_R} \operatorname{sign}(\pi) \prod_{j\in R} \beta_{j\pi(j)}(x)\,.\end{aligned}$$

The kth partial derivative of this expression with respect to λ gives the result

$$\begin{aligned}\frac{\partial^k}{\partial\lambda^k}\det\Big[B(x) - \lambda\mathbb{1}\Big] = \sum_{R+K=\underline{N},|K|\geqslant k} &(-1)^k |K|\ldots(|K|-k+1)(-\lambda)^{|K|-k} \\ &\times \sum_{\pi\in S_R} \operatorname{sign}(\pi) \prod_{j\in R} \beta_{j\pi(j)}(x)\,.\end{aligned}$$

At $\lambda = 0$ only the summands with $|K| = k$ are nonzero and we obtain Eq. (A.7). *Test 1*— As a test we check, whether the sum of the particle densities equals the density of noninteracting fermions $\sum_i \rho^{(i)}(x) = \rho_{\text{fermion gr.}}(x)$. We calculate

$$\sum_{i=1}^N \rho^{(i)}(x) = \frac{d}{dx}\left[\sum_{i=1}^N \sum_{k=0}^{N-i} \frac{(-1)^{N-i}(N-k-1)!}{(i-1)!(N-k-i)!\,k!} \frac{\partial^k}{\partial\lambda^k}\det\Big[B(x) - \lambda\mathbb{1}\Big]\Big|_{\lambda=0}\right].$$

We change the order of the summation $\sum_{i=1}^N \sum_{k=0}^{N-i} \to \sum_{k=0}^{N-1} \sum_{i=1}^{N-k}$ and compute the inner sum

$$\begin{aligned}\sum_{i=1}^N \rho^{(i)}(x) &= \frac{d}{dx}\left[\sum_{k=0}^{N-1} \frac{1}{k!} \frac{\partial^k}{\partial\lambda^k}\det\Big[B(x) - \lambda\mathbb{1}\Big]\Big|_{\lambda=0} \underbrace{\sum_{i=1}^{N-k} \frac{(-1)^{N-i}(N-k-1)!}{(i-1)!(N-k-i)!}}_{(-1)^{N-1}\delta_{k,N-1}}\right] \\ &= \frac{d}{dx}\left[\frac{(-1)^{N-1}}{(N-1)!} \frac{\partial^{N-1}}{\partial\lambda^{N-1}}\det\Big[B(x) - \lambda\mathbb{1}\Big]\Big|_{\lambda=0}\right].\end{aligned}$$

Now we use Eq. (A.7) for $k = N-1$ in order to perform the $(N-1)$th partial derivative. In that case

$$\begin{aligned}\frac{\partial^{N-1}}{\partial\lambda^{N-1}}\det\Big[B(x) - \lambda\mathbb{1}\Big]\Big|_{\lambda=0} &= (N-1)!\,(-1)^{N-1} \sum_{R+K=\underline{N},|K|=N-1} \sum_{\pi\in S_R} \operatorname{sign}(\pi) \prod_{j\in R} \beta_{j\pi(j)}(x) \\ &= (N-1)!\,(-1)^{N-1} \sum_{j=1}^N \beta_{jj}(x)\,.\end{aligned}$$

We finally obtain

$$\sum_{i=1}^N \rho^{(i)}(x) = \frac{d}{dx}\left[\sum_{i=j}^N \beta_{jj}(x)\right] = \sum_{j=1}^N \psi_j^2(x)\,,$$

which is the ground-state density of N noninteracting fermions. *Test 2*— As a second test we check the normalization of $\rho^{(i)}(x)$, which is given by $\int_{-\infty}^{\infty} dx \rho^{(i)}(x) = 1$. We calculate

$$\begin{aligned}\int_{-\infty}^{\infty} dx \frac{\partial}{\partial x}\det\Big[B(x) - \lambda\mathbb{1}\Big] &= \det\Big[\underbrace{B(x=\infty)}_{=\mathbb{1}} - \lambda\mathbb{1}\Big] - \det\Big[\underbrace{B(x=-\infty)}_{=0} - \lambda\mathbb{1}\Big] \\ &= (1-\lambda)^N - (-\lambda)^N\end{aligned}$$

and

$$\frac{\partial^k}{\partial\lambda^k}\Big[(1-\lambda)^N-(-\lambda)^N\Big]_{\lambda=0} = \left[(-1)^k\frac{N!}{(N-k)!}(1-\lambda)^{N-k}-(-1)^k\frac{N!}{(N-k)!}(-\lambda)^{N-k}\right]_{\lambda=0}$$
$$= (-1)^k\frac{N!}{(N-k)!}\,. \qquad \big(\text{since } k\in\{0,\ldots,N-1\}\big)$$

Thus, we obtain from Eq. (A.1)

$$\sum_{i=1}^{N}\rho^{(i)}(x) = \sum_{k=0}^{N-i}\frac{(-1)^{N-i-k}(N-k-1)!N!}{(i-1)!(N-k-i)!k!(N-k)!} = 1\,.$$

The last step can be checked easily with MATHEMATICA.

Appendix B

Weber's differential equation

We want to construct two linearly independent solutions of the differential equation

$$\chi'' - r^2\chi + 2\big[E - V_{\text{box}}\big]\chi = 0.$$

Firstly, I would like to note that the $l = 0$ eigenfunctions of the three-dimensional isotropic harmonic oscillator are solutions of this equation [1]. That is not that surprising since the energy of the particle is only shifted by a constant offset $\big[V_{\text{box}} = V$ if $r \leqslant R$, $V_{\text{box}} = 0$ if $r > R\big]$ compared to the harmonic oscillator problem. The important differences are the two additional boundary conditions at $r = R$. Since we expect that the solutions of the above equation show the same long-range behavior as the eigenfunctions of the harmonic oscillator we perform the transformation

$$\chi(r) =: \phi(r)e^{-r^2/2}$$

and arrive at the differential equation

$$\phi'' - 2r\phi' + \big[2(E - V_{\text{box}}) - 1\big]\phi = 0. \tag{B.1}$$

We introduce the abbreviation

$$a \equiv 2(E - V_{\text{box}}) - 1 \tag{B.2}$$

and assume that the solutions of Eq. (B.1) are given by a power series

$$\phi(r) \equiv \sum_{n=0}^{\infty} c_n r^{s+n}. \tag{B.3}$$

(This ansatz implies $c_0 \neq 0$. Otherwise s has to be changed accordingly.) We insert the power series (B.3) into the differential equation (B.1), multiply Eq. (B.1) with r^2 and obtain

$$\begin{aligned} 0 &= \sum_{n=0}^{\infty}\Big\{c_n(s+n-1)(s+n)r^{s+n} + c_n\big[a - 2(s+n)\big]r^{s+n+2}\Big\} \\ &= (s-1)sc_0r^s + s(s+1)c_1r^{s+1} + \big[c_2(s+1)(s+2) + c_0(a-2s)\big]r^{s+2} + \dots \\ &\quad + \Big\{c_n(s+n-1)(s+n) + c_{n-2}\big[a - 2(s+n-2)\big]\Big\}r^{s+n} + \dots . \end{aligned} \tag{B.4}$$

[1] The construction of the eigenfunctions of the three-dimensional isotropic harmonic oscillator by means of a polynomial ansatz is, e. g., given in Vol. 2 of Ref. [78].

If (B.3) is a solution of (B.1) then all the coefficients of (B.4) have to be zero. From the first term we obtain

$$s(s-1)c_0 = 0 \quad \Rightarrow \quad s = 0 \text{ or } s = 1 \quad (\text{since } c_0 \neq 0).$$

First case— Let us first choose $s = 1$. From the next term of (B.4) we obtain

$$2c_1 = 0 \quad \Rightarrow \quad c_1 = 0.$$

From the following terms we obtain the recurrence relation

$$c_n(s+n-1)(s+n) + c_{n-2}\big[a - 2(s+n-2)\big] = 0 \quad \Rightarrow \quad c_n = \frac{2(s+n-2)-a}{(s+n-1)(s+n)}c_{n-2}.$$

From $c_1 = 0$ and the recurrence formula it follows that all the odd-numbered coefficients are zero. Therefore, the power series (B.3) is given by

$$\phi(r) = r(c_0 + c_2 r^2 + c_4 r^4 + \ldots) \quad \text{with} \quad c_n = \frac{2(n-1)-a}{n(n+1)}c_{n-2}. \tag{B.5}$$

We want to express Eq. (B.5) by means of the confluent hypergeometric function of the first kind

$${}_1F_1(a';b';z) = 1 + \frac{a'}{b'}z + \frac{a'(a'+1)}{b'(b'+1)}\frac{z^2}{2} + \ldots + \frac{a'\ldots(a'+n-1)}{b'\ldots(b'+n-1)}\frac{z^n}{n!} + \ldots . \tag{B.6}$$

We try the following ansatz

$$\phi(r) = r\,{}_1F_1(a';b';r^2). \tag{B.7}$$

In order to bring Eq. (B.7) into agreement with Eq. (B.5) we set $c_0 \equiv 1$. Then, $c_2 = (2-a)/3!$ and $c_4 = (2-a)(6-a)/5!$. Since $(2-a)(6-a) = 4^2\,(1/2 - a/4)\,(3/2 - a/4)$ and $5! = 2\cdot 3\cdot 4\cdot 5 = 2^3\cdot 3\cdot 5 = 2^5\cdot 3/2\cdot 5/2$ the coefficient c_4 may also be written as

$$c_4 = \frac{(1/2 - a/4)\,(1/2 - a/4 + 1)}{2\cdot 3/2\cdot(3/2+1)}.$$

By comparing c_4 with the third coefficient of (B.6) we obtain $a' = 1/2 - a/4$ and $b' = 3/2$. Using (B.2) we obtain the first solution of (B.1)

$$\phi_1(r) = r\,{}_1F_1\left[-\frac{1}{2}(E - V_{\text{box}}) + \frac{3}{4}; \frac{3}{2}; r^2\right].$$

Second case— We now choose $s = 0$. Therefore, the second coefficient of (B.4) is already zero and we can choose an arbitrary value for c_1. But since $(c_1 r + c_3 r^3 + c_5 r^5 + \ldots)$ is proportional to (B.5) we can choose $c_1 = 0$. Again all the odd-numbered coefficients become zero and (B.3) is given by

$$\phi(r) = c_0 + c_2 r^2 + c_4 r^4 + \ldots \quad \text{with} \quad c_n = \frac{2(n-2)-a}{(n-1)n}c_{n-2}.$$

We try the ansatz

$$\phi(r) = {}_1F_1(a'';b'';r^2).$$

We choose $c_0 = 1$. Then, $c_2 = -a/2$ and $c_4 = (-a)(4-a)/4!$. Since $(-a)(4-a) = 4^2(-a/4)(1-a/4)$ and $4! = 2\cdot 3\cdot 4 = 2^3\cdot 3 = 2^5\cdot 3/4 = 2^5\cdot 1/2\cdot(1/2+1)$ the coefficient c_4 may also be written as

$$c_4 = \frac{(-a/4)(-a/4+1)}{2\cdot 1/2\cdot(1/2+1)}.$$

Thus, $a'' = -a/4$ and $b'' = 1/2$ so that the second solution of (B.1) becomes

$$\phi_2(r) = {}_1F_1\left[-\frac{1}{2}(E - V_{\text{box}}) + \frac{1}{4}; \frac{1}{2}; r^2\right].$$

Appendix C

Rabi model

Hamiltonian matrix and Schrödinger equation: We consider a spin-1/2 in a static magnetic and radio-frequency (rf) field (see Fig. C.1)

$$\vec{B}(t) = B_0\vec{e}_z + B_{\text{rf}}\Big(e^{\mathbb{i}\omega t} + e^{-\mathbb{i}\omega t}\Big)\vec{e}_x\,.$$

The magnetic field $\vec{B}(t)$ couples to the spin $\vec{S}$. The model Hamiltonian reads

$$\begin{aligned} H(t) &= -\vec{M}\cdot\vec{B}(t) = -\Big(g\mu_B\vec{S}/\hbar\Big)\cdot\vec{B}(t) = -\frac{1}{2}g\mu_B\vec{\sigma}\cdot\vec{B}(t) \\ &= -\frac{1}{2}g\mu_B\Big[B_0\sigma_z + B_{\text{rf}}\Big(e^{\mathbb{i}\omega t} + e^{-\mathbb{i}\omega t}\Big)\sigma_x\Big]. \end{aligned}$$

Here, $\vec{M} = g\mu_B\vec{S}/\hbar$ is the magnetic moment of the spin $\vec{S}$, g is the g-factor, μ_B is Bohr's magneton, $\vec{S} = (\hbar/2)\vec{\sigma}$ and $\vec{\sigma} = (\sigma_x, \sigma_y, \sigma_y)$ are the Pauli matrices

$$\sigma_x = \begin{pmatrix} 0 & 1 \\ 1 & 0 \end{pmatrix}, \qquad \sigma_y = \begin{pmatrix} 0 & -\mathbb{i} \\ \mathbb{i} & 0 \end{pmatrix}, \qquad \sigma_z = \begin{pmatrix} 1 & 0 \\ 0 & -1 \end{pmatrix}.$$

We define the frequencies $\hbar\omega_0 \equiv g\mu_B B_0$ and $\hbar\omega_{\text{rf}} \equiv g\mu_B B_{\text{rf}}$. The Hamiltonian becomes

$$H(t) = \frac{\hbar}{2}\begin{pmatrix} -\omega_0 & -\omega_{\text{rf}}\left(e^{\mathbb{i}\omega t} + e^{-\mathbb{i}\omega t}\right) \\ -\omega_{\text{rf}}\left(e^{\mathbb{i}\omega t} + e^{-\mathbb{i}\omega t}\right) & \omega_0 \end{pmatrix}.$$

The time-dependent Schrödinger equation is given by

$$\mathbb{i}\hbar\frac{d}{dt}\big|\psi(t)\big\rangle = H(t)\big|\psi(t)\big\rangle$$

where $\big|\psi(t)\big\rangle = \big(\alpha(t), \beta(t)\big)$ is the wave function that describes the time evolution of the spin-1/2.

Transformation into the rotating frame: It turns out further below that an accurate analytical (approximate) solution of the above Hamiltonian is possible if we switch into the framework that rotates with ω around the z-axis. We perform the transformation

$$\big|\widetilde{\psi}(t)\big\rangle = e^{-\mathbb{i}\omega t\sigma_z/2}\big|\psi(t)\big\rangle \quad \Leftrightarrow \quad \big|\psi(t)\big\rangle = e^{\mathbb{i}\omega t\sigma_z/2}\big|\widetilde{\psi}(t)\big\rangle$$

with the rotation matrix

$$e^{\mathbb{i}\omega t\sigma_z/2} = \begin{pmatrix} e^{\mathbb{i}\omega t/2} & 0 \\ 0 & e^{-\mathbb{i}\omega t/2} \end{pmatrix}$$

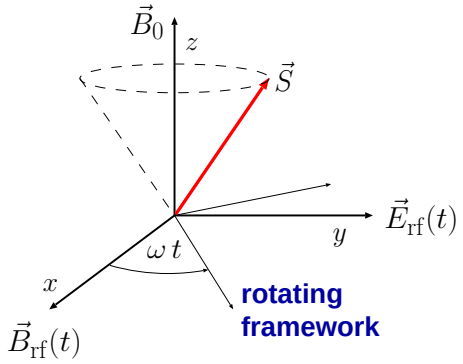

Figure C.1: A spin in a static magnetic and radio-frequency (rf) field. The electric field does not couple to the spin.

so that the transformation is given by $\big(\alpha(t),\beta(t)\big) = \big(e^{\mathrm{i}\omega t/2}\widetilde{\alpha}(t), e^{-\mathrm{i}\omega t/2}\widetilde{\beta}(t)\big)$. Using

$$\mathrm{i}\hbar\frac{d}{dt}\big|\psi(t)\big\rangle = -\frac{\hbar}{2}\omega\sigma_z e^{\mathrm{i}\omega t\sigma_z/2}\big|\widetilde{\psi}(t)\big\rangle + \mathrm{i}\hbar\frac{d}{dt}\big|\widetilde{\psi}(t)\big\rangle$$

the transformed Schrödinger equation reads

$$\mathrm{i}\hbar\begin{pmatrix} e^{\mathrm{i}\omega t/2}\widetilde{\alpha}' \\ e^{-\mathrm{i}\omega t/2}\widetilde{\beta}' \end{pmatrix} = \frac{\hbar}{2}\begin{pmatrix} +(\omega-\omega_0)\,e^{\mathrm{i}\omega t/2} & -\omega_{\rm rf}\left(e^{\mathrm{i}\omega t/2}+e^{-\mathrm{i}3\omega t/2}\right) \\ -\omega_{\rm rf}\left(e^{\mathrm{i}3\omega t/2}+e^{-\mathrm{i}\omega t/2}\right) & -(\omega-\omega_0)\,e^{-\mathrm{i}\omega t/2} \end{pmatrix}\begin{pmatrix}\widetilde{\alpha}\\ \widetilde{\beta}\end{pmatrix}.$$

We multiply the upper equation with $e^{-\mathrm{i}\omega t/2}$ and the lower equation with $e^{+\mathrm{i}\omega t/2}$ and obtain

$$\mathrm{i}\hbar\frac{d}{dt}\begin{pmatrix}\widetilde{\alpha}\\ \widetilde{\beta}\end{pmatrix} = \frac{\hbar}{2}\begin{pmatrix} +\Delta\omega & -\omega_{\rm rf}\left(1+e^{-\mathrm{i}2\omega t}\right) \\ -\omega_{\rm rf}\left(1+e^{\mathrm{i}2\omega t}\right) & -\Delta\omega \end{pmatrix}\begin{pmatrix}\widetilde{\alpha}\\ \widetilde{\beta}\end{pmatrix} \tag{C.1}$$

where we have defined the frequency $\Delta\omega \equiv \omega - \omega_0$.

Rotating wave approximation: We neglect the $-\left(\hbar\omega_{\rm rf}/2\right)e^{\mp\mathrm{i}2\omega t}$ terms of Eq. (C.1) and obtain

$$\mathrm{i}\hbar\frac{d}{dt}\begin{pmatrix}\widetilde{\alpha}\\ \widetilde{\beta}\end{pmatrix} = \frac{\hbar}{2}\begin{pmatrix} +\Delta\omega & -\omega_{\rm rf} \\ -\omega_{\rm rf} & -\Delta\omega \end{pmatrix}\begin{pmatrix}\widetilde{\alpha}\\ \widetilde{\beta}\end{pmatrix}. \tag{C.2}$$

The resulting Hamiltonian matrix is completely time-independent. Thus we can easily solve Eq. (C.2) by diagonalizing H. The approximation is good as long as $|\omega_{\rm rf}/\omega| \ll 1$; see Fig. C.2.

Diagonalization of the time-independent Hamiltonian: We consider the Hamiltonian matrix

$$H = \frac{\hbar}{2}\Delta\omega\begin{pmatrix} 1 & -\omega_{\rm rf}/\Delta\omega \\ -\omega_{\rm rf}^*/\Delta\omega & -1 \end{pmatrix}$$

[according to the above definition $\omega_{\rm rf} = g\mu_B B_{\rm rf}/\hbar$ is real but here I would like to discuss the more general case of a Hermitian 2×2 matrix where $\omega_{\rm rf}$ is complex (and where $\Delta\omega$ is real)]. For convenience, we introduce the angles

$$\tan\theta \equiv -\frac{|\omega_{\rm rf}|}{\Delta\omega} \quad (0\leqslant\theta<\pi) \quad \text{and} \quad \phi \equiv \arg(\omega_{\rm rf}) \quad (0\leqslant\phi<2\pi)$$

to simplify the further calculations. Using this new set of parameters the Hamiltonian reads

$$H = \frac{\hbar}{2}\Delta\omega\begin{pmatrix} 1 & \tan\theta\, e^{\mathrm{i}\phi} \\ \tan\theta\, e^{-\mathrm{i}\phi} & -1 \end{pmatrix}.$$

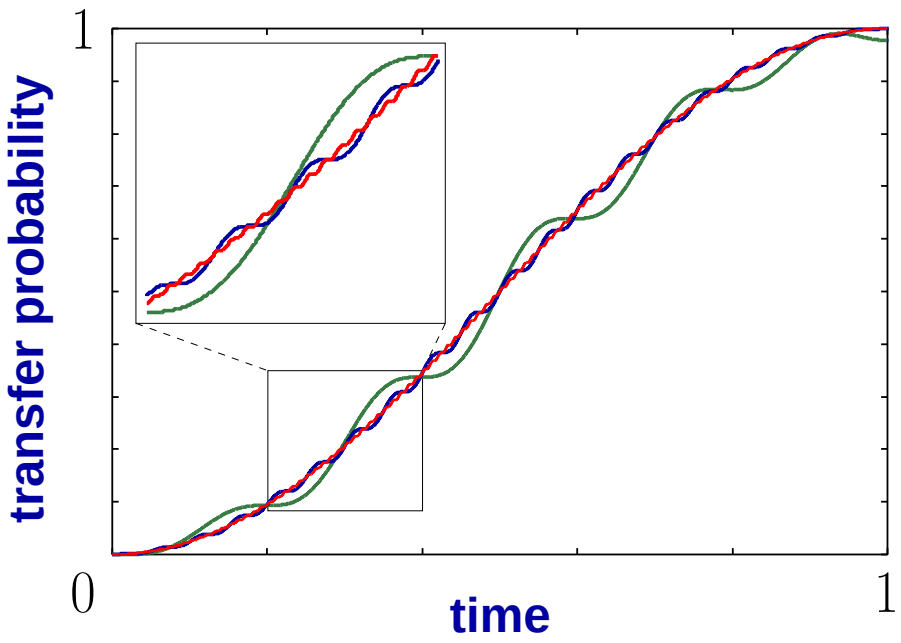

Figure C.2: *Validity of the rotating wave approximation*— Shown is the probability of a spin flip as a function of time for zero detuning ($\Delta\omega = 0$). The transfer probability was obtained from a numerical solution of Eq. (C.1) for $\omega_{\rm rf}/\omega = 1/5$ (green), $\omega_{\rm rf}/\omega = 1/20$ (blue) and $\omega_{\rm rf}/\omega = 1/100$ (red). In the rotating wave approximation (for the chosen rf amplitude $\omega_{\rm rf} = \pi$ Hz) the transfer probability is given by $P_-(t) = \sin^2(\pi t/2)$ [see Eq. (C.5)]. The numerical solutions show fast oscillations around the $\sin^2(\pi t/2)$ curve. The smaller the ratio $\omega_{\rm rf}/\omega$ the smaller the amplitude and the larger the frequency of the oscillations around this curve [see Eq. (C.8)]. As can be seen, the deviation between the red and the $\sin^2(\pi t/2)$ curve is negligibly small.

The eigenenergies are determined by the equation

$$\begin{aligned} 0 = \det(H - \mathbb{1}E) &= \left(\frac{\hbar}{2}\Delta\omega - E\right)\left(-\frac{\hbar}{2}\Delta\omega - E\right) - \frac{\hbar^2}{4}\Delta\omega^2\tan^2\theta \\ &= E^2 - \frac{\hbar^2}{4}\Delta\omega^2\left(1 + \tan^2\theta\right) = E^2 - \left(\frac{\hbar}{2}\Delta\omega\frac{1}{\cos\theta}\right)^2 \\ \Rightarrow\ E_\pm &= \pm\frac{\hbar}{2}\Delta\omega\frac{1}{\cos\theta}\,. \end{aligned}$$

The eigenvector $|\widetilde{\psi}_+\rangle$ is determined by the equation

$$\begin{aligned} &\begin{pmatrix} 1 & \tan\theta\, e^{\mathrm{i}\phi} \\ \tan\theta\, e^{-\mathrm{i}\phi} & -1 \end{pmatrix}\begin{pmatrix} \widetilde{\alpha}_+ \\ \widetilde{\beta}_+ \end{pmatrix} = \frac{1}{\cos\theta}\begin{pmatrix} \widetilde{\alpha}_+ \\ \widetilde{\beta}_+ \end{pmatrix} \\ &\Rightarrow\ \widetilde{\alpha}_+ + \tan\theta\, e^{\mathrm{i}\phi}\widetilde{\beta}_+ = \frac{1}{\cos\theta}\widetilde{\alpha}_+ \\ &\Leftrightarrow\ \widetilde{\alpha}_+\left(\frac{1}{\cos\theta} - 1\right) = \tan\theta\, e^{\mathrm{i}\phi}\widetilde{\beta}_+ \\ &\Leftrightarrow\ \widetilde{\alpha}_+ = \frac{\sin\theta}{1 - \cos\theta}e^{\mathrm{i}\phi}\widetilde{\beta}_+ \end{aligned} \tag{C.3}$$

and the normalization condition

$$
\begin{aligned}
1 = |\widetilde{\alpha}_+|^2 + |\widetilde{\beta}_+|^2 &= \left[\frac{\sin^2\theta}{(1-\cos\theta)^2} + 1\right]|\widetilde{\beta}_+|^2 = \frac{2\cancel{(1-\cos\theta)}}{(1-\cos\theta)\cancel{^2}}|\widetilde{\beta}_+|^2 \\
\Leftrightarrow\ |\widetilde{\beta}_+|^2 &= \frac{1}{2}(1-\cos\theta) = \sin^2\left(\frac{\theta}{2}\right) \\
\Rightarrow\ |\widetilde{\beta}_+| = \sin\left(\frac{\theta}{2}\right) \quad &\Rightarrow \quad \widetilde{\beta}_+ = \sin\left(\frac{\theta}{2}\right) e^{\mathrm{i}\arg(\widetilde{\beta}_+)}.
\end{aligned} \tag{C.4}
$$

The argument of $\widetilde{\beta}_+$ is still undetermined. By inserting (C.4) into (C.3) we obtain $\widetilde{\alpha}_+$:

$$
\begin{aligned}
\widetilde{\alpha}_+ &= \frac{\sin\theta}{1-\cos\theta} e^{\mathrm{i}\phi} \sin\left(\frac{\theta}{2}\right) e^{\mathrm{i}\arg(\widetilde{\beta}_+)} = \frac{\sin\theta}{2\sin^{\cancel{2}}\left(\frac{\theta}{2}\right)} e^{\mathrm{i}\phi} \cancel{\sin\left(\frac{\theta}{2}\right)} e^{\mathrm{i}\arg(\widetilde{\beta}_+)} \\
&= \frac{\cancel{2\sin\left(\frac{\theta}{2}\right)}\cos\left(\frac{\theta}{2}\right)}{\cancel{2\sin\left(\frac{\theta}{2}\right)}} e^{\mathrm{i}\phi} e^{\mathrm{i}\arg(\widetilde{\beta}_+)} = \cos\left(\frac{\theta}{2}\right) e^{\mathrm{i}\phi} e^{\mathrm{i}\arg(\widetilde{\beta}_+)}.
\end{aligned}
$$

The resulting eigenvector $|\widetilde{\psi}_+\rangle$ is given by

$$
|\widetilde{\psi}_+\rangle = e^{\mathrm{i}\arg(\widetilde{\beta}_+)} \left[e^{\mathrm{i}\phi}\cos\left(\frac{\theta}{2}\right)|+\rangle \ +\ \sin\left(\frac{\theta}{2}\right)|-\rangle\right]
$$

with $|+\rangle \equiv (1,0)$ and $|-\rangle \equiv (0,1)$. I choose the global phase according to $\arg(\widetilde{\beta}_+) = 0$ so that we finally obtain

$$
|\widetilde{\psi}_+\rangle = e^{\mathrm{i}\phi}\cos\left(\frac{\theta}{2}\right)|+\rangle \ +\ \sin\left(\frac{\theta}{2}\right)|-\rangle\,.
$$

The second eigenvector $|\widetilde{\psi}_-\rangle$ is most conveniently calculated from the orthogonality condition

$$
\begin{aligned}
0 = \langle\widetilde{\psi}_+|\widetilde{\psi}_-\rangle &= e^{-\mathrm{i}\phi}\cos\left(\frac{\theta}{2}\right)\widetilde{\alpha}_- + \sin\left(\frac{\theta}{2}\right)\widetilde{\beta}_- \\
\Rightarrow\ \widetilde{\alpha}_- = \sin\left(\frac{\theta}{2}\right) \quad &\text{and} \quad \widetilde{\beta}_- = -e^{-\mathrm{i}\phi}\cos\left(\frac{\theta}{2}\right)
\end{aligned}
$$

so that we obtain

$$
|\widetilde{\psi}_-\rangle = \sin\left(\frac{\theta}{2}\right)|+\rangle \ -\ e^{-\mathrm{i}\phi}\cos\left(\frac{\theta}{2}\right)|-\rangle\,.
$$

Probability of a spin flip: The spin shall be initially in state $|+\rangle$ and we want to calculate the probability to find it later in state $|-\rangle$. First I note that

$$
\begin{aligned}
|\langle-|\psi(t)\rangle|^2 &= \langle\psi(t)|-\rangle\langle-|\psi(t)\rangle = \langle\widetilde{\psi}(t)|e^{-\mathrm{i}\omega t\sigma_z/2}|-\rangle\langle-|e^{\mathrm{i}\omega t\sigma_z/2}|\widetilde{\psi}(t)\rangle \\
&= \langle\widetilde{\psi}(t)|-\rangle\langle-|\cancel{e^{-\mathrm{i}\omega t\sigma_z/2}e^{\mathrm{i}\omega t\sigma_z/2}}|\widetilde{\psi}(t)\rangle = |\langle-|\widetilde{\psi}(t)\rangle|^2
\end{aligned}
$$

since $|-\rangle\langle-|$ commutes with σ_z. The initial state is

$$
|\widetilde{\psi}(t=0)\rangle = |+\rangle = |\widetilde{\psi}_+\rangle\langle\widetilde{\psi}_+|+\rangle + |\widetilde{\psi}_-\rangle\langle\widetilde{\psi}_-|+\rangle\,.
$$

The time evolution of this state is given by

$$
|\widetilde{\psi}(t)\rangle = e^{-\mathrm{i}E_+t/\hbar}|\widetilde{\psi}_+\rangle\langle\widetilde{\psi}_+|+\rangle + e^{-\mathrm{i}E_-t/\hbar}|\widetilde{\psi}_-\rangle\langle\widetilde{\psi}_-|+\rangle\,.
$$

We project this wave function on the $|-\rangle$ state

$$\begin{aligned}\langle -|\widetilde{\psi}(t)\rangle &= e^{-\mathrm{i}E_+t/\hbar}\langle -|\widetilde{\psi}_+\rangle\langle\widetilde{\psi}_+|+\rangle + e^{-\mathrm{i}E_-t/\hbar}\langle -|\widetilde{\psi}_-\rangle\langle\widetilde{\psi}_-|+\rangle \\ &= e^{-\mathrm{i}E_+t/\hbar}\sin\left(\frac{\theta}{2}\right)e^{-\mathrm{i}\phi}\cos\left(\frac{\theta}{2}\right) - e^{-\mathrm{i}E_-t/\hbar}e^{-\mathrm{i}\phi}\cos\left(\frac{\theta}{2}\right)\sin\left(\frac{\theta}{2}\right) \\ &= -\mathrm{i}e^{-\mathrm{i}\phi}\sin\theta\,\frac{1}{2\mathrm{i}}\left(e^{-\mathrm{i}E_-t/\hbar} - e^{-\mathrm{i}E_+t/\hbar}\right) = -\mathrm{i}e^{-\mathrm{i}\phi}\sin\theta\sin\left(\frac{\Delta\omega}{2}\frac{1}{\cos\theta}t\right).\end{aligned}$$

Thus, the probability to find the spin in state $|-\rangle$ is given by

$$P_-(t) = |\langle -|\widetilde{\psi}(t)\rangle|^2 = \sin^2\theta\sin^2\left(\frac{\Delta\omega}{2}\frac{1}{\cos\theta}t\right).$$

Since

$$\sin^2\theta = \frac{\tan^2\theta}{1+\tan^2\theta} = \frac{|\omega_{\mathrm{rf}}|^2}{\Delta\omega^2+|\omega_{\mathrm{rf}}|^2}$$

and

$$\begin{aligned}&\cos^2\theta = \frac{1}{1+\tan^2\theta} \quad\Rightarrow\quad \frac{1}{\cos\theta} = \pm\sqrt{1+\tan^2\theta} \\ &\Rightarrow\ \frac{1}{\cos\theta} = \pm\sqrt{1+\frac{|\omega_{\mathrm{rf}}|^2}{\Delta\omega^2}} = \pm\frac{1}{\Delta\omega}\sqrt{\Delta\omega^2+|\omega_{\mathrm{rf}}|^2}\end{aligned}$$

we finally obtain

$$P_-(t) = \frac{|\omega_{\mathrm{rf}}|^2}{\Delta\omega^2+|\omega_{\mathrm{rf}}|^2}\,\sin^2\left(\frac{1}{2}\sqrt{\Delta\omega^2+|\omega_{\mathrm{rf}}|^2}\,t\right). \tag{C.5}$$

Time-dependent rf amplitude and zero detuning: So far we have assumed that the rf amplitude ω_{rf} is time-independent. For zero detuning $\Delta\omega = 0$ the Schrödinger equation (C.2) becomes

$$\mathrm{i}\hbar\frac{d}{dt}\begin{pmatrix}\widetilde{\alpha}\\ \widetilde{\beta}\end{pmatrix} = -\frac{\hbar\omega_{\mathrm{rf}}}{2}\begin{pmatrix}0 & 1\\ 1 & 0\end{pmatrix}\begin{pmatrix}\widetilde{\alpha}\\ \widetilde{\beta}\end{pmatrix}. \tag{C.6}$$

This equation can also be solved analytically if $\omega_{\mathrm{rf}}(t)$ is time-dependent [113]. [1] We perform the transformation

$$\widetilde{\alpha} =: \big(\widetilde{\gamma}+\widetilde{\delta}\big)/\sqrt{2}, \qquad \widetilde{\beta} =: \big(\widetilde{\gamma}-\widetilde{\delta}\big)/\sqrt{2}$$

and obtain from (C.6) the set of equations

$$\mathrm{i}\big(\widetilde{\gamma}'+\widetilde{\delta}'\big) = -\frac{\omega_{\mathrm{rf}}(t)}{2}\big(\widetilde{\gamma}-\widetilde{\delta}\big) \qquad \text{and} \qquad \mathrm{i}\big(\widetilde{\gamma}'-\widetilde{\delta}'\big) = -\frac{\omega_{\mathrm{rf}}(t)}{2}\big(\widetilde{\gamma}+\widetilde{\delta}\big).$$

We sum up (subtract) both equations and obtain the decoupled equations

$$\mathrm{i}\,\widetilde{\gamma}' = -\frac{\omega_{\mathrm{rf}}(t)}{2}\,\widetilde{\gamma} \qquad \text{and} \qquad \mathrm{i}\,\widetilde{\delta}' = +\frac{\omega_{\mathrm{rf}}(t)}{2}\,\widetilde{\delta}\,.$$

We solve both equations by separating variables. The solutions are given by

$$\widetilde{\gamma}(t) = \widetilde{\gamma}_0 e^{\mathrm{i}\Omega_{\mathrm{rf}}(t)/2} \quad \text{and} \quad \widetilde{\delta}(t) = \widetilde{\delta}_0 e^{-\mathrm{i}\Omega_{\mathrm{rf}}(t)/2} \quad \text{with} \quad \Omega_{\mathrm{rf}}(t) = \int_0^t \omega_{\mathrm{rf}}(t')dt'.$$

[1] The calculation works only for a real rf amplitude.

The time evolution of a spin is thus given by

$$|\widetilde{\psi}(t)\rangle = \frac{1}{\sqrt{2}}\left(\widetilde{\gamma}_0 e^{\mathbb{i}\Omega_{\rm rf}(t)/2} + \widetilde{\delta}_0 e^{-\mathbb{i}\Omega_{\rm rf}(t)/2}\right)|+\rangle \;+\; \frac{1}{\sqrt{2}}\left(\widetilde{\gamma}_0 e^{\mathbb{i}\Omega_{\rm rf}(t)/2} - \widetilde{\delta}_0 e^{-\mathbb{i}\Omega_{\rm rf}(t)/2}\right)|-\rangle.$$

The integration constants are determined by the initial condition $|\widetilde{\psi}(t)\rangle = |+\rangle$. It follows, that

$$\left.\begin{aligned} 1 &= \langle +|\widetilde{\psi}(t=0)\rangle = \left(\widetilde{\gamma}_0 + \widetilde{\delta}_0\right)/\sqrt{2} \\ 0 &= \langle -|\widetilde{\psi}(t=0)\rangle = \left(\widetilde{\gamma}_0 - \widetilde{\delta}_0\right)/\sqrt{2} \end{aligned}\right\} \quad \Rightarrow \quad \widetilde{\gamma}_0 = \widetilde{\delta}_0 = 1/\sqrt{2}\,.$$

The time evolution of the spin is now given by

$$|\widetilde{\psi}(t)\rangle = \cos\left[\frac{1}{2}\int_0^t \omega_{\rm rf}(t')dt'\right]|+\rangle \;+\; \mathbb{i}\sin\left[\frac{1}{2}\int_0^t \omega_{\rm rf}(t')dt'\right]|-\rangle\,.$$

Finally we obtain the probability of a spin flip

$$P_-(t) = \sin^2\left[\frac{1}{2}\int_0^t \omega_{\rm rf}(t')dt'\right]. \tag{C.7}$$

Remark— If we neglect the imaginary part of the Hamiltonian matrix of Eq. (C.1) the rf amplitude is given by $\omega_{\rm rf}(t) = \omega_{\rm rf}\big[1+\cos(2\omega t)\big]$ and we obtain the transfer probability

$$P_-(t) = \sin^2\left[\frac{\omega_{\rm rf}}{2}\left(t + \frac{1}{\omega}\sin(2\omega t)\right)\right]. \tag{C.8}$$

Thus, we obtain additional oscillations around the $\sin^2(\omega_{\rm rf}t/2)$ curve with an amplitude which decreases $\propto 1/\omega$ and a frequency which increases $\propto \omega$ similar to the observation of Fig. C.2.

Appendix D

Table of constants

Table D.1: Constants.

Planck's constant	h	$6.62606896 \times 10^{-34}$ Js
	$\hbar = h/(2\pi)$	$1.05457163 \times 10^{-34}$ Js
atomic mass unit	u	$1.660538782 \times 10^{-27}$ kg
mass of ^{87}Rb	m_{Rb}	86.90918053 u
mass of ^{40}K	m_K	39.96399848 u
Bohr's magneton	μ_B	$9.27400915 \times 10^{-24}$ J/T
nuclear magneton	μ_n	$5.05078324 \times 10^{-27}$ J/T
electron g-factor	g_e	2.0023193043622
nuclear g-factor of ^{87}Rb	g_n	0.0009951414
hyperfine constant	C_{hfs}	$3.41734130642 \times 10^9\, h$Hz
Bohr radius	a_B	$0.52917720859 \times 10^{-10}$ m
scattering lengths of spin-1 ^{87}Rb	a_0	$101.8\, a_B$
	a_2	$100.4\, a_B$
constants of Sec. 2.2		
interaction constant	$C_{\text{int.}}$	$3.949099654 \times 10^{-4}$
linear Zeeman energy constant	$C_{Z,\text{lin.}}$	699.8123018×10^3
quadratic Zeeman energy constant	$C_{Z,\text{quad.}}$	71.65471837
constants of Sec. 2.6		
interaction constant	$C^*_{\text{int.}}$	$3.083118598 \times 10^{-5}$
linear Zeeman energy constant	$C^*_{Z,\text{lin.}}$	699.8123018
quadratic Zeeman energy constant	$C^*_{Z,\text{quad.}}$	$2.866188735 \times 10^{-4}$

Bibliography

[1] F. Deuretzbacher. *Spinor Bose-Einstein Kondensate*. Diplomarbeit, Universität Hamburg (2005). The thesis is available on the home page of the condensed matter theory group.

[2] F. Deuretzbacher, K. Bongs, K. Sengstock and D. Pfannkuche. *Evolution from a Bose-Einstein condensate to a Tonks-Girardeau gas: An exact diagonalization study*. Phys. Rev. A **75**, 013614 (2007). doi:10.1103/PhysRevA.75.013614.

[3] F. Deuretzbacher, K. Plassmeier, D. Pfannkuche, F. Werner, C. Ospelkaus, S. Ospelkaus, K. Sengstock and K. Bongs. *Heteronuclear molecules in an optical lattice: Theory and experiment*. Phys. Rev. A **77**, 032726 (2008). doi:10.1103/PhysRevA.77.032726.

[4] F. Deuretzbacher, K. Fredenhagen, D. Becker, K. Bongs, K. Sengstock and D. Pfannkuche. *Exact Solution of Strongly Interacting Quasi-One-Dimensional Spinor Bose Gases*. Phys. Rev. Lett. **100**, 160405 (2008). doi:10.1103/PhysRevLett.100.160405.

[5] L. Tonks. *The Complete Equation of State of One, Two and Three-Dimensional Gases of Hard Elastic Spheres*. Phys. Rev. **50**, 955 (1936). doi:10.1103/PhysRev.50.955.

[6] M. Girardeau. *Relationship between Systems of Impenetrable Bosons and Fermions in One Dimension*. J. Math. Phys. **1**, 516 (1960). doi:10.1063/1.1703687.

[7] E. H. Lieb and W. Liniger. *Exact Analysis of an Interacting Bose Gas. I. The General Solution and the Ground State*. Phys. Rev. **130**, 1605 (1963). doi:10.1103/PhysRev.130.1605.

[8] E. H. Lieb. *Exact Analysis of an Interacting Bose Gas. II. The Excitation Spectrum*. Phys. Rev. **130**, 1616 (1963). doi:10.1103/PhysRev.130.1616.

[9] C. N. Yang. *Some Exact Results for the Many-Body Problem in one Dimension with Repulsive Delta-Function Interaction*. Phys. Rev. Lett. **19**, 1312 (1967). doi:10.1103/PhysRevLett.19.1312.

[10] C. N. Yang and C. P. Yang. *Thermodynamics of a One-Dimensional System of Bosons with Repulsive Delta-Function Interaction*. Journal of Mathematical Physics **10**, 1115 (1969). doi:10.1063/1.1664947.

[11] J. M. Luttinger. *An Exactly Soluble Model of a Many-Fermion System*. Journal of Mathematical Physics **4**, 1154 (1963). doi:10.1063/1.1704046.

[12] D. C. Mattis and E. H. Lieb. *Exact Solution of a Many-Fermion System and Its Associated Boson Field*. Journal of Mathematical Physics **6**, 304 (1965). doi:10.1063/1.1704281.

[13] F. D. M. Haldane. *Effective Harmonic-Fluid Approach to Low-Energy Properties of One-Dimensional Quantum Fluids*. Phys. Rev. Lett. **47**, 1840 (1981). doi:10.1103/PhysRevLett.47.1840.

[14] T. Giamarchi. *Quantum Physics in One Dimension*. Oxford Science Publications (2004).

[15] F. Dalfovo, S. Giorgini, L. P. Pitaevskii and S. Stringari. *Theory of Bose-Einstein condensation in trapped gases*. Rev. Mod. Phys. **71**, 463 (1999). doi:10.1103/RevModPhys.71.463.

[16] A. J. Leggett. *Bose-Einstein condensation in the alkali gases: Some fundamental concepts*. Rev. Mod. Phys. **73**, 307 (2001). doi:10.1103/RevModPhys.73.307.

[17] K. Bongs, S. Burger, S. Dettmer, D. Hellweg, J. Arlt, W. Ertmer and K. Sengstock. *Waveguide for Bose-Einstein condensates*. Phys. Rev. A **63**, 031602(R) (2001). doi:10.1103/PhysRevA.63.031602.

[18] S. Burger, K. Bongs, S. Dettmer, W. Ertmer, K. Sengstock, A. Sanpera, G. V. Shlyapnikov and M. Lewenstein. *Dark Solitons in Bose-Einstein Condensates*. Phys. Rev. Lett. **83**, 5198 (1999). doi:10.1103/PhysRevLett.83.5198.

[19] S. Dettmer, D. Hellweg, P. Ryytty, J. J. Arlt, W. Ertmer, K. Sengstock, D. S. Petrov, G. V. Shlyapnikov, H. Kreutzmann, L. Santos and M. Lewenstein. *Observation of Phase Fluctuations in Elongated Bose-Einstein Condensates*. Phys. Rev. Lett. **87**, 160406 (2001). doi:10.1103/PhysRevLett.87.160406.

[20] M. Greiner, I. Bloch, O. Mandel, T. W. Hänsch and T. Esslinger. *Exploring Phase Coherence in a 2D Lattice of Bose-Einstein Condensates*. Phys. Rev. Lett. **87**, 160405 (2001). doi:10.1103/PhysRevLett.87.160405.

[21] T. Kinoshita, T. Wenger and D. S. Weiss. *Observation of a One-Dimensional Tonks-Girardeau Gas*. Science **305**, 1125 (2004). doi:10.1126/science.1100700.

[22] B. Paredes, A. Widera, V. Murg, O. Mandel, S. Fölling, I. Cirac, G. V. Shlyapnikov, T. W. Hänsch and I. Bloch. *Tonks-Girardeau gas of ultracold atoms in an optical lattice*. Nature **429**, 277 (2004). doi:10.1038/nature02530.

[23] H. Monien, M. Linn and N. Elstner. *Trapped one-dimensional Bose gas as a Luttinger liquid*. Phys. Rev. A **58**, R3395 (1998). doi:10.1103/PhysRevA.58.R3395.

[24] H. Moritz, T. Stöferle, M. Köhl and T. Esslinger. *Exciting Collective Oscillations in a Trapped 1D Gas*. Phys. Rev. Lett. **91**, 250402 (2003). doi:10.1103/PhysRevLett.91.250402.

[25] A. Widera, S. Trotzky, P. Cheinet, S. Fölling, F. Gerbier, I. Bloch, V. Gritsev, M. D. Lukin and E. Demler. *Quantum Spin Dynamics of Mode-Squeezed Luttinger Liquids in Two-Component Atomic Gases*. Phys. Rev. Lett. **100**, 140401 (2008). doi:10.1103/PhysRevLett.100.140401.

[26] O. M. Auslaender, A. Yacoby, R. de Picciotto, K. W. Baldwin, L. N. Pfeiffer and K. W. West. *Tunneling Spectroscopy of the Elementary Excitations in a One-Dimensional Wire*. Science **295**, 825 (2002). doi:10.1126/science.1066266.

[27] M. Bockrath *et al. Luttinger-liquid behaviour in carbon nanotubes*. Nature **397**, 598 (1999). doi:10.1038/17569.

[28] H. Ishii *et al. Direct observation of Tomonaga-Luttinger-liquid state in carbon nanotubes at low temperatures*. Nature **426**, 540 (2003). doi:10.1038/nature02074.

[29] J. Lee, S. Eggert, H. Kim, S.-J. Kahng, H. Shinohara and Y. Kuk. *Real Space Imaging of One-Dimensional Standing Waves: Direct Evidence for a Luttinger Liquid*. Phys. Rev. Lett. **93**, 166403 (2004). doi:10.1103/PhysRevLett.93.166403.

[30] V. Dunjko, V. Lorent and M. Olshanii. *Bosons in Cigar-Shaped Traps: Thomas-Fermi Regime, Tonks-Girardeau Regime, and In Between*. Phys. Rev. Lett. **86**, 5413 (2001). doi:10.1103/PhysRevLett.86.5413.

[31] P. Öhberg and L. Santos. *Dynamical Transition from a Quasi-One-Dimensional Bose-Einstein Condensate to a Tonks-Girardeau Gas*. Phys. Rev. Lett. **89**, 240402 (2002). doi:10.1103/PhysRevLett.89.240402.

[32] D. M. Gangardt and G. V. Shlyapnikov. *Stability and Phase Coherence of Trapped 1D Bose Gases*. Phys. Rev. Lett. **90**, 010401 (2003). doi:10.1103/PhysRevLett.90.010401.

[33] K. V. Kheruntsyan, D. M. Gangardt, P. D. Drummond and G. V. Shlyapnikov. *Finite-temperature correlations and density profiles of an inhomogeneous interacting one-dimensional Bose gas*. Phys. Rev. A **71**, 053615 (2005). doi:10.1103/PhysRevA.71.053615.

[34] K. Sakmann, A. I. Streltsov, O. E. Alon and L. S. Cederbaum. *Exact ground state of finite Bose-Einstein condensates on a ring*. Phys. Rev. A **72**, 033613 (2005). doi:10.1103/PhysRevA.72.033613.

[35] Y. Hao, Y. Zhang, J. Q. Liang and S. Chen. *Ground-state properties of one-dimensional ultracold Bose gases in a hard-wall trap*. Phys. Rev. A **73**, 063617 (2006). doi:10.1103/PhysRevA.73.063617.

[36] D. Blume. *Fermionization of a bosonic gas under highly elongated confinement: A diffusion quantum Monte Carlo study*. Phys. Rev. A **66**, 053613 (2002). doi:10.1103/PhysRevA.66.053613.

[37] G. E. Astrakharchik and S. Giorgini. *Correlation functions and momentum distribution of one-dimensional Bose systems*. Phys. Rev. A **68**, 031602(R) (2003). doi:10.1103/PhysRevA.68.031602.

[38] C. Kollath, U. Schollwöck, J. von Delft and W. Zwerger. *Spatial correlations of trapped one-dimensional bosons in an optical lattice*. Phys. Rev. A **69**, 031601(R) (2004). doi:10.1103/PhysRevA.69.031601.

[39] B. Schmidt and M. Fleischhauer. *Exact numerical simulations of a one-dimensional trapped Bose gas*. Phys. Rev. A **75**, 021601(R) (2007). doi:10.1103/PhysRevA.75.021601.

[40] U. Schollwöck. *The density-matrix renormalization group*. Rev. Mod. Phys. **77**, 259 (2005). doi:10.1103/RevModPhys.77.259.

[41] S. Zöllner, H.-D. Meyer and P. Schmelcher. *Ultracold few-boson systems in a double-well trap*. Phys. Rev. A **74**, 053612 (2006). doi:10.1103/PhysRevA.74.053612.

[42] S. Zöllner. *One-dimensional Few-boson Systems in Single- and Double-well Traps*. Ph.D. thesis, University of Heidelberg (2008). urn:nbn:de:bsz:16-opus-86112.

[43] Y. Hao and S. Chen. *Ground-state properties of interacting two-component Bose gases in a one-dimensional harmonic trap*. Eur. Phys. J. D **51**, 261 (2009). doi:10.1140/epjd/e2008-00266-0.

[44] X. Yin, Y. Hao, S. Chen and Y. Zhang. *Ground-state properties of a few-boson system in a one-dimensional hard-wall split potential*. Phys. Rev. A **78**, 013604 (2008). doi:10.1103/PhysRevA.78.013604.

[45] T. Kinoshita, T. Wenger and D. S. Weiss. *Local Pair Correlations in One-Dimensional Bose Gases*. Phys. Rev. Lett. **95**, 190406 (2005). doi:10.1103/PhysRevLett.95.190406.

[46] D. S. Hall, M. R. Matthews, J. R. Ensher, C. E. Wieman and E. A. Cornell. *Dynamics of Component Separation in a Binary Mixture of Bose-Einstein Condensates*. Phys. Rev. Lett. **81**, 1539 (1998). doi:10.1103/PhysRevLett.81.1539.

[47] J. Stenger, S. Inouye, D. M. Stamper-Kurn, H.-J. Miesner, A. P. Chikkatur and W. Ketterle. *Spin domains in ground-state Bose-Einstein condensates*. Nature **396**, 345 (1998). doi:10.1038/24567.

[48] M.-S. Chang, Q. Qin, W. Zhang, L. You and M. S. Chapman. *Coherent spinor dynamics in a spin-1 Bose condensate*. Nature Phys. **1**, 111 (2005). doi:10.1038/nphys153.

[49] J. Kronjäger, C. Becker, M. Brinkmann, R. Walser, P. Navez, K. Bongs and K. Sengstock. *Evolution of a spinor condensate: Coherent dynamics, dephasing, and revivals*. Phys. Rev. A **72**, 063619 (2005). doi:10.1103/PhysRevA.72.063619.

[50] H. Schmaljohann, M. Erhard, J. Kronjäger, M. Kottke, S. van Staa, L. Cacciapuoti, J. J. Arlt, K. Bongs and K. Sengstock. *Dynamics of $F = 2$ Spinor Bose-Einstein Condensates*. Phys. Rev. Lett. **92**, 040402 (2004). doi:10.1103/PhysRevLett.92.040402.

[51] J. Kronjäger, C. Becker, P. Navez, K. Bongs and K. Sengstock. *Magnetically tuned spin dynamics resonance*. Phys. Rev. Lett. **97**, 110404 (2006). doi:10.1103/PhysRevLett.97.110404.

[52] H. Schmaljohann. *Spindynamik in Bose-Einstein Kondensaten*. Ph.D. thesis, Universität Hamburg (2004). urn:nbn:de:gbv:18-21508.

[53] J. Kronjäger. *Coherent Dynamics of Spinor Bose-Einstein Condensates*. Ph.D. thesis, Universität Hamburg (2007). urn:nbn:de:gbv:18-34281.

[54] T.-L. Ho. *Spinor Bose Condensates in Optical Traps*. Phys. Rev. Lett. **81**, 742 (1998). doi:10.1103/PhysRevLett.81.742.

[55] T. Ohmi and K. Machida. *Bose-Einstein condensation with internal degrees of freedom in Alkali gases*. J. Phys. Soc. Jap. **67**, 1822 (1998). doi:10.1143/JPSJ.67.1822.

[56] C. Law, H. Pu and N. Bigelow. *Quantum Spins Mixing in Spinor Bose-Einstein Condensates*. Phys. Rev. Lett. **81**, 5257 (1998). doi:10.1103/PhysRevLett.81.5257.

[57] C. V. Ciobanu, S.-K. Yip and T.-L. Ho. *Phase diagrams of $F = 2$ spinor Bose-Einstein condensates*. Phys. Rev. A **61**, 033607 (2000). doi:10.1103/PhysRevA.61.033607.

[58] M. Koashi and M. Ueda. *Exact Eigenstates and Magnetic Response of Spin-1 and Spin-2 Bose-Einstein Condensates*. Phys. Rev. Lett. **84**, 1066 (2000). doi:10.1103/PhysRevLett.84.1066.

[59] M. Ueda and M. Koashi. *Theory of spin-2 Bose-Einstein condensates: Spin correlations, magnetic response, and excitation spectra*. Phys. Rev. A **65**, 063602 (2002). doi:10.1103/PhysRevA.65.063602.

[60] W. Zhang, D. L. Zhou, M.-S. Chang, M. S. Chapman and L. You. *Coherent spin mixing dynamics in a spin-1 atomic condensate*. Phys. Rev. A **72**, 013602 (2005). doi:10.1103/PhysRevA.72.013602.

[61] A. Widera, F. Gerbier, S. Fölling, T. Gericke, O. Mandel and I. Bloch. *Coherent Collisional Spin Dynamics in Optical Lattices*. Phys. Rev. Lett. **95**, 190405 (2005). doi:10.1103/PhysRevLett.95.190405.

[62] F. Gerbier, A. Widera, S. Fölling, O. Mandel and I. Bloch. *Resonant control of spin dynamics in ultracold quantum gases by microwave dressing*. Phys. Rev. A **73**, 041602 (2006). doi:10.1103/PhysRevA.73.041602.

[63] A. Widera, F. Gerbier, S. Fölling, T. Gericke, O. Mandel and I. Bloch. *Precision measurement of spin-dependent interaction strengths for spin-1 and spin-2 ^{87}Rb atoms*. New Journal of Physics **8**, 152 (2006). doi:10.1088/1367-2630/8/8/152.

[64] W. Zhang, D. L. Zhou, M.-S. Chang, M. S. Chapman and L. You. *Dynamical Instability and Domain Formation in a Spin-1 Bose-Einstein Condensate*. Phys. Rev. Lett. **95**, 180403 (2005). doi:10.1103/PhysRevLett.95.180403.

[65] H. Saito and M. Ueda. *Spontaneous magnetization and structure formation in a spin-1 ferromagnetic Bose-Einstein condensate*. Phys. Rev. A **72**, 023610 (2005). doi:10.1103/PhysRevA.72.023610.

[66] H. Saito, Y. Kawaguchi and M. Ueda. *Topological defect formation in a quenched ferromagnetic Bose-Einstein condensate*. Phys. Rev. A **75**, 013621 (2007). doi:10.1103/PhysRevA.75.013621.

[67] L. E. Sadler, J. M. Higbie, S. R. Leslie, M. Vengalattore and D. M. Stamper-Kurn. *Spontaneous symmetry breaking in a quenched ferromagnetic spinor Bose-Einstein condensate*. Nature **443**, 312 (2006). doi:10.1038/nature05094.

[68] T. Cheon and T. Shigehara. *Fermion-Boson Duality of One-Dimensional Quantum Particles with Generalized Contact Interactions*. Phys. Rev. Lett. **82**, 2536 (1999). doi:10.1103/PhysRevLett.82.2536.

[69] M. D. Girardeau and A. Minguzzi. *Soluble Models of Strongly Interacting Ultracold Gas Mixtures in Tight Waveguides*. Phys. Rev. Lett. **99**, 230402 (2007). doi:10.1103/PhysRevLett.99.230402.

[70] S. V. Mousavi, A. del Campo, I. Lizuain and J. G. Muga. *Ramsey interferometry with a two-level generalized Tonks-Girardeau gas*. Phys. Rev. A **76**, 033607 (2007). doi:10.1103/PhysRevA.76.033607.

[71] M. D. Girardeau. *Soluble Models of Strongly Interacting Two-level Ultracold Gases in Tight Waveguides with Coupling to the Quantized Electromagnetic Field* (2007). arXiv:0707.1884.

[72] C. Ospelkaus, S. Ospelkaus, L. Humbert, P. Ernst, K. Sengstock and K. Bongs. *Ultracold Heteronuclear Molecules in a 3D Optical Lattice*. Phys. Rev. Lett. **97**, 120402 (2006). doi:10.1103/PhysRevLett.97.120402.

[73] C. Ospelkaus. *Fermi-Bose mixtures: From mean-field interactions to ultracold chemistry*. Ph.D. thesis, Universität Hamburg (2006). urn:nbn:de:gbv:18-32004.

[74] S. Ospelkaus. *Quantum Degenerate Fermi-Bose Mixtures of ^{40}K and ^{87}Rb in 3D Optical Lattices*. Ph.D. thesis, Universität Hamburg (2006). urn:nbn:de:gbv:18-32064.

[75] T. Busch, B. G. Englert, K. Rzążewski and M. Wilkens. *Two Cold Atoms in a Harmonic Trap*. Found. Phys. **28**, 549 (1998). doi:10.1023/A:1018705520999.

[76] M. A. Cirone, K. Góral, K. Rzążewski and M. Wilkens. *Bose-Einstein condensation of two interacting particles*. Journal of Physics B **34**, 4571 (2001). doi:10.1088/0953-4075/34/23/304.

[77] E. G. M. van Kempen, S. J. J. M. F. Kokkelmans, D. J. Heinzen and B. J. Verhaar. *Interisotope determination of ultracold rubidium interactions from three high-precision experiments*. Phys. Rev. Lett. **88**, 093201 (2002). doi:10.1103/PhysRevLett.88.093201.

[78] C. Cohen-Tannoudji, B. Diu and F. Laloë. *Quantum Mechanics*. John Wiley & Sons, New York (1997).

[79] G. Baym. *Lectures on quantum mechanics*. Westview Press (1990).

[80] E. Fick. *Einführung in die Grundlagen der Quantentheorie*. Aula-Verlag (1988).

[81] K. Plassmeier. Private communication (2006/2007).

[82] G. Deuretzbacher. Private communication (2005).

[83] D. J. Griffiths. *Introduction to quantum mechanics*. Prentice Hall, Englewood Cliffs, NJ (1994).

[84] M. Olshanii. *Atomic Scattering in the Presence of an External Confinement and a Gas of Impenetrable Bosons*. Phys. Rev. Lett. **81**, 938 (1998). doi:10.1103/PhysRevLett.81.938.

[85] Z. Idziaszek and T. Calarco. *Two atoms in an anisotropic harmonic trap*. Phys. Rev. A **71**, 050701 (2005). doi:10.1103/PhysRevA.71.050701.

[86] M. D. Girardeau, E. M. Wright and J. M. Triscari. *Ground-state properties of a one-dimensional system of hard-core bosons in a harmonic trap*. Phys. Rev. A **63**, 033601 (2001). doi:10.1103/PhysRevA.63.033601.

[87] O. E. Alon and L. S. Cederbaum. *Pathway from Condensation via Fragmentation to Fermionization of Cold Bosonic Systems*. Phys. Rev. Lett. **95**, 140402 (2005). doi:10.1103/PhysRevLett.95.140402.

[88] E. B. Kolomeisky, T. J. Newman, J. P. Straley and X. Qi. *Low-Dimensional Bose Liquids: Beyond the Gross-Pitaevskii Approximation*. Phys. Rev. Lett. **85**, 1146 (2000). doi:10.1103/PhysRevLett.85.1146.

[89] T. Papenbrock. *Ground-state properties of hard-core bosons in one-dimensional harmonic traps*. Phys. Rev. A **67**, 041601 (2003). doi:10.1103/PhysRevA.67.041601.

[90] A. Minguzzi, P. Vignolo and M. P. Tosi. *High-momentum tail in the Tonks gas under harmonic confinement*. Phys. Lett. A **294**, 222 (2002). doi:10.1016/S0375-9601(02)00042-7.

[91] G. J. Lapeyre, M. D. Girardeau and E. M. Wright. *Momentum distribution for a one-dimensional trapped gas of hard-core bosons*. Phys. Rev. A **66**, 023606 (2002). doi:10.1103/PhysRevA.66.023606.

[92] M. Olshanii and V. Dunjko. *Short-Distance Correlation Properties of the Lieb-Liniger System and Momentum Distributions of Trapped One-Dimensional Atomic Gases*. Phys. Rev. Lett. **91**, 090401 (2003). doi:10.1103/PhysRevLett.91.090401.

[93] K. Fredenhagen. Private communication (2007).

[94] L. Guan, S. Chen, Y. Wang and Z.-Q. Ma. *Exact solution for strongly interacting Fermi gases in tight waveguides* (2008). arXiv:0806.1773.

[95] F. Schwabl. *Quantenmechanik für Fortgeschrittene*. Springer-Verlag, Berlin, 5th edition (2008).

[96] E. Eisenberg and E. H. Lieb. *Polarization of Interacting Bosons with Spin*. Phys. Rev. Lett. **89**, 220403 (2002). doi:10.1103/PhysRevLett.89.220403.

[97] J. J. Sakurai. *Modern Quantum Mechanics*. Addison-Wesley, Reading, MA (1994).

[98] J. F. Bertelsen and K. Mølmer. *Association of heteronuclear molecules in a harmonic oscillator well*. Phys. Rev. A **76**, 043615 (2007). doi:10.1103/PhysRevA.76.043615.

[99] J. F. Bertelsen. *Ultracold Atomic Gases - Mixtures and Molecules*. Ph.D. thesis, University of Aarhus (2007). URL http://www.phys.au.dk/main/publications/PhD/Jesper_Fevre_Bertelsen.pdf.

[100] M. Abramowitz and I. A. Stegun (editors). *Handbook of Mathematical Functions*. Dover, New York (1972).

[101] I. S. Gradshteyn and I. M. Ryzhik. *Table of Integrals, Series, and Products*. Academic Press, San Diego, CA, 6th edition (2000).

[102] Y. Castin. *Basic theory tools for degenerate Fermi gases*. In M. Inguscio, W. Ketterle and C. Salomon (editors), *Proceedings of the International School of Physics - Enrico Fermi*, volume 164. IOS Press (2008). arXiv:cond-mat/0612613v2.

[103] T. Köhler, K. Góral and P. S. Julienne. *Production of cold molecules via magnetically tunable Feshbach resonances*. Rev. Mod. Phys. **78**, 1311 (2006). doi:10.1103/RevModPhys.78.1311.

[104] S. Ospelkaus, C. Ospelkaus, L. Humbert, K. Sengstock and K. Bongs. *Tuning of Heteronuclear Interactions in a Degenerate Fermi-Bose Mixture*. Phys. Rev. Lett. **97**, 120403 (2006). doi:10.1103/PhysRevLett.97.120403.

[105] G. B. Arfken and H. J. Weber. *Mathematical Methods for Physicists*. Academic Press, San Diego, CA, 5th edition (2001).

[106] O. Wille. *Aufbau eines 3D-optischen Gitters für quantenentartete Fermi-Bose-Mischungen aus ^{87}Rb und ^{40}K*. Diplomarbeit, Universität Hamburg (2005). The thesis is available on the home page of the Klaus Sengstock group.

[107] A. Simoni. Private communication (2006).

[108] M. Zaccanti, C. D'Errico, F. Ferlaino, G. Roati, M. Inguscio and G. Modugno. *Control of the interaction in a Fermi-Bose mixture*. Phys. Rev. A **74**, 041605 (2006). doi:10.1103/PhysRevA.74.041605.

[109] A. Derevianko, J. F. Babb and A. Dalgarno. *High-precision calculations of van der Waals coefficients for heteronuclear alkali-metal dimers*. Phys. Rev. A **63**, 052704 (2001). doi:10.1103/PhysRevA.63.052704.

[110] N. Syassen, D. M. Bauer, M. Lettner, D. Dietze, T. Volz, S. Dürr and G. Rempe. *Atom-Molecule Rabi Oscillations in a Mott Insulator*. Phys. Rev. Lett. **99**, 033201 (2007). doi:10.1103/PhysRevLett.99.033201.

[111] D. S. Petrov, C. Salomon and G. V. Shlyapnikov. *Weakly Bound Dimers of Fermionic Atoms*. Phys. Rev. Lett. **93**, 090404 (2004). doi:10.1103/PhysRevLett.93.090404.

[112] D. S. Petrov, C. Salomon and G. V. Shlyapnikov. *Scattering properties of weakly bound dimers of fermionic atoms*. Phys. Rev. A **71**, 012708 (2005). doi:10.1103/PhysRevA.71.012708.

[113] F. Werner. Private communication (2007).

[114] F. Werner. *Trapped cold atoms with resonant interactions: Unitary gas and three-body problem*. Ph.D. thesis, University Paris VI (2008). URL http://tel.archives-ouvertes.fr/tel-00285587.

[115] K.-K. Ni, S. Ospelkaus, M. H. G. de Miranda, A. Pe'er, B. Neyenhuis, J. J. Zirbel, S. Kotochigova, P. S. Julienne, D. S. Jin and J. Ye. *A High Phase-Space-Density Gas of Polar Molecules*. Science **322**, 231 (2008). doi:10.1126/science.1163861.

[116] J. Deiglmayr, A. Grochola, M. Repp, K. Mörtlbauer, C. Glück, J. Lange, O. Dulieu, R. Wester and M. Weidemüller. *Formation of Ultracold Polar Molecules in the Rovibrational Ground State*. Phys. Rev. Lett. **101**, 133004 (2008). doi:10.1103/PhysRevLett.101.133004.

Danksagung

Ich möchte mich zuallererst bei Frau Prof. Daniela Pfannkuche für die Betreuung meiner Arbeit bedanken. Sie hat mir die Wahl dieses interessanten Themas ermöglicht, ein optimales Arbeitsumfeld geschaffen und viele wertvolle Beiträge zu allen Ergebnissen geliefert. Von ihr habe ich gelernt, die wesentlichen physikalischen Mechanismen zu erkennen und die Ergebnisse meiner Arbeit in Publikationen und Vorträgen zu präsentieren. Durch ihre Begeisterung und ihr Engagement hatte ich stets viel Freude bei der Arbeit.

Ich bin sehr dankbar für die enge Zusammenarbeit mit Prof. Klaus Sengstock und seiner Gruppe vom Institut für Laserphysik. In den regelmäßigen Meetings wurden oftmals wichtige Ideen entwickelt und ausgetauscht. Insbesondere danke ich Prof. Kai Bongs für die intensive Betreuung meiner Arbeit. Von besonderem Wert war für mich die Zusammenarbeit mit Christian und Silke Ospelkaus im Zusammenhang mit den ultrakalten Molekülen.

Bei Prof. Klaus Fredenhagen vom II. Institut für Theoretische Physik bedanke ich mich für die fruchtbare Zusammenarbeit im Zusammenhang mit den Spinor Tonks-Girardeau Gasen.

Meiner Gruppe danke ich für das angenehme Arbeitsklima. Ich hatte viele interessante Diskussionen mit Kim Plassmeier, Daniel Becker, Jannes Heinze und Dirk-Sören Lühmann. Bei Daniel Becker und Dirk-Sören Lühmann möchte ich mich außerdem für das Korrekturlesen dieser Arbeit bedanken.

Bei Frau Prof. Stephanie M. Reimann von der Universität Lund bedanke ich mich für die Übernahme des Zweitgutachtens. Sie und Magnus Ögren weckten mein Interesse für eindimensionale Systeme während eines Forschungsaufenthaltes in Lund.

Zu Beginn meiner Arbeit an den ultrakalten Molekülen hatte ich eine sehr anregende Diskussion mit Prof. Kazimierz Rzążewski vom Zentrum für Theoretische Physik der Polnischen Akademie der Wissenschaften über das regularisierte Deltapotential, für die ich mich ebenfalls sehr herzlich bedanken möchte.

Besonders danke ich meinen Eltern für die stets zuversichtliche Unterstützung.